

Development of a Fluorescent Probe Applicable for Screening New Inhibitors Targeting Mitogen- Activated Protein Kinase Kinase 4 (MKK4)

Dissertation

der Mathematisch-Naturwissenschaftlichen Fakultät
der Eberhard Karls Universität Tübingen
zur Erlangung des Grades eines
Doktors der Naturwissenschaften
(Dr. rer. nat.)

vorgelegt von

Theresa Johanna Maria Kircher
aus Fulda

Tübingen

2020

Gedruckt mit Genehmigung der Mathematisch-Naturwissenschaftlichen Fakultät der
Eberhard Karls Universität Tübingen.

Tag der mündlichen Qualifikation:	02.02.2021
Stellvertretender Dekan:	Prof. Dr. József Fortágh
1. Berichterstatter:	Prof. Dr. Stefan A. Laufer
2. Berichterstatter:	Prof. Dr. Michael Lämmerhofer

Nothing is more beautiful than to know all

ATHANASIUS KIRCHER

Preface

Ich bedanke mich bei...

Prof. Stefan Laufer für die Aufnahme in seinen Arbeitskreis, die Betreuung meiner wissenschaftlichen Arbeit und das entgegengebrachte Vertrauen, mein Projekt frei zu bearbeiten.

Prof. Michael Lämmerhofer für die Übernahme des Zweitgutachtens.

Heparegenix, für die Finanzierung der Chemikalien und besonders bei **Dr. Roland Selig** für die Projektkoordination und Syntheseberatung.

der **Screening Unit** des Leibniz-Forschungsinstituts für Molekulare Pharmakologie in Berlin für die Validierung und Durchführung des FP-screens.

Dr. Raimund Niess, für die Organisation des gesamten Arbeitskreises und sein stets lässiges Wesen.

Kristine Schmidt, die durch ihre nette, hilfsbereite Art den Tag immer ein wenig besser gemacht hat.

Mechthild Seyboldt und **Birgit Kailer**, für den Verkauf von Chemikalien und dem ein oder anderen erheiternden Plausch zwischendurch.

Katharina Bauer, **Jens Strobach** und **Gerd Helms** für nette Gespräche, Kaffeerunden und Hilfestellungen jeglicher Art.

AK Böckler: Prof. Frank Böckler, Sebastian Vaas, Marcel Dammann, Marc Engelhardt, Dr. Markus Zimmermann für die gemeinsame Praktikumsbetreuung. Trotz zeitintensiven Klausurkorrekturen war immer für gute Stimmung und Essen gesorgt.

Team-MKK4 (neu und alt). Danke für eine gute und unkomplizierte Zusammenarbeit, insbesondere **Dr. Bent Pfaffenrot** und **Dr. Philip Klövekorn**, die mich die meiste Zeit meiner Promotion begleitet haben. Danke auch an MKK4-Frischling Pascal Sander.

Nordlabor (neu und alt). Danke an alle meine Labor-Kollege, die mich in den vier Jahren Promotion unterstützt haben. Besonders bedanken möchte ich mich bei meinem Leidensgenossen **Juliander Reiner** für die harmonische Atmosphäre und den ein oder anderen lauten Lacher zwischendurch. **Dr. Jùlia Galvez** und **Dr. Ricardo Serafim**. Muito obrigada pelo tempo junto e sua amizade.

4.Ebene: Dr. Michi Forster, Gregor Schmidberger, Teo Dimitrov, Valle Wydra, Carine Abdelmalek, Vanessa Haller, Peter Weißhaupt, Dr. Florian Mohr und vor allem Flo Wittlinger für die Hilfsstellung bei der Imidazol-Synthese und Philipp Nahidino für die gemeinsame Zeit im Praktikum.

8.Ebene, Stefan Gerstenecker und insbesondere Lisa Haarer und Julia Liang für unsere Girls-Snack-Break pünktlich um halb vier.

Docking Crew, especially **Dr. Tatu Pantsar** for intense guiding in academic writing and **Dr. Thales Kronenberger** for Docking- and Pymol-teaching and many useful private conversations.

der Schreibraum-Besetzung: **Stani Andreev** und **Gernôt Haase** für ihren seelischen Beistand und eine Spur Zynismus beim Schreiben.

allen Arbeitskreis-Mitgliedern, die sich zu gemeinsamen Aktivitäten wie „The Kinases“ oder den Staffelläufen haben überreden lassen.

allen ehemaligen Kolleginnen und Kollegen des AK Laufers.

meiner Familie: Gertraude, Werner und Simon (und Paula), die mich bei Urlaub auf dem Bauernhof stets aus der Akademiker-Blase rausgeholt und mein Durchsetzungsvermögen geschult haben.

Philip, der mich immer wieder mit seinem einzigartigen Humor zum Lachen bringen konnte. Ich bin froh, dass das Schicksal in Tübingen zusammengeführt hat <3.

Abbreviations

(COCl) ₂	Oxalyl chloride	ESI-MS	Electrospray ionization mass spectrometry
5-TAMRA	5-Carboxytetramethylrhodamin	EtOAc	Ethyl acetate
ACN	Acetonitrile	EtOH	Ethanol
AcOH	Acetic acid	FA	Formic acid
AlCl ₃	Aluminium chloride	FAK	Focal adhesion kinase
AMP-PNP	Adenylyl-imidodiphosphate	FDA	Food and Drug Administration
ATF2	Cyclic AMP-dependent transcription factor	FGI	Functional group interconversion
ATP	Adenosine triphosphate	FP	Fluorescence polarization
B ₂ pin ₂	Bis(pinacolato)diboran	FTIR	Fourier-transform infrared spectroscopy
BINAP	2,2'-Bis(diphenylphosphino)-1,1'-binaphthyl	GFP	Fluorescent green protein
Boc	Tert-butyloxycarbonyl	HATU	1-[Bis(dimethylamino)methylene]-1 <i>H</i> -1,2,3-triazolo[4,5- <i>b</i>]pyridinium 3-oxide hexafluorophosphate
Br ₂	Bromine	HBTU	2-(1 <i>H</i> -Benzotriazol-1-yl)-1,1,3,3-tetramethyluronium hexafluorophosphate
BRAF	V-Raf murine sarcoma viral oncogene homolog B1	HCl	Hydrogen chloride
bs	Broad singlet	HMBC	Heteronuclear multiple-bond correlation
Btk	Bruton's tyrosine kinase	HPLC	High performance liquid chromatography
BuOH	Butanol	HRMS	High resolution mass spectrometry
Cbz-Cl	Benzyl chloroformate	HSQC	Heteronuclear single quantum coherence
CDCl ₃	Chloroform	HTS	High throughput screening
CDK2	Cyclin-dependent kinase 2	Hz	Hertz
CLD	Chronic liver disease	IC ₅₀	Half maximal inhibitory concentration
d	Doublet	IR	Infrared
DAD	Diode array detector	J	Indirect dipole-dipole coupling constant
DBU	1,8-Diazabicyclo[5.4.0]undec-7-en	JNKs	c-Jun <i>N</i> -terminal kinases
DCB	Dichlorobenzyl	K ₂ CO ₃	Potassium carbonate
DCC	Disuccinimidyl carbonate	K ₃ PO ₄	Potassium phosphate
DCM	Dichloromethane	KH ₂ PO ₄	Monopotassium phosphate
dd	Doublet of doublet	KHCO ₃	Potassium bicarbonate
ddd	Doublet of doublet of doublets	KOAc	Potassium acetate
DIPEA	<i>N,N</i> -Diisopropylethylamine	LiHMDS	Lithium bis(trimethylsilyl)amide
DMA	Dimethylacetamide	m	Multiplet
DMAP	4-Dimethylaminopyridine	MAPK	Mitogen-activated protein kinase
DMDS	Dimethyl disulfide	<i>m</i> CPBA	<i>M</i> -chloroperoxybenzoic acid
DMF	Dimethylformamide	MD	Molecular dynamics
DMSO	Dimethyl sulfoxide	MeOD	Methanol- <i>d</i> ₄
DNA	Deoxyribonucleic acid	MeOH	Methanol
dq	Doublet of quartets		
ELK1	ETS domain-containing protein		

ABBREVIATIONS

MHz	Megahertz	ppm	Parts per million
MKK4	Mitogen-activated protein kinase kinase 4	q	Quartet
MKK7	Mitogen-activated protein kinase kinase 7	RNA	Ribonucleic acid
mRNA	Messenger ribonucleic acid	RP	Reversed-phase
MTBE	Methyl <i>tert</i> -butyl ether	RT	Room temperature
MW	Microwave	r_x	Nuclear distance
NaH	Sodium hydride	s	Singlet
NaNO ₂	Sodium nitrite	S	Spin quantum number
NaOH	Sodium hydroxid	S ₀	Ground state
NaOMe	Sodium methoxide	S ₁	Excited state
NaOtBu	Sodium <i>tert</i> -butoxide	SEM	2-Trimethylsilylethoxymethyl
NBS	<i>N</i> -bromosuccinimide	shRNA	Small hairpin ribonucleic acid
nBuLi	<i>N</i> -butyllithium	S _N AR	Nucleophilic aromatic substitution
NF-κB	Nuclear factor κB	SO ₂ Cl ₂	Sulfury chloride
NH ₃	Ammonia	SOCI ₂	Thionyl chloride
NHS	<i>N</i> -Hydroxysuccinimide	STD	Saturation-transfer-difference
nm	Nanometer	t	Triplet
NMR	Nuclear magnetic resonance	TBTU	2-(1 <i>H</i> -Benzotriazole-1-yl)-1,1,3,3-tetramethylammonium tetrafluoroborate
NP	Normal-phase	td	Triplet of doublets
ns	Nanoseconds	TFA	Trifluoroacetic acid
<i>o</i> -xylol	<i>Ortho</i> -xylol	THF	Tetrahydrofuran
PARP-1	Poly(ADP-ribose)-polymerase 1	THIF	7,3,4-Trihydroxyisoflavone
PCy ₃	Tricyclohexylphosphine	TLC-MS	Thin-layer chromatography mass spectrometry
Pd(dppf)Cl ₂	[1,1'-Bis(diphenylphosphino)ferrocene]palladium(II) dichloride	TNF	Tumor necrosis factor
Pd(OAc) ₂	Palladium(II)-acetate	UV	Ultraviolet
Pd(PPh ₃) ₂ Cl ₂	Bis(triphenylphosphine)palladium(II) dichloride	VEGFR	Vascular endothelial growth factor receptor
Pd(PPh ₃) ₄	Tetrakis(triphenylphosphin)palladium(0)	XPhos Pd G4	9-{Dicyclohexyl[2',4',6'-tris(propan-2-yl)-[1,1'-biphenyl]-2-yl]-1 <i>a</i> -α-carboline 9 <i>H</i> -Pyrido[2,3- <i>b</i>]indole
Pd ₂ (dba) ₃	Tris(dibenzylideneacetone)dipalladium(0)	θ	Rotational correlation time
PDB	Protein Data Bank	λ	Wavelength
PE	Petrolether	ν	Frequency
POC	Percentage of control	τ	Fluorescent lifetime
POCl ₃	Phosphoryl chloride	δ	Chemical shift
PPh ₃	Triphenylphosphine		

Abstract

The number of patients suffering from chronic liver diseases caused by Hepatitis B and C or an unhealthy lifestyle has constantly increased over the last decades. Although the liver has a unique capacity to regenerate completely after injury, this is only valid up to a certain extend of liver tissue damage. MKK4 was identified as the key mediator for liver regeneration in a functional genetic approach. Silencing of MKK4 with shRNA *in vivo* was in direct correlation with increased liver regeneration capacity. Since it was implied that vemurafenib has off-target effects on MKK4 and later its scaffold was successfully used for development of inhibitors, MKK4 is a druggable target. However, up to date only a few MKK4 inhibitors have been published. This gap can be closed with identifying new small molecule inhibitors of MKK4 by developing a fluorescent probe to be utilized in a fluorescence polarization high-throughput screening.

Two orthogonal synthetic strategies were pursued using vemurafenib-derived azaindole and a structural related α -carboline as scaffolds to attach the fluorophore 5-TAMRA by means of a linker system. Linker length, position and connection to the pharmacophore were adjusted with a synthetic, iterative approach to both scaffolds. Compound **55**, containing a carboline scaffold and a linker length of four carbons, exceeded as the compound with the highest binding affinity to MKK4 with a POC of 1.3 (conc. 100 nM) and an IC₅₀-value of 1.03 μ M. This fluorescent probe was capable to confirm previously reported MKK4 inhibitors in a competition assay fitting to its prior determined binding affinities. Finally, the developed probe was able to identify new scaffolds in a HT screen from a compound library with more than 7000 compounds which can be utilized to develop new selective inhibitors. These hits were confirmed in a binding affinity assay and evaluated regarding chemical tractability, drug likeness and stability. Two striking hits, containing an aminopyrimidine and imidazole core, were selected for further investigations. For both actives straightforward synthesis has been established, which enabled fast early-stage structure-activity-relationship assessment. From aminopyrimidine-based compounds new knowledge of the SAR, especially regarding the hydrophobic back pocket, could be generated. The optimization of the second imidazole-based hit provided compound **142**

with a high affinity to MKK4 (POC of 26) which is comparable to vemurafenib (**1**, POC = 14) and can be seen as new class of MKK4 inhibitors, even if this compound class is well known for kinase inhibition. These structural results pave the way for further Hit-to-lead modification to inhibit MKK4.

Zusammenfassung

In den letzten Jahren ist die Anzahl an Patienten, welche unter chronischen Lebererkrankungen leiden, konstant gestiegen. Obwohl die Leber das einzige Organ darstellt, welches sich nach Gewebeschädigung in Kürze komplett regenerieren kann, ist dies nur bis zu einem bestimmten Anteil an verbleibendem gesundem Lebergewebe möglich. MKK4 wurde dabei als Schlüsselregulator der Leberregeneration identifiziert. Unter Laborbedingungen konnte eine direkte Korrelation zwischen reduzierter Protein-Expression von MKK4 mit shRNA und einer erhöhten Regenerationsfähigkeit der Hepatozyten gezeigt werden. Zeitgleich wurde mit dem BRAF-Inhibitor Vemurafenib ein Startpunkt gefunden, welcher MKK4 als off-target bindet. Bis heute gibt es jedoch nur wenige veröffentlichte Inhibitoren mit guter Selektivität für MKK4, was den dringenden Bedarf an neuen Strukturklassen zu Adressierung von MKK4 unterstreicht. Diese Lücke kann mit der Identifizierung neuer Inhibitoren für MKK4 in einem Fluoreszenzpolarisations-basierten Hochdurchsatz-Screening geschlossen werden. Dafür bedarf es der Entwicklung einer fluoreszenten Sonde zur Adressierung von MKK4 in einem entsprechenden Assay.

Diesbezüglich wurden zwei parallele Synthesestrategien verfolgt, welche auf strukturell verwandten Grundgerüsten des Vemurafenibs, Azaindol und Carbolin, basieren. Mit Hilfe von Linker-Systemen, welche sich in Länge, Basis und Positionierung des Fluoreszenzfarbstoffes am Grundgerüst unterscheiden, konnte die Carbolin-basierte Verbindung **55** entwickelt werden, welche eine hohe Affinität (POC = 1.3, Konz. 100 nM) und Inhibition ($IC_{50} = 1.03 \mu\text{M}$) zu MKK4 zeigte. Mit Hilfe dieser fluoreszenten Sonde konnten bekannte MKK4 Inhibitoren in ihrer Potenz bestätigt werden. Außerdem war diese Verbindung fähig neue Strukturklassen in einem HT-screening zu finden, welche zur Weiterentwicklung neuer Inhibitoren geeignet sind. Die gefundenen Hits wurden in einem zweiten Assay bestätigt und anhand ihrer synthetischen Zugänglichkeit, Struktur und Stabilität bewertet. Diese zwei Hits, welche ein Aminopyrimidin- und ein Imidazol-Grundgerüst enthalten, wurden für weitere Untersuchungen ausgewählt. Für beide Verbindungen konnte eine zugängliche Synthese etabliert werden, die in kurzer Zeit eine

hohe Anzahl an Derivaten zuließ, welche Aussagen über den Bindemodus der Kinase erlaubten. Besonders Verbindung **142** hob sich durch eine hohe Bindeaffinität zu MKK4 (POC = 26) hervor, welche sich im gleichen Bereich wie Vemurafenib bewegt und ist trotz bekanntem Imidazol Strukturmotiv eine neue Substanzklasse zur Inhibition von MKK4. Diese Ergebnisse ebener den Weg für die Entwicklung neuer Leitstrukturen zur Adressierung von MKK4.

Table of contents

Preface	I
Abbreviations	III
Abstract	V
Zusammenfassung	VII
1. Introduction	1
1.1. Biological target.....	1
1.1.1. Liver as therapeutic target	1
1.1.2. Drug target MKK4.....	2
1.1.3. Target identification and validation: Hepatocyte proliferation by MKK4 silencing	5
1.2. Strategies for new lead compounds	6
1.2.1. Natural sources for MKK4 inhibitors	6
1.2.2. Improving existing drugs: New drugs from old drugs.....	7
1.2.3. High-throughput screening	9
1.3. Basics and applications of Fluorescence polarization (FP)	9
1.3.1. Fundamentals of fluorescence spectroscopy.....	9
1.3.2. Chromophores and fluorescent dyes	12
1.3.3. Visible-absorbing dyes	13
1.4. Fluorescence polarization assay	14
1.4.1. Polarised light and anisotropy.....	14
1.4.2. Fluorescence polarization.....	15
1.4.3. Considerations in FP-assay design	16
1.4.4. Applications of fluorescent probes	17
2. Objectives of the thesis	19
3. Chemistry	21

TABLE OF CONTENTS

3.1.	Molecular design.....	21
3.1.1.	Structural Information about vemurafenib – MKK4	21
3.2.	Azaindole -Series	22
3.2.1.	Retrosynthesis of vemurafenib (1)	22
3.2.2.	Azaindole key intermediate.....	23
3.3.	α -Carboline-Series	24
3.3.1.	Carboline key intermediate.....	24
3.4.	Spacer and linkage design.....	27
3.5.	Connection of key intermediates 6 and 10 to spacer	32
3.6.	Fluorescent molecules.....	34
3.7.	Results from the fluorescence polarization screen	42
3.8.	Aminopyrimidine series	42
3.8.1.	Representative NMR discussion of compound 91	48
3.9.	Thioimidazole series.....	49
3.9.1.	Introduction of sulfur substituents	49
3.9.2.	Introduction of ring-systems in 5-position of imidazole.....	56
4.	Results and discussion	62
4.1.	Biological testing.....	62
4.1.1.	Commercial KINOMEscan® binding assay from DiscoverX ^[104]	62
4.2.	Chemical probe for finding new MKK4 scaffolds	63
4.2.1.	Comparison of azaindole Boc-protected precursors.....	64
4.2.2.	Incorporation of 5-TAMRA for azaindoles	65
4.2.3.	5-TAMRA tagged linkers systems.....	66
4.2.4.	Incorporation of 5-TAMRA on the sulfonamide side of 1.....	66
4.2.5.	Comparison of carboline Boc-protected precursors.....	67
4.2.6.	Incorporation of 5-TAMRA for carbolines	68

TABLE OF CONTENTS

4.2.7.	Influence on binding affinity of the linker core	70
4.2.8.	Further investigations of 47 and 55	70
4.2.9.	Comparison of fluorescently tagged scaffolds azaindole and carboline.....	72
4.3.	Competition assay with known MKK4-inhibitors.....	74
4.3.1.	Fluorescence polarization assay.....	74
4.4.	Hit identification – High-throughput screen.....	76
4.4.1.	Validation and performance of the HT screen	76
4.5.	Investigation of aminopyrimidine-based 72.....	78
4.6.	Investigation of imidazole-based 73	83
5.	Summary of the results	89
6.	Experimental methods	92
6.1.	Materials and methods	92
6.2.	General procedures	93
6.3.	Experimental procedures.....	96
6.3.1.	Azaindole derivatives	96
6.3.2.	Carboline synthesis.....	98
6.3.3.	Linker synthesis.....	102
6.3.4.	Linker implementation.....	107
6.3.5.	5-TAMRA implementation	121
6.3.6.	Sulfonamide linker.....	135
6.3.7.	Aminopyrimidine series	142
6.3.8.	Thioimidazole series.....	167
7.	Appendix.....	178
8.	Bibliography	184

1. Introduction

Modern rational drug discovery and development can be subdivided into four main phases: Target selection, probe selection and screening of chemical libraries, lead selection and lead optimization. According to a definition provided by Arrowsmith (2015), a chemical probe is a "... small-molecule modulator of a protein's function that allows the user to ask mechanistic and phenotypic questions about its molecular target in biochemical, cell-based or animal studies".^[1] This study followed the conceptual framework of drug discovery and focused on developing a probe for hit identification. Target selection and probe development were the first two steps approaching drug discovery. Important information about biochemical and biophysical background of these two steps were given in the following introducing part of this study.

1.1. Biological target

1.1.1. Liver as therapeutic target

Chronic liver disease (CLD) has risen to become one of the leading causes of death all over the world. Although there is a large-scale vaccination in progress for viral infections causing CLD such as Hepatitis B, the number of patients constantly increases due to metabolic syndrome and alcohol abuse. ^[2]

The liver is the largest internal gland in the human body and is acting as the key mediator in homeostasis of glycogenolysis and lipid metabolism. In protein processing it influences the production of important carrier proteins such as albumin or transferrin. Additionally, the liver is involved in biotransformation of lipophilic xenobiotics such as nutrients, drugs, and alcohol by utilizing cytochrome P450 enzymes. The most fascinating fact about the liver is, that it can regenerate damaged tissue endogenously. This ability for tissue regeneration is only known for some metazoan such as axolotl.^{[3][4]}

The cellular mechanism of endogenous regeneration has been studied intensively over the past decades. Models to investigate this ability start from partial hepatectomy or chemical-induced hepatotoxicity, such as the treatment with carbon tetrachloride. Subsequently, the regeneration process starts with an increased liver cell size followed by a rising cell number

until retaining complete tissue restoration. The initiation phase is related to expression of cytokines and growth factors. In particular, tumor necrosis factor α (TNF) is involved in activating nuclear factor- κ B (NF- κ B) signaling pathway and stimulating stress activated protein kinases, including MKK4, in hepatocytes. The induced kinase cascade activity results in a transcription of genes such as cyclin-dependent kinase 2 (*CDK2*) initiating hepatocyte proliferation.^[5] With this information, kinase cascade activity can be utilized to identify latent targets for induced liver regeneration.

1.1.2. Drug target MKK4

In order to understand the response from a drug-target interaction the molecular structure of the drug binding site needs to be examined. Functional macromolecular structures can be receptors, ion channels or enzymes such as protein kinases. Their response is usually initiated by a complex formation with a ligand further processing biochemical and physiological functions. Regarding protein kinases, complex cascades involving up- and downstream proteins are modulated by drugs including alterations in the physiological functions of kinases.

As all protein kinases share highly conserved structural organization, the architecture of mitogen-activated protein kinase kinase 4 (MKK4) can serve as an illustration for explaining the key domains of kinases. Figure 1 depicts the crystal structure of non-phosphorylated MKK4 (PDB ID: 3ALO) in complex with adenylyl-imidodiphosphate (AMP-PNP).^[6]

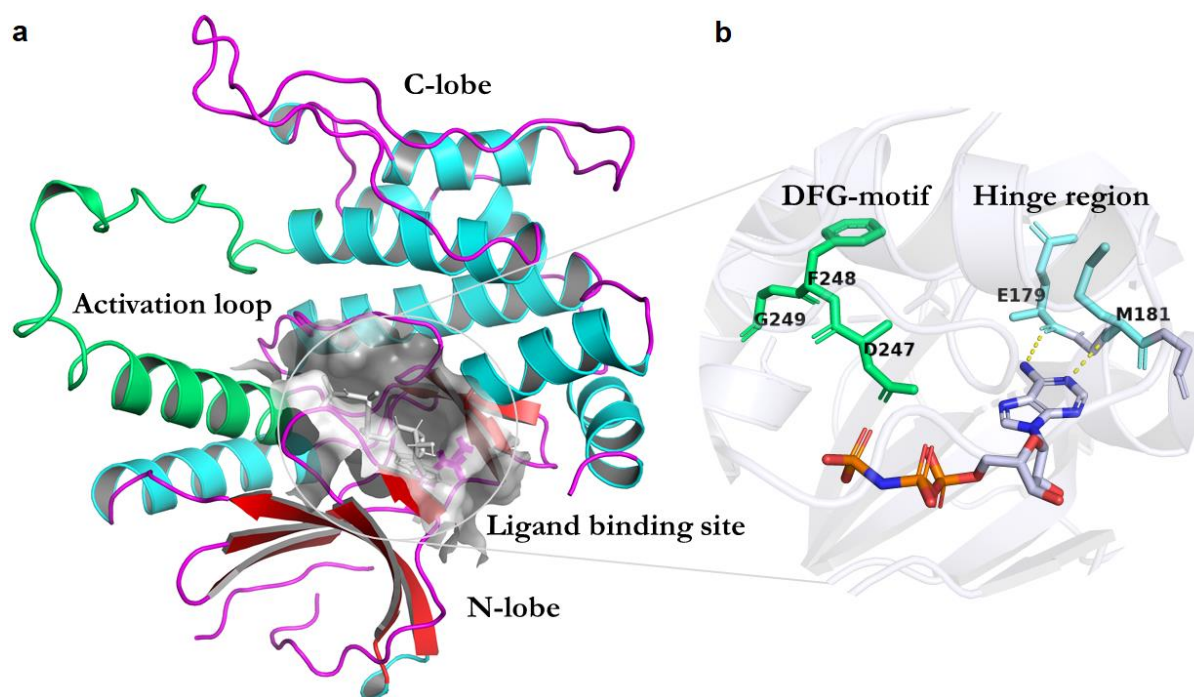


Figure 1 Crystal structure of non-phosphorylated MKK4 kinase domain complexed with AMP-PNP (PDB ID: 3ALO) (a) Cartoon representation of the tertiary structure of MKK4 highlighting the N- and C-lobes, the open formation of the activation loop (green) and binding site as surface (grey) occupied by AMP-PNP (sticks). α -Helices are coloured in cyan, β -sheets in red and loops in pink; (b) Cut-out of the ligand binding site occupied by AMP-PNP, DFG-motif (green) and hinge region (blue) are highlighted. Hydrogen bonds are shown as dashed lines.

The small N-lobe, consisting of five β -sheets, is connected to the large dominant α -helical C-lobe by a small cleft. In between these lobes the cleft or hinge region can bind ATP. The hinge is connected to the activation loop, which is the most disordered part in the crystal structure. More than 30 amino acids are not resolved in the MKK4/AMP-PNP-complex, which demonstrates the flexibility of this segment. The activation loop can be either open or closed, depending on the activation status of the kinase. If the loop is closed, the access to the binding site is occluded. In the large C-lobe close to the binding site, the DFG(Asp-Gly-Phe)-motif is located, which contributes to ATP-binding and regulates catalysis. Figure 1 b shows a magnified view in the binding site with the ligand AMP-PNP bond to the hinge region and depicts the adjacent residues from the DFG-motif.^[7]

Evaluation of available crystal structures of protein-ligand complexes is one method which helps to understand binding modes of ligands to their targets. For MKK4 inhibition the binding mode is still poorly known. No study to date has published a crystal structure of

MKK4 in complex with inhibitors. Besides two crystal structures of MKK4 bound to AMP-PNP (PDB IDs: 3vut; 3aln) there is an additional one published as apo structure.^[8,9]

Most of the reported kinase inhibitors compete with adenosine triphosphate (ATP), which provides the phosphate group, and blocks the binding pocket. Phosphorylation causes the transfer of the γ -phosphate of ATP to hydroxyl groups of several substrates. This kind of post-translational modification is involved in cellular and extracellular processes and can be displayed as signal transduction pathway.^[10]

The kinase family can be classified based on its phosphorylation-acceptor amino acid. The two most important classes are Ser/Thr- and Tyr-specific kinases. These classes create a phosphate ester with their specific alcohol group. MKK4 is a dual specific protein kinase, which is either Tyr or Ser/Thr-specific, anchored in two stress-activated signaling pathways, p38 MAPK and c-Jun *N*-terminal kinases (JNKs). Caused by cellular stress and inflammatory cytokines, the cell responds with phosphorylation of MKK4. MKK4 is then able to phosphorylate its downstream targets JNK and p38. Besides MKK4, mitogen-activated protein kinase kinase 7 (MKK7) can activate JNK simultaneously and favours the Thr residue for phosphorylation. MKK4 preferentially phosphorylates the Tyr residue of JNK. Both contribute to a maximum activation of JNK which causes the phosphorylation of transcription factors such as cyclic AMP-dependent transcription factor 2 (ATF2) and ETS domain-containing protein 1 (ELK1).^[11]

There are two different binding modes of inhibitor-kinase complexes which allow a distinction. The first one is represented by non-covalent inhibitors. This class can be divided into subclasses depending on the position of the activation loop and the DFG-motif. For type-1 inhibition the activation loop is open and permits access to the binding site. Simultaneously the DGF-motif is occupying a hydrophobic pocket close to the hinge region (“DFG-in”). In consequence the type-1 inhibitor has access to the ATP site. Type-2 inhibitors bind to the hydrophobic back pocket and the ATP site. Due to the movement of the activation loop to a “closed” confirmation, the hydrophobic back pocket is released by an accompanied switch to DFG-out motif. Type-3 inhibition is described by allosteric binding to clefts outside the binding site and no interaction to the hinge region.^[12] Recently

there have been published new types of kinase inhibitors in between type-1 and type-2 termed as type-1^{1/2}.^[13]

The second class of kinase inhibitors binds irreversible to the protein. These covalent inhibitors usually incorporate a chemical module or warhead, which can bind near the binding site. These modules utilize amino acids such as Lys or Cys for covalent binding and are termed as type-4 inhibitors.^[14]

1.1.3. Target identification and validation: Hepatocyte proliferation by MKK4 silencing

For target validation it needs to be demonstrated that the aimed target is associated with a therapeutic benefit. Model system using clinically relevant conditions can help to proof that modulation of the identified target has the desired therapeutic effect. A major tool for a proof of principle is small interfering RNA technique such as small hairpin RNA (shRNA). shRNA is an artificial molecule used to silence target gene expression via RNA interference. In these experiments delivering shRNA to the cytoplasm of certain cells results in mRNA destruction and subsequently to a loss of specific genetic information.^[15,16]

In 2013 Wuestefeld *et al.* used an shRNA experiment to identify MKK4 as a regulator of liver regeneration in hepatocytes. In a mouse model silencing of MKK4 with shRNA resulted in an increased liver tissue regeneration and cell cycle induction.^[16]

Regarding the signaling pathway, silencing of MKK4 with shRNA had an extensive impact on molecular mechanisms. Figure 2 illustrates the differences between a physiological signaling pathway (Figure 2 a) and the consequences of silencing MKK4 (Figure 2 b).^[17]

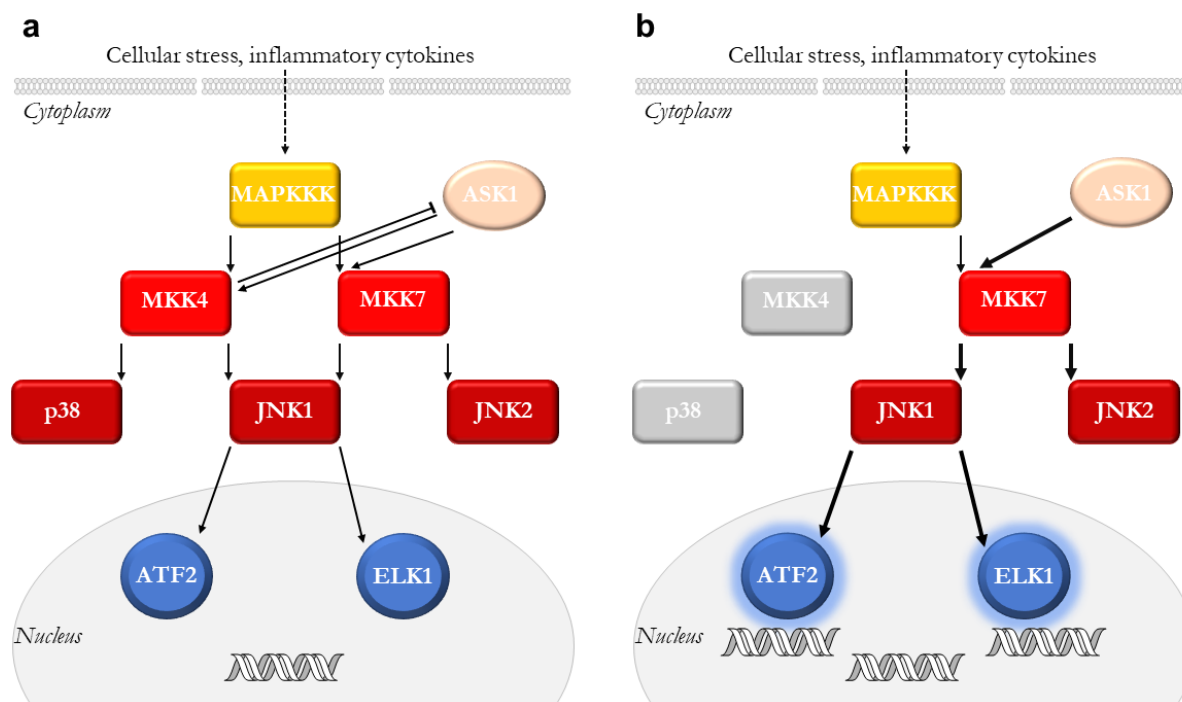


Figure 2 Signaling pathways of MKK4 (a) Stress-induced JNK pathway; (b) MKK4 silencing causing changes in signal transduction. Figure modified according to Wuestefeld *et al.*^[16]

The knockdown of MKK4 resulted in a strong induction of ASK1 activity and subsequently in downstream activation of JNK1. Meanwhile the activation of p38 MAP kinase decreased. Enhanced activation of JNK1, controlling transcription factors ATF2 and ELK1, resulted in an increased cell differentiation rate and hepatocyte proliferation.

This experiment is decisive for validation of MKK4 as a molecular target. Silencing MKK4 *in vivo* with shRNA technique is in direct correlation with increased regeneration capacity of hepatocytes.^[16]

1.2. Strategies for new lead compounds

1.2.1. Natural sources for MKK4 inhibitors

One strategy in searching new lead compounds for disease related targets is the investigation of natural derived compounds. For MKK4 three naturally occurring small molecules, depicted in Figure 3, show *in vivo* inhibition.

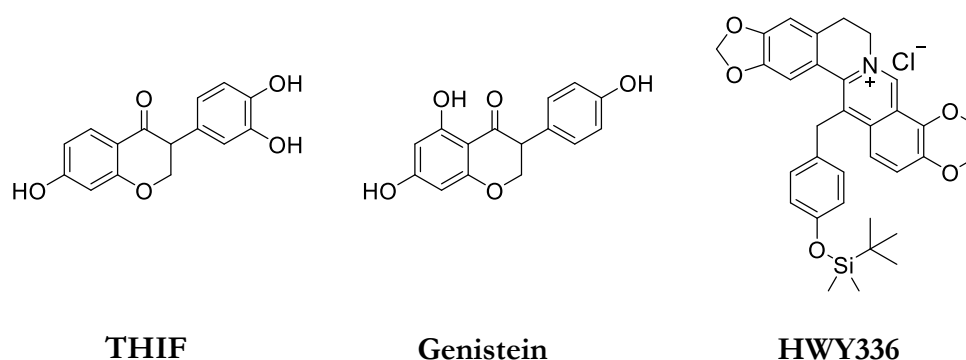


Figure 3 Structures of naturally occurring MKK4 inhibitors THIF, Genistein and HWY336.

7,3,4-Trihydroxyisoflavone (THIF) is a metabolite of an isoflavone derived from soybeans or sprouts. In 2011 THIF was found to inhibit NF- κ B transcription activity in mice skin epidermal cells and could potentially be used for skin cancer chemoprevention. In particular Lee *et al.* identified THIF as an MKK4 inhibitor.^[18] A second soybean derived isoflavone is genistein, which is reported as metalloproteinase-2 inhibitor and silencer of p38 MAP kinase. It was considered to be a promising treatment for metastatic prostate cancer, but lacked bioavailability.^[19]

A few years later Kim *et al.* investigated the impact of protoberberine-alkaloid derivative HWY336 on the MAPK cascades in mammalian cells and revealed the interaction of HWY336 with the activation loop close to the binding pocket. This caused a non-ATP competitive inhibition of MKK4 which prevented substrate binding due to structural rearrangements.^[20]

1.2.2. Improving existing drugs: New drugs from old drugs

Designing an inhibitor targeting a certain kinase is a challenging task. Non-specific binding caused by unselective addressing of a target can induce off-target effects. Due to the structural similarities of kinases many small molecule inhibitors are promiscuous.

V-Raf murine sarcoma viral oncogene homolog B1 (BRAF) kinase was published to be selectively addressed by vemurafenib in the cutaneous squamous cell carcinoma therapy in 2012.^[21] Surprisingly, Vin *et al.* discovered in 2013 novel side-effects of vemurafenib on JNK pathway, particular by inhibition of MKK4.^[22]

In previous work from our group, Kloevekorn *et al.* benefited from these effects and used vemurafenib as a template for the development of novel selective MKK4 inhibitors.^[23] Additionally, vemurafenib-related tricycles (carbolines) have been published as MKK4 inhibitors.^[24] These α -carbolines are reported to inhibit MKK4 selectively and were previously published by Lowinger *et al.* in 2003.^[25] Figure 4 shows the structures of vemurafenib (**1**) and the related tricycle α -carboline.

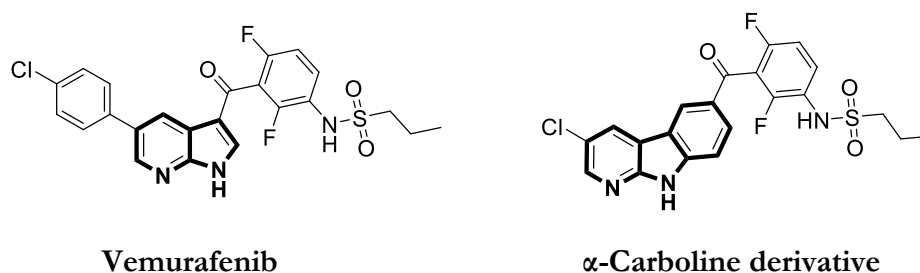


Figure 4 Structures of published MKK4 inhibitors. Azaindole and carboline scaffolds are highlighted.

In 2017 Deibler *et al.* investigated the binding mode of former FDA-approved renal cell carcinoma multi-kinase inhibitor Pazopanib to MKK4 by performing docking experiments and saturation-transfer-difference (STD)-NMR-experiments. Their study gives more information about the SAR of MKK4 inhibitors and the distinction to members of the MKK-family such as MKK7.^[26]

In summary MKK4 is a promising and valid mechanistic and druggable target in acute and chronic liver failure as demonstrated by an RNA interference *in vivo* model. Exploiting the vemurafenib scaffold for lead generation brought an improved glimpse of the pharmacophore of this structural class but left limited space for further development.^[27]

Therefore, screening compound libraries as a third strategy of drug discovery is justified and can provide more chemical entities for further investigation to discover next level MKK4 inhibitors. Although several MKK4 inhibitors have been reported, none of them has reached clinical stages. Establishing new molecular scaffolds could be valuable in the treatment of chronic liver diseases for addressing unmet medical needs.

1.2.3. High-throughput screening

An automated method for identifying new leads from compound libraries is high-throughput screening (HTS). One of the first kinase inhibitors on the market, sunitinib, was found in an HTS targeting tumor angiogenesis by inhibiting the vascular endothelial growth factor receptor (VEGFR) kinase activity.^[28] Usually the data from HTS is analysed by a change of a fluorescent signal. It is advantageous that this signal is not dependent on the intensity of the emitted light or on the fluorophore concentration. A specific application which uses fluorescence is fluorescence polarization (FP). FP-HTS is a non-radioactive method with high sensitivity and is compatible to automated read-outs.^[29] The following part of the introduction will be dedicated to the principle and application of FP screenings and their physical basics.

1.3. Basics and applications of Fluorescence polarization (FP)

The technique of FP can be used to interrogate the change of molecular weight of a fluorescent probe binding to a protein in solution by emitting light. This gives insight in biological processes such as molecular interaction or enzymatic activity. In combination with automatic read-out assays this enables rapid measurement of a large number of samples, which is compelling for screening compound libraries.^[30]

1.3.1. Fundamentals of fluorescence spectroscopy

Transitions of electronic states in molecules can be divided in radiative and non-radiative processes (Figure 5). Radiative transition occurs after a molecule absorbs a photon moving to a higher electronic state (S_1). In an excited vibrational state, it can move back to the ground state of the excited state by non-radiative transitions involving vibrational relaxation with dissipation of energy from the molecule to its surroundings. To move from the excited state S_1 to the ground state S_0 , the surrounding environment of the molecule is not capable to absorb excess energy of the molecule. The remaining energy is then emitted through spontaneous emission (fluorescence) in a vertical transition back to the ground state of the molecule.^[31]

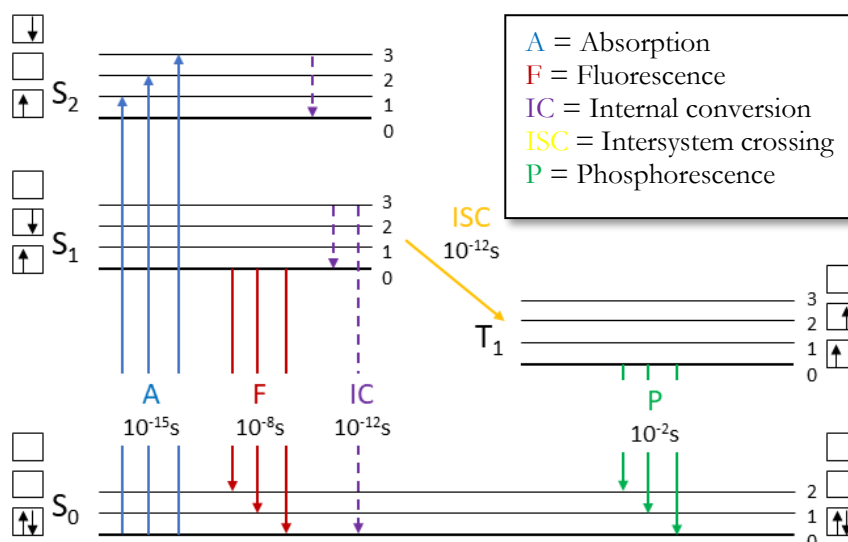


Figure 5 Jablonski diagram and timescales of the respective processes.

Processes occurring after absorption of photons are illustrated in a Jablonski diagram (Figure 5). After absorption of photons, the molecule transits from the ground state S_0 to various vibrational states of excited states S_1 and S_2 . This usually happens fast in about 10^{-15} seconds. Then the molecule moves from higher vibrational states to the vibrational ground state of S_1 under relaxation. This process is called internal conversion and happens prior to emission in 10^{-12} seconds. Initiated by the emission of fluorescence the thermally equilibrated excited state S_1 photons descend to vibrational levels of S_0 in approximately 10^{-8} seconds. Besides internal conversion and fluorescence, molecules resting in S_1 can undergo intersystem crossing in a spin conversion from singlet to triplet state. A triplet state is a quantum mechanical description of two unpaired spins with a spin quantum number of $S = 1$. Molecules in an excited triplet state are trapped because it is forbidden to directly move back to the singlet ground state, which implies that the transition back to S_0 is slow ($\geq 10^{-2}$ seconds). This transition is termed phosphorescence and shifted to lower energy or longer wavelengths than fluorescence.^[32]

Electronic transitions proceed in a time scale whereby nuclear motion of the ground and excited state can be neglected. In the quantum mechanical approach, the dynamic status of a molecule can be described as a wavefunction. The chance of transition from the ground to the excited state is more likely for the maximum compliance of two wavefunctions. The theoretical basis for this principle is the Born-Oppenheimer-approximation which allows

the separation from movements of nuclei and electrons in dynamic molecular systems, due to their difference in mass.^[33]

Figure 6 a illustrates the quantum mechanical description for vibrational transitions from ground state S_0 to excited state S_1 , termed as Franck-Condon principle. Both states have several vibrational levels ν . The excited state has a greater nuclear distance than the ground state and is referred to as r_x . The probability for transitions from the ground to the excited state is proportional to the square of the overlap of the vibrational wavefunctions and proceeds in a vertical way. Usually there are several vibrational levels in the excited states with an overlapping vibrational state, thus more than one transition from ground to excited state can occur.^[34]

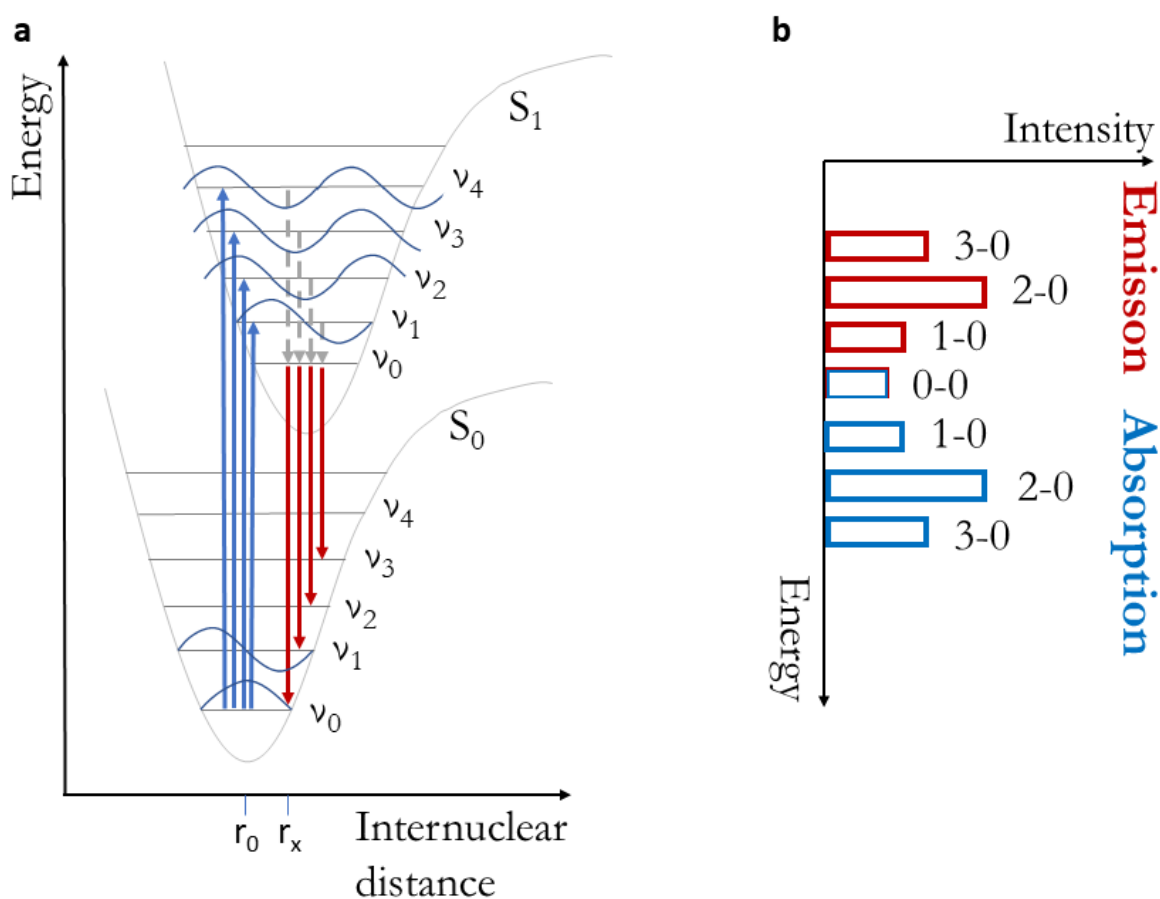


Figure 6 Energy diagram of the Franck-Condon principle (a) Transitions from ground state S_0 to excited state S_1 (blue) and from excited to ground state (red). Non-radiative processes are shown as grey arrows. (b) Absorption and emission spectrum for the corresponding transitions indicated as numbers.

Figure 6 b shows the influence of the previously described principle on the representation of the energy diagram of absorption and fluorescence. Absorptions from ground state to vibrational levels of the excited state have higher energies and shorter wavelengths. Losing energy to the surroundings of the molecule, emission transitions occur from the lowest vibrational state to various vibrational states of the ground state. This phenomenon of fluorescence occurring at longer wavelengths than emission is called Stokes shift. The loss of energy can be traced back to effects such as energy transfer to solvent molecules by quenching, excited-state reactions, and complex formations.^[35]

1.3.2. Chromophores and fluorescent dyes

Many simple molecules containing double- or triple-bonds or aromatic systems can be excited with comparatively low amounts of energy. The most important electric transition is the π - π^* transition, which can be detected in the visible spectrum. Substituents attached to aromatic systems with I- or M-effects can extensively alter electronic transitions. In conjugated π -systems for instance, delocalization can lower the orbital energies of π^* resulting in a shift of the absorption band to longer wavelengths.^[36]

π - π^* Transitions are also the reason for chromophoric properties of certain amino acids. For instance, Trp, Tyr and Phe contribute to fluorescent effects of proteins and belong to the intrinsic fluorophores. Intrinsic fluorophores contain a structure which can absorb and emit light.^[37] Figure 7 a highlights the structure of the mentioned amino acids with its spectroscopic data.

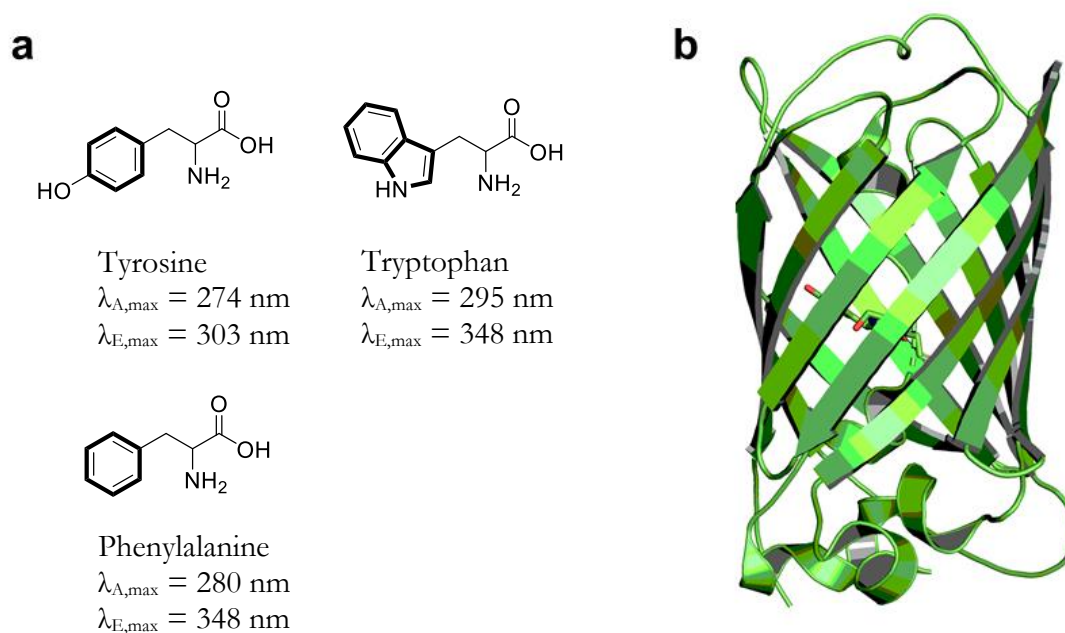


Figure 7 Structures of intrinsic fluorophores: (a) Amino acids and their absorption and emission maxima.^[38] Conjugating π -systems are highlighted. (b) Cartoon representation of green fluorescent protein (GFP) (PDB ID: 2QLE^[39]).

In contrast, extrinsic fluorophores are dyes which can be used for covalent binding or accumulation to non-fluorescent molecules.^[38] Figure 7 b illustrates the structure of the green fluorescent protein (GFP). GFP was found in the jellyfish *Aequorea Victoria* and emits green light when it is exposed to blue or purple light.^[40] Besides GFP there are several extrinsic fluorescent dyes which can be used for labeling of proteins or small molecules.

1.3.3. Visible-absorbing dyes

The most important visible fluorophores are fluorescein and rhodamine analogues.^[41] The chemical structures of fluorescein and 5-TAMRA are shown in Figure 8. Fluorescein is a green, fluorescent dye used in immunoassays and high-throughput screenings. Notably its spectral properties, such as quantum yield and fluorescent lifetime, are highly dependent on the pH resulting from its different prototropic forms.^[42]

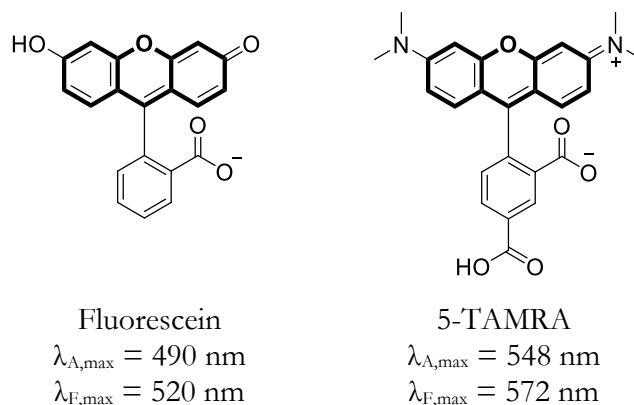


Figure 8 Fluorophores for covalent labeling of biomolecules and their absorption and emission maxima. Fluorescein is depicted as its monoanion form. Maxima are given at alkaline pH.^[43] 5-TAMRA is shown as its zwitterionic form^[44]. Xanthene moiety is highlighted.

A second example is 5-carboxytetramethylrhodamine (5-TAMRA), a member of the rhodamine family. The properties of these xanthene derivatives depend on the substitution pattern of the tricyclic system and therefore are easily adjustable to the aimed application.^[44] For instance, 5-TAMRA bears two dimethylamino substituents which result in a bathochromic emission compared to its parent structure ($\lambda_{F,max} = 572 \text{ nm}$). The fluorescent lifetime of 5-TAMRA is approximately 2.5 ns.^[45] This property will be important in the next chapter.

1.4. Fluorescence polarization assay

1.4.1. Polarised light and anisotropy

In the previous chapter the fundamentals of fluorescence and properties of fluorescent dyes have been introduced. In this section basics about polarized light anisotropy will be presented to explain the principles of fluorescence polarization.

Light in a quantum mechanical interpretation is an electromagnetic wave described with a specific wavelength λ and frequency ν . It bears magnetic and electric properties. The electronic wave component is cosine-shaped and has an oscillating magnetic field perpendicular to its dispersion direction. The visible spectrum of light ranges between wavelengths of 380 and 780 nm. Besides this high-energetic γ -radiation and low-frequency radio waves complete the range of the light spectrum. The individual sectors are separated

by their frequency and energy. Usually light is spread out undirected but can be directed or linearly polarized with special polarization filters.^[46]

The term of anisotropy refers to the directional dependency of molecule properties. Photoselective excitation of fluorophores by polarized light depends on anisotropy. In an ideal case, maximum excitation of the fluorophore takes place when its transition dipole moment is parallel to the electric field vector of polarized light. Subsequently the resulting emission of light is pointing in the same direction. The decisive factor for the magnitude of fluorescence anisotropy is the rotational angle between both transition states. One important factor which lowers the anisotropy is the rotational movement of the molecule in the timescale between emission and excitation termed fluorescent lifetime (τ). This movement is highly dependent on the size of the fluorescent molecule. Small molecules rotate fast, while huge proteins move relatively slow.^[43]

This phenomenon can be used for detecting changes in volume of fluorescently tagged molecules, especially for binding of small molecules to huge proteins and is called fluorescence polarization. In the next chapter the applications of fluorescence polarization are described in detail.

1.4.2. Fluorescence polarization

The time in which the rotational diffusion of fluorophores occurs is defined as rotational correlation time θ . If this time is significantly faster than the fluorescent lifetime τ the emission of the molecule is mostly depolarized. On the other hand, if the rotational diffusion is insignificant, for instance for huge protein-dye complexes, the emission is strongly polarized. Equation 1 shows the dependency of the rotational movement on the volume of the molecule.^[47]

$$\theta = \frac{\eta V}{RT}$$

Equation 1 Dependency of the rotational correlation time θ to solvent viscosity η , volume of the molecule V , gas constant R and temperature T .

Figure 9 a shows the movement occurring after polarized light excitation of a small molecule in τ . An unbound fluorescently tagged molecule containing a structure capable to

interact with the binding site of a protein, rotates fast in the fluorescent lifetime τ due to its small size. As a result, the emission of this molecule is depolarized.^[48]

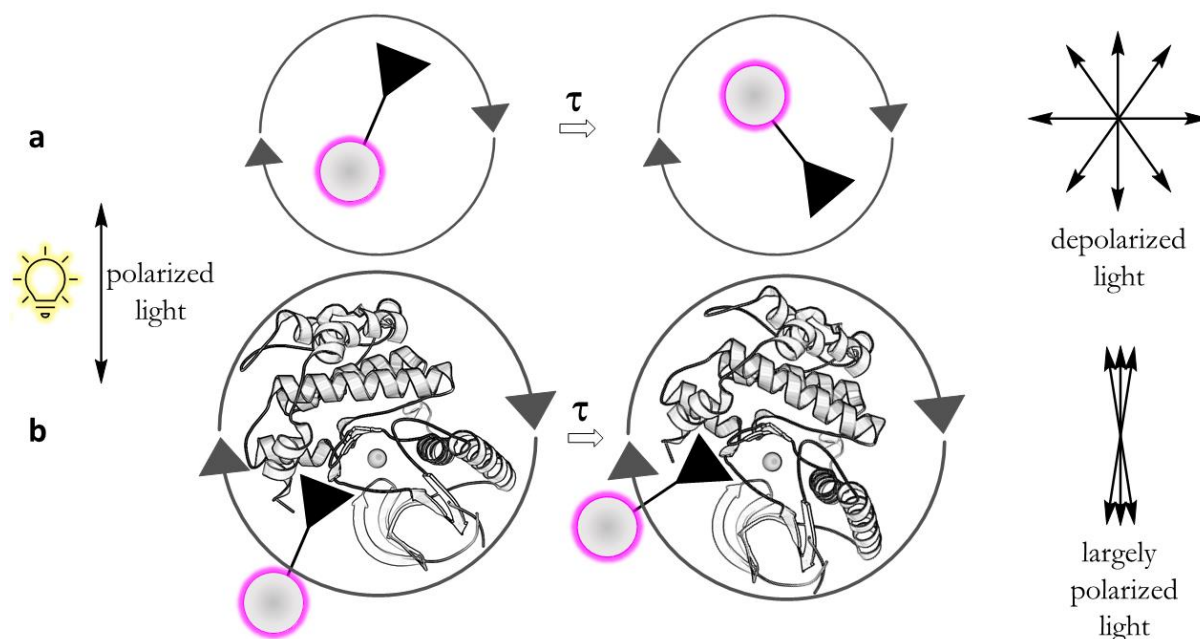


Figure 9 The basic principles of fluorescence polarization for unbound (a) and bound (b) fluorescent molecules to a certain protein within the fluorescence lifetime τ . The fluorescent dye (pink circle) is attached to a pharmacophore (black triangle) and a protein (grey cartoon). (a) A fluorescently tagged molecule is excited with polarized light and rotates during the specific time τ . (b) A fluorescently tagged molecule bound to a protein is excited with polarized light and rotates slowly in τ . The Figure was inspired by Moerke (2009).^[49]

In Figure 9 b this small molecule is bound to the binding site of a protein. After absorption of polarized light, the movement of this vast complex in τ is slower than for the unbound molecule and results in a largely polarized signal. Thus, the observed polarization is dependent on the rotational diffusion rate of a molecule and can be used to detect the binding status of a fluorescently tagged molecule.

1.4.3. Considerations in FP-assay design

For addressing a specific enzyme target in FP-assays, the tool compound needs to consist of a recognition element (or pharmacophoric group), a linker and a dye. In terms of the recognition element, the incorporation of the linker and dye must not result in adverse effects on the binding affinity of the pharmacophoric group. Therefore, the pharmacophoric scaffold should be capable to attach the linker system preferably in a position, which is tolerated without losing binding affinity. This linker system should position the dye, which usually has a bulky volume, outside of the binding pocket. If the

linker is too short, the recognition element is impeded from entering the active site of the enzyme. Contrarily if the linker length is too long the dye causes negative local rotational movements which lower the polarization. The reason of this so called “propeller effect” is the simulated increased rotational correlation time, which has been explained in the previous chapter.^[50] The conjugational chemistry of an appropriate tool compound is an empirical process which needs to be adjusted to the target protein in each case. Throughout this thesis, the term “linker” is used to refer to the chemical connective element between the pharmacophoric group and the dye. The term spacer will be used solely when referring to the chain included in the linker.

Considering the read-out, two main factors contribute to interferences in fluorescence polarization assays. In the case of screening large compound libraries for finding new chemical entities, usually most evaluated compounds are substituted aromatic systems. Thus, these compounds can simulate a positive hit in the assay and lower the quality of the results. Additionally, the compounds can cause interference if their inherent fluorescence overlaps with the area of detection of the reader.^[51]

One way to overcome these problems is the proper choice of the fluorescent dye. Knowing that aromatic compounds tend to have a major interference in a wavelength range about 300 nm, selecting a red-shifted fluorescent dye can alleviate the mentioned interference.^[52] In consequence, in this work the fluorescent dye of choice was 5-TAMRA due to its bathochromic shift of the emission wavelength.

1.4.4. Applications of fluorescent probes

Fluorescent tool compounds can be used for many diagnostic or imaging applications. Recently there is a growing number of studies describing the role of fluorescent tools *in vivo*. In 2013 Thurber *et al.* described a novel single-cell imaging tool to investigate the pharmacokinetic behaviour of poly(ADP-ribose)-polymerase 1 (PARP-1) inhibitors. They were able to monitor real-time drug distribution and determine drug concentration in tumor cells.^[53] One year later Kim *et al.* reported a fluorescently tagged Bruton’s tyrosine kinase (Btk) inhibitor, based on the covalent inhibitor Ibrutinib. The red-shifted silicon rhodamine

imaging tool was used for local profiling of the Btk expression and enabled measurements of the receptor inhibition with competing non-fluorescent compounds.^[54]

2. Objectives of the thesis

This study focused on the development and synthesis of a fluorescent probe, based on vemurafenib (**1**) and α -carboline, to allow the identification of new lead structures in a HTS-screening for inhibition of MKK4. At the outset of the project, MKK4 was identified as a promising target to enhance the liver hepatocyte proliferation and promote liver regeneration. Meanwhile, the BRAF inhibitor **1** was found to possess off-target activity on MKK4. Unfortunately, no crystal structure of an inhibitor-protein-complex was published to facilitate the design of the fluorescent probe without losing crucial interactions to the target. The previously obtained structure-activity relationships allowed to hypothesize that an implementation of the bulky fluorophore 5-TAMRA and a linker is possible. Figure 10 illustrates parts of the process of rational drug discovery and highlights the steps which are covered in this study.

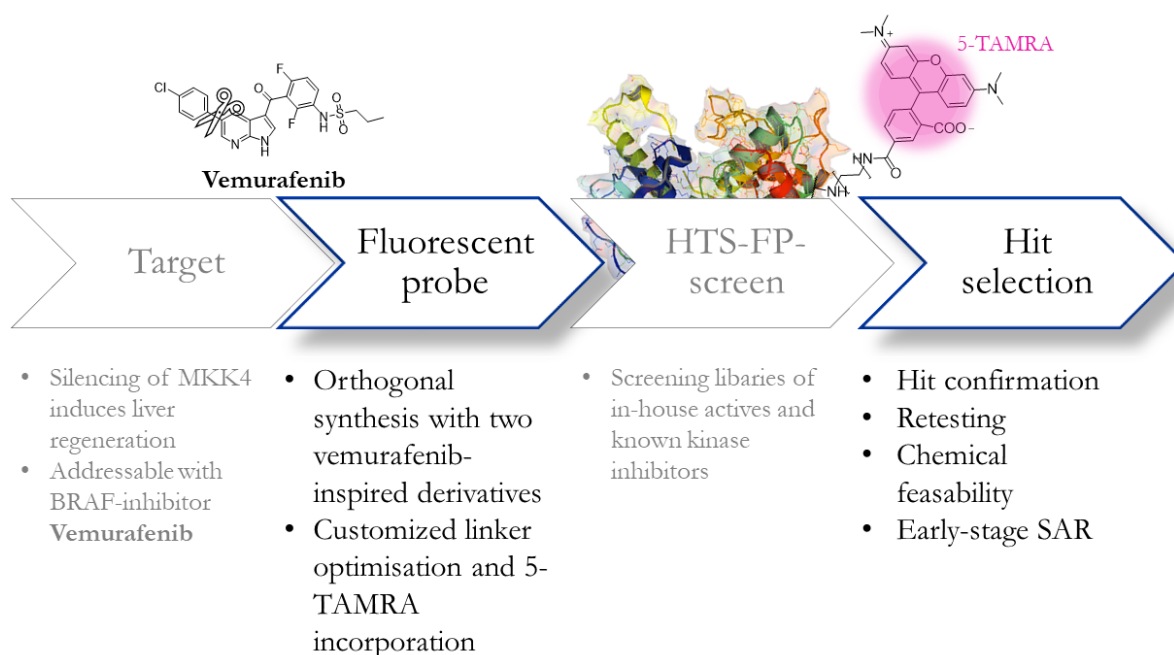


Figure 10 Process of rational drug discovery, highlighting fluorescent probe design and hit selection.

Iterative searching for the ideal connector between the fluorophore and the derived pharmacophoric group is important for finding a balance between sufficient binding affinity of the pharmacophore and restricted movement of the attached dye. Therefore, linker elements differing in their spacer, connection and basis were tested to find the optimal linker and subsequently attached to two vemurafenib-derived hinge binding motifs with

high affinity to MKK4 (Figure 11). Additionally, the implementation of the fluorophore 5-TAMRA was revised to maintain crucial interactions of the pharmacophore to the binding pocket. The developed suitable probe was applied to discover new small molecule inhibitors of MKK4 in a fluorescence polarization screening.

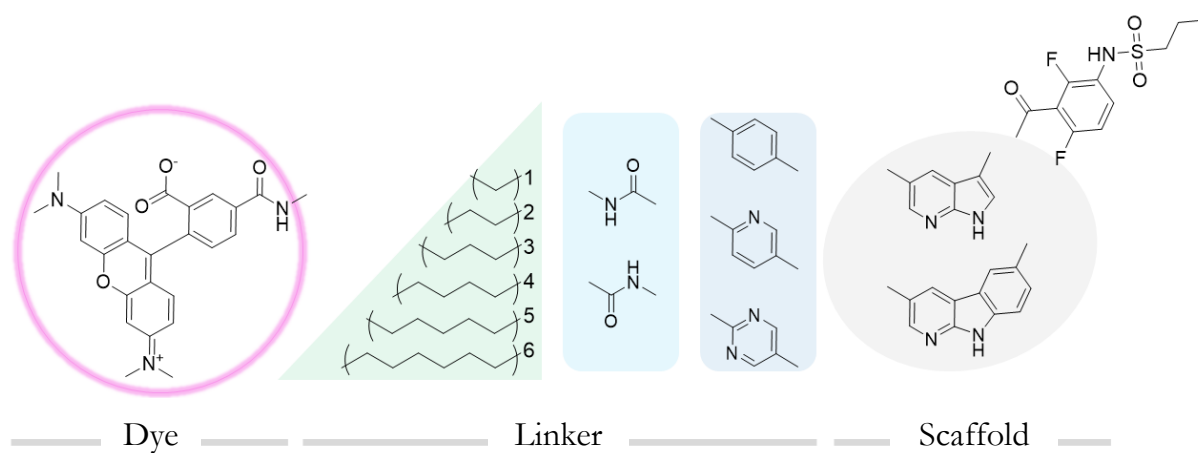


Figure 11 Simplified representation of the development of a fluorescent probe targeting MKK4 containing dye, linker, and a suitable scaffold.

Based on the output of the performed HT-screen, the second objective was to identify and confirm hits regarding chemical tractability, drug likeness and stability. The new synthetic route aligned to the hit should guarantee flexible and fast access to a comprehensive collection of compounds. The developed synthetic approach was used for preliminary attempts to improve the binding affinity of new scaffolds for MKK4 and provide further understanding of the active site.

3. Chemistry

3.1. Molecular design

3.1.1. Structural Information about vemurafenib – MKK4

As outlined earlier in the introduction, BRAF inhibitor vemurafenib (**1**, Figure 12) has strong off-target activity on MKK4.^[22] Recently Kloevekorn *et al.* depicted a broad spectrum of structure-activity correlations of **1** to MKK4.^[23] They enhanced the ability of the vemurafenib scaffold to inhibit MKK4 by variation of the *para*-chlorophenyl- and the sulfonamide moiety. With this information first hints are given to develop a hypothesis on how to attach a bulky fluorophore to the scaffold of **1**.

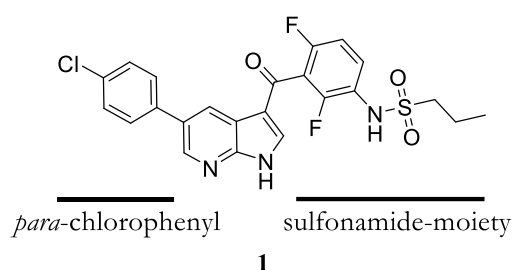


Figure 12 Structure of BRAF inhibitor vemurafenib **1** and the key terminology.

In this work, first steps to investigate binding modes of inhibitor-protein complexes were done by computer-aided analysis of available crystal structures of the target protein. Among the three published MKK4 crystal structures, two are in complex with adenylyl-imidodiphosphat, while the third is an apo structure. (PDB IDs: 3vut; 3aln; 3alo)^[9,8,6]. Since there is no available crystal structure of a MKK4-inhibitor complex, MD-derived simulation of the protein-**1** complex was done and supported information gained by structure-activity relationships.^[55] As expected, the *para*-chlorophenyl part protrudes out of the ATP binding pocket towards the solvent (Figure 13). This binding orientation provided a rational starting point for the ligand design of fluorescent derivatives for MKK4 and is consistent with the previously described binding data.^[56]

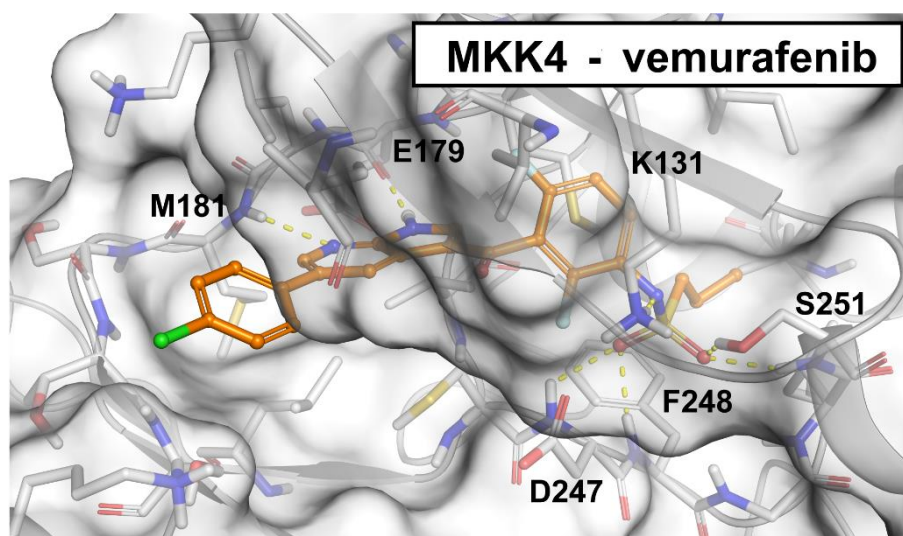
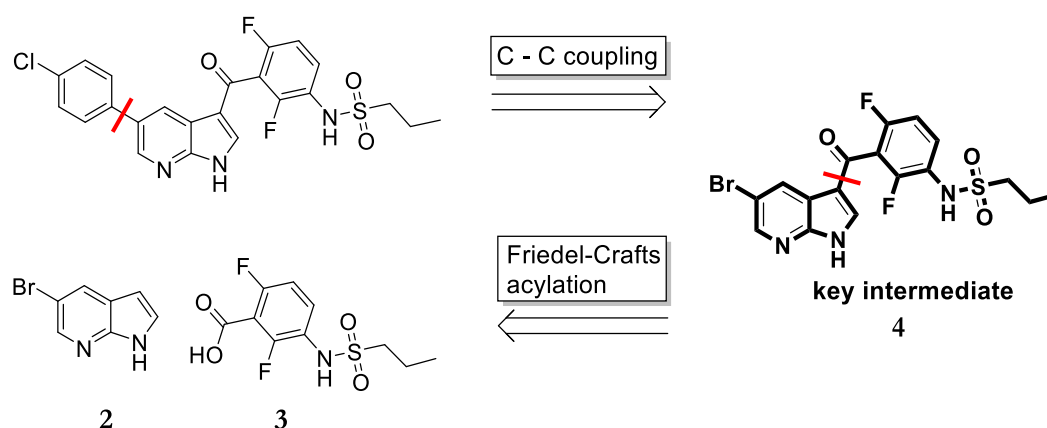


Figure 13 Docking pose of **1** in MD derived MKK4 structure prepared by Tatu Pantsar. Residues showing polar interactions (dashed yellow lines) with the ligand are labeled.^[56]

3.2. Azaindole -Series

3.2.1. Retrosynthesis of vemurafenib (**1**)

Previous synthetic approaches from the group started the synthesis of vemurafenib-based derivatives from 7-bromoazaindole (**2**) and the corresponding carboxylic acid **3** using Friedel-Crafts acylation conditions (Scheme 1). The *para*-chlorophenyl moiety was subsequently introduced via Suzuki carbon-carbon-coupling with an appropriate boronate species in a microwave reactor.^[57]

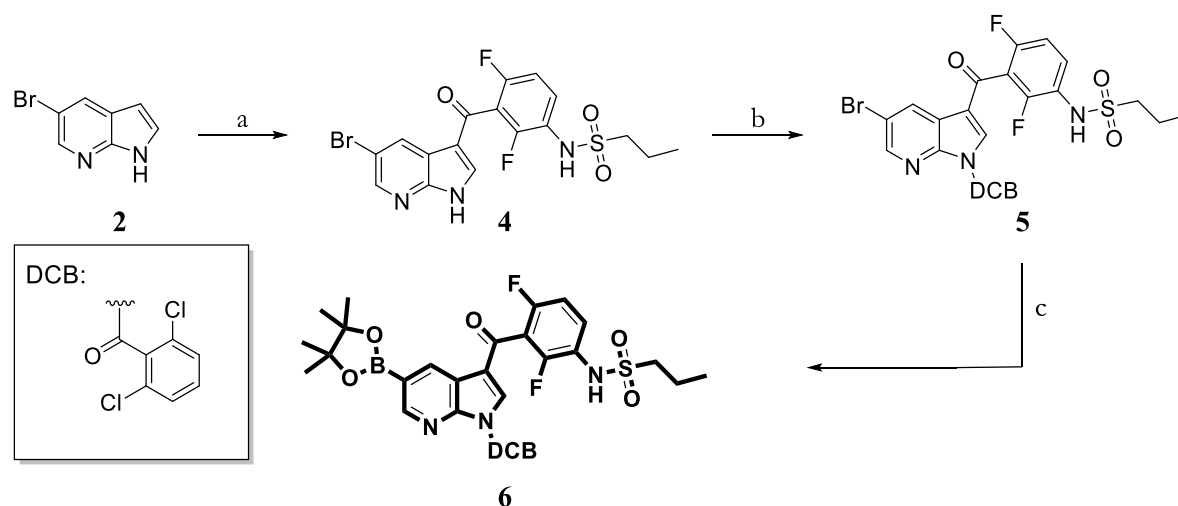


Scheme 1 Retrosynthetic analysis of vemurafenib. Red lines indicate bond breaking.

To introduce functional groups which can be connected to linking systems, the key intermediate **4** served as the starting material to plan further synthesis.

3.2.2. Azaindole key intermediate

The synthetic strategy was planned according to patent literature and is illustrated in Scheme 2.^[57] Instead of using the unprotected bromo-azaindole derivative **4**, the nitrogen was protected with DCB to yield **5** and subsequently transformed to the boronate species **6**.



Scheme 2 Synthetic path to intermediate **6**. Reagents and conditions: (a) AlCl_3 , 2,6-difluoro-3-(propylsulfonamido)benzoic acid, $(\text{COCl})_2$, DCM, 50°C , 6 h, 85%; (b) 2,6-dichlorobenzoyl chloride, Et_3N , 4-DMAP, THF, 0°C -RT, 17 h, 68%; (c) B_2pin_2 , KOAc, $\text{Pd}(\text{PPh}_3)_2\text{Cl}_2$, 1,4-dioxane, 80°C , 2 h, 68%.

In the first step, the Friedel-Crafts acylation was carried out with commercially available 7-bromo azaindole (**2**) and 2,6-difluoro-3-(propylsulfonamido) benzoic acid (**3**) in the presence of excessive aluminum chloride forming key intermediate **4**.

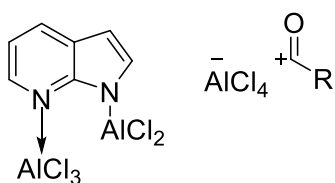


Figure 14 Proposed transition state of azaindole, the acylium cation and aluminium chloride in a Friedel-Crafts acylation.

For azaindole compounds three equivalents of aluminum chloride were required to generate the active acylium ion (Figure 14). The second equivalent is coordinating the pyridine nitrogen and the third one deprotonates the N-H group of the azaindole. The reaction yielded the intermediate in good yields (85%).^[58]

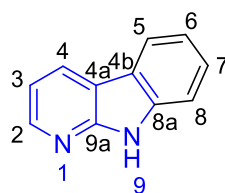
To transform aryl bromides into the corresponding pinacolates, Miyaura coupling conditions can be used. The typical borylation setup uses borylation reagents such as B_2pin_2 and transition metal catalysts. Pinacolates are generally more stable than the related boronic acids, as the σ -donation of the adjacent carbon atoms influences the lone pairs of the oxygen atoms and alters the electron density in the deficient boron centre.^[59] Many of the standard protocols for palladium catalysed cross-couplings fail in the presence of acidic N–H groups.^[60]

Therefore, a 2,6-dichlorobenzoyl (DCB) protecting group was installed on the indole nitrogen of key intermediate **4**, which allowed performing the Miyaura borylation of **5** at lower temperatures. Moreover, fewer side products such as dehalogenation of the bromoazaindole precursor were observed. The resulting pincolato-ester **6** served as a basis for a convenient and efficient introduction of linkage systems.

3.3. α -Carboline-Series

3.3.1. Carboline key intermediate

In addition to the azaindole-core of **1**, a tricyclic α -carboline (*9H*-pyrido[2,3-*b*]indole) scaffold was used, because derivatives of α -carbolines also show high affinity and selectivity for MKK4.^[24] As noted in the introduction, the α -carboline scaffold was preliminarily designed by Bayer in 2003 as MKK4 and MKK7 inhibitor.^[25] Figure 15 shows the structure of α -carboline and the resemblance to the azaindole core.

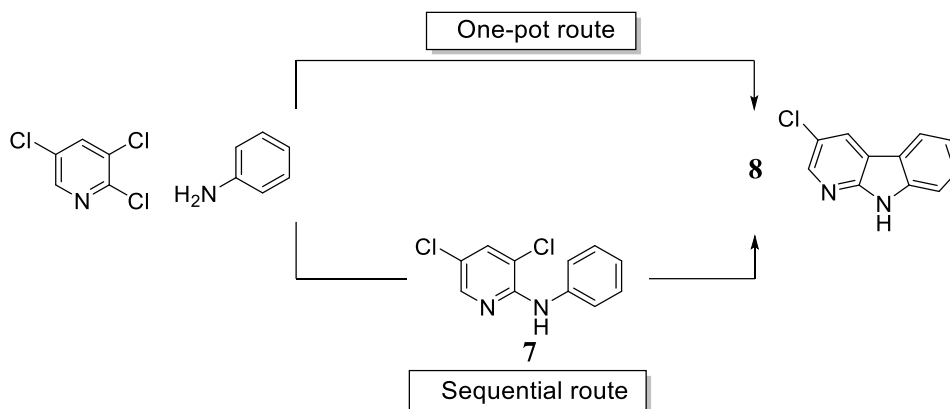


9H-pyrido[2,3-*b*]indole

Figure 15 Structure and numbering of the tricyclic *9H*-pyrido[2,3-*b*]indole, highlighting the resemblance to the previously described azaindole core in blue.

Carbolines with the *para*-chlorophenyl- and difluoroaryl moiety attached at the 3- and 6-position have a slightly different geometry with an additional ring system compared to azaindoles. Therefore, the linker system evaluation was done for both scaffolds.

The approach to access the α -carboline precursor **8** started from trichloropyridine, which was coupled with aniline under Buchwald Hartwig conditions (Scheme 3). The following intramolecular ring-closure of diarylamine **7** yielded 3-chloro-carboline (**8**). This conversion can be achieved either by an one-pot approach or a sequential route via **7** as isolated intermediate.^[61]



Scheme 3 Synthetic preparation of 3-chloro-carboline can be achieved via a one-pot- or a sequential route.

Table 1 summarizes the reaction conditions and yields to the final product **8**.

Table 1 Reaction conditions via one-pot or sequential route to **8**.

		<i>Pd-source</i>	<i>Ligand</i>	<i>Base</i>	<i>Solvent</i>	<i>Yield (7)^a</i>	<i>Yield (8)^b</i>	
120 °C, 17 h	One-pot	Pd(OAc) ₂	PPh ₃	NaO <i>t</i> Bu	<i>o</i> -xylol	n.d. ^c	n.d. ^c	
		Pd(OAc) ₂	PCy ₃	DBU	<i>o</i> -xylol	n.d. ^c	43%	
	Sequential	1.	Pd(OAc) ₂	PPh ₃	NaO <i>t</i> Bu	<i>o</i> -xylol	82% ^a	n.d. ^c
		2.	Pd(OAc) ₂	PCy ₃	DBU	DMA/ <i>o</i> -xylol	59% ^a	48%

^aYield of the isolated intermediate; ^bCalculated overall yield; ^cNot determined.

Although trichloropyridine offers three chloro atoms as a potential leaving group, the regioselectivity of the palladium catalysed cross coupling reaction can be predicted quite precisely from ¹H-NMR shifts of the parent non-halogenated heteroaromatic ring.^[62]

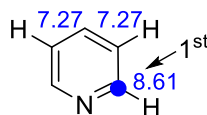
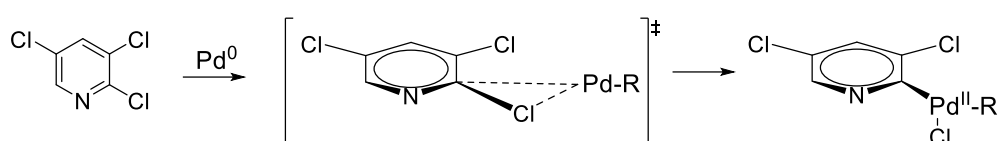


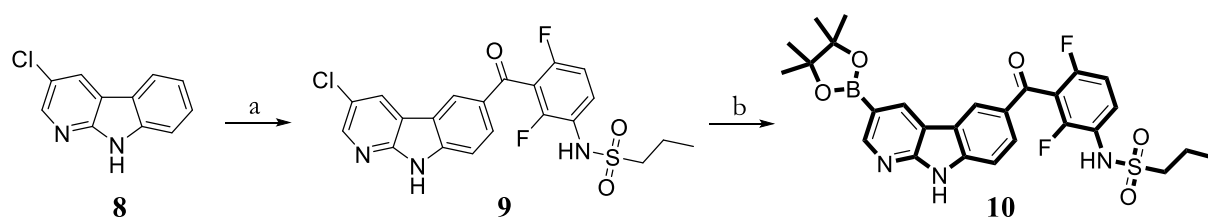
Figure 16 Prediction of regioselectivity in palladium catalysed cross coupling using $^1\text{H-NMR}$ shifts.^[63]

In cross couplings oxidative addition is the regioselectivity-controlling step.^[64] For pyridine, the 2-position has the highest degree of electron deficiency and therefore the C-Cl-bond in this position breaks in the first transition state of Buchwald coupling (Scheme 4). Regarding the sequential route to **7** only mono substitution was observed and yielded the desired intermediate in good yields (82%).



Scheme 4 Transition state of palladium catalysed oxidative addition for trichloropyridine.

After N-arylation of trichloropyridine, the next step was C-H activation of the 3-position of **7**.^[65] The subsequent ring closure led to the formation of the desired tricycle. The use of DBU as a base at elevated temperatures was optimal to prevent competing hydrodehalogenation during the C-H activation step. In case of the one-pot-two-step cyclization procedure the reagents required for the second step were added successively after 3 hours at 120 °C without any workup.^[66] Since there was no significant difference between the yields of the one-pot and the sequential route, it is preferable to use the one-pot route conditions because of temporal expenditure and economic reasons.



Scheme 5 Friedel-Crafts Acylation and Miyaura borylation of **8**. Reaction conditions: (a) AlCl_3 , 2,6-difluoro-3-(propylsulfonamido)benzoic acid **3**, $(\text{COCl})_2$, DCM, 50 °C, 17 h, 69%; (b) B_2pin_2 , KOAc, XPhos Pd G3, MW (50 W), 1,4-dioxane, 110 °C, 40 min, 89%.

Similar to the azaindole synthesis, **8** was acylated via Friedel-Crafts acylation with the carboxylic acid **3** yielding **9** and subsequently borylated using Miyaura borylation to obtain

10 in good yields which is surprisingly possible without a protection group of the carboline N-H. Intermediate **10** could be merged with the linker systems which will be described in the next chapter.

3.4. Spacer and linkage design

The design of a fluorescent small molecule-based tracer addressing the binding pocket of a protein is an iterative procedure. Usually, the ATP binding pocket of kinases is highly conserved and not accessible for sterically hindered moieties. Thus, the bulky fluorophore needs to be spatially separated from the pharmacophore by a chemical linker, containing a spacer, without adverse effects on binding affinity. Figure 17 shows the definition of the terms related to the synthetic strategy utilized in this work. Besides a spacer with a certain length, the installation to a specific position of the ligand is important to consider. To retain the main interactions of the pharmacophore to the protein, the spacer should be attached in a region pointing outside of the binding pocket.

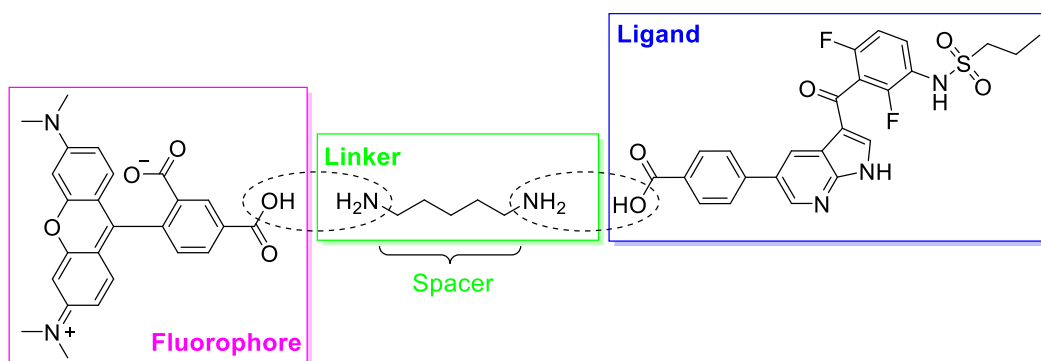


Figure 17 Overview of the synthetic strategy of connecting ligand, spacer, and fluorophore to a ligand and the definition of used terms.

Combining structural information with molecular modeling helps to guide the design of the probe. As previously described (3.1, design), MD simulation of MKK4 supported the hypothesis based on SAR. The *para*-chlorophenyl substituent of **1** seemed to point into the solvent region out of the binding pocket and can be introduced in the latest synthetic step. As it is part of the pharmacophore, the *para*-chlorophenyl moiety could be replaced for further improvement of spacer systems.

Figure 18 compares the binding affinity of three different core systems, which allow an attachment of linkages in the *para*-position of the phenyl ring.

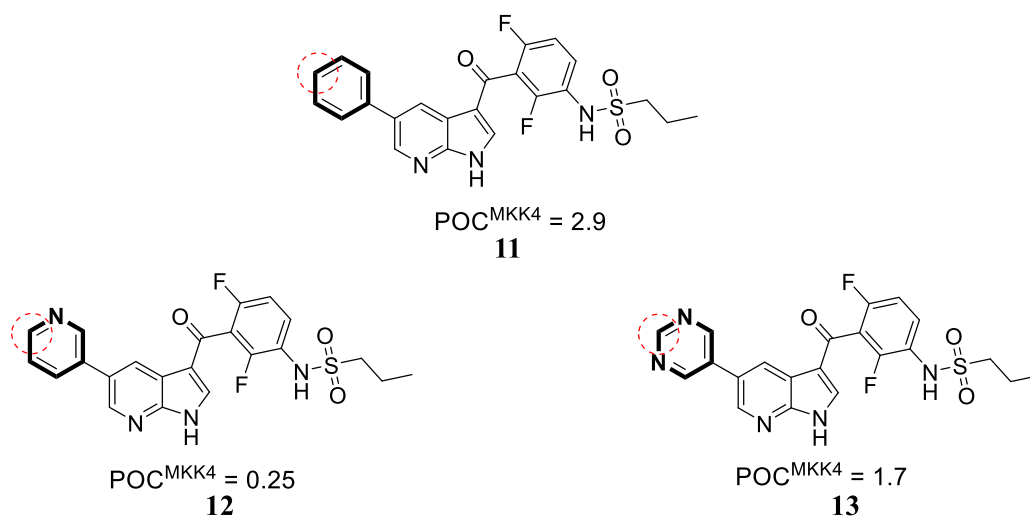
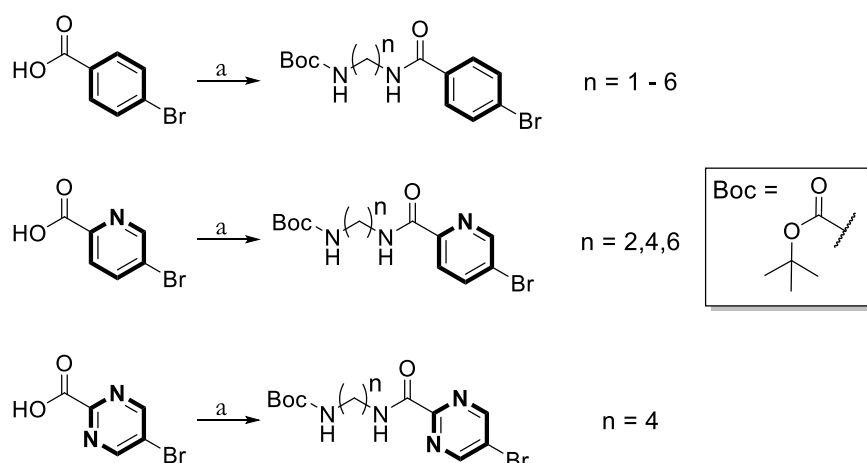


Figure 18 Binding affinities at a screening concentration of 0.1 μM and structure of different derivatives with pyridine and pyrimidine moieties. The *para*-position of the moiety directed towards the solvent region is highlighted in red.

The advantage of pyridinyl- and pyrimidinyl moieties is the increased affinity to the target protein compared to **1** ($\text{POC}^{\text{MKK4}} = 14$).^[23] Furthermore, linking systems with an additional nitrogen atom offer a hydrogen bond acceptor to fixate the linker and reduce rotation. The relevance of the rotational movement of the compound for the results of the fluorescence polarization assay was described in detail in the introduction.

Scheme 6 illustrates the three different linker systems which were used for synthetic design. For all three species the carboxylic acid derivative bears a bromo atom in the 4-position.



Scheme 6 Synthetic strategy to different linker core derivatives. Reaction conditions: (a) Corresponding amine, HATU, DIPEA, DMF, RT, 17 h.

The next important consideration was which kind of functional group would be the best to connect spacer systems in the *para*-position. The requirements were a decreased rotational movement of the attached spacer, easy chemical accessibility and reaction conditions aiming high yields.

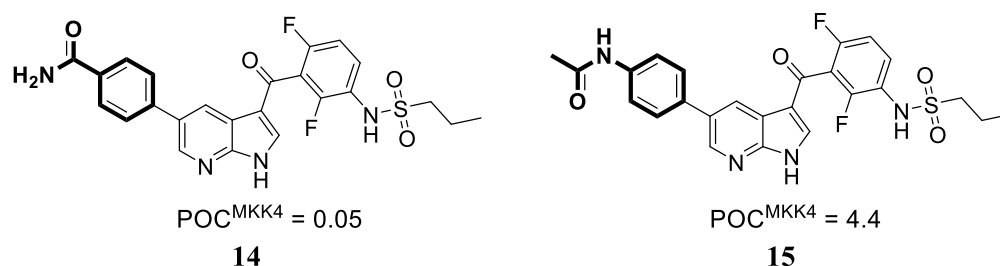
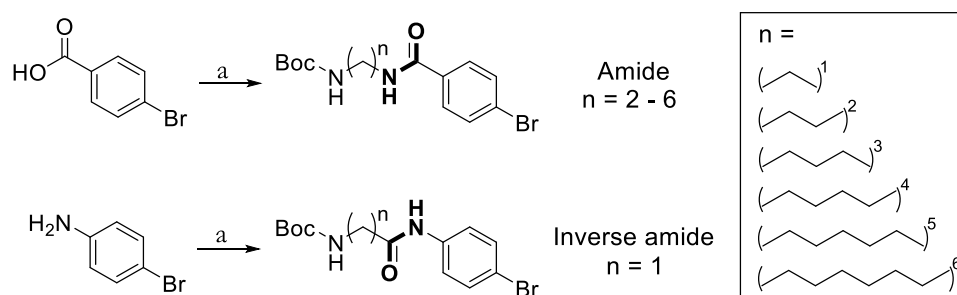


Figure 19 Binding affinities and structure of amide and inverse amide derivatives of **1**.

Amide bonds have a restricted rotation which can be explained by delocalization of electrons among O-C-N bond and a resulting partial double bond character. Based on the high binding affinity of derivatives **14**, this structural element was selected for introducing spacers (Figure 19).

The next step was the introduction of spacer systems differing in length. The easiest way to build up long spacers was using alkyl-chains in between the fluorophore and the scaffold of **1**. Diamino chains offer two functional groups to connect both ends. The optimal length of the spacer depends on the depth of the binding of the inhibitor to the active side, which allows the sterically hindered fluorophore to be attached with an appropriate distance.

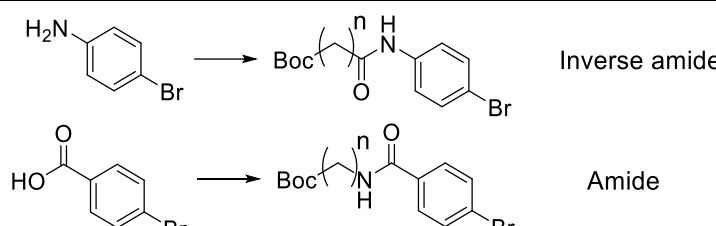
Scheme 7 illustrates the synthetic strategy to install alkyl chain spacers of varying lengths for the attachment of the fluorophore. The spacer was established via mono Boc-protected diamino chains containing one to six carbon atoms or Boc-protected amino carboxylic acid with one carbon atom.



Scheme 7 Synthetic approach to amide and inverse amide spacer systems. Reaction conditions: (a) Corresponding amine or carboxylic acid, HATU, DIPEA, DMF, RT, 17h.

Amide bonds can be introduced using amide coupling reagents, which transform the unreactive carboxylic acid into an activated species. Especially uronium salts, like *N*-[(dimethylamino)-1*H*-1,2,3-triazolo[4,5-*b*]pyridin-1-ylmethylene]-*N*-methylmethanaminium hexafluorophosphate (HATU) are widely used in pharmaceutical chemistry.^[67]

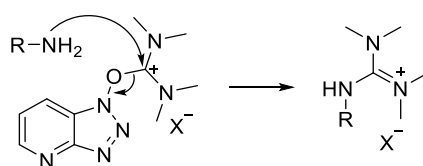
In this work HATU was used as a coupling reagent in combination with the sterically hindered base DIPEA in DMF as solvent. Table 2 gives a summary of all synthesized linker system and their structure.

Table 2 Summary of all Boc-protected linker systems.


<i>Linker core</i>	<i>Linker connection</i>	<i>Spacer length</i>	<i>Yield^a</i>	<i>Product</i>
Phenyl	Inverse amide	n = 1	36%	16
Phenyl	Amide	n = 2	quant.	17
Phenyl	Amide	n = 3	62%	18
Phenyl	Amide	n = 4	73%	19
Phenyl	Amide	n = 5	45%	20
Phenyl	Amide	n = 6	78%	21
Pyridine	Inverse amide	n = 1	59%	22
Pyridine	Amide	n = 3	32%	23
Pyridine	Amide	n = 4	66%	24
Pyridine	Amide	n = 6	69%	25
Pyrimidine	Amide	n = 4	48%	26

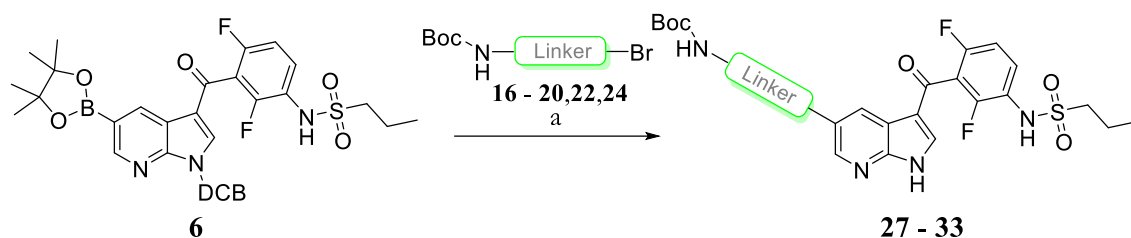
^aIsolated yield.

In general, the isolated yields of the amide coupling using HATU were moderate. A side reaction which can occur using uronium salts like HATU is the reaction of the free amine and the uronium salt resulting in a guanidinium salt (Scheme 8).^[68]

**Scheme 8** Side reaction of a free amine and the uronium salt.

3.5. Connection of key intermediates 6 and 10 to spacer

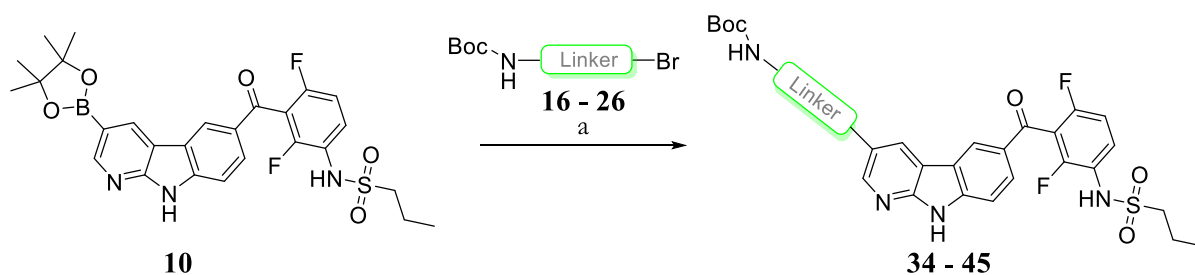
As previously described compound **6** and **10** serve as key intermediates for further linking synthesis. Scheme 9 illustrates the synthetic path to the Boc-protected precursors **27 - 33** from **6**.



Scheme 9 Synthetic strategy to fluorescently tagged compounds. Reaction conditions (a) (i) Pd(dppf)Cl₂, K₂CO₃, 1,4-dioxane/water; 110 °C, 3 – 17 h; (ii) K₂CO₃, MeOH, 4 h.

For azaindoles, **6** was treated with Boc-protected amines **16 - 26** under Suzuki coupling conditions with Pd(dppf)Cl₂ at high temperatures. Subsequently the DCB protection group was removed under basic conditions in MeOH yielding compounds **27 – 33**. The products were obtained in moderate yields between 39 – 66%. In contrast to the azaindole scaffold, where an introduction of the DCB protection group was favourable, Suzuki coupling with carbolines did not necessarily need a nitrogen protecting group.

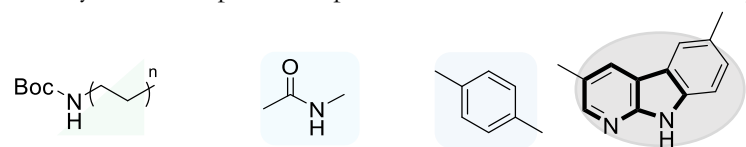
Carboline **10** could be connected to linker systems **16 – 26** with palladium catalyst Pd(PPh₃)₄ under milder conditions at 55 °C yielding the products in yields between 19 – 75% (Scheme 10). The Suzuki products could be obtained in high purity after recrystallization from EtOAc and *n*heptan or *n*hexan.



Scheme 10 Synthetic strategy of the linker attachment to the carboline scaffold. Reaction conditions (a) Pd(PPh₃)₄, K₂CO₃, 1,4-dioxane/water; 55 °C, 17h.

Table 3 summarises all Boc-protected intermediates containing azaindole or carboline structures and different spacer systems.

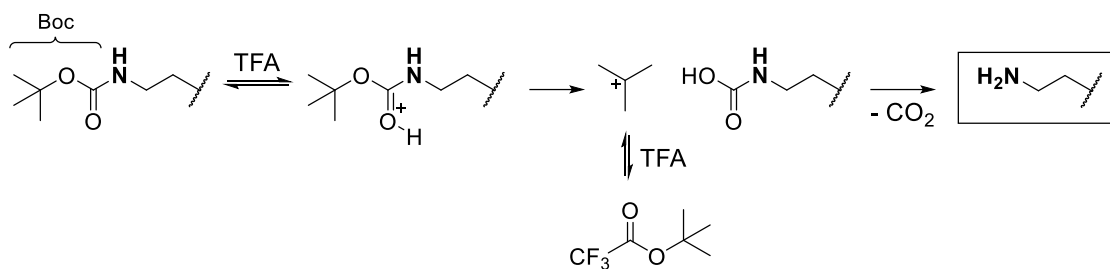
Table 3 Summary of all Boc-protected precursors **27** - **45** which can be conjugated to the fluorophore.



<i>Spacer length</i>	<i>Linker connection</i>	<i>Linker core</i>	<i>Scaffold</i>	<i>Yield^a</i>	<i>Product</i>
n = 1	Inverse amide	Phenyl	Azaindole	66%	27
n = 1	Inverse amide	Pyridine	Azaindole	49%	28
n = 2	Amide	Phenyl	Azaindole	39%	29
n = 3	Amide	Phenyl	Azaindole	59%	30
n = 4	Amide	Phenyl	Azaindole	57%	31
n = 4	Amide	Pyridine	Azaindole	49%	32
n = 5	Amide	Phenyl	Azaindole	58%	33
n = 1	Inverse amide	Phenyl	Carboline	65%	34
n = 1	Inverse amide	Pyridine	Carboline	27%	35
n = 2	Amide	Phenyl	Carboline	40%	36
n = 3	Amide	Phenyl	Carboline	20%	37
n = 3	Amide	Pyridine	Carboline	33%	38
n = 4	Amide	Phenyl	Carboline	75%	39
n = 4	Amide	Pyridine	Carboline	42%	40
n = 4	Amide	Pyrimidine	Carboline	19%	41
n = 5	Amide	Phenyl	Carboline	35%	42
n = 5	Amide	Pyridine	Carboline	32%	43
n = 6	Amide	Phenyl	Carboline	75%	44
n = 6	Amide	Pyridine	Carboline	30%	45

^aIsolated yields.

Before connecting the ligand-linker system to the fluorophore, the Boc-group was neatly removed under strong acidic conditions with TFA in toluene (Scheme 11).



Scheme 11 Mechanism of the deprotection of Boc-protected linker systems using TFA.^[69]

Due to their high polarity, primary amines typically suffer from peak broadening and bad separation when subjected to normal phase column chromatography, which can result in a loss of product and low yields. Thus, the Boc-protected intermediate **27 – 45** were used after traceless deprotection in the final amide coupling with 5-TAMRA without further purification.

3.6. Fluorescent molecules

Fluorescently tagged molecules can be used for many *in vitro* assay systems to monitor cellular events, for instance protein-protein interactions or monitoring cellular movements.^[70] The wide range of available fluorophores differs in emission wavelength, quantum yield and chemical properties such as solubility and stability.^[44] Depending on the desired result of the pursued assay system, some fluorophores are more favorable than others.

As reported earlier, some small molecules from compound libraries are native fluorophores as they bear (hetero)aromatic ring systems. Commonly used fluorophores such as fluorescein overlap with these intrinsic fluorophores. This impairs the assay result and leads to false positive and negative results. Using red-fluorescent signals at 550 nm, however, limits the occurrence of fluorescence interference and reduces the overlap, because interference with bathochromic shifts is rarely observed.^[51]

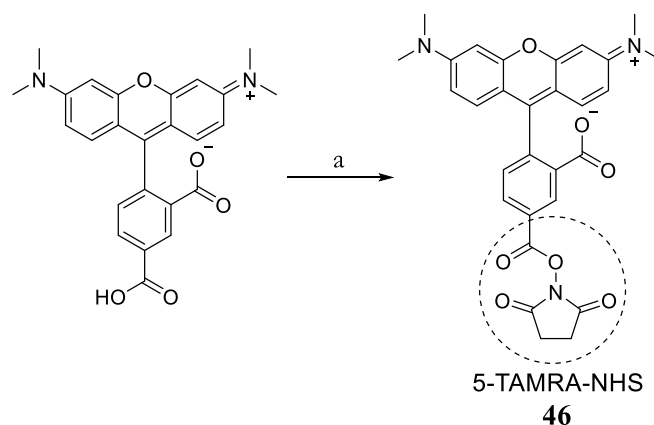
Labeling of small molecules with fluorophores can be achieved using different methods of conjugation. Some commercially available fluorophores are already transferred to a reactive

species bearing isothiocyanate or succinimidyl ester as functional groups for connection with amines. Isothiocyanate derivatives form a thiourea bond to the corresponding amine and succinimidyl ester (SE) are transformed to the corresponding amide linkage.

Rhodamines have a polycyclic xanthene-based ring system similar to fluorescein but bear two additional amino substituents on the tricyclic scaffold. The modification of the functional groups close to the planar ring structure may cause alteration of electronical values, such as absorption and emission wavelengths.^[71] As outlined in the introduction, 5-TAMRA was selected as the fluorescent dye of choice due to favorable red-shifted emission wavelength.

The structure of 5-TAMRA bears a carboxylic acid group in 5-position, capable to connect under amide coupling conditions to amines of biomolecules. Conjugation of the fluorophore 5-TAMRA can be performed either by using activating agents for the carboxylic acid group or using the preactivated derivative of 5-TAMRA.

The preactivated dyes are restricted for high quantity applications due to economic reasons. First attempts to synthesize the *N*-hydroxysuccinimide (NHS) ester of 5-TAMRA by activating it with disuccinimidyl carbonate (DCC) were barely successful.

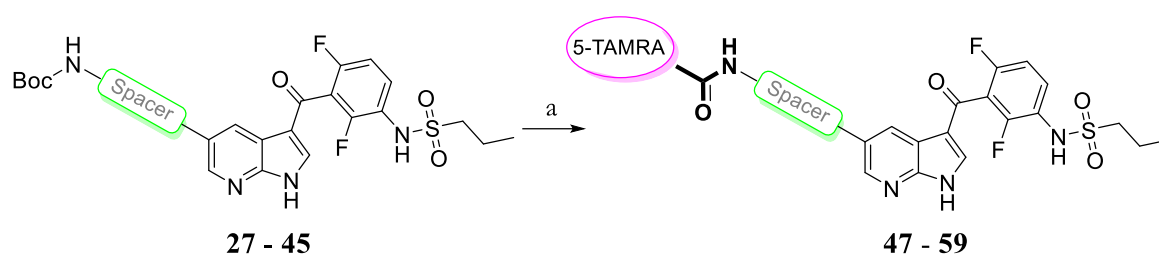


Scheme 12 Activation of 5-TAMRA using DCC to form 5-TAMRA-NHS. Reaction conditions (a) DCC, DMAP, DMF, RT, 17 h, 51%.

Scheme 12 illustrates the activating step of 5-TAMRA using DCC and DMAP to obtain the storage-stable 5-TAMRA-NHS (**46**). There is only little literature about synthesizing compound **46**, and Thermo Fisher Scientific published its synthesis without mentioning a

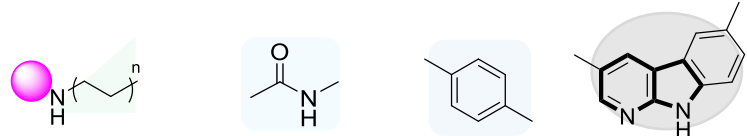
yield.^[72] The obtained yield in this work was 51% and therefore not satisfying for synthesising a library of fluorescent compounds.

The application of *in situ* activating agents such as HATU was previously described in the linker synthesis. Additionally, HATU was used to form the amide bond between the linker system and the fluorophore (Scheme 13).



Scheme 13 Deprotection and conjugation to 5-TAMRA shown on an azaindole. Reaction conditions: (a) (i) TFA/toluene (1:10, v/v), RT, 17 h; (ii) HATU, DIPEA, 5-TAMRA, DMF; RT, 17 h.

To prevent side reactions (3.4, Spacer and linkage design), HATU was used in an equimolar ratio to the fluorophore. Then a solution of the unprotected amine in DMF and DIPEA was added and stirred at RT. Table 4 summarizes all fluorescently tagged compounds containing azaindole and carboline scaffolds.

Table 4 Summary of all 5-TAMRA tagged compounds **47** - **59**.


<i>Spacer length</i>	<i>Linker connection</i>	<i>Linker core</i>	<i>Scaffold</i>	<i>Yield^a</i>	<i>Product</i>
n = 1	Inverse amide	Phenyl	Azaindole	64%	47
n = 4	Amide	Pyridine	Azaindole	44%	48
n = 1	Inverse amide	Phenyl	Carboline	52%	49
n = 1	Inverse amide	Pyridine	Carboline	30%	50
n = 2	Amide	Phenyl	Carboline	54%	51
n = 3	Amide	Phenyl	Carboline	65%	52
n = 3	Amide	Pyridine	Carboline	59%	53
n = 4	Amide	Phenyl	Carboline	39%	54
n = 4	Amide	Pyridine	Carboline	47%	55
n = 4	Amide	Pyrimidine	Carboline	42%	56
n = 5	Amide	Phenyl	Carboline	31%	57
n = 6	Amide	Phenyl	Carboline	24%	58
n = 6	Amide	Pyridine	Carboline	58%	59

^aIsolated yields.

All compounds could be obtained after normal-phase (NP) chromatography using TFA as an acidic additive in DCM/MeOH mixture or reversed-phase (RP) column chromatography. After purification, all solids were recrystallized from EtOAc and *n*hexane or *n*heptane yielding the products in high purity.

To eliminate false positive assay hits, chemical stability of the fluorescent compounds was investigated by exposing DMSO solutions of azaindole **47** and carboline **50** to sunlight. Figure 20 compares the photostability of fluorescently tagged compounds **47** and **50** in DMSO over a period of one week.

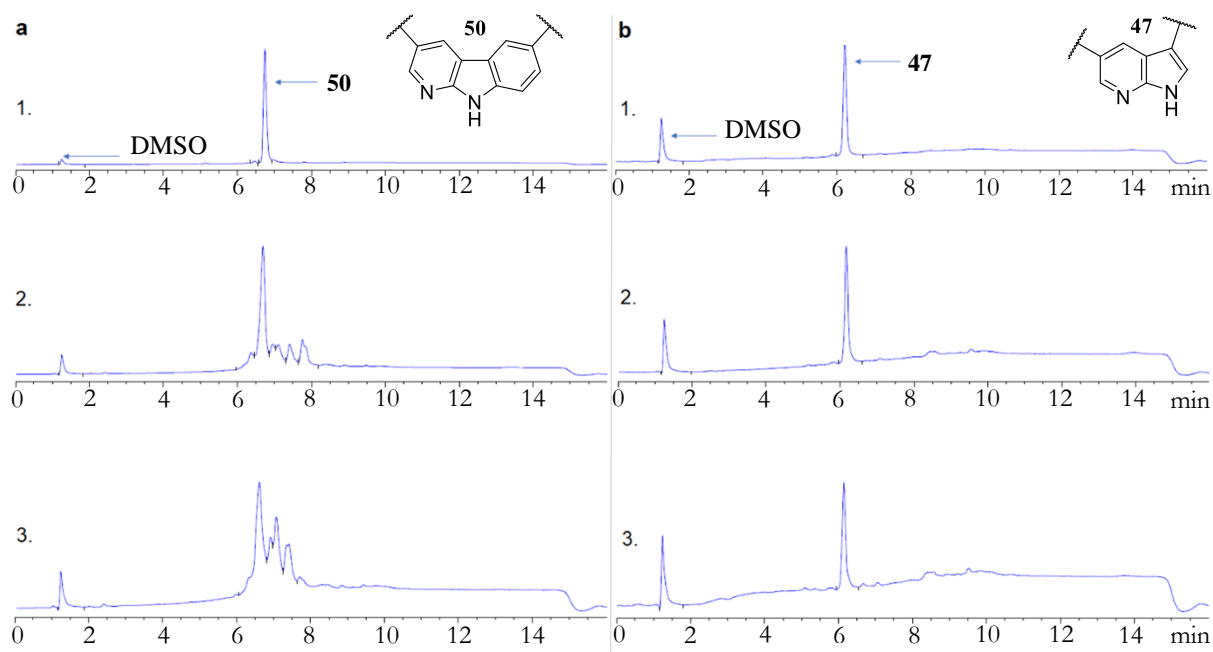


Figure 20 Photostability of fluorescently tagged carboline **50** and azaindole **47** under light exposure in DMSO solutions. Analysis carried out by HPLC (detection at 230 nm); 1. Pure product peak; 2. 72 hours light exposure; 3. One-week light exposure.

Surprisingly only the azaindole derivative **47** was stable under such extreme conditions over a time of one week. The carboline derivative **50** started to decompose after 72 hours to unidentified fragments. Nevertheless, both compounds were stable in DMSO over a period of one week without light exposure and therefore fulfill the requirements of chemical stability for upcoming assay investigation.

In addition to standard ^1H - and ^{13}C -NMR experiments, 2D experiments (HSQC and HMBC) were performed to determine the connectivity of a representative fluorescent compound. It is noticeable that almost all protons of the 5-TAMRA spin system showed broad signals in the ^1H -spectrum. Hydrogens belonging to the xanthene moiety showed a broad multiplet at 6.46 and 7.00 ppm. Especially the CH_3 -groups attached to the nitrogen showed a broad singlet at 3.08 ppm, indicating that both CH_3 -groups were in a rotational movement.

The confirmation of the structure of a representative fluorescent compound (Figure 21 a-d) was obtained by NMR assignment of compound **53** in $\text{DMSO-}d_6$ using a ^1H -NOESY-experiment.

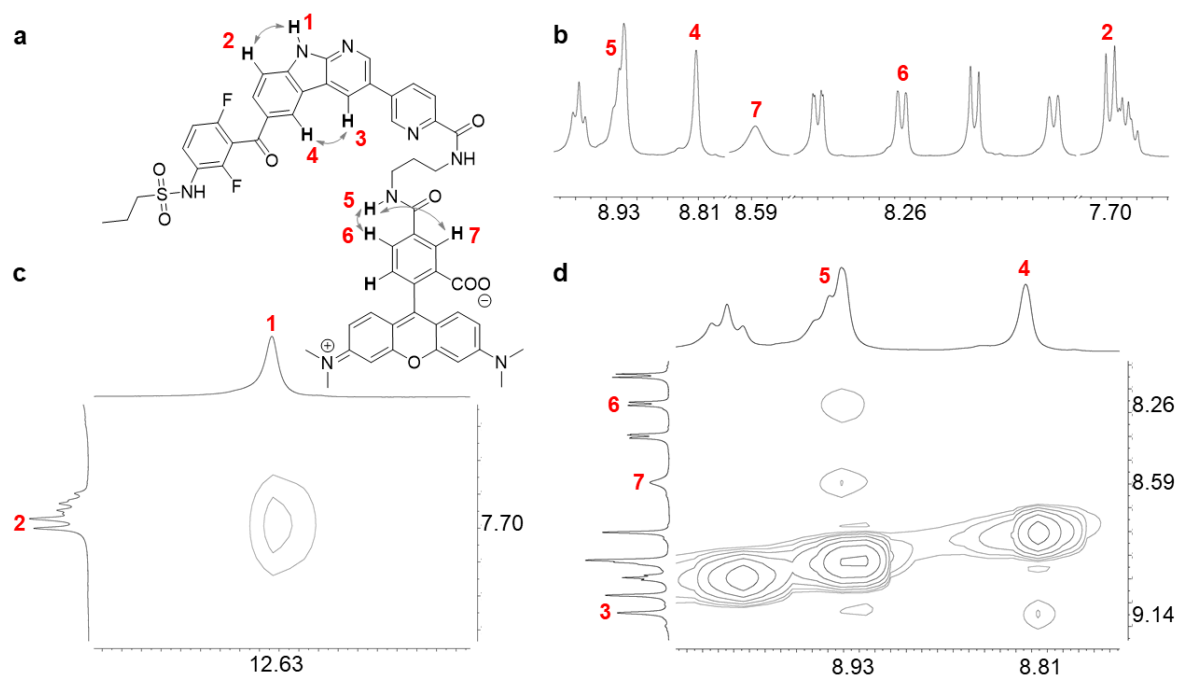


Figure 21 NMR assignment of **53**. (a) Structure of compound **53** in DMSO- d_6 : Important hydrogens are highlighted bold and numbered (red). Spatially close resonances derived from the NOESY-NMR experiment are displayed as grey arrows. (b) ^1H -NMR spectrum from 7.60 – 9.00 ppm of **53**. Important peaks are highlighted and numbered in red. (c) Cut-out from 12.50 – 12.75 ppm (x-axis) and 7.55 – 7.90 ppm (y-axis) derived from the NOESY-experiment, showing cross peaks of hydrogen 1 and 2; (d) Cut-out from 8.70 – 9.10 ppm (x-axis) and 8.2 – 9.2 ppm (y-axis) derived from the NOESY experiment illustrating cross peaks between hydrogens 5/6, 5/7 and 4/3.

The correlation between hydrogen 5/6 and 5/7 verified that the amide bond was connected in the 5-position of 5-TAMRA, demonstrating that these hydrogens are in spatial proximity. Additionally, spatially close resonances can be observed for the carboline scaffold of **53**, in particular hydrogen 1/2 and 3/4. Finally, Figure 22 shows all ^1H -shifts of compound **53** in DMSO- d_6 .

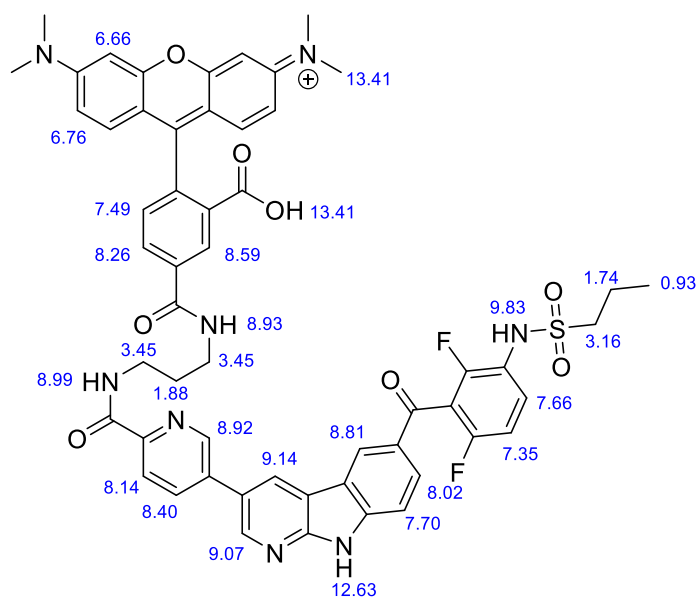
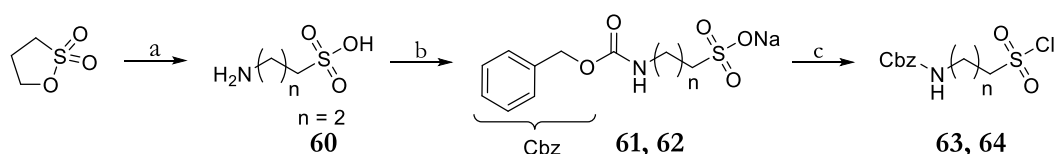


Figure 22 $^1\text{H-NMR}$ assignment of compound **53** in $\text{DMSO-}d_6$, highlighting the shifts in blue.

To prove that labeling is only applicable at one site of the molecule (*para*-chlorophenyl), 5-TAMRA was also introduced at the other site of the molecule. Therefore, two fluorescent molecules were synthesized to confirm the structural hypothesis. Binding affinities of these compounds were expected to decrease.

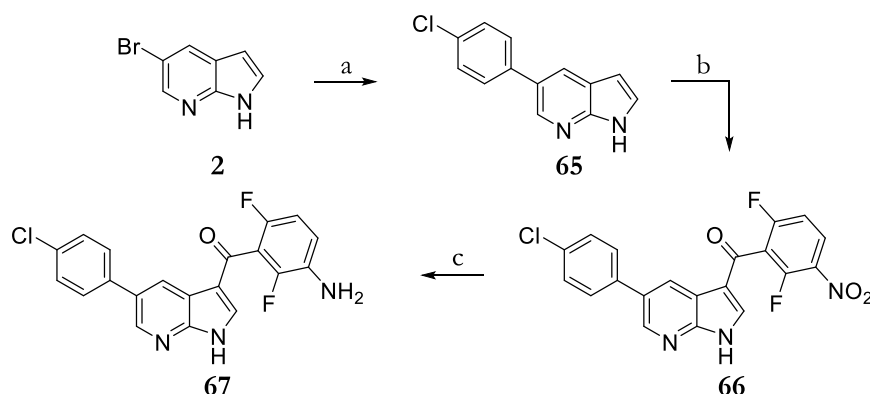
The sulfonamide was chosen as an attachment point to introduce a spacer with a functional group to connect 5-TAMRA. In general, this sulfonamide moiety was connected by the treatment of the free aniline with 1-propanesulfonyl chloride. Thus, two spacer systems with two (**63**) or three (**64**) carbon atoms in between a sulfonyl chloride group and a Boc-protected amine were prepared.



Scheme 14 Synthetic route to **63** and **64**. Reaction conditions: (a) NH_3 (7N in MeOH) RT, 4 h, 49%; (b) NaOH, Cbz-Cl, water, RT, 17 h, quant.; $n = 1,2$; (c) PPh_3 , SO_2Cl_2 , 0°C , 1 h, 58 – 74%.

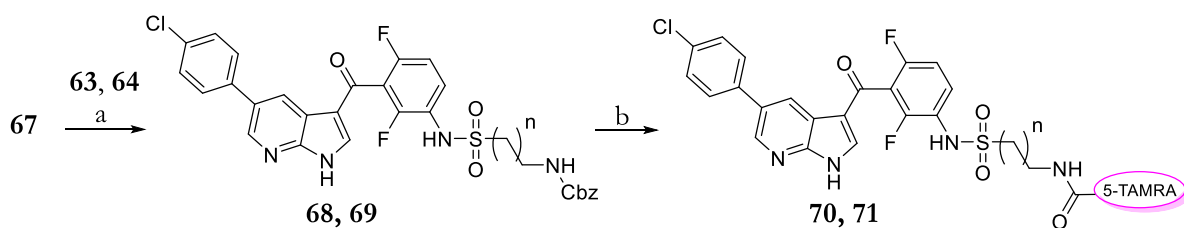
Scheme 14 describes the synthetic route to compounds **63** and **64**. 3-Amino-1-propane sulfonic acid (**60**) was obtained after a ring opening reaction of commercially available 1,2-oxathiolane 2,2-dioxide. After a protection with benzyl chloroformate, the resulting sodium

salts **61** and **62** were transferred into the corresponding sulfonyl chlorides, which could be purified using column chromatography.



Scheme 15 Synthetic route to **67**. Reaction conditions: (a) (*para*-chlorophenyl) boronic acid, K_2CO_3 , ACN/water, $Pd(PPh_3)_4$, 80 °C, 17 h, 69%; (b) 2,6-difluoro-3-nitrobenzoic acid, $AlCl_3$, DCM, $(COCl)_2$, 40 °C, 6 h, 70%; (c). $SnCl_2$ dihydrate, THF/EtOAc, 60 °C, 17 h, 48%.

The vemurafenib scaffold synthesis was reordered to gain access to the free aniline attached to the difluoro moiety. 7-Bromoazaindole **2** was connected to (*para*-chlorophenyl) boronic acid using Suzuki conditions yielding **65** and subsequently connected to 2,6-difluoro-3-nitrobenzoic acid in a Friedel-Crafts reaction. The nitro group of **66** was then reduced with stannous chloride dihydrate to yield the desired free aniline derivative **67**.



Scheme 16 Synthetic route to **70** and **71**. Reaction conditions: (a) Pyridine, THF, RT, 6 h, 30 %; $n = 1,2$; (b) (i) HCl, EtOH, MW, 100 °C, 1 h; (ii) 5-TAMRA-SE, DIPEA, DMF, RT, 17 h, 72% $n = 1,2$.

Compound **67** was treated with **63** and **64**, respectively, yielding sulfonamides **68** and **69** and finally attached to 5-TAMRA to afford the fluorescent compounds **70** and **71** (Scheme 16).

3.7. Results from the fluorescence polarization screen

The preselection of the probes, assay validation and performance for a fluorescence polarization assay on MKK4 was executed by the Screening Unit of the Leibniz Forschungsinstitut für molekulare Pharmakologie.

Figure 23 illustrates the selection of hits which were found in this fluorescence polarization screen with the designed fluorescent probe based on the previously described results similar to **55**. Two compounds (RN2716 and LN850) are part of a Laufer group in-house compound library and belong to p38 MAP kinase projects. AZD5438 (**72**) is a known kinase inhibitor for CDK1/2/9.

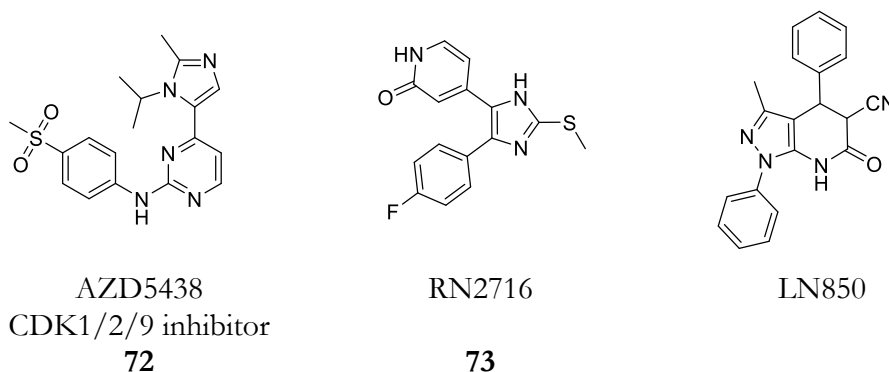


Figure 23 Structure of three hits identified in the fluorescence polarization screening.

Part of the process of the hit identification was the analysis of stability and retesting of activity in an assay system which differs in the assay set up from the HTS screen, which was described in the introduction. **72** and **73** were chosen for activity and stability confirmation. Later, both compounds were used to implement for further investigations on structure-activity relationship.

3.8. Aminopyrimidine series

Cyclin dependent kinase (CDK) inhibitor AZD5438 (**72**) was primary developed by AstraZeneca in 2008.^[73] Analyzing the crystal structure of **72** to CDK2 (PDB ID: 6GUH)^[74] can give first insights in the binding mode of **72** in kinases and allows the guidance of further synthesis of derivatives of **72** targeting MKK4. Comparison of the binding site of both proteins showed a high concordance of the hinge region (Figure 24 a). Representation of **72** in CDK2 (Figure 24 b) demonstrates that the phenyl-ring in 2-position of the

pyrimidine core is located outside the ATP binding pocket pointing into the solvent accessible area. The main hinge interaction in CDK2 can be observed from Leu83 and NH from the aniline and N1 of pyrimidine. The bulky isopropyl substituent attached to the imidazole ring in 4-position of the pyrimidine core projects into a hydrophobic pocket in the ribose binding domain.^[75]

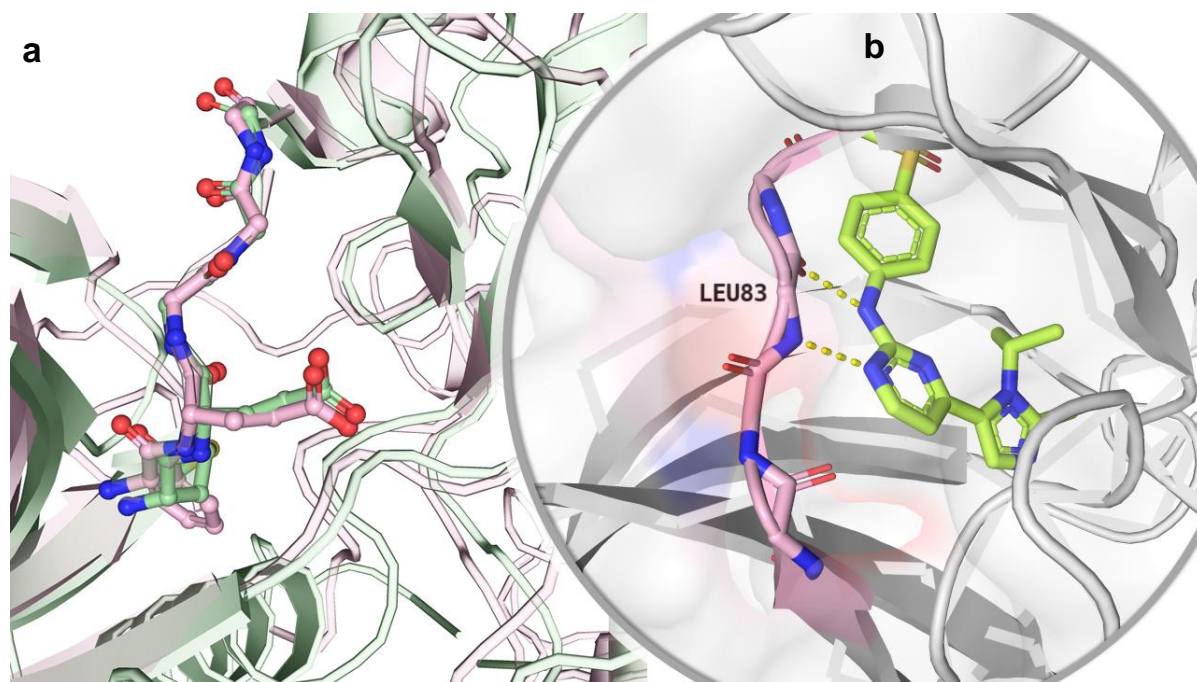
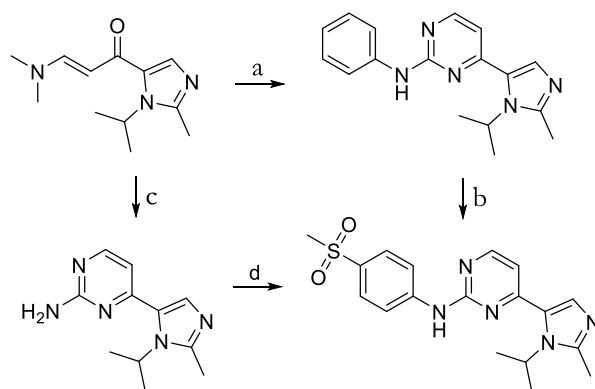


Figure 24 (a) Structural alignment of CDK2 (pink., PDB ID: 6GUH)^[74] and MKK4 (green, PDB ID: 3ALO)^[6] using Schrodinger Maestro “binding site alignment” highlighting the resemblance of the hinge main chain of both proteins. (b) Binding mode of AZD5438 **72** (green) in complex with CDK2 highlighting hinge binding residue Leu83. Residues that show polar interactions (dashed yellow lines) with the ligand are labeled in the figure.

Hence, it could conceivably be hypothesized that **72** occupies the binding pocket of MKK4 in a similar manner, assuming that the methylsulfonyl-moiety points into the solvent. The imidazole moiety leaves only little tractability for chemical alterations. Thus, retaining the methylsulfonyl-moiety, the hinge binding motive, and exchanging the imidazole heterocycle seemed to be a good starting point for developing new compounds addressing MKK4.

Compound **72** contains an aminopyrimidine scaffold as primary core system. There are two known synthetic strategies to obtain aminopyrimidine derivatives. One was the heterocyclic ring closure where the substituent in 4-position was introduced in the first step. Scheme 13 shows the two published routes to synthesize **72**.^[75]



Scheme 17 Published synthesis of imidazole **72**. Reagents and conditions: (a) phenyl-guanidine hydrogencarbonate, NaOMe, DMA, 150 °C, 24 h, 96%; (b) ClSO₃CH₃, SOCl₂, 0 °C-reflux, 1 h; 44–81%; (c) guanidine hydrochloride, NaOMe, BuOH, reflux, 18 h, 84%; (d) 4-I-C₆H₄-SO₂NH(CH₂)₂OMe, Pd₂(dba)₃, BINAP, NaOtBu, dioxane, 80 °C, 18 h, 84 %.

This synthesis introduced 1-isopropyl-2-methyl-1*H*-imidazole in the first step and allowed only little synthetic variation for moieties in 4-position of the aminopyrimidine. Additionally, the aminopropenone precursor, which was used as a starting material in Scheme 17, had to be synthesized in a four-step reaction path in advance.

The second synthetic route to aminopyrimidines included regioselective substitution of the pyrimidine core. In some publications regioselective zinc-mediated exchange reactions of halogen substituents in 2-position of the pyrimidine core is discussed.^[76]

Compared to pyridines from the previous sections, pyrimidine regioselectivity regarding S_NAr and palladium catalyzed reactions is in direct contrast to the prediction using ¹H-NMR shifts.^{[62][77]} Illustrated in Figure 25, reactions of polyhalogenated pyrimidine occur faster in 4-position than in 2-position. This hypothesis is highly dependent on reaction conditions and often yields regioisomeric mixtures.^[78]

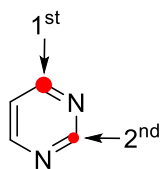
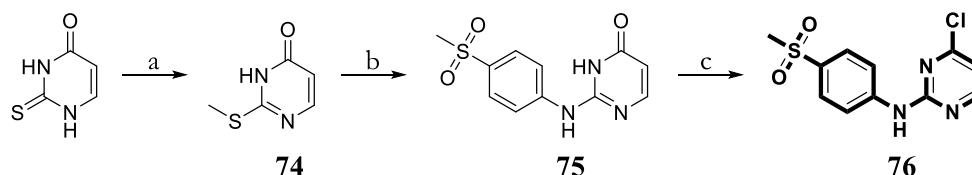


Figure 25 Predicted reactivity of pyrimidine regarding S_NAr and palladium catalysed functionalization.

This strategy led to a new regioselective synthetic approach, which generated the key intermediate **76** in good yields without column chromatography and avoided previously

described regioselective mixtures of pyrimidine intermediates and an inconvenient strategy of the pyrimidine ring closure.

Scheme 18 describes the synthetic route to aminopyrimidine derivatives with different substituents in 4-position.



Scheme 18 Synthetic route to Aminopyrimidine derivatives. Reaction and conditions: (a) iodomethane, NaOH, EtOH/water (2:1, v/v), 0 - 60°C, 20 hours, 63%; (b) 4-(methylsulfonyl)anilin, crude, 180 °C, 73%; (c) POCl₃, 110 °C, 1 hour, 68%.

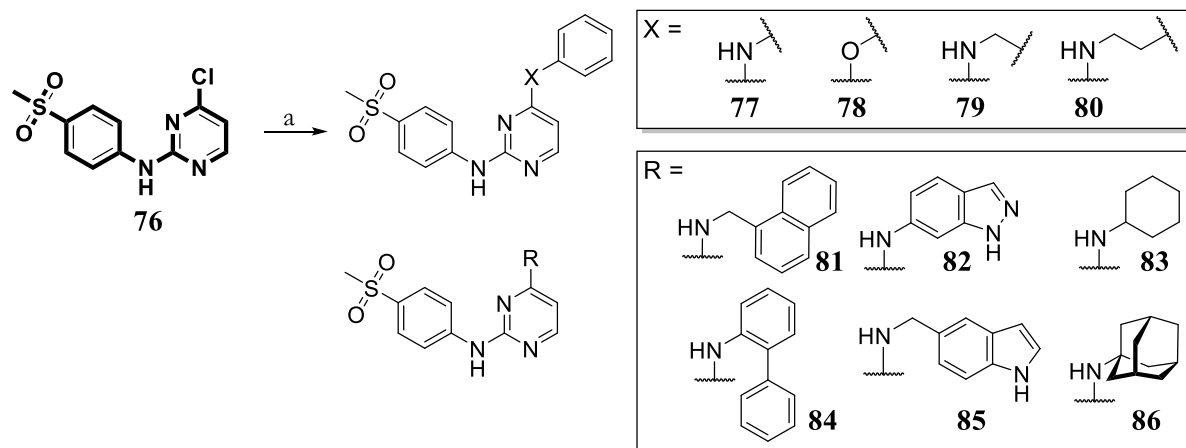
The new established route blocked the 4-position of pyrimidine with a keto function and yielded the product of 2 substitution in regioselective pure intermediates. Later the inaccessible position 4 of the pyrimidine core was transformed to the corresponding chloro-derivative and could be used for further substitution.

This route allowed a fast synthesis with regioselective pure intermediates. Starting with the methylation of commercially available 2-thiouracil using iodomethane and grinded NaOH in an EtOH/water mixture described by Maddess *et al.*^[79] yielded the pure intermediate **74** from crystallization in EtOH/water.

In the next step the methylthio-group was substituted by S_NAr with 4-(methylsulfonyl)anilin at high temperatures without any solvent. After full consumption, the pure product **75** could be obtained after crushing the crude solid in acetonitrile and collection via suction filtration. Subsequently the pyrimidone derivative **75** was chlorinated with POCl₃ at high temperatures yielding the key intermediate **76**. After recrystallization in acetonitrile the pure intermediate could be isolated using suction filtration.

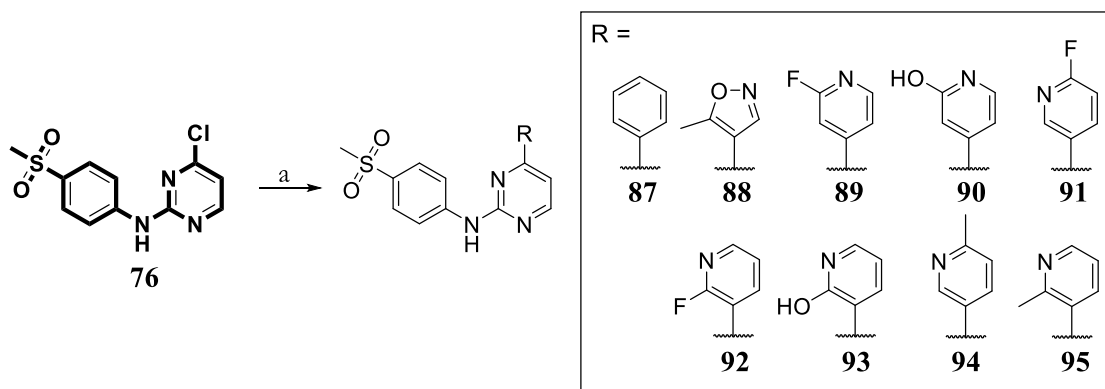
The key intermediate **76** with a chlorine atom in 4-position allowed the introduction of substituents with reactions such as S_NAr or palladium-catalysed reactions. With this approach a broad range of compounds differing in their electronic properties, sterical nature and substitution pattern could be achieved easily with the purpose to find new scaffolds substituting the imidazole from **72**.

Scheme 19 shows the synthetic step to compounds having different connective elements X (**77** – **80**) and ring systems (**81** – **86**). Almost all compounds could be recrystallized from EtOAc and *n*hexane to yield the pure final product.



Scheme 19 Final synthetic step to aminopyrimidine derivatives connected via $\text{S}_{\text{N}}\text{Ar}$. Reaction conditions: (a) corresponding nucleophile, K_2CO_3 , DMF, $150\text{ }^\circ\text{C}$, 1 – 17 h.

The next compound class connected via carbon-carbon coupling from intermediate **76** was obtained utilizing Suzuki conditions without the need of high temperatures. Scheme 20 depicts the final step to compounds **87** – **95**.

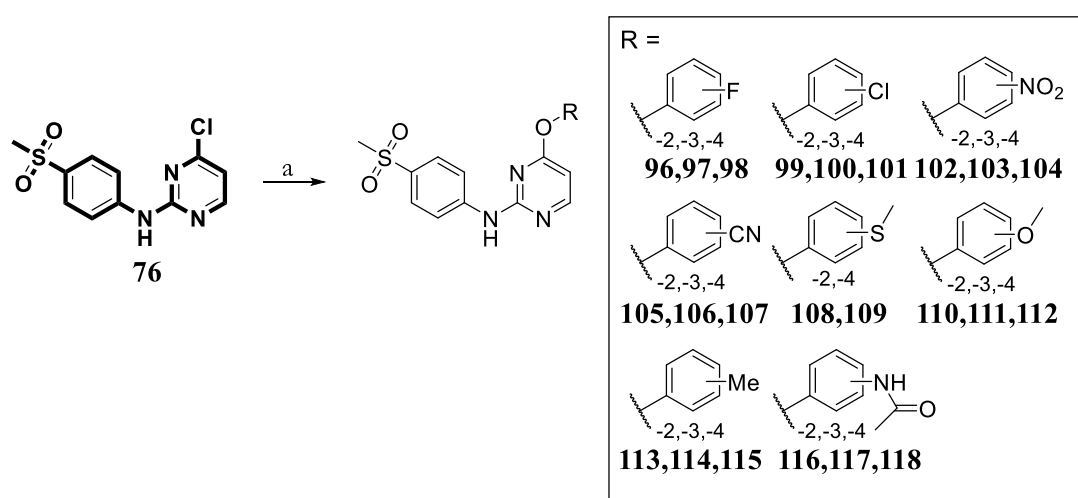


Scheme 20 Final synthetic step to carbon-carbon connected aminopyrimidines. Reaction conditions: (a) Corresponding boronic acid, K_2CO_3 , $\text{Pd}(\text{dppf})\text{Cl}_2$, 1,4-dioxane/water, $55\text{ }^\circ\text{C}$, 2 h.

Having the demand to synthesize a broad range of compounds in a short time, some heterocyclic precursors were disregarded. For Suzuki coupling, especially 2-pyridinyl boronic acids suffer from protodeboronation and therefore were not used for synthesizing a broad range of compounds.^[80] With the general procedure using $\text{Pd}(\text{dppf})\text{Cl}_2$ and standard Suzuki conditions, all compounds from Scheme 20 could be isolated in moderate yields

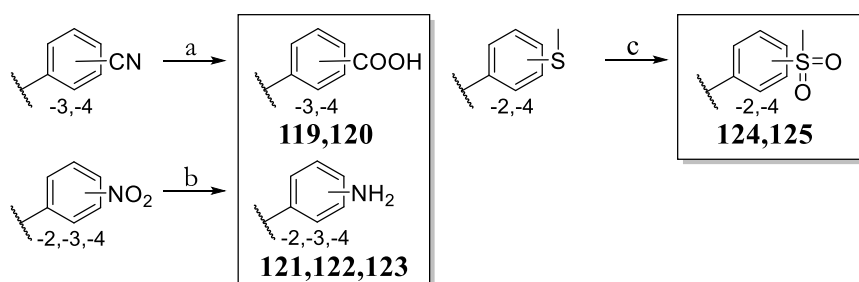
from 42 - 70%. Although heteroaromatic boronic acids are known to be less stable in solution, reaction efficacy was not reduced in a significant manner.

After structure-activity analysis of unsubstituted moieties **77** – **86**, phenolic derivative **78** seems to be the most promising and was used for introducing functional groups differing in their electronic properties yielding in **96** – **118** (Scheme 21).



Scheme 21 Final synthetic step to aminopyrimidine connected phenol derivatives via S_NAr . Reaction conditions: (a) Corresponding phenol, K_2CO_3 , DMF, $150\text{ }^\circ\text{C}$, 1 – 17 h.

Some of the compounds bearing functional groups were used as starting material for further compounds by simple reaction conditions. Scheme 22 sums up the three derivatisation reactions to obtain **119** – **125**.



Scheme 22 Final synthetic step to aminopyrimidine connected phenol derivatives via functional group transformation. Reaction conditions: (a) HCl (12N), $100\text{ }^\circ\text{C}$, 2 h; (b) H_2 , Raney nickel, MeOH, RT, 17 h; (c) *m*CPBA, DCM, $0\text{ }^\circ\text{C}$ - RT, 17 h.

The nitrile in 2-, 3- or 4-position of the attached phenol was transferred to the corresponding carboxylic acid using concentrated HCl and high temperature. After full conversion and cooling to $0\text{ }^\circ\text{C}$ the final product precipitated from the reaction solution

and could be obtained after suction filtration as a pure solid. Nitro-group containing phenols could be reduced with Raney nickel and hydrogen without additional column chromatography. Finally, the methylsulfonyl derivatives could be obtained by oxidation of methylthio-compounds with *m*CPBA.

Compounds **116** – **125** bear a functional group which again could be used as a possible link for new moieties.

3.8.1. Representative NMR discussion of compound **91**

Figure 26 displays the ^1H NMR spectrum of compound **91** in $\text{DMSO-}d_6$. Due to ^1H - ^{19}F coupling, all hydrogens could be assigned without additional 2D-NMR experiments. The sharp singlet at 10.32 ppm resulted from the N-H of the aniline and the two multiplets with an intensity of 2 at 7.86 and 8.06 ppm from the aromatic hydrogens from methylsulfonylphenyl. The hydrogen of the pyrimidine core next to the nitrogen showed a down shielded doublet at 8.69 ppm with a coupling constant of $J = 5.2$ Hz. The corresponding hydrogen also showed a doublet at 7.62 ppm. Due to the presence of an additional fluorine atom in 2-position of the pyridine, all hydrogens on the pyridine ring were split by ^1H - ^{19}F coupling and can be seen in Figure 26.

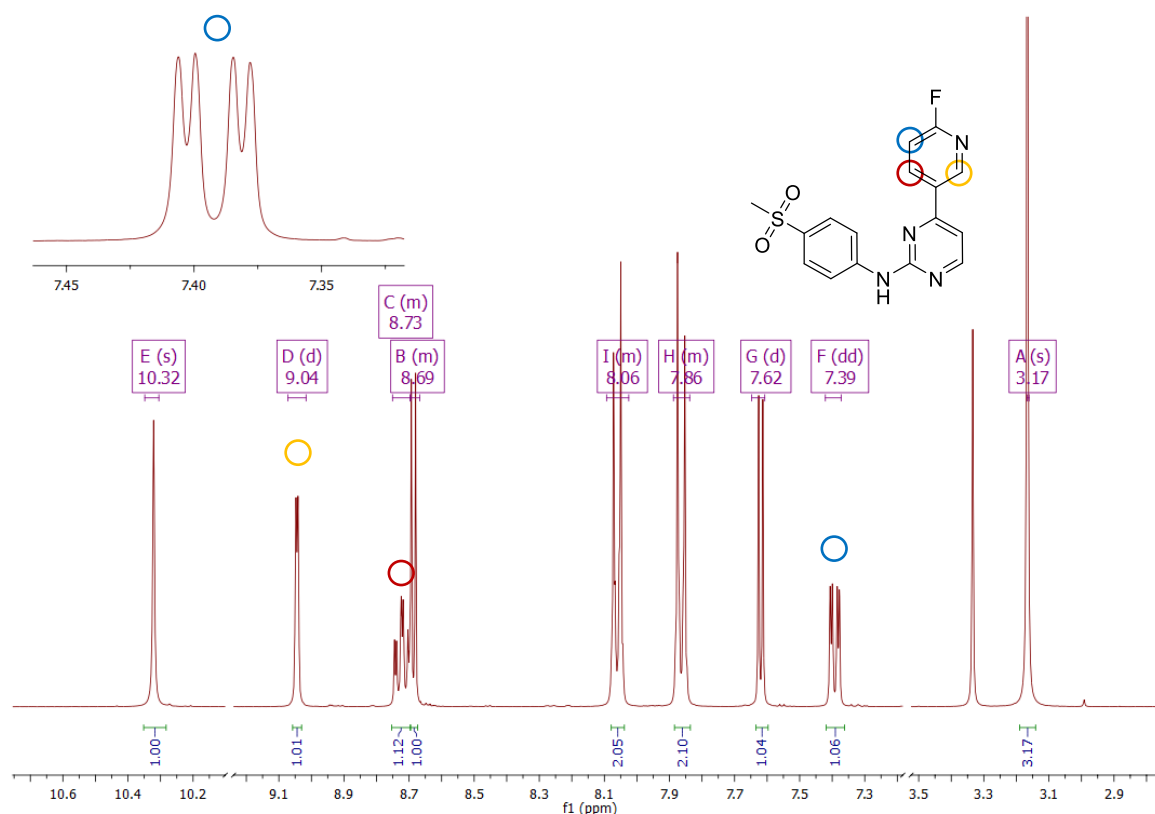


Figure 26 Representative ¹H-NMR (DMSO-*d*₆, 400 Hz) spectrum displaying a cutoff between 2.6 and 10.9 ppm. The doublet of doublet at 7.39 ppm is zoomed for detailed presentation. The signals resulting from the 2-fluoropyridine are highlighted with colors.

3.9. Thioimidazole series

3.9.1. Introduction of sulfur substituents

The initial hit RN2713 (**73**) was found as a Laufer group in-house library compound which was originally a side product from a S_NAr reaction of 2-substituted pyridines in a p38 MAP kinase project.

To gain more insight in the binding mode of thioimidazole compounds, a structural related derivative was investigated in the available crystal structure. Figure 27 shows the binding mode of the imidazole-based inhibitor SB203580 in a complex with p38. The main hydrogen bond is formed between the pyridinyl nitrogen, and the Met109 backbone NH of the protein. For the aspired goal of inhibiting p38 **73**, containing a pyridone structure, the hinge binding motif is altered due to inversed hydrogen bonding.^[81]

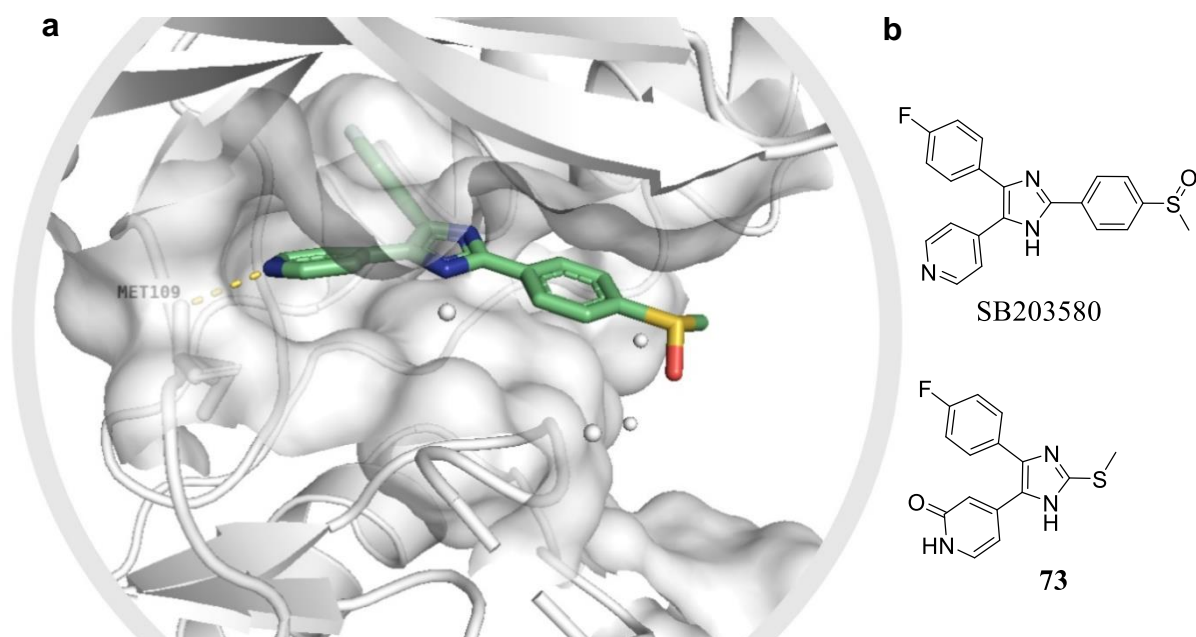
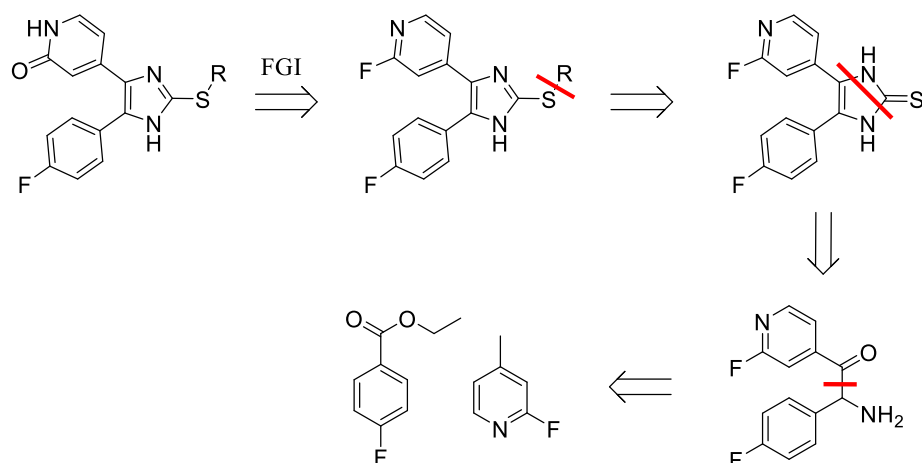


Figure 27 (a) Crystal structure of SB203580 (green) in complex with p38 MAP kinase (PDB ID: 3GCP)^[82]. Residues that show polar interactions (dashed yellow lines) with the ligand are labeled in the figure. (b) Structure of SB203580 and **73**.

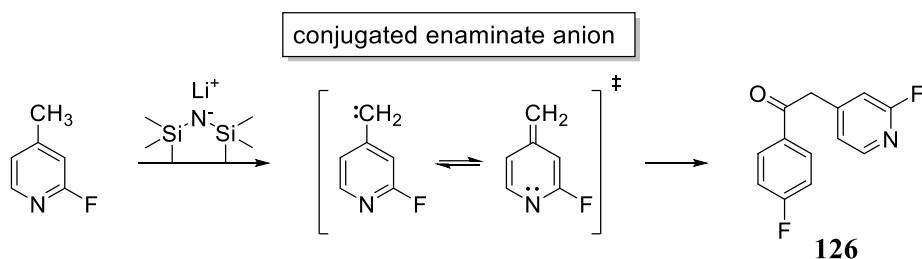
Various approaches have been proposed to prepare imidazole-based compounds.^[83] Depending on the desired substitution pattern imidazoles can be synthesized by ring closing strategies or regioselective introduction of functionalized substituents.^[84] In order to analyze the influence on the substitution of the imidazole-C₂-thio position, the synthetic route should offer a possibility to add different substituents to the previously prepared thio-structure in one of the final synthetic steps.

Guenther *et al.* had investigated a synthetic route, where the heterocycle of the 2-thioimidazole is closed by Marckwald cyclisation and therefore offered the desired synthetic approach.^[85] The retrosynthetic analysis of the thioimidazole-based scaffold is shown in Scheme 23. In the first step the pyridone structure of the 5-position is interconverted in the corresponding functional group of 2-fluoropyridine moiety. After retrosynthetic breaking of the thioether bond in 2-position of the imidazole, the imidazole ring is disconnected in a *retro*-Marckwald-cyclisation and yielded the corresponding α -aminoketone. This can be prepared from deprotonating the methyl group of 2-fluoro-4-picoline and ethyl 4-fluorobenzoate.



Scheme 23 Retrosynthetic analysis of thioether derivatives of imidazole. Red lines indicate a breaking bond. FGI = functional group interconversion.

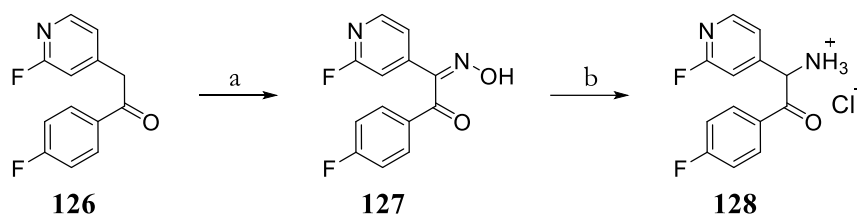
The synthetic route started from the two compounds 2-fluoro-4-picoline and ethyl 4-fluorobenzoate derived from the retrosynthetic analysis. Due to the presence of the nitrogen, the methyl-group of 2-fluoro-4-picoline could be easily deprotonated in 4-position using a strong base like LiHMDS to yield the conjugated enamine anion (Scheme 24).^[86] The resonance stabilized structure could be used to interact with the ethyl ester to provides the desired intermediate **126** in very good yields (93%).



Scheme 24 Reaction path to 1-(4-fluorophenyl)-2-(2-fluoropyridin-4-yl)ethan-1-one **126** via conjugated enamine anion equilibrium.

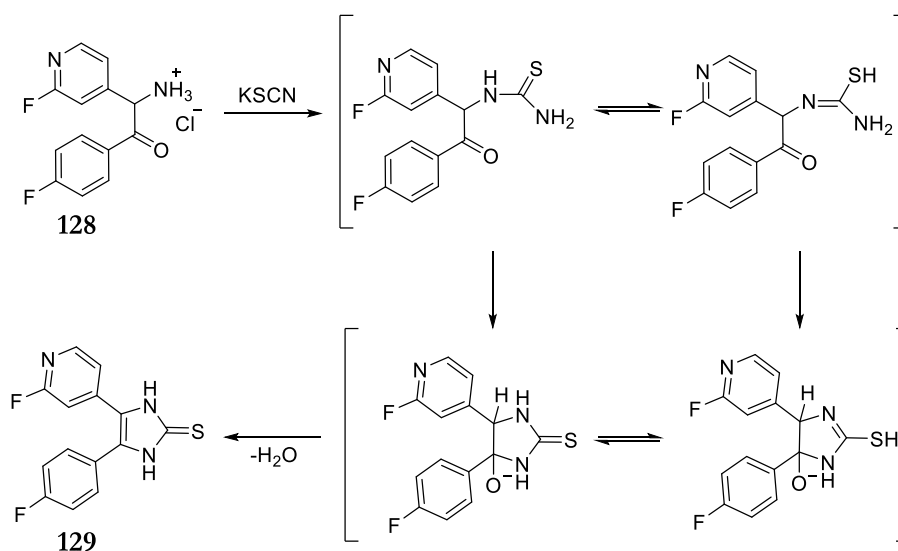
In the second step the precursor for thioimidazole ring-closing could be achieved by nitrosation and subsequently reduction from oxime to amine (Scheme 25). **126** could be transferred to the corresponding oximinoketone **127** by nitrosation of the α -methylene group with sodium nitrite in glacial acetic acid in moderate yields of 61%.^[81] The reduction of this oxime was described by Wagner *et al.* using hydrogen and palladium on carbon under acidic conditions.^[81] Although nucleophilic replacement of the 2-fluoro position of the pyridine is outlined as a side reaction in some solvents, the reduction could not be

reproduced in high yields. The main limitation of this step could be the low solubility of the oximinoketone. However, the oxime could be reduced with zinc dust in formic acid/MeOH over 20 hours. **128** could be precipitated from ethyl acetate as a salt by adding HCl in 1,4-dioxane (4N).



Scheme 25 Reaction path to **128**: (a) NaNO_2 , glacial acetic acid, 10 °C, 61%; (b) Zn dust, MeOH/formic acid, 10 °C, 34%.

As previously stated, there are several approaches for imidazole cyclization. Depending on the substitution pattern of the imidazole in 2-, 4- or 5-position, different starting materials can be chosen. The condensation of an α -dicarbonyl with an aldehyde and ammonia is called Radziszewski reaction.^[87] This procedure seemed to be favorable aiming to synthesize imidazole heterocycles with carbon based substituents in 2-position. For the desired 2-thioimidazoles the condensation of potassium thiocyanate and the salt of α -aminoketones **128**, a Marckwald-like heterocyclization, had been published.^[88]

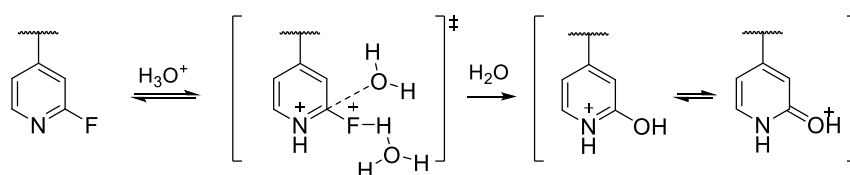


Scheme 26 Marckwald imidazole cyclisation: Condensation of the HCl salt of 2-amino-1-(4-fluorophenyl)-2-(2-fluoropyridin-4-yl)ethan-1-one with potassium thiocyanate.^[89]

Scheme 26 depicts the proposed mechanism of the condensation of the HCl salt **128** with potassium thiocyanate, including two equilibrium states. The first equilibrium is described as a thion/thiol-tautomerism leading to the ring closure with an exocyclic sulfur atom. The final product **129** exists as well as both thione/thiol-tautomers, but is not shown for reasons of clarity.^[90]

Nucleophilic substitution of appropriate halogenoalkanes at the 2-position of thioimidazole represented the last step in the straightforward synthesis of alkylsulfanyl imidazoles. Therefore, **129** could be applied as important precursor for introducing new moieties on the exocyclic sulfur atom and was treated with potassium carbonate as a base and the corresponding halogenalkane in THF yielding **130 - 132**.

After nucleophilic substitution of the thione, the 2-fluoro-pyridine moiety was hydrolyzed under acidic conditions yielding the corresponding pyridone in moderate yields. A possible mechanism acid-promoted S_NAr-reaction is outlined in Scheme 27.



Scheme 27 Reaction mechanism of acid-promoted S_NAr-reaction of 2-fluoro-pyridine derivatives.^[91]

In the presence of an acid, water attacks the π-deficient pyridine in 2-position and displaces the fluorine atom to generate an ionic transition state, which further reacts with water to the desired pyridone/pyridol-tautomer. Finally compounds **133 – 135** could be obtained.

Table 5 Acid-promoted S_NAr-reaction of thioimidazole **133 - 135** and the corresponding yields.

Structure	No.	R =	Yield [%]
	133		75
	134		57
	135		32

Figure 28 illustrates the ^1H - and ^{13}C -NMR assignment including coupling constants derived from 2D NMR experiments (HSQC, HMBC) of compound **133**. Figure 28 a shows the proton signals resulting from the pyridone structure. The highlighted protons gave information about the positions of two quaternary carbons (blue) based on heteronuclear correlations. As shown in Figure 28 b, all carbons could be assigned due to the specific carbon-fluorine correlations which corresponded with related literature.^[92]

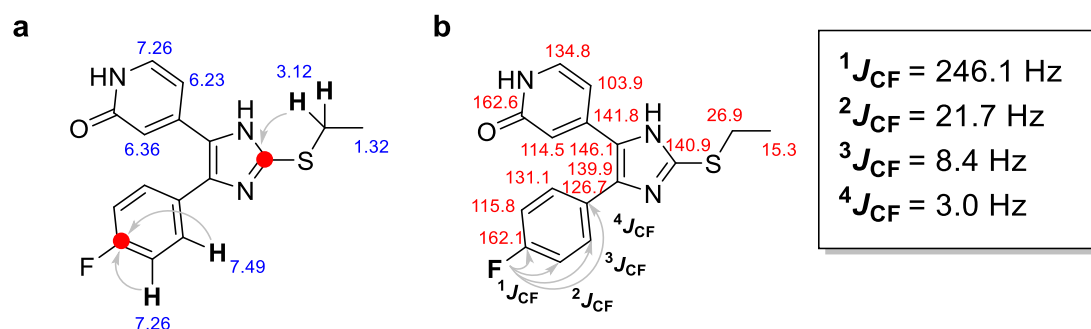


Figure 28 2D-NMR assignment of **133** (a) including proton (blue) and (b) carbon (red) shifts. Correlations between some carbons (red) and protons or fluorine and carbons are presented as grey arrows.

Interestingly, pyridone/pyridinol-tautomerism could be observed in the ^1H -NMR of **133** (Figure 29). Separate resonances from the three hydrogens in the pyridone ring can be seen in NMR time scale, especially for proton H_a and H_b . The resulting doublet is shifted by one ppm and gives insight in the tautomeric equilibrium. The dominant pyridone structure, favoured in the polar solvent DMSO, is present in the ration 3:2 to the compared pyridinol form.

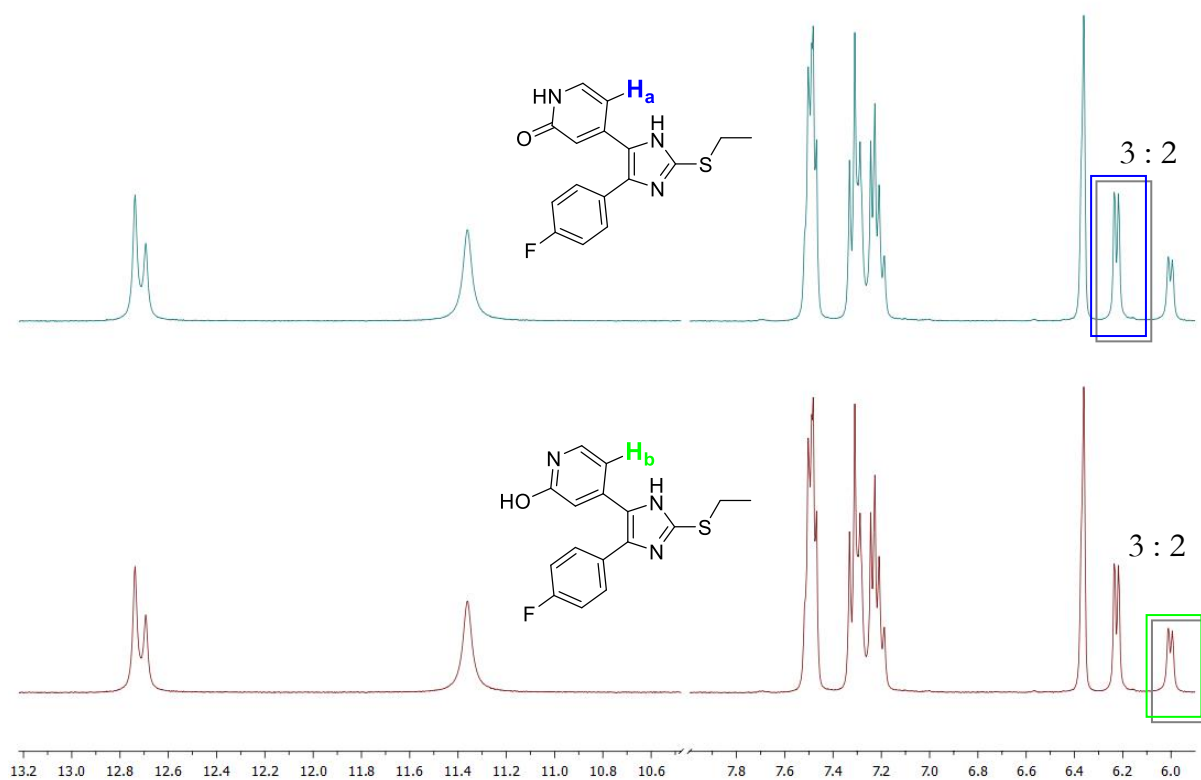


Figure 29 Comparison of the ¹H-NMR in the range of 6.0 to 13.2 ppm showing tautomers of **133**.

Further investigations of the pyridone/pyridol tautomerism were performed using HPLC. Figure 30 compares a freshly prepared solution of compound **133** in DMSO (a) with a solution of **133** in DMSO, which was stored for 5 days (b).

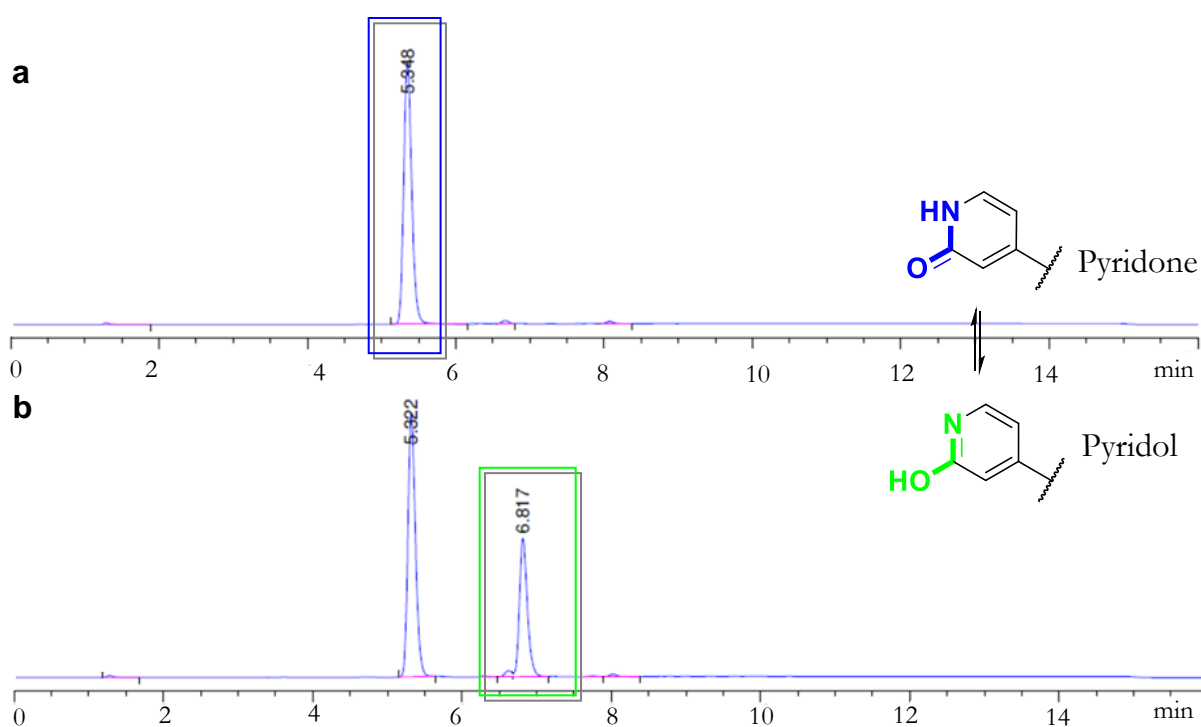


Figure 30 HPLC analysis of pyridone (green)/pyridol (blue)-tautomerism: (a) Compound **133** aliquot in DMSO. (b) Compound **133** aliquot in DMSO stored for 5 days.

Compound **133** was dissolved in DMSO and an aliquot was directly investigated using HPLC, showing only one peak with a retention time of 5.35 minutes. After storing compound **133** for 5 days in DMSO a stable equilibrium with the ratio 3:2 was set up and resulted in an additional peak in the HPLC after 6.82 minutes. As expected from the previous investigations using NMR technique, the additional peak which can be seen after 5 days is the pyridol form of **133** and supports the previously mentioned ratio of 3:2 of the equilibrium in from the NMR experiment.

The solvent dependency of tautomerism of 2-pyridone has been investigated by Miletti *et al.* in 2009. 2-Pyridones mainly exist in their oxo-form in water and other polar solvents such as DMSO. Analysing related crystal structures of ligands containing 2-pyridones in the Protein Data Bank (PDB) revealed that in complex with a protein only two structures contained a pyridol fragment and 24 interacted with the pyridone structure.^[93]

3.9.2. Introduction of ring-systems in 5-position of imidazole

In contrast to the previously described synthetic route to thioimidazole compounds differing in their thioether substitution pattern, the synthetic route to enable the substitution in 5-position of the imidazole core took a different approach. As earlier

described this moiety had been introduced in one of the first steps in synthesis because it was kept as an important interaction partner.^[94]

The following approach used a regioselective functionalization of the imidazole core instead of a cyclization reaction. This regiocontrolled synthesis was particularly useful to introduce the replaceable substituent in one of the final steps and therefore strategically important.

The following is a brief description of the synthetic route which started from imidazole and introduced substituents step by step based on the reactivity against halogen-metal-interactions, like lithium halogen exchange and C-C-cross coupling. Again, the reactivity can be predicted for cross-coupling and metalation reactions by electron deficiency of the bromo-carbon binding. Figure 31 shows this trend of reactivity of SEM-protected tribromoimidazole.

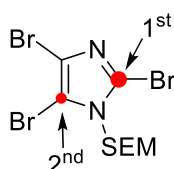
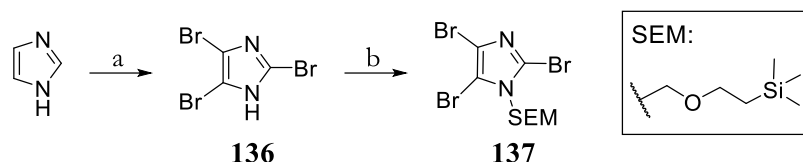


Figure 31 Predicted reactivity of tribromoimidazole for cross-coupling and metalation reactions.^[95]

For this approach, the protecting group must be stable to strong bases and direct metalation and ideally increase regioselectivity in the following steps. Protecting the nitrogen of imidazole with the 2-trimethylsilylethoxymethyl (SEM)-protection group was advantage because the SEM group can direct the metalation reaction with organolithium reagents selectively in a neighbouring position.^[96] Thus protection with SEM increases the selectivity of many reactions occurring on the imidazole scaffold. Also reactions with electrophiles (e.g. MeI in DMF) yield regioselective substituted products.^[97]

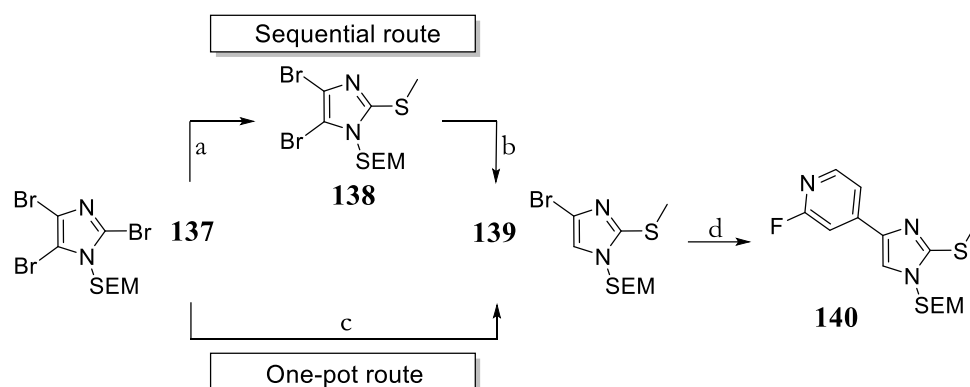
Scheme 28 illustrates the synthetic step to the key intermediate **137**. Bromination of imidazole was performed with Br₂ and a base in DMF and yielded the tribromo-species of imidazole **136**. In literature bromination with the common bromination reagent NBS led to a mixture of mono-, di- and tribromoimidazole.^[98] The desired product could be purely isolated by precipitation in water.



Scheme 28 Bromination and SEM-protection of 1*H*-imidazole. Reaction conditions: a) Br₂, KHCO₃, DMF, 0 – 70 °C, 61%; b) NaH, SEM-Cl, THF, RT, 42%.

In the next step the N-H group of imidazole was protected with SEM-Cl. SEM was introduced using sodium hydride as a base and yielded compound **137** in moderate yields. Now, the protected imidazole with three bromines **137** could be treated regioselective in the order of substitution 2-,4- and finally 5-position of imidazole using lithium halogen exchange.^[99]

As detailed in Scheme 29, the thiomethyl group was introduced in the first step by lithium halogen exchange in position 2 and subsequently adding dimethyl disulfide to yield **138**.^[100] Following second lithium halogen exchange in 4-position and quenching with water resulted in the mono brominated imidazole **139**, which could be used for Suzuki cross-coupling in the next step. The lithium halogen exchanges could be done in either a sequential route or a one-pot route.



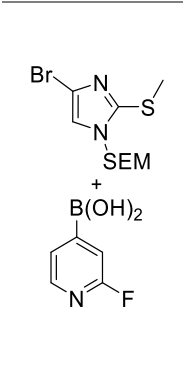
Scheme 29 Reaction path to **140** via sequential route or one-pot route. Reactions conditions: (a) *n*BuLi, DMDS, THF, -78°C - RT, 22 h, 95%; (b) *n*BuLi, THF, -78°C - RT, 15 min, 94%; (c) 1. *n*BuLi, DMDS, THF, -78°C - RT, 1 h; 2. *n*BuLi, THF, -78°C - RT, 17 h; (d) (2-Fluoropyridin-4-yl)boronic acid, K₃PO₄, XPhos Pd G4, 1,4-dioxane/water, 65 °C, 8 h, 80%.

The sequential route first introduced the thiomethyl group by adding one equivalent of *n*BuLi at low temperatures and subsequently dimethyl disulfide (DMDS). After stopping the reaction with HCl solution and purification, the intermediate **138** was once more treated

with one equivalent of *n*BuLi to exchange the second halogen in 4-position of imidazole. This procedure could be reduced to a one-pot route, where the addition of *n*BuLi was done in each case with one equivalent successively. Both procedures yielded the intermediate **139** in good to very good yields.

So far, the imidazole core structure had been edited to a point where all substituents can be introduced regioselective. The next step was the implementation of the 2-fluoro-pyridine moiety, which was later converted to the pyridone structure. This moiety could be introduced using Suzuki coupling conditions. Suzuki coupling with heteroaryl boronic acids usually suffer from protodeboronation, a formal hydrolysis of a boronic acid to the parent arene and boric acid.^[101] Protodeboronation can be avoided by less harsh coupling conditions, like weaker base or a different ligand system. The results from the screening of different reaction conditions for Suzuki coupling of **139** can be seen in Table 6.

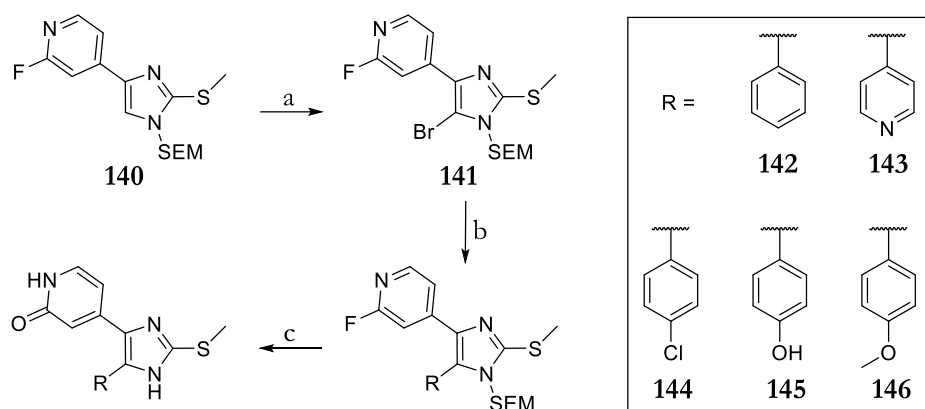
Table 6 HPLC analysis of optimal Suzuki conditions to yield **140**.

	<i>Ligand</i>	<i>Pd generation</i>	<i>Base</i>	<i>Yield</i> ^a
	dppf	-	K ₃ PO ₄	76%
	(<i>t</i> Bu) ₃	Pd G3	K ₃ PO ₄	89%
	XPhos	Pd G3	K ₃ PO ₄	60%
	(PPh ₃) ₄	-	K ₃ PO ₄	81%
	(<i>t</i> Bu) ₃	Pd G3	K ₂ CO ₃	73%
	(<i>t</i> Bu) ₃	Pd G3	KO <i>t</i> Bu	80%

^a Yield was calculated comparing absorption integrals of HPLC peaks at 254 nm.

Reaction conditions were compared using 1,4-dioxane/water as a solvent at 60 °C for 2.5 hours. In a small scale all reaction conditions afforded high yields, highlighting the combination (*t*Bu)₃ as a ligand and K₃PO₄ as base. In a large scale (more than 1 g of the imidazole compound) the yield did not fit to the results from the initial screen. Consequently, hypothesizing that the stability of the boronic acid was the limiting factor, (2-fluoropyridin-4-yl) boronic acid was added in small portions. This procedure increased the overall yield of **140** to 80%.

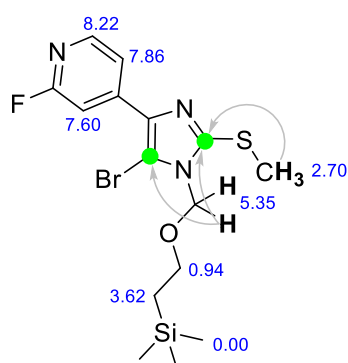
Scheme 30 depicts the last steps in the synthesis to 4-position aryl derivatives **142** - **146**.



Scheme 30 Synthetic route to final compounds **144** – **148** for aryl derivatization in 4-position of imidazole. Reaction conditions: (a) NBS, ACN, $-30\text{ }^{\circ}\text{C}$ -RT, 69%; (b) R-B(OH)₂, K₃PO₄, *t*BuXPhos, 1,4-dioxane/water (4:1, v/v), 17 h; (c) AcOH, $100\text{ }^{\circ}\text{C}$, 17 h.

The first step was the bromination of the 4-position of the imidazole derivative **140** to obtain **141**. In contrast to the previously described method, NBS was used for brominating of the 4-position. The reaction with NBS in acetonitrile was fast and the starting material is fully converted at $-30\text{ }^{\circ}\text{C}$ within one hour.

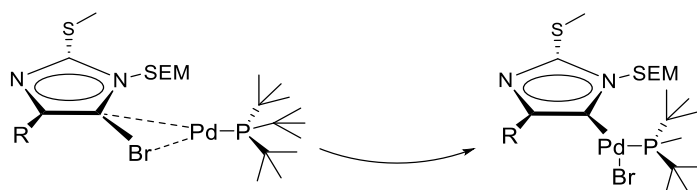
The NMR-assignment of the purified product **141** gave an insight in the regioselectivity described in previous chapters. Scheme 31 highlights the most important couplings derived from 2D-NMR (HSQC, HMBC) experiments.



Scheme 31 2D-NMR assignment of **141**. Correlations between carbons (green) and protons (shift in blue) are presented as grey arrows.

The alkyl-hydrogens from methylthio- and SEM-group at 2.70 and 5.35 ppm showed correlations to the adjacent quaternary carbons of the imidazole ring. This matched well with the hypothesis of the lithium halogen exchange occurring regioselectivity at 4-position and confirmed the influence of the neighboring SEM group.

The final step was proceeded using the same Suzuki conditions as earlier described. A possible side reaction was the dehalogenation of the imidazole-core. Additionally, the imidazole halide seemed to be a sterically demanding heterocyclic halide. Though bulky, electron-rich phosphine ligands like XPhos or P(*t*Bu)₃, could decrease side reactions.^[102] These ligands led to a mono-ligand-palladium species LPd(0), which had increase reactivity in the oxidative addition. The unsaturated 12e-palladium-complex drove the formation of the transition state shown in Scheme 32.^[103]



Scheme 32 Sterically hindered transition state of mono ligand complex Pd(0)[P(*t*Bu)₃] and aryl bromide.

After purification of the Suzuki product, the acidic hydrolysis was performed in refluxing acidic acid and yielded the pure final compounds **142** - **146** after precipitation from EtOAc/*n*hexane-mixture.

The described straightforward approach to substituted 2-thioimidazole could be used to obtain derivatives in 4- and 5- position of imidazole without the need of economically difficult ring closing strategies. Table 7 shows the structure of two additional compounds **147** and **148** derived from the compound library of the Laufer group, which have been used for comparison in the discussion of the structure-activity relationship of imidazole derivatives.

Table 7 Compounds **147** and **148** derived from an internal library similar to **73**.

No.	Structure	No.	Structure
147		148	

4. Results and discussion

4.1. Biological testing

For the determination of binding affinity to the protein target MKK4 a commercial binding assay from DiscoverX was used. Assay concentrations between 10 nM and 10 μ M have been used and are annexed to the table, respectively. All binding affinities were quantified using percentage of control (POC). High POC values up to 100 indicated low binding affinity to MKK4 and low POC values imply high binding affinity with the maximum of 0 (resolution limit).

4.1.1. Commercial KINOMEScan® binding assay from DiscoverX^[104]

Figure 32 illustrates the principle of the binding assay interaction between potential kinase inhibitors, a DNA-tagged kinase and an immobilised ligand on a bead.

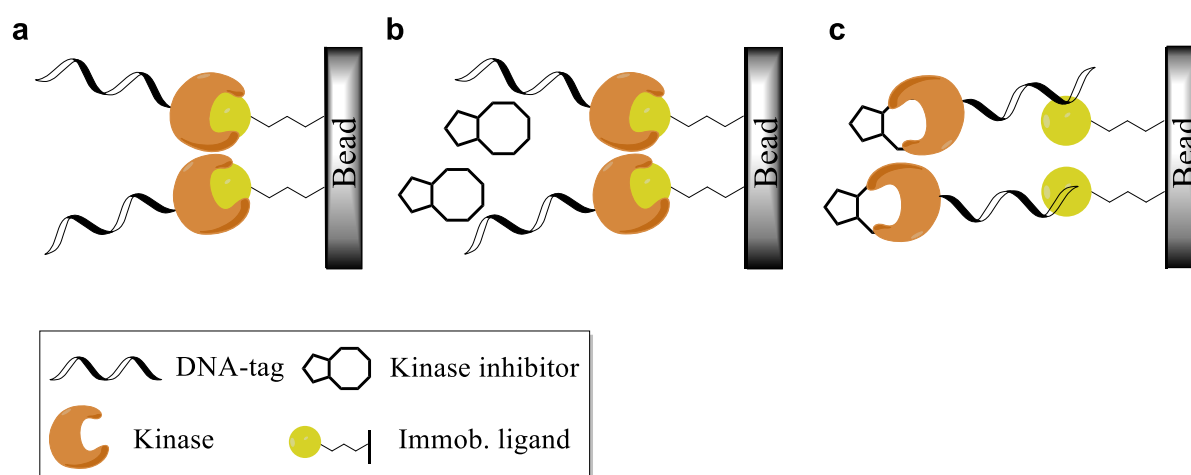


Figure 32 Principle of the KINOMEScan® binding assay for small-molecule kinase interaction by DiscoverX. (a) DNA-tagged kinase binds to immobilised ligand; (b) Additional kinase inhibitor is not able to displace the immobilized ligand; (c) Kinase inhibitor is able to displace immobilized ligand.

The binding assay is an active site competition assay without the presence of ATP and uses DNA-tagged kinases and immobilized ligands with a specific binding affinity to detect and determine binding affinity (Figure 32 a). In general, the displacement of the test inhibitor quantifies the binding affinity of the tested compounds. Compounds with lower affinity to the kinase than the utilized ligand are not able to bind to the DNA-tagged kinase (Figure 32 b). Compounds with a higher binding affinity than the immobilized ligand, reduce the amount of kinase connected to a solid phase (Figure 32 c).

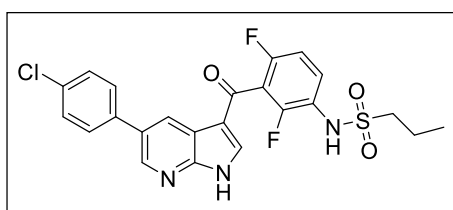
Binding affinity of the inhibitor is determined by measuring the amount of DNA-tagged kinase versus a control sample. Therefore, qPCR methods are used which detect associated DNA labels.

$$POC = \left(\frac{\text{test compound signal} - \text{positive control signal}}{\text{negative control signal} - \text{positive control signal}} \right) * 100$$

Equation 2 Calculation POC: test compound signal = synthesized test compound, negative control = DMSO (POC = 100), positive control (POC = 0).

4.2. Chemical probe for finding new MKK4 scaffolds

To address the binding pocket of MKK4 with a fluorescent probe, azaindole and carboline attached linker systems have been synthesised. For all tested linkage systems, the difluoro-moiety and the sulfonamide part of azaindole **1** are kept as substituents and were transferred to a α -carboline scaffold in 6-position. The former *para*-chlorophenyl moiety of **1** was utilized for implementing different linking systems and is attached in 3-position of the carboline and 5-position of the azaindole. The resulting binding affinity of the linker systems should decrease in the case of sterical clashes caused by the attached linkages or wrong positioning of the connection to the pharmacophoric group of **1**, since both scaffolds are known inhibitors of MKK4 with high affinities. Though earlier investigations using structure-activity relationships and MD-simulation confirm the assumption of positioning of the linkage substituting the *para*-chlorophenyl part. For comparing binding affinity, **1** serves as a reference compound with a POC^{MKK4} of 14 at a screening concentration of 100 nM (Figure 33).



1
 $POC^{MKK4} = 14$

Figure 33 Binding affinity of vemurafenib (**1**) to MKK4 at a screening concentration of 100 nM.

In the introduction the principles of fluorescence polarizations and the choice of 5-TAMRA as a fluorophore have already been explained in detail. Developing a suitable FP-screening-probe is an iterative process and should imply a balance between retained binding

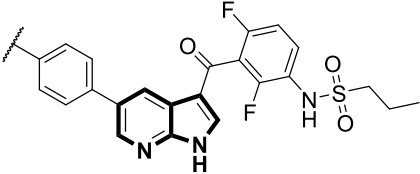
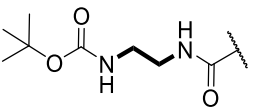
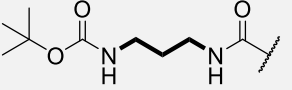
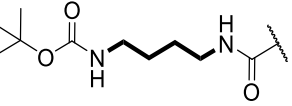
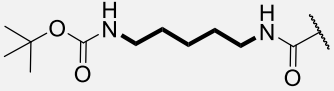
affinity of the scaffold and restricted movement of the attached fluorophore outside of the binding pocket guaranteed by the preferably shortest linker.

4.2.1. Comparison of azaindole Boc-protected precursors

Under the assumption that azaindoles and carbolines have a slightly different geometry in occupying the binding pocket of MKK4, the investigation regarding positioning and linker length for both scaffolds was investigated separately.

In order to assess a positioning of the linking systems for azaindoles, the influence on binding affinity for different spacer lengths was investigated. The results obtained from the preliminary analysis of the spacer length are presented in Table 8.

Table 8 Comparison of binding affinities of compounds **27** – **32**, containing azaindole scaffold, to MKK4 at a screening concentration of 100 nM.

No.	Structure	Spacer	POC
27		n = 1	15
29		n = 2	1.9
30		n = 3	2
31		n = 4	7.2
32		n = 5	5.3

The introduction of the shortest spacer system with n = 1 (**27**) showed almost the same binding affinity with a POC^{MKK4} of 15 as the reference compound **1** (POC^{MKK4} = 11). Increasing the spacer length from n = 2 – 5 (**29** - **32**), it is noticeable, that all linker systems

were well tolerated ($\text{POC}^{\text{MKK4}} < 7.2$) and the attachments had no adverse effect on binding affinity. Remarkably **29** and **30** had an excellent binding affinity, even higher than the reference compound **1**. Although the linker systems have a huge sterical demand, which could cause a clash with the protein, binding affinities remained high. Hence, introduction of a linker in 4-position of the former *para*-chlorophenyl of **1** was possible and stood implementations of linker system with a spacer length of $n = 5$.

4.2.2. Incorporation of 5-TAMRA for azaindoles

To further evaluate which spacer length would be the best for implementation of the bulky fluorophore, a selection of Boc-protected azaindoles with high binding affinity were used for fluorescent tagging with 5-TAMRA.

It seemed to be reasonable to connect 5-TAMRA with the shortest precursor with a spacer containing $n = 1$ carbon atoms. As already mentioned in the introduction, spacer length which position the fluorophore too far away from the binding site, lower the results of the FP assay, which is described as “propeller effect”. Although **27** was not the precursor with the highest binding affinity, its spacer length seemed to be long enough to attach 5-TAMRA Figure 34.

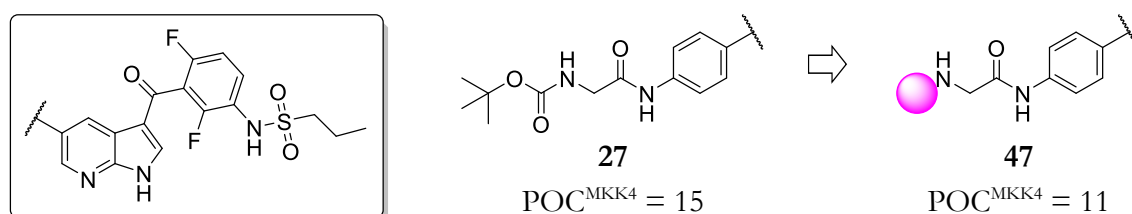


Figure 34 Effect of the incorporation of 5-TAMRA on binding affinity to MKK4.

With the implementation of the sterically demanding fluorophore 5-TAMRA to the shortest linkage (**27**), binding affinity remained sufficient with a POC^{MKK4} of 11 (**47**). It is a rather significant outcome that the binding affinity of fluorescent **47** (POC^{MKK4} of 11) was in the same range as the starting point **1** (POC^{MKK4} of 14) without any linkage.

4.2.3. 5-TAMRA tagged linkers systems

Knowing that the inclusion of the fluorophore is possible for azaindole **27**, the next step was to approach the optimal spacer length for each scaffold, by comparing binding affinity of all fluorophore-attached spacer systems.

Figure 35 summarizes the effect of the 5-TAMRA tag on a short ($n = 1$, **47**) and medium ($n = 4$, **48**) linker system on binding affinity.

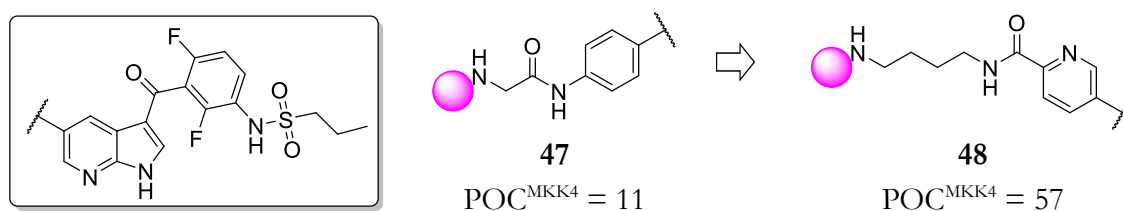


Figure 35 Comparison between short and medium linker length of azaindoles.

Surprisingly, the longer linkage **48** lacks binding affinity towards MKK4 with a POC of 57 and therefore **47** seemed to be the fluorescent compound of choice.

4.2.4. Incorporation of 5-TAMRA on the sulfonamide side of **1**

As a proof of concept, a negative feasibility analysis was done by synthesizing two fluorescent compounds which have been introduced to the scaffold of **1** close to the sulfonamide moiety at the other distal end of **1**.

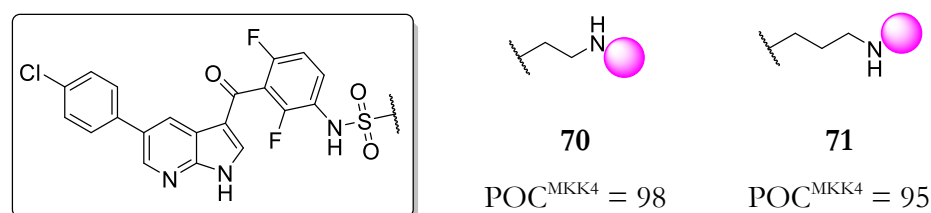


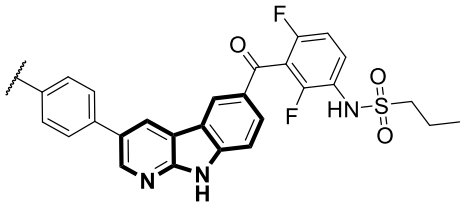
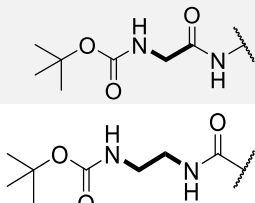
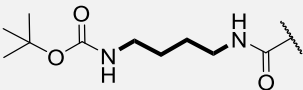
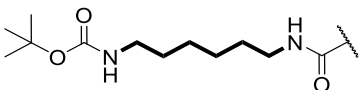
Figure 36 Comparison between $n = 2$ (**70**) and $n = 3$ (**71**) fluorescently tagged azaindoles close to the sulfonamide part of the molecule.

Both compounds **70** and **71** showed a complete loss of binding affinity to the target MKK4 ($\text{POC} > 95$). Although the incorporation of linker and fluorophore on the former *para*-chlorophenyl part was successful, this experiment proved the hypothesis about the orientation and binding mode of **1** to MKK4.

4.2.5. Comparison of carboline Boc-protected precursors

In comparison to the azaindole scaffold, carboline derivatives have a slightly different geometry due to the additional ring system close to the keto-bridge. Although both scaffolds share the same hinge-binding motif, it was assumable that the orientation of the linker system could be different. Therefore, the attachment of the linker system was also investigated for a selection of Boc-protected precursors containing a carboline scaffold (Table 9).

Table 9 Comparison of binding affinities of compounds **34**, **39** and **44** to MKK4 at a screening concentration of 100 nM.

No.	Structure	Spacer	POC
34		n = 1	9.2
36		n = 2	3.5
39		n = 4	5.2
44		n = 6	21

Similar to the results from the investigations of azaindole linker systems, almost all prepared linkages (**34** – **39**) were well tolerated and showed a high affinity with a POC < 9.2 to MKK4. Only the longest linker with n = 6 shows a slightly decrease of binding affinity in comparison to **1**.

4.2.6. Incorporation of 5-TAMRA for carbolines

Having in mind, that the shortest linker was sufficient to connect 5-TAMRA to the azaindole scaffold, the incorporation of the bulky 5-TAMRA fluorophore was evaluated between a short ($n = 1$) and medium spacer system ($n = 4$) (Figure 37).

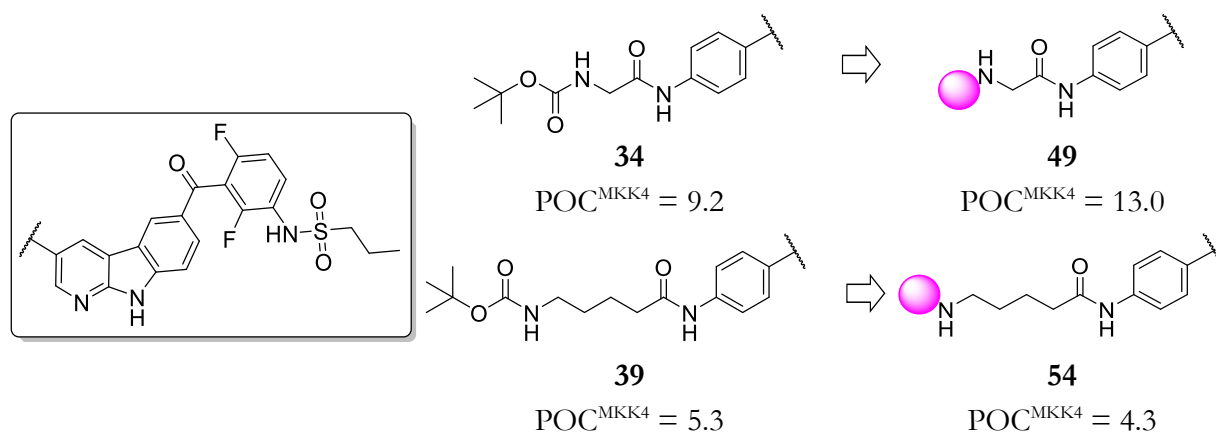


Figure 37 Comparison of the incorporation of 5-TAMRA to two carboline-based precursors with different lengths.

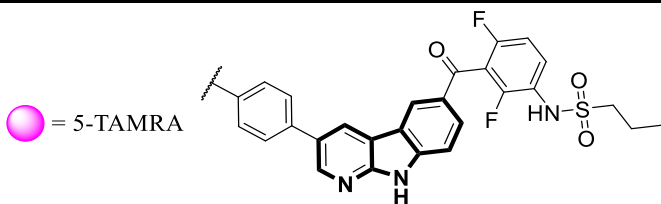
For the shortest spacer system, the binding affinity slightly decreased from a POC of 9.2 for the Boc intermediate **34** to 13 with incorporation of 5-TAMRA (**49**). It could be hypothesized, that for $n = 1$ there is a low steric repulsion resulting from the bulky fluorophore. Moving forward to the longer spacer length with $n = 4$, the incorporation of 5-TAMRA was tolerated and showed high binding affinity with a POC of 4.3 (**54**) to MKK4.

The trend of the binding affinity of the fluorophore tagged compounds with different scaffolds was not consistent. For carboline compounds the spacer length of $n = 4$ (**54**) seemed favourable, though for azaindole derivatives spacer length with $n = 1$ (**49**) had the highest binding affinity. The corresponding azaindole compound **54** with $n = 4$ had a decreased POC of 57 and a lower binding affinity on MKK4. Hence, the influence on binding mode of the additional phenyl ring in the scaffold of carboline seemed to be greater than expected.

These conclusions indicated that the bulky fluorophore was positioned outside of the binding pocket in the solvent area but maintained crucial interactions of the pharmacophore. This confirmed the hypothesis of the positioning and attachment of the

fluorophore which were made based on structural and computational investigations and gave a hint about the favoured linker system.

Table 10 Summary of all fluorophore tagged carboline compounds containing a phenyl linker core, investigated at a screening concentration of 100 nM.



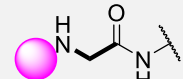
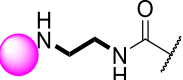
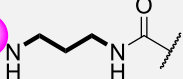
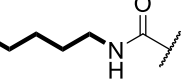
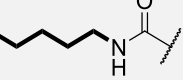
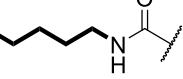
No.	Linker	Spacer	POC ^{MKK4a}
49		n = 1	13.0
51		n = 2	19.0
52		n = 3	13.0
54		n = 4	4.3
57		n = 5	32.0
58		n = 6	6.6

Table 10 summarizes all binding affinities from fluorescent carbolines (**49,51,52,54,57,58**). Carboline derivatives **52** (POC 4.3) and **58** (POC 6.6) possessed a sufficient binding affinity to MKK4. **49**, **51**, **52** and **57** had a decreased binding affinity compared to their corresponding Boc-protected precursors, which allowed to conclude that there is a steric repulsion with the fluorophore moiety with spacer systems having a shorter carbon length than n = 4. Thus compound **54** seemed to be a good compromise between linker length and remaining pharmacophoric affinity.

4.2.7. Influence on binding affinity of the linker core

For compound **54** with the highest binding affinity, further investigations with a different linker basis have been performed and are summarized in Figure 38.

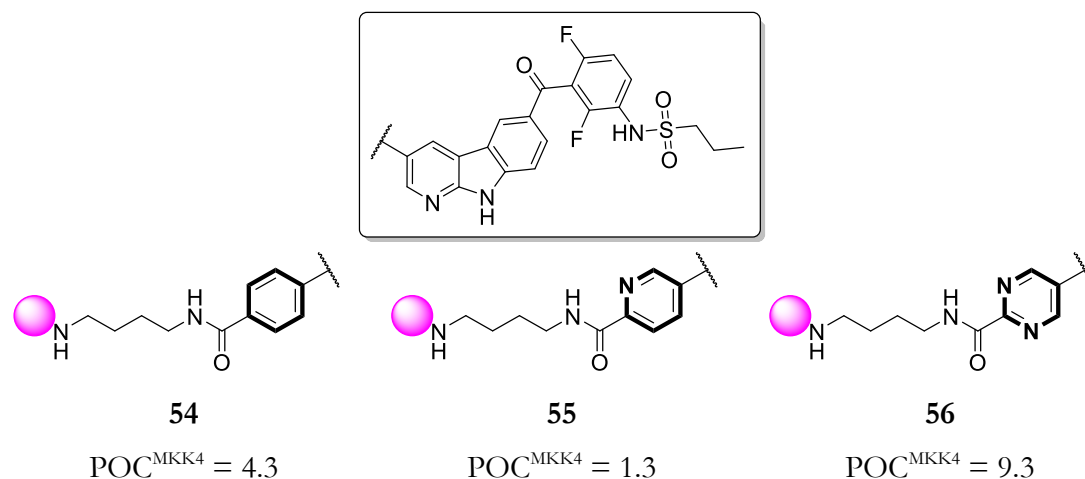


Figure 38 Comparison of compound **54** to the corresponding pyridinyl- (**55**) and pyrimidyl (**56**) compounds.

Binding affinity of **55** containing a pyridinyl core increased in comparison to corresponding phenyl derivatives **54**. This simple substitution seemed to have an additional interaction with the protein. The pyrimidyl compound **56** showed a slightly decreased binding affinity of 9.3 POC.

4.2.8. Further investigations of **47** and **55**

Having now two possible tool molecules with high binding affinity to MKK4 derived from an azaindole and carboline scaffold, these compounds were evaluated in a radiometric phosphorylation assay environment by measuring IC₅₀-values to gain insight in their binding properties. Figure 39 highlights potency of compound **47** and **55**.

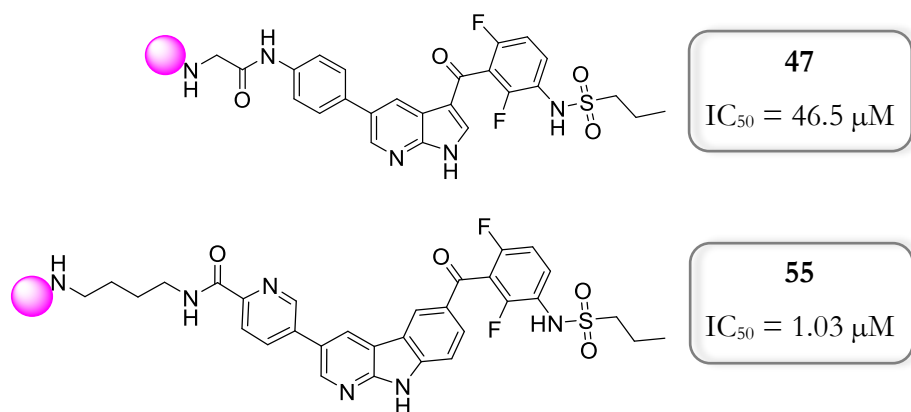
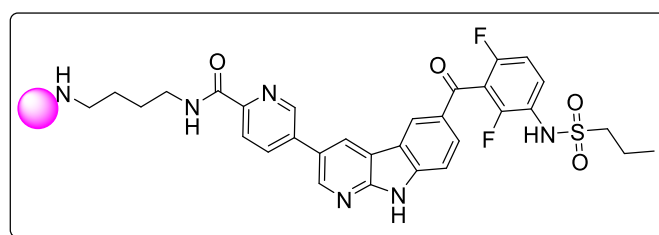


Figure 39 Comparison of potencies between compound **47** and **55**

Although chemical probes are not designed to have a clinical output, the potency of the fluorescently tagged ligand has a major influence on the validation of the fluorescence polarization assay. High potent ligands lower the required amount of protein or its concentration in the assay. Additionally, ligands with strong affinity to the target extended the range of inhibitory potency that could be resolved in the utilized assay. It was remarkable that both compounds showed a major difference in potency. Starting from the scaffold of **1**, the azaindole compound **47** (IC₅₀ = 46.5 μM) was inferior to the carboline compound **55** with a sufficient IC₅₀ of 1.03 μM. Compound **55** with the ideal linker length was further investigated at lower screening concentrations. Table 11 illustrates the binding affinity at three different concentrations.

Table 11 Binding affinity of **55** at three different screening concentrations.



55

Screening concentration:		
100 nM	30 nM	10 nM
POC ^{MKK4} = 1.3	POC ^{MKK4} = 4.1	POC ^{MKK4} = 18

Usually measuring binding affinity at 100 nM, compound **55** maintained high binding affinity at assay concentrations of 30 nM with a POC of 4.1. Even at 10 nM concentration the fluorescent tagged molecule had high affinity to the target.

Accordingly compound **55** excelled from the previously selected fluorescent compounds. With a high binding affinity and potency to inhibit MKK4 met the requirements (1.4.3, Considerations in FP-assay design) of a tool molecule.

4.2.9. Comparison of fluorescently tagged scaffolds azaindole and carboline

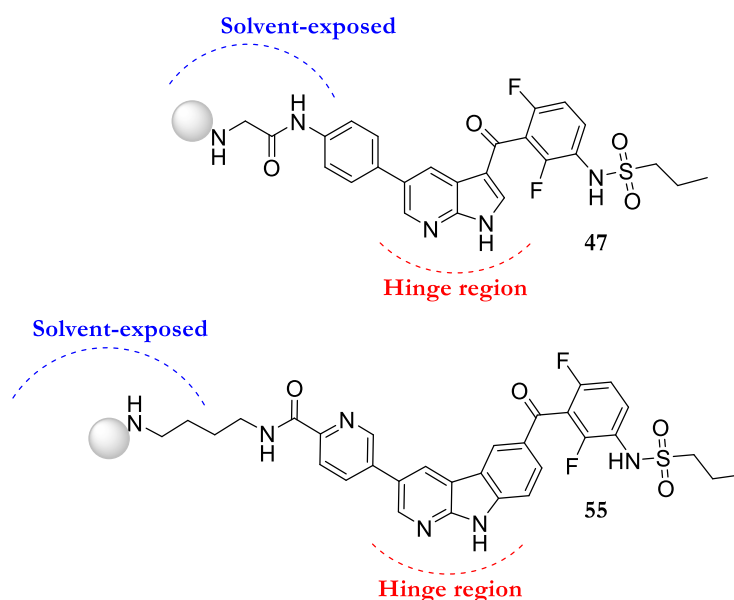


Figure 40 Differences of the occupied space of azaindole and carboline.

Figure 40 depicts the presumed occupancy of the two different scaffolds to MKK4. On the basis of the linker evaluation the additional ring system included in the carboline scaffold might lead to a slightly different occupation in the binding pocket. It was likely that carboline interaction was not as close to the solvent accessible area as it could be seen in azaindole interaction. This led to the requirement of a longer linker system possessing more flexibility to attach the fluorophore outside of the protein binding site for retaining binding affinity.

For further extending the binding properties of compound **55** MD-simulations were again performed for explaining the specific spacer length of the carboline scaffold. All docking experiments were done by Tatu Pantsar (University of Tübingen, University of Eastern Finland). Figure 41 shows the docking results of **55** bond to MKK4.

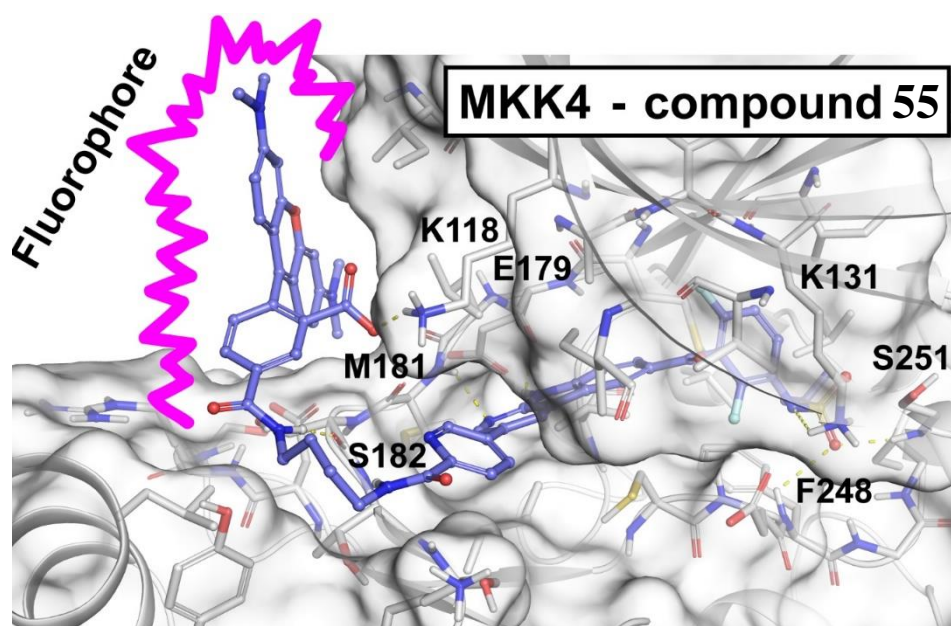


Figure 41 Docking pose of fluorescent compound **55** in MKK4 prepared by Tatu Pantsar. Residues that show polar interactions (dashed yellow lines) with the ligand are labeled in the figures.

Structural insights suggested that the bulky fluorophore 5-TAMRA was in the adjacent cleft outside the binding pocket of MKK4. The positively charged lysine residue, Lys118, seemed to form an ionic interaction with the negatively charged carboxylate group in the fluorophore fixating the ligand molecule. Therefore, previously theories about the solvent accessible area were disproven and underlined, that the phenyl-moiety in both scaffolds occupied the entrance of the binding pocket.

The selectivity profile (Figure 42) of compound **55** indicated no binding affinity to the off-target BRAF ($\text{POC}^{\text{BRAF}} = 92$) which was used as a starting point for the ligand design based on **1**. The superimposition of the docking pose of **55** bound to MKK4 and the crystal structure of BRAF in complex with **1**. Figure 42 demonstrated that BRAF is missing the hollow close to the binding pocket. This allowed the beneficial positioning of 5-TAMRA in MKK4 and explained the weak interaction between **55** and BRAF. Especially BRAF residues Asp479, Lys473, Trp531 and Glu533 showed sterical clashes with the attached fluorophore.

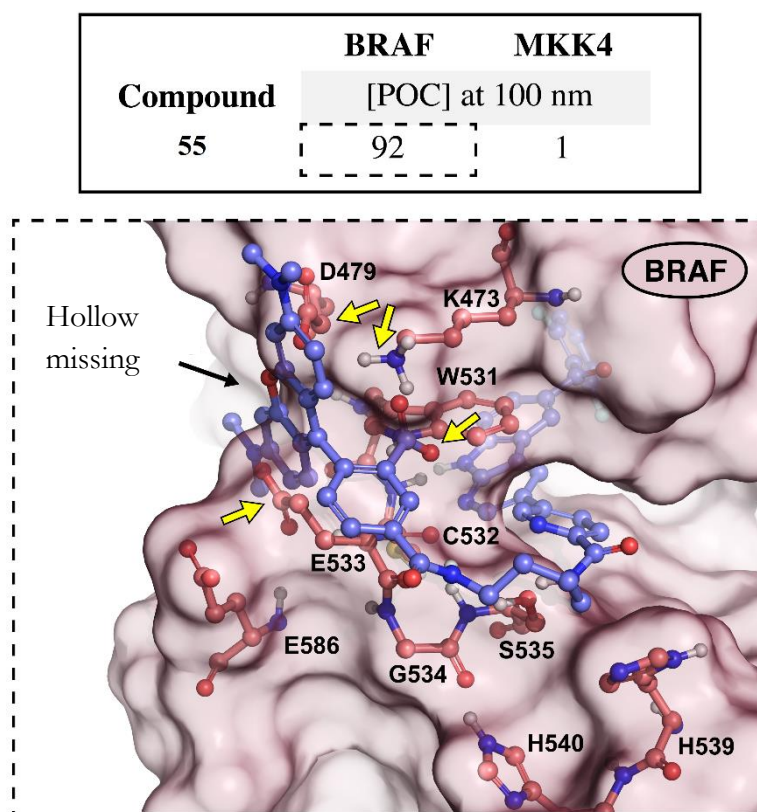


Figure 42 Superimposition of docking pose of **55** (purple) in MKK4 (hidden) and the crystal structure of BRAF (PDB ID: 4rzv)^[105]. The nearby amino acids of BRAF within 4Å of **55** are highlighted in red in the figure. The yellow arrows indicate the major sterical clashes between BRAF and **55**. The molecular surface of BRAF is shown in red.

4.3. Competition assay with known MKK4-inhibitors

4.3.1. Fluorescence polarization assay

To evaluate the usability of compound **55** as an FP-screening probe, assay related validations were performed. The assay development and measurements were executed by the Screening Unit of the Leibniz-Forschungsinstitut für Molekulare Pharmakologie in Berlin.

Previously SAR of vemurafenib-related compounds of earlier studies from the group have been used as a starting point for hypothesizing about the implementation of the dye. These studies yielded in a range of compounds differing in their binding affinity. Three compounds (BP762, PKL306, PKL608) derived from these studies have been used for a competition assay.

The FP-compound probe **55** was used at a concentration of 20 nM and MKK4 at 64 nM. Binding competition to MKK4 with BP762, PKL306 and PKL608 was tested in a concentration range from 12 nM to about 6 μ M.

With the developed probe pre-evaluation have been done to prove the reliability of the fluorescent probe in a competition assay with known MKK4-inhibitors. These three compounds, containing azaindole- and pyrazolo pyridine-cores, differ in their binding affinity to MKK4 and were designed in previous studies from the Laufer group. The positive control BP762 has a high binding affinity to MKK4 with a POC of 0.25 at a concentration of 100 nM and showed an EC_{50} -value of 31 nM. The reference compound PKL306 had a weaker binding affinity to MKK4 ($POC^{MKK4} = 11$) than **55** and showed a decreased EC_{50} -value of 164 nM. PKL608 was used as negative control ($POC^{MKK4} = 47$) and resulted in an EC_{50} -value of 628 nM. Using MKK4 at 64 nM and compound **55** at 20 nM in a competition binding experiment, all known inhibitors showed EC_{50} -values fitting their binding properties and could be properly classified.

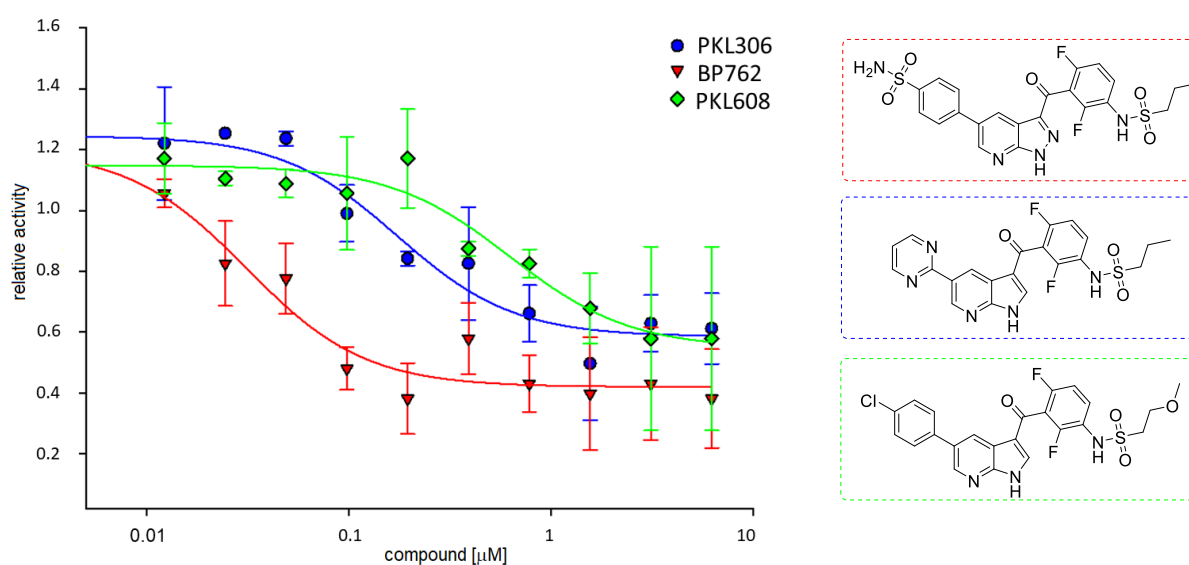


Figure 43 MKK4 Fluorescence polarization assay. Compound **55** in competition with MKK4 inhibitors BP762 (red), PKL306 (blue) and PKL608 (green) showed EC_{50} -values of 31, 164 and 628 nM respectively. The competition assay was performed at the Screening Unit of the Leibniz-Forschungsinstitut für Molekulare Pharmakologie in Berlin.

Both POC- and EC_{50} -values are compared in Table 12 and showed a proper correlation.

Table 12 Comparison of EC₅₀-values and POC-values of the three reference compounds BP 762, PKL306 and PKL608 at a screening concentration of 100 nM.

<i>Reference</i>	<i>POC^{MKK4}</i>	<i>EC₅₀ [nM]</i>
BP762	0.25	31
PKL306	11	164
PKL608	47	628

Additionally, the comparison demonstrated that the fluorescent compound **55** was able to identify potential inhibitors of MKK4 with a low nanomolar inhibitory potency.

Overall, the emerged compound **55** fulfilled the criteria of a FP-assay tool compound as an inhibitor of MKK4 with high binding affinity and a potency of 1.03 μ M. The implementation of this compound was investigated in a competition assay, using similar conditions as the HTS screening. Finally compound **55** was able to detect known inhibitors and classify their potency as expected from compared binding affinity.

4.4. Hit identification – High-throughput screen

4.4.1. Validation and performance of the HT screen

All assay related validations and evaluations for the fluorescence polarization HTS were done by the Screening Unit of Leibniz-Forschungsinstitut für Molekulare Pharmakologie (FMP). More than 7000 compounds from an in-house library and a commercially available Selleckchem compound library were screened against the developed fluorescent probe. The probe was able to identify more than 100 primary hits. Three of the most promising hits are described and displayed in

Figure 44.

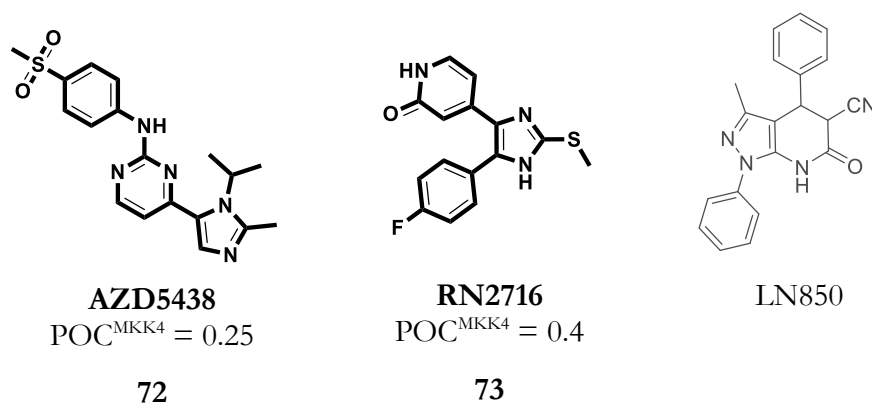


Figure 44 Three compounds found as a hit in a fluorescence polarization assay and the corresponding binding affinities at a screening concentration of 1 μ M.

To evaluate the reliability of these compounds found in the HTS fluorescence polarization screen, the selection of hits has been re-evaluated by determination of their binding affinity at 1 μ M to MKK4.

Compound LN850, part of the in-house compound library, was excluded from the selection because it was found to be not stable in solution and started to degrade after a short time in DMSO.

RN2716 (**73**) was part of a project with the aim to address the p38 MAP kinase with a pyridine as hinge binding motif. **73** was found as a side product of a cyclisation reaction, where the ring closure of the imidazole core immediately merged with an intermolecular methyl-group transfer from 2-methoxy-pyridine to the thiol next to the imidazole ring. The resulting pyridone structure has an altered hinge binding motif and could interact with MKK4 in a favourable way.

In the introduction some published MKK4 inhibitors have already been mentioned. Regarding its three-dimensional structure, it is known, that active MKK4 has a small lipophilic binding pocket close to the hinge region, which is preferentially occupied with aromatic residues such as benzyl or indazole (1.2.2 Improving existing drugs).^[23,26] Driven by the ability to attach bulky linker systems close to the hinge region, it could be hypothesized that the entrance to the binding pocket is shallow. STD-NMR-studies of pazopanib which was presumably connected to the hinge with an aminopyrimidine

structure indicate, that the 4-position of the pyrimidine core offered space for introducing sterical demanding moieties.^[26]

Thus **72** and **73** have been selected for further investigation and structure-activity relationship studies.

4.5. Investigation of aminopyrimidine-based **72**

72 had a restricted chemical tractability, especially regarding its imidazole residue in 4-position of the pyrimidine. This residue left no room for generating a large quantity of compounds (Figure 45).

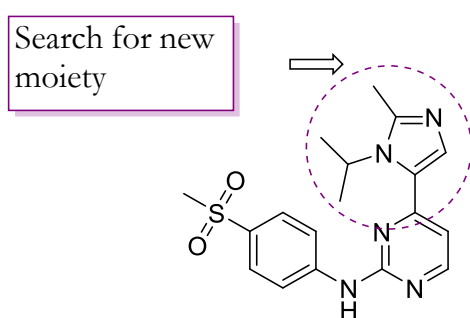
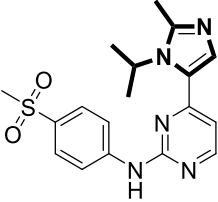
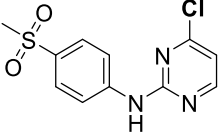


Figure 45 Structure of **72** containing 2- and 3-substituted imidazole residue in 4-position.

As already discussed in detail in the Chemistry part, substitution of the residue in 4-position was easily accessible and planning to new compound was straight forward and could be implemented rapidly.

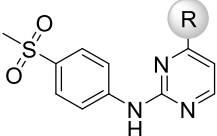
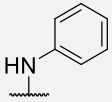
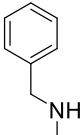
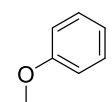
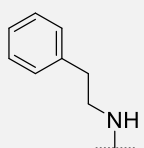
For analysing the influence of the imidazole residue, this heterocyclic ring was removed and the synthetic precursor with a chloro atom in 4-position was investigated (Table 13).

Table 13 Influence of the removal of the imidazole ring on binding affinity at a screening concentration of 1 μM .

	
72	76
$\text{POC}^{\text{MKK4}} = 0.4$	$\text{POC}^{\text{MKK4}} = 90$

The removal of the imidazole core caused a loss of binding affinity towards MKK4, and consequently had a significant contribution to its binding to the kinase. Closer investigations of the crystal structure of **72** bound to its on-target CDK2 showed, that the isopropyl residue is interacting favourably with the hydrophobic pocket in the ATP-ribose binding domain. An edge-to-face interaction between isopropyl and Phe close to the cleft explained the high binding affinity. This observation suggested that this branched aliphatic chain was also pointing to a lipophilic area in MKK4. To enable the envisioned interaction different bridge elements for ring systems have been synthesised to target the hydrophobic back pocket (Table 14).

Table 14 Compound **72** containing a substituted imidazole residue in 4-position of the pyrimidine.

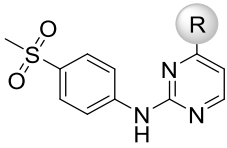
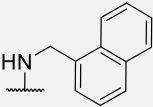
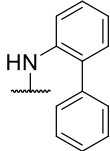
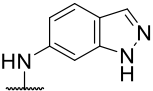
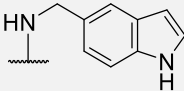
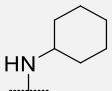
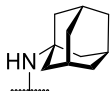
					
Screening concentration: 1 μM					
No.	R =	POC^{MKK4}	No.	R =	POC^{MKK4}
77		73	79		62
78		15	80		62

All compounds containing a nitrogen- or oxygen-bridge ring system (**77**, **79** and **80**) had a low binding affinity towards MKK4 at a screening concentration of 1 μM . Only compound

78 containing a phenol, had a moderate binding affinity with a POC of 15. The discrepancy between aniline **77** and phenol **78** could be traced back to the loss of resonance stabilization for phenol and the resulting increased acidity of the hinge binding nitrogen of the pyrimidine thus influencing the ability to interact with the hinge region.

As previously reported SAR indicated that a back pocket can be addressed with lipophilic residues, the available space close to the hinge was investigated by synthesizing sterical demanding aromatic and aliphatic rings differing in 4-position of the aminopyrimidine scaffold (Table 15).

Table 15 Binding affinities of substitution of 4-position of aminopyrimidine **72** using S_NAr conditions.

					
Screening concentration: 1 μ M					
No.	R =	POC ^{MKK4}	No.	R =	POC ^{MKK4}
81		100	84		60
82		28	85		70
83		46	86		62

The annulated ring **81** with an additional CH_2 -group had no binding affinity at a screening concentration of 1 μ M to the target. Compound **84** with an isolated ring system (biphenyl) showed a higher binding affinity (POC = 60) than **81** (POC = 100). Nitrogen containing annulated heterocycle **85** showed only moderate binding affinity. Nevertheless, the previously reported indazole derivative **82** derived from pazopanib showed good binding affinity at a screening concentration of 1 μ M with a POC of 28 in comparison to the other bulky ring-systems. Somewhat unexpected the strongly lipophilic cyclohexyl containing **83** showed a moderate binding affinity and even the introduction of an adamantyl-substituent with a high sterical demand showed a moderate binding affinity. These results support the previously mentioned assumption that the aminopyrimidine scaffold could be improved by introducing bulky lipophilic residues in 4-position.

Seeking further improvement, the phenol core derived from **78** was selected for further derivatization as it bore a promising binding affinity (POC of 15 at a screening concentration of 1 μ M). Thus, the binding affinity of derivatives of **78** was investigated by generating a broad range of compounds differing in their electronic and lipophilic properties, shown in Table 16.

Table 16 Binding affinities of phenol substituted derivatives of **72**.

Screening concentration: 0.1 μ M								
<i>No.</i>	<i>R=</i>	<i>POC</i>	<i>No.</i>	<i>R=</i>	<i>POC</i>	<i>No.</i>	<i>R=</i>	<i>POC</i>
			78	2,3,4-H	15 ^a			
96	2-F	100	107	4-CN	78	118	4-NH-COCH ₃	99
97	3-F	100	108	2-S-CH ₃	100	119	3-COOH	81
98	4-F	100	109	4-S-CH ₃	96	120	4-COOH	100
99	2-Cl	100	110	2-O-CH ₃	100	121	2-NH ₂	96
100	3-Cl	98	111	3-O-CH ₃	100	122	3-NH ₂	100
101	4-Cl	100	112	4-O-CH ₃	98	123	4-NH ₂	99
102	2-NO ₂	100	113	2-CH ₃	100	124	2-SO ₂ CH ₃	100
103	3-NO ₃	100	114	3-CH ₃	100	125	4-SO ₂ CH ₃	100
104	4-NO ₃	92	115	4-CH ₃	91			
105	2-CN	100	116	2-NH-COCH ₃	89			
106	3-CN	100	117	3- NH-COCH ₃	98			

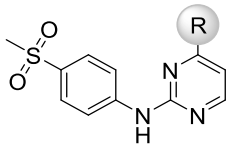
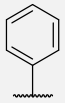
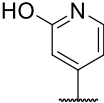
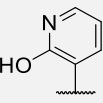
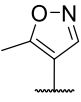
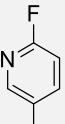
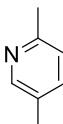
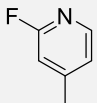
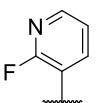
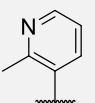
^aScreening concentration: 1 μ M.

The collection of compounds based on a rational design approach, where *ortho*-, *meta*- and *para*-position were varied with functional groups are differing in their electronic and mesomeric effects. Unfortunately, all compounds **96** – **125** showed almost no binding affinity to MKK4 at a screening concentration of 100 nM and therefore no structure-activity conclusion could be drawn from the obtained results.

Further modifications included the C-C-connection between the pyrimidine core in 4-position and nitrogen-containing heterocycles. This approach based on the reduced degree

of freedom by removing the nitrogen- or oxygen-containing connectivity element. Thus, different ring equivalents to imidazole have been introduced in 4-position of the pyrimidine core resulting in compounds **87** – **95** (Table 17).

Table 17 Binding affinities of C-C-coupled derivatives in 4-position of **72**.

								
Screening concentration: 0.1 μ M								
No.	R =	POC ^{MKK4}	No.	R =	POC ^{MKK4}	No.	R =	POC ^{MKK4}
87		31 ^a	90		94	93		99
88		96	91		100	94		83
89		100	92		63	95		100

^aScreening concentration of 1 μ M.

Substitution of the imidazole with a related isoxazole **88** resulted in a loss of binding affinity. Pyridines with the nitrogen in 4-position (**89** and **90**) showed no binding affinity to the target. Having the nitrogen in 3-position only **92** showed a moderate binding affinity with a POC of 63 in comparison to **91**, **93**, **94** and **95** (POC > 83). It is noticeable that not the position of the nitrogen contributed to improved binding affinity, but the position of the fluorine atom in 2-position.

4.6. Investigation of imidazole-based **73**

Moving now to compound **73** with a POC^{MKK4} of 60 at a screening concentration of 100 nM, this trisubstituted imidazole showed a promising starting point for further improvement of the binding affinity to the target MKK4. Therefore, characteristic structural elements were chemically changed.

Researching literature the structure of hit **73** has been reported with no activity to its on-target p38.^[81] Additionally only one patent was describing pyridone moiety attached to thioimidazoles as kinase inhibitors for targeting Janus kinase and therefore this scaffold had an interesting structure lacking information about its interaction.^[106]

Regarding the chemical flexibility, thioimidazole **73** offered four positions for chemical modifications illustrated in Figure 46.

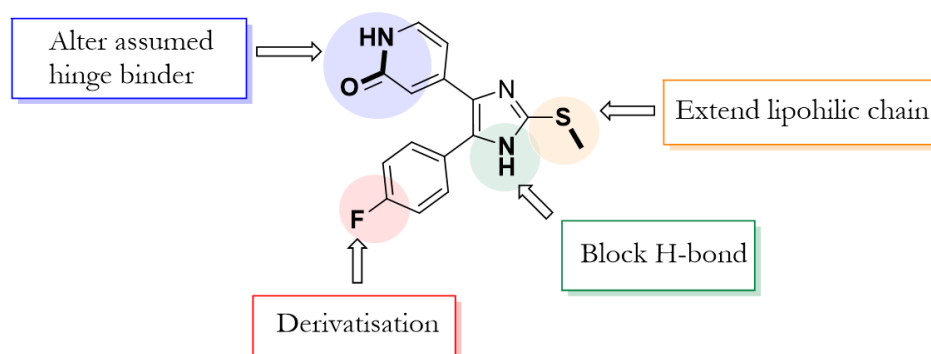


Figure 46 Structure of compound **73**. Chemical alterations are highlighted.

Four different sides of interaction were evaluated starting with the imidazole ring. The significance of the potential H-bond interaction arising from the imidazole nitrogen could be analysed by blocking **73** with a methyl-group attached to the nitrogen.

Table 18 compares the binding affinities of the unsubstituted imidazole ring **73** with the methylated species **147**.

Table 18 Comparison of binding affinities between unsubstituted imidazole **73** and methylated **147** at a screening concentration of 1 μ M.

	<i>No.</i>	<i>Structure</i>	<i>POC^{MKK4}</i>
	73		0.4
	147		100

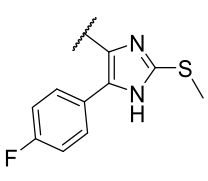
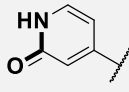
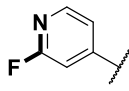
The binding affinity to MKK4 decreased significantly from a POC of 0.4 to no observed binding affinity at a screening concentration of 1 μ M for the methylated **147** with a POC of 100. Unfortunately, this left no space for the introduction of residues and capability of

tetrasubstituted imidazoles as MKK4 inhibitors. Nevertheless, it could be assumed that this specific hydrogen was interacting favourably with the protein and was crucial for improved binding affinity.

As regards the assumed hinge binding motif, pyridone/pyridol tautomerism was already investigated in detail in the Chemistry part. The favoured equilibrium state in solution is highly dependent on the solvent. Under physiological conditions in water the pyridone/pyridol-tautomerism favours the pyridone structure with a protonated nitrogen.^[107]

In order to elaborate the interaction of the pyridone residue as a putative hinge binding motif, Table 19 compares the pyridone moiety with a 2-fluoro-pyridine residue at a screening concentration of 0.1 μM .

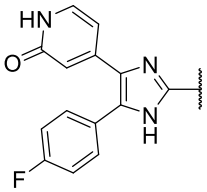
Table 19 Comparison of binding affinities between pyridone **73** and 2-fluoro-pyridine **148** containing derivatives at a screening concentration of 0.1 μM .

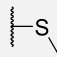
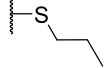
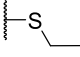
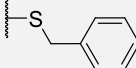
	No.	Structure	POC^{MKK4}
	73		60
	148		92

148 was easily accessible as it is the precursor of pyridone **73**. Remarkably this change had a major influence on the binding affinity considering that the hydrogen bond donor switches to an acceptor and vice versa. The comparison between **73** ($\text{POC}^{\text{MKK4}} = 60$) and **148** ($\text{POC}^{\text{MKK4}} = 92$) presented a loss of binding affinity to MKK4, pointing out that the protonated nitrogen served as hydrogen bond donor and the oxygen as the acceptor.

This crucially observation was important since the structure subjects tautomerism in solution and therefore the binding affinity decreases due to a percentage of **73** in its pyridol state.

Turning now to the exocyclic sulfur atom, its influence on the binding affinity was investigated by extending the aliphatic side chain length with ethyl, propyl and benzyl (Table 20).

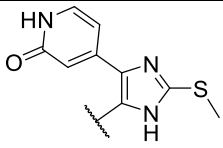
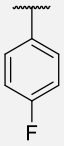
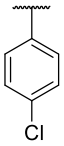
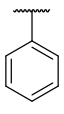
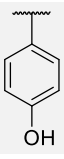
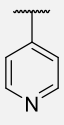
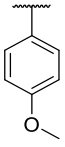
Table 20 Binding affinities of thioimidazole substituted derivatives **133** – **135** compared to **73** at a screening concentration of 0.1 μM .


No.	Structure	POC ^{MKK4}	No.	Structure	POC ^{MKK4}
73		60	134		98
133		68	135		87

Extension of the residue next to the thioimidazole from methyl to ethyl was tolerated and remained high binding affinity with a POC of 68 (**133**). Substitutions with larger residues such as propyl (**134**) with a POC of 98 or benzyl (**135**, POC = 87) resulted in lower binding affinities to MKK4. Thus, keeping the methyl residue on the sulfur atom seemed to be beneficial.

As structural data of a complex between a derivative of **72** and p38 was available, investigations were made regarding the environment of the *para*-fluorophenyl moiety. Hypothesizing that this residue occupies a special hydrophobic pocket, the fluorine atom was substituted with certain residues differing in specific interaction patterns such as lipophilicity and electronic values. Table 21 gives an overview about the relating binding affinities of compounds **142** - **146**.

Table 21 Binding affinities of compounds **142** – **146** in comparison with **73**.

					
No.	Structure	POC ^{MKK4}	No.	Structure	POC ^{MKK4}
73		60	144		100
142		26	145		100
143		96	146		68

Starting from the parent structure of **73**, exchanging fluorine (POC = 60) with the related chloro atom (**144**) decreased binding affinity significantly to a POC of 100. Although both residues are lipophilic, chlorine has an increased van der Waals radius comparing to fluorine. Also, the introduction of a polar residue in *para*-position represented by a phenol-group (**145**) had no observed binding affinity to MKK4 (POC = 100). Surprisingly the methoxy-derivative **146** recovered the binding affinity similar to the starting point **73** with a POC of 68. Removing the residue in *para*-position (**142**) significantly improved binding affinity (POC = 26), which was almost as high as for **1** (POC = 14). Although fluorine and hydrogen resemble each other, hydrogen has a smaller van der Waals radius. Additionally, introducing a pyridinyl-residue (**143**) instead of a *para*-fluorophenyl decreased binding affinity from a POC of 60 to 96.

In summary, the replacement of the imidazole moiety of compound **72** was reasonably accessible by synthesis, the changes with NH- or O- connected aromatic moieties did not result in a compound with strong binding affinity. Also, the replacement with bulky ring-systems and non-classical bioisosters resulted in a decrease in binding affinity. Nevertheless, the results contribute to a clearer understanding of the back pocket of MKK4. Additionally, the imidazole residue featured important lipophilic interactions with the protein. The

observed decrease in binding affinity could be attributed to the geometry of the imidazole ring containing a branched isopropyl chain, which forces the residue in a rigid conformation in the binding pocket and interacts with the protein favourably. The imidazole residue was therefore presumably accommodated in a hydrophobic back pocket, which appeared in outlines recently.

Summing up, investigation of **73** led to early SAR. Hypothesizing that the pyridone structure serves as a hinge binding motif, there were two possible occupations for the phenyl-residue in 5-position of the imidazole, a hydrophobic back pocket, or a solvent accessible pocket next to the hinge region. Having in mind, that introducing residues in *para*-position was not favourable, it might be reasonable, that this residue protruded into a small hydrophobic back pocket similar to the described binding mode for imidazole derivatives in p38. In future it could be beneficial to exchange the aromatic ring system with branched aliphatic chains. This approach needs a new synthetic design and was out of the scope of this study.

Two essential interactions were elaborated for binding to MKK4. The imidazole nitrogen provides an acidic hydrogen for H-bond interaction to the protein and the pyridone structure could serve as a possible hinge binding motif. Extending aliphatic chains next to the sulfur atom outside of the imidazole ring up to ethyl is tolerable, propyl and benzyl had almost no binding affinity. Gratifyingly the removal of the *para*-fluoro-residue at the aromatic ring in 5-position of the imidazole improved binding affinity, hypothesizing, that this residue occupied a small lipophilic back pocket.

5. Summary of the results

In order to assess the attachment of the bulky dye 5-TAMRA to MKK4 inhibitors with retained binding affinity, previously published SAR of vemurafenib derivatives were investigated. Starting with an azaindole scaffold, spacer length was tolerated up to a chain length of $n = 5$ in *para*-position of the former chlorophenyl moiety of **1** with a Boc-protection group and did not decrease the binding affinity. The incorporation of the dye was optimal for a spacer length of $n = 1$. As a proof of concept, the incorporation of the dye on the opposite part of **1** (sulfonamide) resulted in a complete loss of binding affinity. Unfortunately, the best azaindole compound **47** ($n = 1$) with a POC of 11 (conc. 100 nM) showed a low IC_{50} -value of 46.5 μ M. Regarding the carboline scaffold, linker inclusion up to spacer lengths of $n \leq 4$ was feasible in *para*-position of the former chlorophenyl moiety. Surprisingly, the incorporation of the dye was ideal for a spacer length of $n = 4$ (**54**) with a POC of 4.3 (conc. 100 nM). Changing the linker basis from phenyl to pyridinyl (**55**) slightly increased binding affinity (POC of 1.3, conc. 100 nM). Additionally compound **55** showed an IC_{50} -value of 1.03 μ M. Further analysis at lower screening concentrations revealed, that compound **55** retained high binding affinity, even higher than the starting point **1**. Thus, the most promising compound **55** is an applicable probe for an fluorescence polarization high-throughput screening (Figure 47).

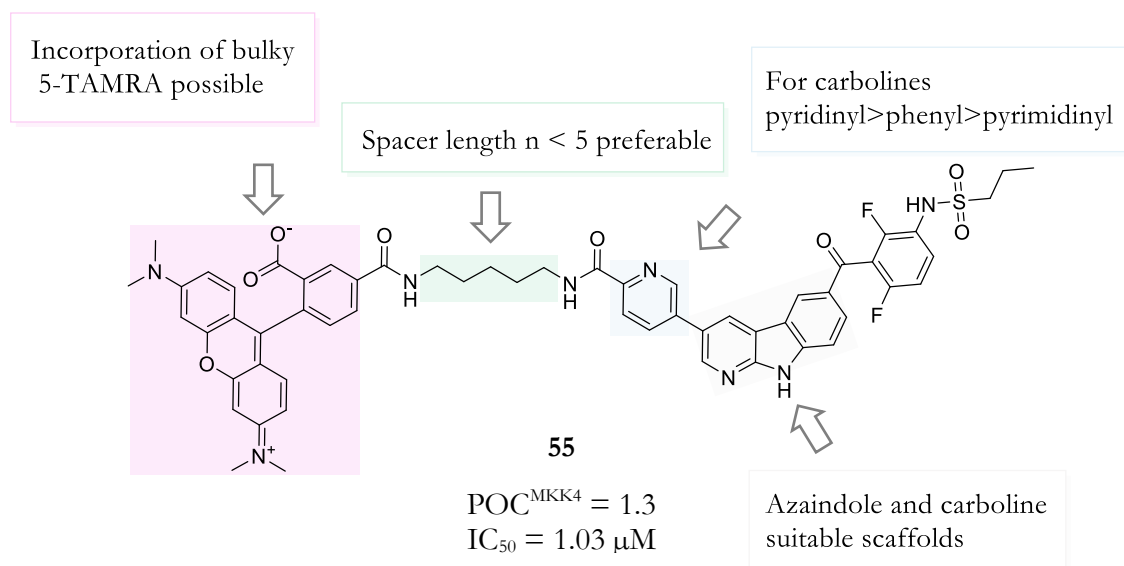


Figure 47 Structure and elaborated properties of compound **55**.

The correlation between binding affinity and potency was validated by a competition assay with known MKK4 inhibitors and showed consistency between binding affinity and potency of the compounds. The applicability of compound **55** was thus demonstrated. In the final HTS-assay the fluorescent probe was able to identify certain aminopyrimidine-based compounds and revealed imidazole-derivatives as novel unknown MKK4 inhibitors. For two selected hits a fast and efficient synthesis was established which yielded a broad range of compounds in a short time.

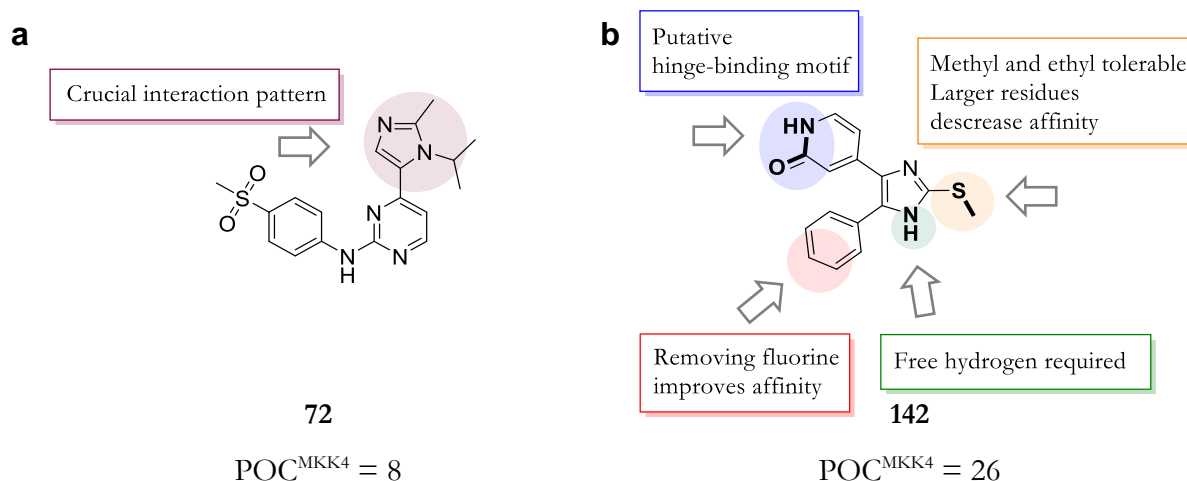


Figure 48 Summary of early SAR investigation (a) Structure of hit **72**, highlighting the crucial interaction pattern of the residue in 4-position of the aminopyrimidine. (b) Structure of compound **142**, important interactions are highlighted. For both compounds a screening concentration of 100 nM has been used.

Starting from hit compound **72**, different ring equivalents, phenol- and aniline derivatives were introduced in 4-position of the aminopyrimidine, substituting the imidazole-moiety. No significant increase in binding affinity was found compared to compound **72** ($\text{POC} = 8$, conc. 100 nM). Notwithstanding, these results confirm the crucial interaction pattern of the imidazole-moiety to a hypothesized lipophilic back pocket.

The SAR from imidazole-based compound **73** was significantly meaningful. Substituting the pyridone moiety ($\text{POC} = 60$, conc. 100 nM) with the precursor 2-fluoro-pyridine resulted in a considerable decrease in binding affinity ($\text{POC} = 92$, conc. 100 nM). Presumably the pyridone structure serves as hinge binding motif. Extending the methyl group on the sulfur atom, only ethyl was tolerable ($\text{POC} = 68$, conc. 100 nM), while larger residues such as propyl and benzyl decreased binding affinity ($\text{POC} \geq 87$, conc. 100 nM). Additionally, the hydrogen attached to the imidazole ring seemed to have important

interactions, since blocking the imidazole with a methyl-group resulted in a loss of binding affinity. Due to sterical hindrance, substitution of the *para*-position of the aromatic moiety in 5-position of the imidazole was only tolerated for the unsubstituted phenyl-derivative **142**. Finally compound **142** with a POC of 26 (conc. 100 nM) showed high binding affinity to MKK4.

In the framework of this thesis a vemurafenib-inspired fluorescent probe was developed with high binding affinity to MKK4 and optimal positioning of the bulky fluorophore 5-TAMRA to guarantee utilization in a FP-screening meeting essential requirements. The probe revealed a novel scaffold for MKK4 inhibition and contributed to existing knowledge of the binding mode of MKK4 by early SAR investigation of two selected hit compounds.

6. Experimental methods

6.1. Materials and methods

Materials: All reagents and solvents are commercially available from Acros Organics, Activate Scientific, Alfa Aesar, BLD Pharm, ChemPUR, Fluka, Fluorochem, Sigma Aldrich, Tokio Chemical Industry Co. and were used without further purification.

NMR: ^1H and ^{13}C NMR spectra were obtained with Bruker Avance 200, Bruker Avance 400 or Bruker Avance 600. The spectra were obtained in the indicated solvent and calibrated against the residual proton peak of the deuterated solvent. Chemical shifts (δ) are reported in parts per million.

Mass Spectrometry: Mass spectra were obtained by TLC-MS (ESI) and from the Mass Spectrometry Department (HRMS), Institute of Organic Chemistry, Eberhard Karls Universität Tübingen.

TLC: Analyses were performed on fluorescent silica gel 60 F₂₅₄ plates (Merck) and visualized under UV illumination at 254 and 366 nm.

Column Chromatography. Column chromatography was performed on Davisil LC60A 20–45 μm silica from Grace Davison and Geduran Si60 63–200 μm silica from Merck for the precolumn using an Interchim PuriFlash 430 automated flash chromatography system.

HPLC: The purity of all compounds is, unless otherwise stated, >95% and was determined via reverse-phase high-performance liquid chromatography on Hewlett-Packard HP 1090 series II LC equipped with a UV diode array detector (DAD, detection at 230 and 254 nm or 430 nm). The chromatographic separation was performed on a Phenomenex Luna 5u C8 column (150 mm \times 4.6 mm, 5 μm) at 35 °C oven temperature. The injection volume was 5 μL , and the gradient of the used method was the following (flow, 1.5 mL/min), with 0.01 M KH_2PO_4 , pH 2.3 (solvent A), MeOH(solvent B): from 40% B to 85% B in 8 min, 85% B for 5 min, from 85% to 40% B in 1 min, 40% B for 2 min, stop time 16 min.

IR-Spectroscopy: IR spectra were measured using Thermo Scientific Nicolette 380-FTIR and Agilent Cary 630 FTIR Spectrometer. Transmission peaks are reported in cm^{-1} .

Biological assays: All compounds were investigated by a commercial binding assay by DiscoverX (Kinomescan™) at a screening concentration of 100 nM which uses an immobilised ligand competing with the measured compound for the kinase.

MKK4 Fluorescence Polarization assay

Table 22 MKK4 Fluorescence Polarization assay. Presented are relative activities in relation to the non-inhibited interaction of compound 55 and MKK4.

conc. MKK4 [μM]	BP762		PKL306		PKL608	
6.25	0.07	0.30	0.49	0.33	0.16	0.59
3.13	0.10	0.36	0.49	0.36	0.16	0.59
1.56	0.07	0.33	0.16	0.43	0.40	0.56
0.78	0.16	0.30	0.40	0.53	0.59	0.66
0.39	0.30	0.46	0.76	0.49	0.66	0.69
0.20	0.26	0.10	0.63	0.66	0.86	1.09
0.10	0.23	0.33	0.72	0.86	0.72	0.99
0.05	0.49	0.66	1.05	1.02	0.92	0.86
0.02	0.72	0.53	1.05	1.05	0.89	0.92
0.01	0.82	0.89	1.15	0.89	0.89	1.05

6.2. General procedures

A Amide coupling:

To a suspension of 4-bromobenzoic acid (1 eq), the corresponding Boc protected amine (1.1 eq) and triethylamine or DIPEA (2 or 3 eq) in DMF was added HATU (1 eq). The reaction mixture was stirred at room temperature until TLC indicated complete conversion of the starting material. Then the reaction mixture was diluted with EtOAc, washed with water, and saturated sodium chloride solution and dried over sodium sulfate. The organic layer was dried over sodium sulfate and the solvent was evaporated under reduced pressure. Column chromatography (PE/EtOAc, v/v, 25-75%) yielded the pure product.

C Suzuki coupling α -carboline:

N-(2,4-difluoro-3-(3-(4,4,5,5-tetramethyl-1,3,2-dioxaborolan-2-yl)-9*H*-pyrido[2,3-*b*]indole-6-carbonyl)phenyl)propane-1-sulfonamide (1 eq), the corresponding Boc protected amine

(1.1 eq) and K_2CO_3 (2 eq) were suspended in 1,4-dioxane/water (1:1, v/v) and purged with argon for 15 minutes. Subsequently $Pd(PPh_3)_4$ (5 mol%) was added and stirred under microwave irradiation (50 W, 110 °C) for 40 minutes. Showing full consumption of the starting material, EtOAc was added, and the organic layer was washed with water and saturated sodium chloride. The organic layer was dried over sodium sulphate and the solvent was removed under reduced pressure. Column chromatography (DCM/EtOAc, v/v, 0-65%) yielded the pure product.

Suzuki coupling azaindole

N-(3-(1-(2,6-dichlorobenzoyl)-5-(4,4,5,5-tetramethyl-1,3,2-dioxaborolan-2-yl)-1*H*-pyrrolo[2,3-*b*]pyridine-3-carbonyl)-2,4-difluorophenyl)propane-1-sulfonamide (1 eq), corresponding Boc-protected bromo derivative (1.1 eq) and K_2CO_3 (2.5 eq) were suspended in 1,4-dioxane/water (4:1, v/v) and purged with argon for 20 minutes. Subsequently $Pd(dppf)Cl_2$ (5 mol%) was added and stirred at 55 °C until TLC revealed full consumption of the starting material. Then the solvent was removed under reduced pressure and the crude product was dissolved in MeOH and excess K_2CO_3 was added. After 4 hours EtOAc was added, and the organic layer was washed with saturated ammonium chloride solution and saturated sodium chloride. The organic layer was dried over sodium sulphate and the solvent was evaporated under reduced pressure. The pure product could be obtained after column chromatography (DCM/MeOH, v/v, 0–6%).

Suzuki coupling amino pyrimidine

4-Chloro-*N*-(4-(methylsulfonyl)phenyl)pyrimidin-2-amine (1 eq), corresponding boronic acid (1.1 eq) and K_2CO_3 (2.5 eq) were suspended in 1,4-dioxane/water (4:1, v/v) and purged with argon for 20 minutes. Subsequently $Pd(dppf)Cl_2$ (5 mol%) was added and the reaction mixture was stirred at 55 °C until TLC revealed full consumption of the starting material. Then EtOAc was added, and the organic layer was washed with saturated ammonium chloride solution and saturated sodium chloride. The organic layer was dried over sodium sulphate and the solvent was evaporated under reduced pressure. The pure product could be obtained after column chromatography (PE/EtOAc, v/v, 10–50%) and recrystallization in EtOAc and *n*hexane.

D Amide coupling 5- TAMRA derivatives:

The corresponding Boc protected amine (1.5 eq) was deprotected in toluene/TFA (10:1, v/v) and stirred for 17 hours. Then the solvent was evaporated under reduced pressure and the residue was dissolved again in DMF (0.5 mL) and DIPEA (excess). The mixture was added to a solution of 5-TAMRA (1 eq) and HATU (1 eq) in DMF. After 17 hours at room temperature the solvent was removed under reduced pressure. The crude product was purified using column chromatography to obtain the pure product as a purple solid.

B Nucleophilic aromatic substitution:

To a solution of 4-chloro-*N*-(4-(methylsulfonyl)phenyl)pyrimidin-2-amine (1 eq) in DMF and K₂CO₃ (3 eq) was added an excess of the corresponding nucleophile (amine, aniline or phenol) and heated up to 150 °C for 1 – 17 hours. After full consumption of the starting material the mixture was cooled to room temperature, diluted with EtOAc and washed with water. The organic phase was dried over sodium sulphate and concentrated. After column chromatography (PE/EtOAc, v/v, 25-75%) the desired compounds could be received as white solids in good purity (>95% judged by HPLC).

E Suzuki coupling imidazole and acidic hydrolysis:

4-(4-Bromo-2-(methylthio)-1-((2-(trimethylsilyl)ethoxy)methyl)-1*H*-imidazol-5-yl)-2-fluoropyridine (1 eq), the corresponding boronic acid (1 eq) and K₃PO₄ (3 eq) were suspended in 1,4-dioxane/water (4:1, v/v) and purged with argon for 15 minutes. Subsequently the *t*BuXPhos Pd G3 (2 mol) was added and stirred under argon (50 W, 110 °C). After TLC analysis the boronic acid (1-3 eq) was added in portions until TLC indicated full consumption. Then EtOAc was added and the organic layer was washed with water and saturated sodium chloride. The organic layer was dried over sodium sulphate and the solvent was removed under reduced pressure. Column chromatography (DCM/EE, v/v, 0-65%) yielded the pure product. Subsequently the pure product was dissolved in glacial acetic acid (2-4 mL) and heated to reflux until HPLC revealed full consumption. The solvent was removed under reduced pressure and the crude product was recrystallized from EtOAc and *n*hexane.

F S-alkylation of mercaptoimidazole and acidic hydrolysis

The corresponding alkylhalide (1.2 eq), 4-(4-Fluorophenyl)-5-(2-fluoropyridin-4-yl)-1,3-dihydro-2*H*-imidazole-2-thione (1 eq) and K₂CO₃ (1.2 eq) were suspended in dry THF (2-5 mL) and heated to reflux until TLC revealed full consumption of the thione. The cooled solution was diluted with EtOAc and washed with saturated ammonium chloride solution and water. The organic layer was dried over sodium sulphate and the solvent was removed under reduced pressure. Column chromatography (PE/EtOAc, v/v, 0-50%) yielded the pure intermediate. Subsequently the intermediate was solved in glacial acetic acid and heated to reflux until HPLC revealed full consumption of the starting material. The solvent was removed under reduced pressure and the crude product was recrystallized from EtOAc and *n*hexane.

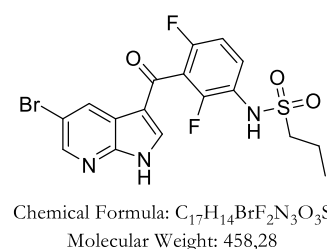
6.3. Experimental procedures

6.3.1. Azaindole derivatives

***N*-(3-(5-bromo-1*H*-pyrrolo[2,3-*b*]pyridine-3-carbonyl)-2,4-difluorophenyl)propane-1-sulfonamide (4)**

5-Bromo-1*H*-pyrrolo[2,3-*b*]pyridine (5 g, 25.4 mmol, 1 eq) and AlCl₃ (10.15 g, 76 mmol, 3 eq) were dissolved in DCM (100 mL) and stirred for 1 hour. Meanwhile 2,6-difluoro-3-(propylsulfonamido)benzoic acid (7.8 g, 27.9 mmol, 1.1 eq) was suspended in DCM (50 mL) and oxalyl chloride (2.4 mL, 27.9 mmol, 1.1 eq) and DMF (1 mL) was added dropwise. After the gas evolution stopped, both mixtures were combined and stirred for 6 hours at 40 °C. The reaction was stopped by adding MeOH, water and EtOAc at 0 °C. The organic layer was washed with saturated sodium chloride solution and dried over sodium sulfate. The yellow solid (9.9 g, 21 mmol, 85%) was obtained after column chromatography (PE/EtOAc, v/v, 20-50%).

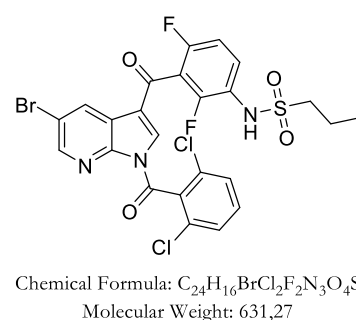
^1H NMR (200 MHz, DMSO): δ 13.14 (s, 1H), 9.78 (s, 1H), 8.59 (d, $J = 1.8$ Hz, 1H), 8.51 (d, $J = 2.0$ Hz, 1H), 8.28 (s, 1H), 7.59 (td, $J = 9.0, 6.4$ Hz, 1H), 7.28 (t, $J = 8.8$ Hz, 1H), 3.19 – 3.06 (m, 2H), 1.86 – 1.62 (m, 2H), 0.96 (t, $J = 7.3$ Hz, 3H) ppm. ^{13}C NMR (50 Hz, DMSO): δ 180.6, 156.6 (dd, $J = 184.1, 7.6$ Hz), 151.7 (dd, $J = 187.1, 7.7$ Hz), 147.8, 145.3, 139.3, 131.1, 128.9 (dd, $J = 10.1, 2.1$ Hz), 122.0 (dd, $J = 13.6, 3.8$ Hz), 119.0, 117.8 (dd, $J = 24.3, 22.1$ Hz), 114.9, 114.3, 112.4 (dd, $J = 22.8, 3.8$ Hz), 53.5, 16.8, 12.6 ppm. ESI-MS (m/z) 456.0 $[\text{M} - \text{H}]^-$.



***N*-(3-(5-bromo-1-(2,6-dichlorobenzoyl)-1*H*-pyrrolo[2,3-*b*]pyridine-3-carbonyl)-2,4-difluorophenyl)propane-1-sulfonamide (5)**

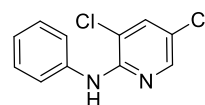
N-(3-(5-bromo-1*H*-pyrrolo[2,3-*b*]pyridine-3-carbonyl)-2,4-difluorophenyl)propane-1-sulfonamide (2.5 g, 5.46 mmol, 1 eq) and triethylamine (912 mL, 6.55 mmol, 1.2 eq) were dissolved in THF (50 mL) and cooled to 0 °C with an ice-bath. Then 2,6-dichlorobenzoyl chloride (938 mL, 6.55 mmol, 1.2 eq) was added over 5 minutes. After DMAP (67 mg, 545 μmol , 0.1 eq) was added, the ice bath was removed, and the mixture was stirred overnight. The reaction was stopped by adding EtOAc and the organic phase was washed with water and saturated sodium chloride solution and dried over sodium sulfate. Next the solvent was evaporated under reduced pressure. The purified product (2.35 g, 3.72 mmol, 68%) was obtained by column chromatography (PE/EtOAc, v/v, 2:1).

^1H NMR (200 MHz, DMSO) δ 9.83 (s, 1H), 8.90 (s, 1H), 8.73 (d, $J = 2.3$ Hz, 1H), 8.33 (d, $J = 2.1$ Hz, 1H), 7.77 – 7.55 (m, 4H), 7.34 (t, $J = 8.3$ Hz, 1H), 3.22 – 3.09 (m, 2H), 1.76 (dq, $J = 14.7, 7.4$ Hz, 2H), 0.97 (t, $J = 7.4$ Hz, 3H) ppm. ^{13}C NMR (50 MHz, DMSO) δ 182.3, 161.3, 156.86 (d, $J = 191.7$ Hz), 152.53 (dd, $J = 249.6, 9.8$ Hz), 147.0, 145.2, 135.6, 133.4, 133.1, 132.9, 130.9, 130.20 (dd, $J = 9.4, 2.8$ Hz), 128.4, 122.20 (dd, $J = 13.5, 3.9$ Hz), 121.0, 117.4, 116.58 – 116.40 (m), 112.68 (dd, $J = 22.3, 3.2$ Hz), 53.5, 39.5, 16.8, 12.5 ppm. ESI-MS (m/z) 629.0 $[\text{M} - \text{H}]^-$.



sulphate and the solvent was removed under reduced pressure. Column chromatography (PE/EtOAc, v/v, 0-50%) yielded the pure product (215 mg, 899 μ mol, 82%).

^1H NMR (200 MHz, DMSO) δ 8.51 (d, $J = 2.4$ Hz, 1H), 8.12 (d, $J = 2.3$ Hz, 1H), 7.99 (d, $J = 2.3$ Hz, 1H), 7.62 (d, $J = 7.7$ Hz, 2H), 7.29 (t, $J = 7.9$ Hz, 2H), 7.01 (t, $J = 7.3$ Hz, 1H) ppm. ^{13}C NMR (50 MHz, DMSO) δ 150.3, 146.6, 143.7, 139.9, 136.7, 128.3, 122.5, 120.9, 119.8, 116.0, 39.5 ppm.

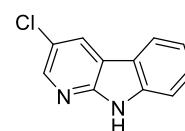


Chemical Formula: $\text{C}_{11}\text{H}_8\text{Cl}_2\text{N}_2$
Molecular Weight: 239,10

3-Chloro-9H-pyrido[2,3-*b*]indole (8)

3,5-Dichloro-*N*-phenylpyridin-2-amine (8.14 g, 34 mmol, 1 eq) was dissolved in a mixture of *o*-xylol and DMA (1:1, v/v, 2M) and DBU (10.2 mL, 68 mmol, 2 eq), PCy₃ (1.91 g, 6.8 mmol, 0.2 eq) and Pd(OAc)₂ (764 mg, 3.4 mmol, 10 mol%) were added. The reaction mixture was heated to 150 °C for 17 hours. After TLC revealed full consumption of the starting material, the mixture was cooled to room temperature and EtOAc was added. The organic phase was washed with ammonium chloride solution and water. After drying the organic phase over sodium sulphate, the solvent was removed under reduced pressure. Column chromatography (PE/EtOAc, v/v, 0-50%) yielded the pure product (4.1 g, 20.2 mmol, 59%).

^1H NMR (200 MHz, DMSO) δ 11.99 (s, 1H), 8.68 (d, $J = 2.0$ Hz, 1H), 8.41 (d, $J = 2.2$ Hz, 1H), 8.20 (d, $J = 7.9$ Hz, 1H), 7.54 – 7.48 (m, 2H), 7.24 (ddd, $J = 8.0, 5.5, 2.7$ Hz, 1H) ppm. ^{13}C NMR (50 MHz, DMSO) δ 150.1, 144.0, 139.7, 128.0, 127.4, 121.7, 121.7, 119.8, 119.6, 116.4, 111.5 ppm. ESI-MS (m/z) 201.0 [M - H].



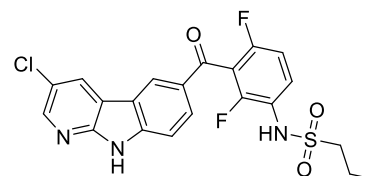
Chemical Formula: $\text{C}_{11}\text{H}_7\text{ClN}_2$
Molecular Weight: 202,64

N-(3-(3-chloro-9H-pyrido[2,3-*b*]indole-6-carbonyl)-2,4-difluorophenyl)propane-1-sulfonamide (9)

3-Chloro-9H-pyrido[2,3-*b*]indole (1.03 g, 5.08 mmol, 1 eq) and AlCl₃ (3.39 g, 25.41 mmol, 5 eq) were dissolved in DCM (50 mL) and stirred at room temperature for 60 minutes. Meanwhile 2,6-difluoro-3-(propylsulfonamido)benzoic acid (2.13 g, 7.62 mmol, 1.5 eq) was suspended in DCM (20 mL) and oxalyl chloride (654 μ L, 1.5 mmol, 1.5 eq) and DMF (500

μL) were added dropwise. After the gas evolution stopped, both mixtures were combined and stirred at 50 °C until no starting material was left. The reaction was stopped by adding MeOH and water at 0 °C, then the aqueous phase was extracted with EtOAc. The organic phase was concentrated and the forming precipitate (1.53 g, 3.3 mmol, 65%) was collected and dried under reduced pressure.

^1H NMR (200 MHz, DMSO) δ 12.63 (s, 1H), 9.85 (s, 1H), 8.88 (d, $J = 1.8$ Hz, 1H), 8.80 (s, 1H), 8.48 (d, $J = 2.0$ Hz, 1H), 8.06 (d, $J = 8.6$ Hz, 1H), 7.75 – 7.60 (m, 2H), 7.34 (t, $J = 8.7$ Hz, 1H), 3.21 – 3.11 (m, 2H), 1.85 – 1.61 (m, 2H), 0.93 (t, $J = 7.3$ Hz, 3H) ppm. ^{13}C NMR (50 MHz, DMSO) δ 187.1,



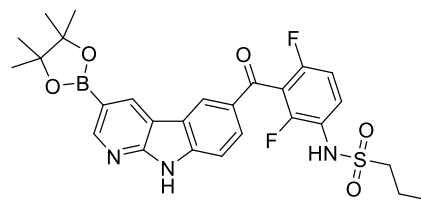
Chemical Formula: $\text{C}_{21}\text{H}_{16}\text{ClF}_2\text{N}_3\text{O}_3\text{S}$
Molecular Weight: 463,88

156.22 (dd, $J = 246.8, 6.8$ Hz), 152.38 (dd, $J = 250.0, 8.4$ Hz), 151., 145.4, 143.8, 129.4, 129.2, 128.6, 128.3, 128.47 (d, $J = 7.5$ Hz), 125.8, 123.1, 122.14 (dd, $J = 13.4, 3.7$ Hz), 119.9, 117.52 (dd, $J = 23.9, 22.1$ Hz), 116.8, 112.60 (dd, $J = 21.5, 2.5$ Hz), 112.4, 53.5, 16.9, 12.6 ppm. ESI-MS (m/z) 462.1 $[\text{M} - \text{H}]^-$.

***N*-(2,4-difluoro-3-(3-(4,4,5,5-tetramethyl-1,3,2-dioxaborolan-2-yl)-9*H*-pyrido[2,3-*b*]indole-6-carbonyl)phenyl)propane-1-sulfonamide (10)**

N-(3-(3-chloro-9*H*-pyrido[2,3-*b*]indole-6-carbonyl)-2,4-difluorophenyl)propane-1-sulfonamide (514 mg, 1.1 mmol, 1 eq), 4,4,4',4',5,5,5',5'-octamethyl-2,2'-bi(1,3,2-dioxaborolane) (295 mg, 1.16 mmol, 1.1 eq) and KOAc (217 mg, 2.2 mmol, 2 eq) were suspended in 1,4-dioxane/water (1:1, v/v, 4 mL) and purged with argon for 15 minutes. Subsequently XPhos Pd G3 (29 mg, 33 μmol , 3 mol%) was added and stirred under microwave irradiation (50 W, 115 °C) for 40 minutes. Showing full consumption of the starting material, EtOAc was added, and the organic layer was washed with water and saturated sodium chloride. The organic layer was dried over sodium sulphate and the solvent was removed under reduced pressure. After column chromatography (DCM/EtOAc, v/v, 0-50%) the pure product could be obtained as an off-white solid (550 mg, 990 μmol , 89%).

^1H NMR (200 MHz, DMSO) δ 12.54 (s, 1H), 9.78 (s, 1H), 8.96 (s, 1H), 8.87 (s, 1H), 8.71 (s, 1H), 8.09 (d, $J = 9.0$ Hz, 1H), 7.72 – 7.57 (m, 1H), 7.33 (t, $J = 8.7$ Hz, 1H), 3.24 – 3.08 (m, 2H), 1.74 (dd, $J = 15.1, 7.5$ Hz, 2H), 1.33 (s, 12H), 0.93 (t, $J = 7.3$ Hz, 3H) ppm. ^{13}C NMR (101 MHz, DMSO) δ 187.6, 158.0, 157.9, 157.9, 156.69 (dd, $J = 246.7, 6.7$ Hz), 155.5, 155.4, 155.4, 154.8, 154.1, 154.0, 153.4, 152.79 (dd, $J = 249.2, 8.0$ Hz), 151.6, 151.5, 143.4, 136.5, 129.65 (d, $J = 9.3$ Hz), 129.2, 127.8, 126.6, 122.40 (dd, $J = 13.2, 3.2$ Hz), 121.1, 118.00 (t, $J = 22.9$ Hz), 115.7, 112.92 (dd, $J = 22.7, 3.8$ Hz), 112.6, 84.3, 53.9, 25.1, 17.1, 13.0 ppm. ESI-MS (m/z) 554.1 [M - H] $^-$.



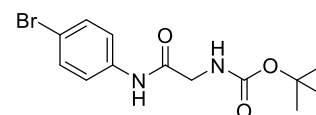
Chemical Formula: $\text{C}_{27}\text{H}_{28}\text{BF}_2\text{N}_3\text{O}_5\text{S}$
Molecular Weight: 555,40

6.3.3. Linker synthesis

***Tert*-butyl (2-((4-bromophenyl)amino)-2-oxoethyl)carbamate (16)**

To a suspension of 4-bromoaniline (1 g, 5.81 mmol, 1.2 eq), (*tert*-butoxycarbonyl) glycine (849 mg, 4.84 mmol, 1 eq) and triethylamine (1.32 mL, 9.69 mmol, 2 eq) in DMF (10 mL) was added TBTU (1.56 g, 4.84 mmol, 1 eq). The reaction mixture was stirred at room temperature for 2 hours. Then it was diluted with EtOAc, washed with water, and saturated sodium chloride solution and dried over sodium sulfate. The organic layer was dried over sodium sulfate and the solvent was evaporated under reduced pressure. After column chromatography the pure product could be obtained as an off-white oil (190 mg, 664 μ mol, 36%).

^1H NMR (200 MHz, DMSO) δ 10.07 (s, 1H), 7.51 (q, J = 8.9 Hz, 5H), 7.04 (t, J = 6.0 Hz, 1H), 3.71 (d, J = 5.8 Hz, 2H), 1.38 (s, 9H) ppm. ^{13}C NMR (50 MHz, DMSO) δ 168.5, 156.1, 138.4, 131.6, 121.1, 114.8, 78.2, 43.9, 39.5, 28.3 ppm.

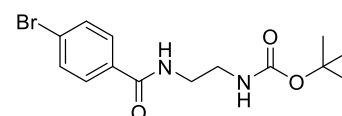


Chemical Formula: $\text{C}_{13}\text{H}_{17}\text{BrN}_2\text{O}_3$
Molecular Weight: 329,19

***Tert*-butyl (2-(4-bromobenzamido)ethyl)carbamate (17)**

Oxalyl chloride (118 μ L, 1.37 mmol, 1.1 eq) was added to 4-bromobenzoic acid (276 mg, 1.37 mmol, 1.1 eq) in THF (10 mL) and DMF (0.5 mL) and stirred at room temperature until gas evolution stopped. Subsequently the mixture was added dropwise to a solution of (2*H*-imidazol-2-yl)methanone (200 mg, 1.25 mmol, 1 eq) in THF at 0 $^\circ\text{C}$ and stirred at room temperature for 3 hours. Then it was diluted with EtOAc, washed with water, and saturated sodium chloride solution and dried over sodium sulfate. The organic layer was dried over sodium sulfate and the solvent was evaporated under reduced pressure. After column chromatography (PE/EtOAc, v/v, 1:1) the pure product could be obtained as a white solid (430 mg, 1.25 mmol, quant.).

^1H NMR (200 MHz, DMSO) δ 8.58 – 8.47 (m, 1H), 7.77 (d, J = 8.6 Hz, 2H), 7.66 (d, J = 8.7 Hz, 2H), 6.80 (t, J = 5.7 Hz, 1H), 3.23 (dd, J = 12.7, 6.7 Hz, 2H), 2.96 (dd, J = 13.0, 6.8 Hz, 2H), 1.71 – 1.49 (m, 2H), 1.36 (s, 9H) ppm. ^{13}C NMR (50 MHz,



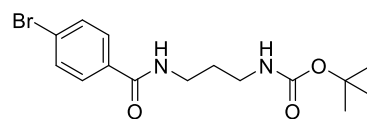
Chemical Formula: $\text{C}_{14}\text{H}_{19}\text{BrN}_2\text{O}_3$
Molecular Weight: 343,22

DMSO) δ 165.4, 155.7, 133.7, 131.4, 129.3, 124.9, 77.6, 38.5 (under DMSO-signal), 37.1, 29.6, 28.3 ppm.

***Tert*-butyl (3-(4-bromobenzamido)propyl)carbamate (18)**

Following the general procedure for amide coupling, the reaction of 4-bromobenzoic acid (200 mg, 995 μ mol, 1 eq), *tert*-butyl (3-aminopropyl)carbamate (190 mg, 1.09 mmol, 1.1 eq) and HATU (378 mg, 995 μ mol, 1 eq) yielded *tert*-butyl (3-(4-bromobenzamido)propyl)carbamate (220 mg, 615 μ mol, 62%) as a colorless oil.

^1H NMR (200 MHz, DMSO) δ 8.58 – 8.47 (m, 1H), 7.77 (d, J = 8.6 Hz, 1H), 7.66 (d, J = 8.7 Hz, 1H), 6.80 (t, J = 5.7 Hz, 1H), 3.23 (dd, J = 12.7, 6.7 Hz, 2H), 2.96 (dd, J = 13.0, 6.8 Hz, 2H), 1.71 – 1.49 (m, 2H), 1.36 (s, 9H). ^{13}C NMR (50 MHz,



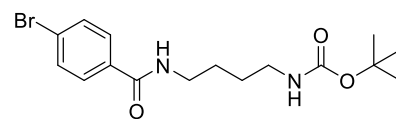
Chemical Formula: $\text{C}_{15}\text{H}_{21}\text{BrN}_2\text{O}_3$
Molecular Weight: 357,25

DMSO) δ 165.4, 155.7, 133.7, 131.4, 129.3, 124.9, 77.6, 39.5, 37.1, 29.6, 28.3 ppm. ESI-MS (m/z) 354.9 [M - H] $^-$.

***Tert*-butyl (4-(4-bromobenzamido)butyl)carbamate (19)**

Following the general procedure for amide coupling, the reaction of 4-bromobenzoic acid (335 mg, 1.67 mmol, 1 eq), *tert*-butyl (4-aminobutyl)carbamate (345 mg, 1.83 mmol, 1.1 eq), DIPEA (968 μ L, 5 mmol, 3 eq) and HATU (634 mg, 1.67 mmol, 1 eq) yielded *tert*-butyl (4-(4-bromobenzamido)butyl)carbamate (450 mg, 1.21 mmol, 73%) as a colorless solid.

^1H NMR (200 MHz, CDCl_3) δ 7.69 (d, J = 8.4 Hz, 2H), 7.54 (d, J = 8.6 Hz, 2H), 6.72 (s, 1H), 4.68 (s, 2H), 3.47 (q, J = 6.4 Hz, 2H), 3.15 (q, J = 6.5 Hz, 2H), 1.76 – 1.53 (m, 4H), 1.43 (s, J = 4.5 Hz, 9H) ppm. ^{13}C NMR (50 MHz, CDCl_3) δ 133.6, 131.8, 128.8, 126.1, 125.6, 82.3, 77.2, 39.9, 28.5 ppm.



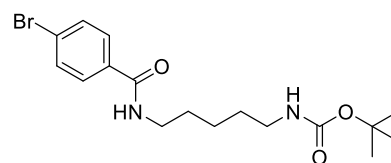
Chemical Formula: $\text{C}_{16}\text{H}_{23}\text{BrN}_2\text{O}_3$
Molecular Weight: 371,28

***Tert*-butyl (5-(4-bromobenzamido)pentyl)carbamate (20)**

Following the general procedure for amide coupling, the reaction of 4-bromobenzoic acid (300 mg, 1.49 mmol, 1.1 eq), *tert*-butyl (4-aminopentyl)carbamate (274 mg, 1.36 mmol, 1 eq), DIPEA (474 μ L, 2.71 mmol, 2 eq) and HATU (567 mg, 1.49 mmol, 1.1 eq) yielded *tert*-

butyl (5-(4-bromobenzamido)pentyl)carbamate (234 mg, 607 μmol , 45%) as a colorless solid.

^1H NMR (200 MHz, CDCl_3) δ 7.68 – 7.61 (m, 2H), 7.58 – 7.50 (m, 2H), 6.40 (s, 1H), 4.61 (s, 1H), 3.42 (dd, $J = 12.7$, 6.8 Hz, 2H), 3.11 (q, $J = 6.4$ Hz, 2H), 1.61 (dd, $J = 14.2$, 7.2 Hz, 2H), 1.55 – 1.43 (m, 4H), 1.41 (s, 9H) ppm. ^{13}C NMR (50 MHz, CDCl_3) δ 156.3, 133.7, 131.9, 128.7, 126.1, 82.2, 77.2, 40.1, 29.9, 28.5, 24.1 ppm. ESI-MS (m/z) 407.0 $[\text{M} + \text{Na}]^+$.

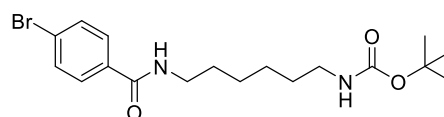


Chemical Formula: $\text{C}_{17}\text{H}_{25}\text{BrN}_2\text{O}_3$
Molecular Weight: 385,30

***Tert*-butyl (6-(4-bromobenzamido)hexyl)carbamate (21)**

Following the general procedure for amide coupling, the reaction of 4-bromobenzoic acid (296 mg, 1.37 mmol, 1.1 eq), *tert*-butyl (4-aminohexyl)carbamate (250 mg, 1.24 mmol, 1 eq), DIPEA (331 μL , 2.49 mmol, 2 eq) and HATU (473 mg, 1.24 mmol, 1.1 eq) yielded *tert*-butyl (5-(4-bromobenzamido)pentyl)carbamate (388 mg, 972 μmol , 78%) as a colorless solid.

^1H NMR (200 MHz, DMSO) δ 7.78 (d, $J = 8.6$ Hz, 1H), 7.65 (d, $J = 8.5$ Hz, 1H), 6.75 (t, $J = 5.1$ Hz, 1H), 3.23 (dd, $J = 12.8$, 6.6 Hz, 1H), 2.94 – 2.83 (m, 1H), 1.36 (s, 4H) ppm. ^{13}C NMR (50 MHz, DMSO) δ 165.1, 155.6, 133.8, 131.2, 129.3, 124.7, 77.3, 39.5, 29.5, 29.0, 28.3, 26.2, 26.0 ppm. ESI-MS (m/z) 421.1 $[\text{M} + \text{Na}]^+$.



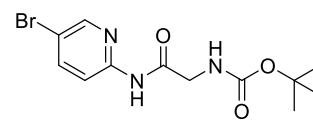
Chemical Formula: $\text{C}_{18}\text{H}_{27}\text{BrN}_2\text{O}_3$
Molecular Weight: 399,33

***Tert*-butyl (2-((5-bromopyridin-2-yl)amino)-2-oxoethyl)carbamate (22)**

To a suspension of 4-bromopyridine-2-amine (500 mg, 2.89 mmol, 1 eq) and (*tert*-butoxycarbonyl) glycine (759 mg, 4.33 mmol, 1.2) in THF (6 mL) was added di(2H-imidazol-2-yl)methanone (703 mg, 4.33 mmol, 1.2 eq). The reaction mixture was stirred at room temperature for 17 hours. Then it was diluted with EtOAc, washed with water, and saturated sodium chloride solution and dried over sodium sulfate. The organic layer was dried over sodium sulfate and the solvent was evaporated under reduced pressure. After

column chromatography (PE/EtOAc, v/v, 1:1) the pure product could be obtained as a white solid (576 mg, 1.71 mmol, 59%).

^1H NMR (200 MHz, DMSO) δ 10.58 (s, 1H), 8.43 (d, $J = 1.0$ Hz, 1H), 8.12 – 7.91 (m, 2H), 7.06 (t, $J = 5.7$ Hz, 1H), 3.78 (d, $J = 6.1$ Hz, 2H), 1.38 (s, 9H) ppm. ^{13}C NMR (50 MHz, DMSO) δ 169.3, 155.9, 150.7, 148.6, 140.7, 115.0, 113.4, 78.1, 43.8, 39.5, 28.2 ppm.

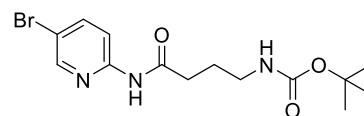


Chemical Formula: $\text{C}_{12}\text{H}_{16}\text{BrN}_3\text{O}_3$
Molecular Weight: 330,18

***Tert*-butyl (2-(5-bromopicolinamido)propyl)carbamate (23)**

The reaction was done with *tert*-butyl (2-aminoethyl)carbamate (200 mg, 1.25 mmol, 1 eq) and 5-bromopicolinic acid (794 mg, 2.48 mmol, 1 eq). The pure product could be obtained after column chromatography (acetone + 1% triethylamine) as a colorless solid (270 mg, 0.27 mmol, 32%).

^1H NMR (200 MHz, DMSO) δ 8.82 (t, $J = 5.6$ Hz, 1H), 8.76 (d, $J = 2.0$ Hz, 1H), 8.24 (dd, $J = 8.4, 2.3$ Hz, 1H), 8.02 – 7.92 (m, 1H), 6.91 (t, $J = 4.7$ Hz, 1H), 3.31 (d, $J = 6.0$ Hz, 2H), 3.11 (q, $J = 5.8$ Hz, 2H), 1.34 (s, 9H) ppm.

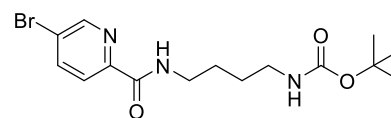


Chemical Formula: $\text{C}_{14}\text{H}_{20}\text{BrN}_3\text{O}_3$
Molecular Weight: 358,24

***Tert*-butyl (4-(5-bromopicolinamido)butyl)carbamate (24)**

Oxalyl chloride (1.11 mL, 12.99 mmol, 1.05 eq) was added to 5-bromopicolinic acid (2.5 g, 12.38 mmol, 1 eq) in DCM (5 mL) and DMF (0.5 mL) and stirred at room temperature until gas evolution stopped. Subsequently the solvent was evaporated under reduced pressure and the residue was dissolved in DCM (5 mL) again. The mixture was added dropwise to a solution of *tert*-butyl (4-aminobutyl)carbamate (200 mg, 1.25 mmol, 1 eq) in DCM (10 mL) at 0 °C and stirred at room temperature for 17 hours. Then it was diluted with EtOAc, washed with water, and saturated sodium chloride solution and dried over sodium sulfate. The organic layer was dried over sodium sulfate and the solvent was evaporated under reduced pressure. After column chromatography (PE/EtOAc, v/v, 1:1) the pure product could be obtained as a white solid (3 g, 8.06 mmol, 66%).

^1H NMR (200 MHz, DMSO) δ 8.81 (t, $J = 5.8$ Hz, 1H), 8.75 (d, $J = 1.6$ Hz, 2H), 8.24 (dd, $J = 8.2, 1.7$ Hz, 1H), 7.95 (d, $J = 8.5$ Hz, 2H), 6.78 (t, $J = 4.4$ Hz, 1H), 3.26 (dd, $J = 12.0, 6.0$ Hz, 4H), 2.91 (dd, $J = 12.2, 6.3$ Hz, 1H), 1.58 – 1.38 (m, 2H), 1.35 (s, 9H) ppm. ^{13}C NMR (50 MHz, DMSO) δ 163.1, 155.6, 149.1, 149.0, 140.4, 123.8, 123.2, 77.4, 40.8, 39.6, 28.3, 27.0, 26.6, 26.5 ppm. ESI-MS (m/z) 393.8 [$\text{M} + \text{Na}$] $^+$.

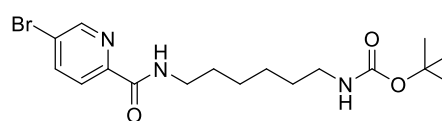


Chemical Formula: $\text{C}_{15}\text{H}_{22}\text{BrN}_3\text{O}_3$
Molecular Weight: 372,26

***Tert*-butyl (6-(5-bromopicolinamido)hexyl)carbamate (25)**

Following the general procedure for amide coupling, the reaction of 4-bromopicolinic acid (250 mg, 1.24 mmol, 1 eq), *tert*-butyl (4-aminohexyl)carbamate (294 mg, 1.36 mmol, 1.1 eq), DIPEA (186 μL , 1.36 mmol, 1,1 eq) and HATU (469 mg, 1.24 mmol, 1 eq) yielded *tert*-butyl (6-(5-bromopicolinamido)hexyl)carbamate (340 mg, 849 μmol , 69%) as a colorless solid.

^1H NMR (200 MHz, DMSO) δ 8.78 (dd, $J = 11.4, 3.9$ Hz, 2H), 8.23 (dd, $J = 8.4, 2.2$ Hz, 1H), 7.95 (d, $J = 8.3$ Hz, 1H), 6.74 (t, $J = 4.3$ Hz, 1H), 3.26 (dd, $J = 13.1, 6.8$ Hz, 2H), 2.87 (dd, $J = 12.2, 6.3$ Hz, 2H), 1.50 (s, 2H),



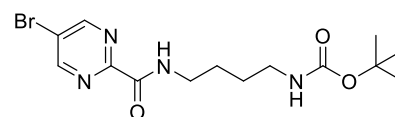
Chemical Formula: $\text{C}_{17}\text{H}_{26}\text{BrN}_3\text{O}_3$
Molecular Weight: 400,32

1.35 (s, 9H), 1.26 (m, 6H) ppm. ^{13}C NMR (101 MHz, DMSO) δ 162.9, 155.5, 149.1, 149.0, 140.4, 123.7, 123.1, 77.2, 38.8, 29.4, 29.1, 28.2, 26.1, 26.0 ppm.

***Tert*-butyl (4-(5-bromopyrimidine-2-carboxamido)butyl)carbamate (26)**

To a suspension of 4-bromobenzoic acid (500 mg, 2.46 mmol, 1 eq), *tert*-butyl (4-aminobutyl)carbamate (529 μL , 2.96 mmol, 1.2 eq) and DIPEA (674 μL , 4.93 mmol, 2 eq) in DMF (8 mL) was added HBTU (791 mg, 2.46 mmol, 1 eq). The reaction mixture was stirred at room temperature for 17 hours. Then it was diluted with EtOAc, washed with water, and saturated sodium chloride solution and dried over sodium sulfate. The organic layer was dried over sodium sulfate and the solvent was evaporated under reduced pressure. After column chromatography (acetone + 1% triethylamine) the pure product could be obtained as a colorless solid (440 mg, 1.18 mmol, 48%).

^1H NMR (200 MHz, CDCl_3) δ 8.88 (s, 2H), 7.93 (s, 1H), 4.64 (s, 1H), 3.49 (dd, $J = 12.7, 6.4$ Hz, 2H), 3.13 (dd, $J =$



Chemical Formula: $\text{C}_{14}\text{H}_{21}\text{BrN}_4\text{O}_3$
Molecular Weight: 373,25

^{13}C NMR (50 MHz, CDCl_3) δ 161.6, 158.2, 156.1, 155.8,

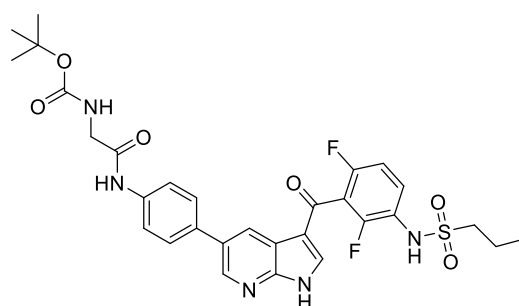
122.6, 77.2, 39.6, 28.5, 27.6, 26.9 ppm. ESI-MS (m/z) 394.8 $[\text{M} + \text{Na}]^-$.

6.3.4. Linker implementation

***Tert*-butyl (2-((4-(3-(2,6-difluoro-3-(propylsulfonamido)benzoyl)-1*H*-pyrrolo[2,3-*b*]pyridin-5-yl)phenyl)amino)-2-oxoethyl)carbamate (27)**

Following the general procedure C for Suzuki coupling of azaindoles, coupling of *N*-(3-(1-(2,6-dichlorobenzoyl)-5-(4,4,5,5-tetramethyl-1,3,2-dioxaborolan-2-yl)-1*H*-pyrrolo[2,3-*b*]pyridine-3-carbonyl)-2,4-difluorophenyl)propane-1-sulfonamide (100 mg, 147 μmol , 1 eq), *tert*-butyl (2-((4-bromophenyl)amino)-2-oxoethyl)carbamate (53 mg, 162 μmol , 1.1 eq) and K_2CO_3 (51 mg, 369 μmol , 2.5 eq) in afforded the product after purification and recrystallization in a mixture of EtOAc and *n*hexane as a colorless solid (61 mg, 97 μmol , 66%).

^1H NMR (600 MHz, DMSO) δ 12.96 (s, 1H), 10.06 (s, 1H), 9.76 (s, 1H), 8.69 (d, $J = 2.2$ Hz, 1H), 8.69 (d, $J = 2.2$ Hz, 1H), 8.59 (s, 1H), 8.59 (s, 1H), 8.21 (s, 1H), 8.21 (s, 1H), 7.74 (t, $J = 7.3$ Hz, 2H), 7.71 (d, $J = 8.6$ Hz, 2H), 7.59 (td, $J = 9.0, 6.1$ Hz, 1H), 7.28 (t, $J = 8.5$ Hz, 1H), 7.06 (t, $J = 6.0$ Hz, 1H), 3.76 (d, $J = 6.0$ Hz, 2H), 3.14 – 3.10 (m,



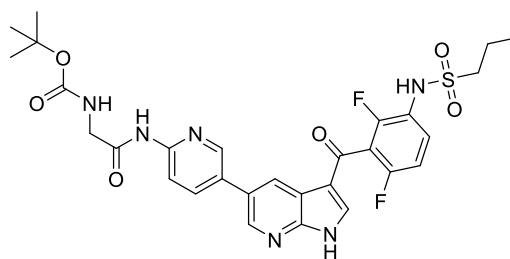
Chemical Formula: $\text{C}_{30}\text{H}_{31}\text{F}_2\text{N}_5\text{O}_6\text{S}$
Molecular Weight: 627,66

2H), 1.78 – 1.70 (m, 2H), 1.41 (s, $J = 18.5$ Hz, 9H), 0.96 (t, $J = 7.4$ Hz, 3H) ppm. ^{13}C NMR (151 MHz, DMSO) δ 180.6, 168.4, 156.03 (dd, $J = 246.6, 6.6$ Hz), 152.35 (dd, $J = 249.6, 8.5$ Hz), 148.7, 143.8, 138.6, 132.8, 131.2, 128.78 (d, $J = 8.8$ Hz), 127.5, 126.5, 121.96 (d, $J = 12.4$ Hz), 119.7, 118.22 (t, $J = 23.6$ Hz), 117.5, 115.7, 112.34 (d, $J = 22.5$ Hz), 78.1, 78.1, 53.5, 43.9, 39.5, 28.2, 16.8, 12.6 ppm. ESI-MS (m/z) 626.5 $[\text{M} - \text{H}]^-$.

***Tert*-butyl (2-((5-(3-(2,6-difluoro-3-(propylsulfonamido)benzoyl)-1*H*-pyrrolo[2,3-*b*]pyridin-5-yl)pyridin-2-yl)amino)-2-oxoethyl)carbamate (28)**

Following the general procedure C for Suzuki coupling of azaindoles, coupling of *N*-(3-(1-(2,6-dichlorobenzoyl)-5-(4,4,5,5-tetramethyl-1,3,2-dioxaborolan-2-yl)-1*H*-pyrrolo[2,3-*b*]pyridine-3-carbonyl)-2,4-difluorophenyl)propane-1-sulfonamide (200 mg, 295 μ mol, 1 eq) *tert*-butyl ((5-bromopicolinamido)methyl)carbamate (108 mg, 324 μ mol, 1.1 eq) and K_2CO_3 (102 mg, 737 μ mol, 2.5 eq) in afforded the product after purification and recrystallization in a mixture of EtOAc and *n*hexane as a colorless solid (90 mg, 143 μ mol, 49%).

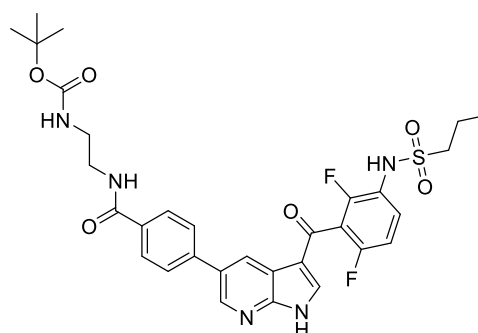
1H NMR (400 MHz, DMSO) δ 13.02 (s, 1H), 10.57 (s, 1H), 9.77 (s, 1H), 8.74 (t, $J = 2.7$ Hz, 1H), 8.72 (s, 1H), 8.66 (s, 1H), 8.26 (d, $J = 11.0$ Hz, 1H), 8.20 (s, 1H), 7.59 (td, $J = 9.0, 5.9$ Hz, 1H), 7.28 (t, $J = 8.1$ Hz, 1H), 7.09 (t, $J = 6.1$ Hz, 1H), 3.81 (t, $J = 12.3$ Hz, 2H), 3.12 (dd, $J = 8.7, 6.6$ Hz, 2H), 1.80 – 1.68 (m, 2H), 1.40 (s, 9H), 0.96 (t, $J = 7.4$ Hz, 3H). ^{13}C NMR (101 MHz, DMSO) δ 180.7, 169.2, 156.08 (dd, $J = 246.6, 6.9$ Hz), 152.40 (dd, $J = 248.9, 9.3$ Hz), 151.2, 150.0, 149.0, 146.2, 143.8, 138.9, 136.9, 129.4, 128.3, 126.9, 121.98 (d, $J = 13.7$ Hz), 118.82 – 117.78 (m), 117.6, 115.7, 113.4, 112.41 (d, $J = 22.5$ Hz), 78.2, 53.5, 43.8, 28.2, 16.9, 12.6 ppm. ESI-MS (m/z) 627.8 [$M - H$].



***Tert*-butyl (2-(4-(3-(2,6-difluoro-3-(propylsulfonamido)benzoyl)-1*H*-pyrrolo[2,3-*b*]pyridin-5-yl)benzamido)ethyl)carbamate (29)**

Following the general procedure C for Suzuki coupling of azaindoles, coupling of *N*-(3-(1-(2,6-dichlorobenzoyl)-5-(4,4,5,5-tetramethyl-1,3,2-dioxaborolan-2-yl)-1*H*-pyrrolo[2,3-*b*]pyridine-3-carbonyl)-2,4-difluorophenyl)propane-1-sulfonamide (50 mg, 99 μ mol, 1 eq), *tert*-butyl (2-(4-bromobenzamido)ethyl)carbamate (37 mg, 109 μ mol, 1.1 eq) and K_2CO_3 (34 mg, 247 μ mol, 2.5 eq) in afforded the product after purification and recrystallization in a mixture of EtOAc and *n*hexane as a colorless solid (25 mg, 39 μ mol, 39%).

^1H NMR (600 MHz, DMSO) δ 13.04 (s, 1H), 9.76 (s, 1H), 8.77 (d, $J = 2.2$ Hz, 1H), 8.69 (s, 1H), 8.54 (t, $J = 5.4$ Hz, 1H), 8.26 (s, 1H), 7.99 (d, $J = 8.2$ Hz, 2H), 7.86 (d, $J = 8.2$ Hz, 2H), 7.59 (td, $J = 9.0, 6.0$ Hz, 1H), 7.29 (t, $J = 8.3$ Hz, 1H), 6.93 (t, $J = 5.7$ Hz, 1H), 3.34 – 3.30 (m, 3H), 3.13 (dt, $J = 7.7, 7.1$ Hz, 4H), 1.80 – 1.69 (m, 2H), 1.38 (s, 9H), 0.96 (t, $J = 7.4$ Hz, 3H) ppm. ^{13}C NMR (151 MHz, DMSO) δ 180.7, 166.0, 156.04 (dd, $J = 246.5, 6.8$ Hz), 152.38 (dd, $J = 249.7, 8.4$ Hz), 149.2, 144.2, 140.7, 139.0, 133.4, 130.6, 128.85 (d, $J = 9.3$ Hz), 128.1, 127.2, 126.9, 121.98 (d, $J = 13.4$ Hz), 118.45 – 117.86 (m), 117.5, 112.36 (d, $J = 22.7$ Hz), 77.7, 53.5, 40.1, 39.5, 28.3, 16.8, 12.6 ppm. ESI-MS (m/z) 663.5 $[\text{M} + \text{Na}]^+$.

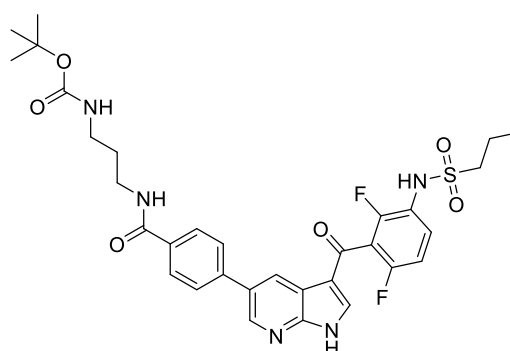


Chemical Formula: $\text{C}_{31}\text{H}_{33}\text{F}_2\text{N}_5\text{O}_6\text{S}$
Molecular Weight: 641.69

***Tert*-butyl (3-(4-(3-(2,6-difluoro-3-(propylsulfonamido)benzoyl)-1*H*-pyrrolo[2,3-*b*]pyridin-5-yl)benzamido)propyl)carbamate (30)**

Following the general procedure C for Suzuki coupling of azaindoles, coupling of *N*-(3-(1-(2,6-dichlorobenzoyl)-5-(4,4,5,5-tetramethyl-1,3,2-dioxaborolan-2-yl)-1*H*-pyrrolo[2,3-*b*]pyridine-3-carbonyl)-2,4-difluorophenyl)propane-1-sulfonamide (100 mg, 58 μmol , 1 eq), *tert*-butyl (3-(4-bromobenzamido)propyl)carbamate (58 mg, 162 μmol , 1.1 eq) and K_2CO_3 (51 mg, 87 μmol , 2.5 eq) in afforded the product after purification and recrystallization in a mixture of EtOAc and *n*hexane as a colorless solid (57 mg, 87 μmol , 59%).

^1H NMR (600 MHz, DMSO) δ 13.04 (s, 1H), 9.77 (s, 1H), 8.77 (d, $J = 2.2$ Hz, 1H), 8.68 (s, 1H), 8.53 (t, $J = 5.6$ Hz, 1H), 8.25 (s, 1H), 7.99 (d, $J = 8.4$ Hz, 2H), 7.86 (d, $J = 8.3$ Hz, 2H), 7.62 – 7.53 (m, 3H), 7.28 (dd, $J = 18.6, 10.3$ Hz, 2H), 6.82 (t, $J = 5.6$ Hz, 1H), 3.32 – 3.25 (m, 2H), 3.15 – 3.09 (m, 2H), 3.00 (dd, $J = 12.9, 6.6$ Hz, 2H), 1.78 – 1.70 (m, 2H), 1.70 – 1.61 (m, 2H), 1.38 (s, 9H), 0.96 (t,



Chemical Formula: $\text{C}_{32}\text{H}_{35}\text{F}_2\text{N}_5\text{O}_6\text{S}$
Molecular Weight: 655.72

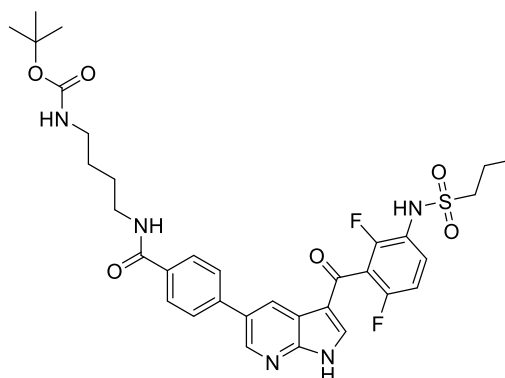
$J = 7.4$ Hz, 3H) ppm. ^{13}C NMR (151 MHz, DMSO) δ 180.7, 165.8, 165.8, 156.06 (dd, $J = 247.3, 7.5$ Hz), 155.7, 152.38 (dd, $J = 250.1, 8.9$ Hz), 144.2, 140.7, 139.0, 133.5, 130.6, 128.69

(dd, $J = 52.5, 11.1$ Hz), 128.0, 127.0, 121.99 (d, $J = 13.4$ Hz), 118.16 (t, $J = 23.5$ Hz), 117.5, 115.8, 112.37 (d, $J = 22.6$ Hz), 77.5, 53.5, 39.5, 37.7, 37.0, 28.3, 16.8, 12.6 ppm. ESI-MS (m/z) 678.6 $[M + Na]^+$.

***Tert*-butyl (4-(4-(3-(2,6-difluoro-3-(propylsulfonamido)benzoyl)-1*H*-pyrrolo[2,3-*b*]pyridin-5-yl)benzamido)butyl)carbamate (31)**

Following the general procedure C for Suzuki coupling of azaindoles, coupling of *N*-(3-(1-(2,6-dichlorobenzoyl)-5-(4,4,5,5-tetramethyl-1,3,2-dioxaborolan-2-yl)-1*H*-pyrrolo[2,3-*b*]pyridine-3-carbonyl)-2,4-difluorophenyl)propane-1-sulfonamide (50 mg, 99 μ mol, 1 eq), *tert*-butyl (4-(4-bromobenzamido)butyl)carbamate (40 mg, 109 μ mol, 1.1 eq) and K_2CO_3 (41 mg, 296 μ mol, 2.5 eq) in afforded the product after purification and recrystallization in a mixture of EtOAc and *n*hexane as a colorless solid (38 mg, 57 μ mol, 57%).

1H NMR (600 MHz, $CDCl_3$) δ 9.76 (s, 1H), 8.77 (d, $J = 2.2$ Hz, 1H), 8.68 (s, 1H), 8.58 – 8.48 (m, 1H), 8.25 (s, 1H), 8.02 – 7.93 (m, 2H), 7.86 (d, $J = 8.3$ Hz, 1H), 7.64 – 7.56 (m, 1H), 7.33 – 7.26 (m, 1H), 6.85 – 6.76 (m, 1H), 3.28 (dd, $J = 12.6, 6.5$ Hz, 2H), 3.12 (dd, $J = 8.7, 6.7$ Hz, 2H), 2.95 (dd, $J = 12.8, 6.6$ Hz, 2H), 1.79 – 1.68 (m, 2H), 1.56 – 1.49 (m, 2H), 1.43 (dt, $J = 13.8, 6.8$ Hz, 2H), 1.37



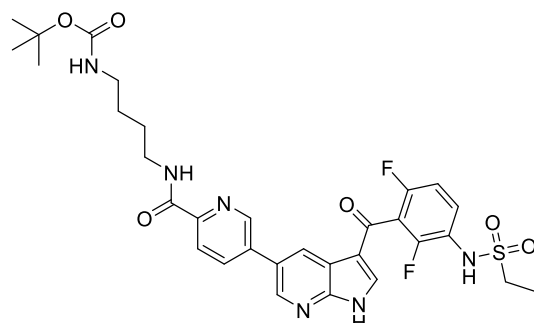
Chemical Formula: $C_{33}H_{37}F_2N_5O_6S$
Molecular Weight: 669,74

(s, 9H), 0.99 – 0.93 (m, 3H) ppm. ^{13}C NMR (151 MHz, $CDCl_3$) δ 180.71 (d, $J = 4.0$ Hz), 165.73 (d, $J = 3.5$ Hz), 156.06 (dd, $J = 246.8, 7.1$ Hz), 155.7, 152.38 (dd, $J = 249.6, 8.5$ Hz), 150.8, 149.1, 144.2, 140.6, 138.9, 133.6, 130.7, 128.9, 128.1, 127.2, 126.9, 121.96 (d, $J = 13.6$ Hz), 118.10 (d, $J = 18.5$ Hz), 117.5, 115.8, 115.0, 112.3, 77.37 (d, $J = 5.2$ Hz), 53.5, 40.1, 39.0, 28.32 (d, $J = 8.1$ Hz), 27.1, 26.6, 16.9, 12.6 ppm

***Tert*-butyl (4-(5-(3-(2,4-difluoro-3-(propylsulfonamido)benzoyl)-1*H*-pyrrolo[2,3-*b*]pyridin-5-yl)picolinamido)butyl)carbamate (32)**

Following the general procedure C for Suzuki coupling of azaindoles, coupling of *N*-(3-(1-(2,6-dichlorobenzoyl)-5-(4,4,5,5-tetramethyl-1,3,2-dioxaborolan-2-yl)-1*H*-pyrrolo[2,3-*b*]pyridine-3-carbonyl)-2,4-difluorophenyl)propane-1-sulfonamide (200 mg, 317 μ mol, 1 eq), *tert*-butyl (4-(5-bromopicolinamido)butyl)carbamate (130 mg, 349 μ mol, 1.1 eq) and K_2CO_3 (131 mg, 950 μ mol, 2.5 eq) in afforded the product after purification and recrystallization in a mixture of EtOAc and *n*hexane as a yellow solid (90 mg, 143 μ mol, 49%).

1H NMR (400 MHz, DMSO) δ 13.00 (bs, 1H), 9.66 (bs, 1H), 9.01 (s, 1H), 8.84 (t, $J = 5.8$ Hz, 1H), 8.81 (d, $J = 1.9$ Hz, 1H), 8.77 (d, $J = 2.1$ Hz, 1H), 8.36 (dd, $J = 7.9, 1.3$ Hz, 1H), 8.14 (d, $J = 11.0$ Hz, 2H), 7.66 (dd, $J = 14.5, 7.7$ Hz, 1H), 7.35 (t, $J = 8.8$ Hz, 1H), 6.80 (t, $J = 5.3$ Hz, 1H, N-H), 3.35 – 3.30 (m, 4H), 3.18 – 3.13 (m, 2H),



Chemical Formula: $C_{32}H_{36}F_2N_6O_6S$
Molecular Weight: 670,73

2.94 (dd, $J = 12.6, 6.4$ Hz, 3H), 1.86 – 1.75 (m, 2H), 1.53 (dd, $J = 14.5, 6.8$ Hz, 2H), 1.47 – 1.38 (m, 3H), 0.99 (t, $J = 7.4$ Hz, 3H)ppm. ^{13}C NMR (101 MHz, DMSO) δ 184.6, 163.5, 159.89 (dd, $J = 255.5, 3.6$ Hz), 156.10 (dd, $J = 253.4, 4.9$ Hz), 155.5, 149.2, 148.9, 146.6, 144.0, 138.2, 136.2, 136.0, 128.98 – 128.67 (m), 127.9, 127.4, 125.13 (d, $J = 17.9$ Hz), 122.1, 118.1, 114.9, 114.4, 112.22 (d, $J = 20.8$ Hz) 77.3, 54.7, 39.5, 38.5, 28.2, 27.0, 26.6, 16.9, 12.6 ppm. ESI-MS (m/z) 669.0 [M - H].

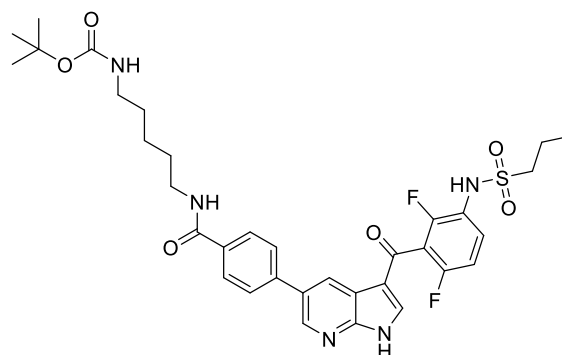
***Tert*-butyl (5-(4-(3-(2,6-difluoro-3-(propylsulfonamido)benzoyl)-1*H*-pyrrolo[2,3-*b*]pyridin-5-yl)benzamido)pentyl)carbamate (33)**

Following the general procedure C for Suzuki coupling of azaindoles, coupling of *N*-(3-(1-(2,6-dichlorobenzoyl)-5-(4,4,5,5-tetramethyl-1,3,2-dioxaborolan-2-yl)-1*H*-pyrrolo[2,3-*b*]pyridine-3-carbonyl)-2,4-difluorophenyl)propane-1-sulfonamide (73 mg, 108 μ mol, 1 eq), *tert*-butyl (5-(4-bromobenzamido)pentyl)carbamate (46 mg, 118 μ mol, 1.1 eq) and K_2CO_3

(37 mg, 269 μmol , 2.5 eq) in afforded the product after purification and recrystallization in a mixture of EtOAc and *n*hexane as a yellow solid (43 mg, 63 μmol , 58%).

^1H NMR (600 MHz, CDCl_3) δ 9.77 (s, 1H), 8.75 (t, $J = 14.3$ Hz, 1H), 8.68 (s, 1H), 8.52 (t, $J = 5.5$ Hz, 1H), 8.25 (s, 1H), 7.99 (d, $J = 8.3$ Hz, 2H), 7.85 (d, $J = 8.2$ Hz, 2H), 7.59 (td, $J = 9.0, 6.0$ Hz, 1H), 7.29 (t, $J = 8.4$ Hz, 1H), 6.77 (t, $J = 5.2$ Hz, 1H), 3.28 (dd, $J = 12.7, 6.6$ Hz, 2H), 3.14 – 3.11 (m, 2H), 2.92 (dd, $J = 12.9, 6.6$ Hz, 2H), 1.78 – 1.70 (m, 2H), 1.57 – 1.51

(m, 2H), 1.42 (dt, $J = 13.0, 6.4$ Hz, 2H), 1.36 (s, 9H), 1.30 (dd, $J = 14.8, 7.9$ Hz, 2H), 0.96 (t, $J = 7.4$ Hz, 3H) ppm. ^{13}C NMR (151 MHz, CDCl_3) δ 180.7, 180.7, 165.7, 165.7, 156.05 (dd, $J = 246.8, 6.6$ Hz), 155.6, 152.38 (dd, $J = 249.7, 8.3$ Hz), 149.1, 144.16 (d, $J = 8.9$ Hz), 140.6, 138.98 (d, $J = 25.3$ Hz), 133.6, 130.7, 128.9, 128.0, 127.2, 126.9, 121.97 (d, $J = 13.5$ Hz), 118.16 (t, $J = 23.5$ Hz), 117.5, 115.8, 112.60 – 111.84 (m), 77.3, 53.5, 40.1, 39.5, 31.3, 29.2, 28.9, 28.3, 23.8, 22.1, 16.8, 14.0, 12.6 ppm. ESI-MS (m/z) 706.7 [$\text{M} + \text{Na}$] $^+$.

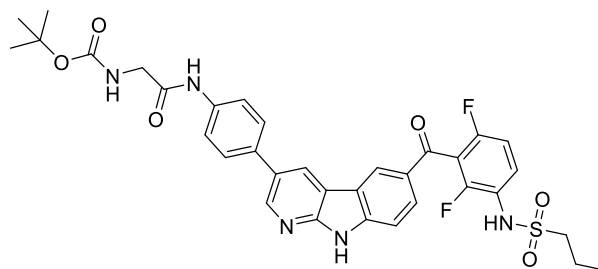


Chemical Formula: $\text{C}_{34}\text{H}_{39}\text{F}_2\text{N}_5\text{O}_6\text{S}$
Molecular Weight: 683.77

***Tert*-butyl (2-((4-(6-(2,6-difluoro-3-(propylsulfonamido)benzoyl)-9*H*-pyrido[2,3-*b*]indol-3-yl)phenyl)amino)-2-oxoethyl)carbamate (34)**

Following standard procedure C for Suzuki coupling *N*-(2,4-difluoro-3-(3-(4,4,5,5-tetramethyl-1,3,2-dioxaborolan-2-yl)-9*H*-pyrido[2,3-*b*]indole-6-carbonyl)phenyl)propane-1-sulfonamide (120 mg, 216 μmol , 1 eq), *tert*-butyl (2-((4-bromophenyl)amino)-2-oxoethyl)carbamate (78 mg, 238 μmol , 1.1 eq), K_2CO_3 (60 mg, 432 μmol , 2 eq) and $\text{Pd}(\text{PPh}_3)_4$ (12 mg, 11 mol, 5 mol%) were suspended in 1,4-dioxane/water (1:1, v/v, 2 mL) and yielded the product as a colorless solid (95 mg, 140 μmol , 65%).

^1H NMR (200 MHz, DMSO) δ 12.48 (s, 1H), 10.04 (s, 1H, NH-23), 9.82 (s, 1H), 9.02 (d, $J = 2.0$ Hz, 1H), 8.81 (d, $J = 1.4$ Hz, 1H), 8.03 (d, $J = 7.2$ Hz, 1H), 7.71 (dd, $J = 16.6, 5.4$ Hz, 7H), 7.35 (t, $J = 8.5$ Hz, 1H), 7.07 (s, 1H), 3.76 (d, $J = 5.7$ Hz, 2H), 3.23 – 3.11 (m, 2H), 1.74 (dd, $J = 15.4, 7.7$ Hz, 3H), 0.93 (t, $J = 7.5$ Hz, 3H) ppm. ^{13}C NMR (50 MHz, DMSO) δ 187.7, 168.3, 156.0, 152.0, 145.8, 143.5, 138.3, 132.8, 128.5, 128.2, 127.8, 127.3, 127.1, 125.3, 122.06 (dd, $J = 13.3, 3.6$ Hz), 120.8, 119.6, 115.7, 112.54 (dd, $J = 20.4, 3.6$ Hz), 112.1, 78.1, 53.5, 44.2, 28.2, 16.8, 12.6 ppm. ESI-MS (m/z) 700.6 [$\text{M} + \text{Na}$] $^+$.

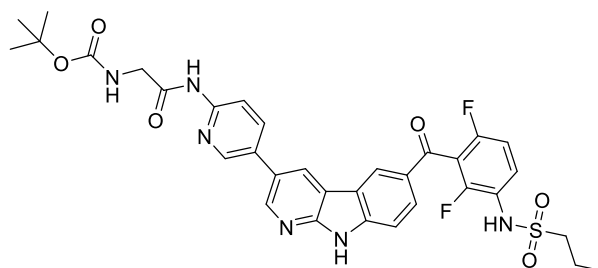


Chemical Formula: $\text{C}_{34}\text{H}_{33}\text{F}_2\text{N}_5\text{O}_6\text{S}$
Molecular Weight: 677,72

***Tert*-butyl (2-((5-(6-(2,6-difluoro-3-(propylsulfonamido)benzoyl)-9*H*-pyrido[2,3-*b*]indol-3-yl)pyridin-2-yl)amino)-2-oxoethyl)carbamate (35)**

Following standard procedure C for Suzuki coupling *N*-(2,4-difluoro-3-(3-(4,4,5,5-tetramethyl-1,3,2-dioxaborolan-2-yl)-9*H*-pyrido[2,3-*b*]indole-6-carbonyl)phenyl)propane-1-sulfonamide (200 mg, 360 μmol , 1 eq), *tert*-butyl (2-((5-bromopyridin-2-yl)amino)-2-oxoethyl)carbamate (131 mg, 396 μmol , 1.1 eq), K_2CO_3 (100 mg, 720 μmol , 2 eq) and $\text{Pd}(\text{PPh}_3)_4$ (21 mg, 18 μmol , 5 mol%) were suspended in 1,4-dioxane/water (1:1, v/v, 3.5 mL) and yielded the product as a colorless solid (65 mg, 96 μmol , 27%).

^1H NMR (200 MHz, DMSO) δ 12.55 (s, 1H), 10.56 (s, 1H), 9.83 (s, 1H), 9.10 (s, 1H), 8.86 (s, 1H), 8.81 (s, 1H), 8.20 (s, 1H), 8.04 (d, $J = 8.2$ Hz, 1H), 7.68 (d, $J = 8.6$ Hz, 1H), 7.37 (d, $J = 8.8$ Hz, 1H), 7.09 (s, 1H), 3.81 (s, 2H), 3.16 (s, 2H), 1.73 (d, $J = 7.1$ Hz, 2H), 1.40 (s, 12H), 0.92 (t, $J = 7.3$ Hz, 3H) ppm. ^{13}C NMR (50 MHz, DMSO) δ 187.3, 152.6, 146.3, 143.9, 136.7, 129.6, 121.1, 116.1, 78.5, 44.1, 41.1, 40.7, 40.3, 39.9, 39.5, 39.1, 38.6, 28.6, 28.6, 17.2, 12.9 ppm. ESI-MS (m/z) 701.7 [$\text{M} + \text{Na}$] $^+$.

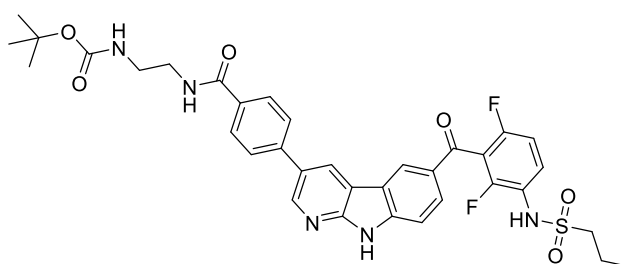


Chemical Formula: $\text{C}_{33}\text{H}_{32}\text{F}_2\text{N}_5\text{O}_6\text{S}$
Molecular Weight: 678,71

***Tert*-butyl (2-(4-(6-(2,6-difluoro-3-(propylsulfonamido)benzoyl)-9*H*-pyrido[2,3-*b*]indol-3-yl)benzamido)ethyl)carbamate (36)**

Following standard procedure C for Suzuki coupling *N*-(2,4-difluoro-3-(3-(4,4,5,5-tetramethyl-1,3,2-dioxaborolan-2-yl)-9*H*-pyrido[2,3-*b*]indole-6-carbonyl)phenyl)propane-1-sulfonamide (213 mg, 384 μmol , 1 eq), *tert*-butyl (2-(4-bromobenzamido)ethyl)carbamate (145 mg, 422 μmol , 1.1 eq), K_2CO_3 (106 mg, 767 μmol , 2 eq) and $\text{Pd}(\text{PPh}_3)_4$ (22 mg, 19 μmol , 5 mol%) were suspended in 1,4-dioxane/water (1:1, v/v, 3.5 mL) and yielded the product as a colorless solid (109 mg, 154 μmol , 40%).

^1H NMR (200 MHz, DMSO) δ 12.57 (s, 1H), 9.83 (s, 1H), 9.15 (d, $J = 1.3$ Hz, 1H), 8.91 (d, $J = 1.3$ Hz, 1H), 8.86 (s, 1H), 8.54 (t, $J = 4.5$ Hz, 1H), 8.10 – 7.89 (m, 2H), 7.76 – 7.59 (m, 2H), 7.35 (t, $J = 8.6$ Hz, 1H), 6.94 (t, $J = 4.8$ Hz, 1H), 3.34 – 3.26 (m, 2H), 3.21 – 3.07 (m, 4H), 1.87 – 1.63



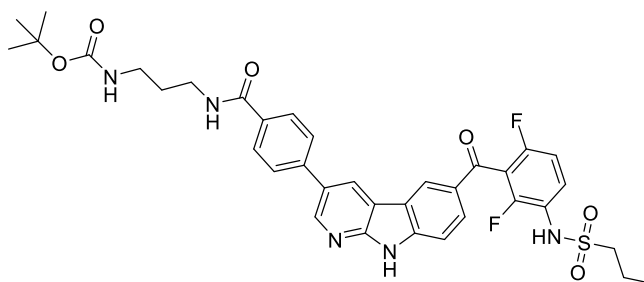
Chemical Formula: $\text{C}_{33}\text{H}_{35}\text{F}_2\text{N}_5\text{O}_6\text{S}$
Molecular Weight: 691,75

(m, 2H), 1.38 (s, 3H), 0.92 (t, $J = 7.4$ Hz, 3H) ppm. ^{13}C NMR (101 MHz, DMSO) δ 186.9, 166.0, 155.8, 152.4, 146.0, 143.5, 140.6, 133.0, 128.4, 127.9, 127.8, 126.4, 125.0, 122.1, 122.0, 122.0, 122.0, 120.8, 115.7, 112.6, 112.5, 112.3, 112.3, 112.0, 77.7, 53.6, 39.5, 28.2, 16.8, 12.5 ppm. ESI-MS (m/z) 714.8 $[\text{M}+\text{Na}]^+$.

***Tert*-butyl (3-(4-(6-(2,6-difluoro-3-(propylsulfonamido)benzoyl)-9*H*-pyrido[2,3-*b*]indol-3-yl)benzamido)propyl)carbamate (37)**

Following standard procedure C for Suzuki coupling *N*-(2,4-difluoro-3-(3-(4,4,5,5-tetramethyl-1,3,2-dioxaborolan-2-yl)-9*H*-pyrido[2,3-*b*]indole-6-carbonyl)phenyl)propane-1-sulfonamide (100 mg, 180 μmol , 1 eq), *tert*-butyl (3-(4-bromobenzamido)propyl)carbamate (71 mg, 198 μmol , 1.1 eq), K_2CO_3 (75 mg, 540 μmol , 3 eq) and Xphos Pd G3 (8 mg, 9 μmol , 5 mol%) were suspended in 1,4-dioxane/water (1:1, v/v, 3.5 mL) and yielded the product as a colorless solid (25 mg, 34 μmol , 20%).

^1H NMR (400 MHz, MeOD) δ 8.80 (d, $J = 2.1$ Hz, 1H), 8.73 (d, $J = 2.1$ Hz, 1H), 8.69 (s, 1H), 8.07 (dd, $J = 8.6, 1.5$ Hz, 1H), 7.95 (d, $J = 8.4$ Hz, 2H), 7.81 (d, $J = 8.4$ Hz, 2H), 7.73 (td, $J = 9.0, 5.7$ Hz, 1H), 7.64 (d, $J = 8.6$ Hz, 1H), 7.22 – 7.17 (m, 1H), 3.46 (t, $J = 6.8$ Hz, 2H), 3.20 –



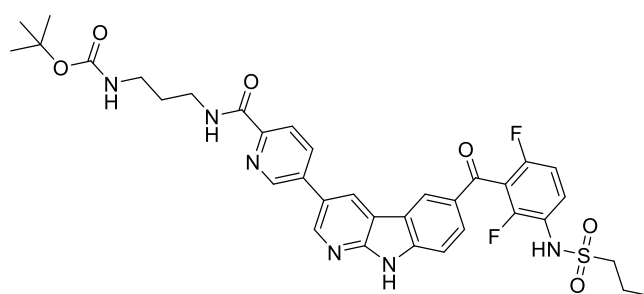
Chemical Formula: $\text{C}_{36}\text{H}_{37}\text{F}_2\text{N}_5\text{O}_6\text{S}$
Molecular Weight: 705,78

3.12 (m, 4H), 1.92 – 1.76 (m, 4H), 1.46 (s, 9H), 1.01 (t, $J = 7.5$ Hz, 3H) ppm. ^{13}C NMR (101 MHz, MeOD) δ 188.9, 169.8, 158.7, 158.21 (dd, $J = 248.3, 7.2$ Hz), 153.9 (dd, $J = 249.4, 8.3$ Hz), 153.6, 146.7, 145.2, 142.9, 134.4, 130.5, 130.2, 129.76 (d, $J = 9.8$ Hz), 129.5, 129.1, 128.1, 126.0, 123.53 (dd, $J = 13.4, 4.0$ Hz), 122.4, 119.15 (dd, $J = 23.8, 22.0$ Hz), 118.0, 113.35 (dd, $J = 22.7, 3.6$ Hz), 113.0, 80.1, 55.2, 49.0, 38.8, 38.4, 30.9, 28.8, 18.3, 13.2 ppm.

***Tert*-butyl (3-(5-(6-(2,6-difluoro-3-(propylsulfonamido)benzoyl)-9H-pyrido[2,3-*b*]indol-3-yl)picolinamido)propyl)carbamate (38)**

Following standard procedure C for Suzuki coupling *N*-(2,4-difluoro-3-(3-(4,4,5,5-tetramethyl-1,3,2-dioxaborolan-2-yl)-9H-pyrido[2,3-*b*]indole-6-carbonyl)phenyl)propane-1-sulfonamide (200 mg, 360 μmol , 1 eq), *tert*-butyl(3-(5-bromopicolinamido)propyl)carbamate (194 mg, 540 μmol , 1.5 eq), K_2CO_3 (100 mg, 720 μmol , 2 eq) and $\text{Pd}(\text{PPh}_3)_4$ (21 mg, 18 μmol , 5 mol%) were suspended in 1,4-dioxane/water (1:1, v/v, 3.5 mL) and yielded the product as a colorless solid (85 mg, 65 μmol , 33%).

^1H NMR (200 MHz, MeOD) δ 8.96 (s, 1H), 8.89 (s, 1H), 8.74 (dd, $J = 11.6, 2.1$ Hz, 1H), 8.65 (s, 1H), 8.19 (dd, $J = 8.3, 2.0$ Hz, 1H), 8.09 (d, $J = 8.1$ Hz, 1H), 8.03 (dd, $J = 8.7, 1.4$ Hz, 1H), 7.71 (td, $J = 9.1, 5.9$ Hz, 1H), 7.58 (d, $J = 8.7$ Hz, 1H), 7.17 (t, $J = 8.7$ Hz, 1H), 3.47 (t, $J = 5.3$ Hz, 2H), 3.31 (dt, $J = 3.2, 1.6$ Hz, 2H), 3.14 (m, 4), 1.96 – 1.70 (m, 2H), 1.44 (s, 9H),



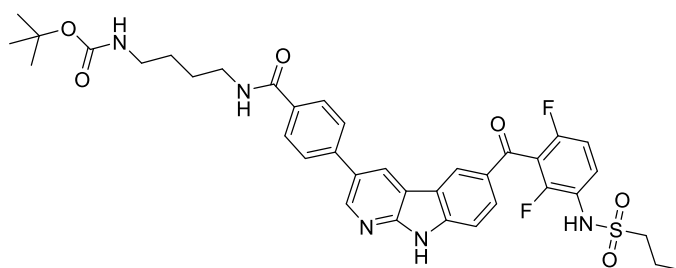
Chemical Formula: $\text{C}_{33}\text{H}_{36}\text{F}_2\text{N}_6\text{O}_6\text{S}$
Molecular Weight: 706,77

1.00 (t, $J = 7.4$ Hz, 3H) ppm. ^{13}C NMR (50 MHz, MeOD) δ 188.8, 166.6, 165.0, 155.4, 153.9, 153.8, 149.6, 147.9, 146.7, 145.1, 138.1, 136.6, 130.6, 129.6, 126.9, 123.2, 122.2, 118.0, 113.0, 55.2, 49.0, 37.9, 31.0, 28.8, 18.3, 13.2 ppm. ESI-MS (m/z) 729.2 $[\text{M}+\text{Na}]^+$.

***Tert*-butyl (4-(4-(6-(2,6-difluoro-3-(propylsulfonamido)benzoyl)-9*H*-pyrido[2,3-*b*]indol-3-yl)benzamido)butyl)carbamate (39)**

Following standard procedure C for Suzuki coupling *N*-(2,4-difluoro-3-(3-(4,4,5,5-tetramethyl-1,3,2-dioxaborolan-2-yl)-9*H*-pyrido[2,3-*b*]indole-6-carbonyl)phenyl)propane-1-sulfonamide (200 mg, 360 μmol , 1 eq), *tert*-butyl (4-(4-bromobenzamido)butyl)carbamate (147 mg, 396 μmol , 1.1 eq), K_2CO_3 (100 mg, 720 μmol , 2 eq) and $\text{Pd}(\text{PPh}_3)_4$ (21 mg, 18 μmol , 5 mol%) were suspended in 1,4-dioxane/water (1:1, v/v, 3.5 mL) and yielded the product as a colorless solid (199 mg, 271 μmol , 75%).

^1H NMR (200 MHz, DMSO) δ 12.57 (s, 1H), 9.83 (s, 1H), 9.14 (d, $J = 2.1$ Hz, 1H), 8.90 (d, $J = 2.0$ Hz, 1H), 8.85 (s, 1H), 8.53 (t, $J = 5.6$ Hz, 1H), 8.10 – 7.87 (m, 5H), 7.76 – 7.58 (m, 2H), 7.35 (t, $J = 8.7$ Hz, 1H), 6.81 (t, $J = 5.4$ Hz, 1H), 3.28 (d, $J = 5.6$ Hz, 2H),



Chemical Formula: $\text{C}_{37}\text{H}_{39}\text{F}_2\text{N}_5\text{O}_6\text{S}$
Molecular Weight: 719,80

3.22 – 3.11 (m, 2H), 2.95 (d, $J = 6.0$ Hz, H), 1.85 – 1.62 (m, 2H), 1.47 (s, 4H), 1.37 (s, 9H), 0.92 (t, $J = 7.4$ Hz, 3H) ppm. ^{13}C NMR (50 MHz, DMSO) δ 187.0, 165.7, 155.6, 152.5, 146.1, 143.5, 140.5, 133.2, 128.4, 127.9, 127.8, 126.5, 120.8, 115.7, 77.4, 53.5, 39.5, 28.3, 16.8, 12.6 ppm. ESI-MS (m/z) 742.8 $[\text{M}+\text{Na}]^+$.

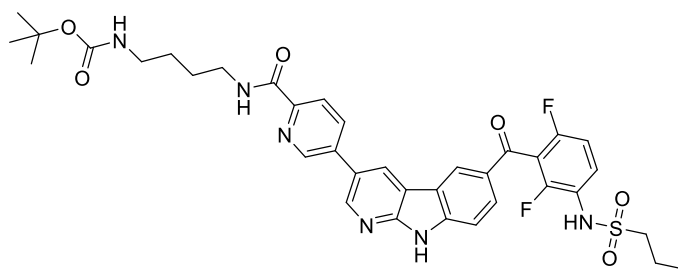
***Tert*-butyl (4-(5-(6-(2,6-difluoro-3-(propylsulfonamido)benzoyl)-9*H*-pyrido[2,3-*b*]indol-3-yl)picolinamido)butyl)carbamate (40)**

Following standard procedure C for Suzuki coupling *N*-(2,4-difluoro-3-(3-(4,4,5,5-tetramethyl-1,3,2-dioxaborolan-2-yl)-9*H*-pyrido[2,3-*b*]indole-6-carbonyl)phenyl)propane-1-sulfonamide (200 mg, 360 μmol , 1 eq), *tert*-butyl(4-(5-bromopicolinamido)butyl)carbamate (147 mg, 396 μmol , 1.1 eq), K_2CO_3 (100 mg, 720

μmol , 2 eq) and $\text{Pd}(\text{PPh}_3)_4$ (21 mg, 18 μmol , 5 mol%) were suspended in 1,4-dioxane/water (1:1, v/v, 3.5 mL) and yielded the product as a colorless solid (110 mg, 153 μmol , 42%).

^1H NMR (200 MHz, DMSO) δ 12.65 (s, 1H), 9.84 (s, 1H), 9.21 (d, $J = 2.1$ Hz, 1H), 9.09 (d, $J = 1.5$ Hz, 1H), 8.97 (d, $J = 2.1$ Hz, 1H), 8.88 – 8.79 (m, 2H), 8.41 (dd, $J = 8.0, 2.2$ Hz, 1H), 8.14 (d, $J = 8.0$ Hz, 1H), 8.04 (dd, $J = 8.6, 1.4$ Hz, 1H), 7.77 – 7.59 (m, 2H),

7.35 (t, $J = 8.5$ Hz, 1H), 6.81 (s, 1H), 3.32 – 3.25 (m, 2H), 3.22 – 3.09 (m, 2H), 2.94 (d, $J = 6.3$ Hz, 2H), 1.73 (dd, $J = 14.9, 7.2$ Hz, 2H), 1.40 (s, 2H), 1.36 (s, 9H), 0.91 (t, $J = 7.4$ Hz, 3H) ppm. ^{13}C NMR (50 MHz, DMSO) δ 187.0, 163.6, 155.6, 152.8, 148.8, 146.4, 143.6, 136.1, 135.5, 128.5, 125.1, 124.9, 122.0, 120.8, 115.8, 112.2, 77.4, 53.5, 39.5, 28.3, 25.0, 16.8, 12.6 ppm. ESI-MS (m/z) 743.3 $[\text{M}+\text{Na}]^+$.

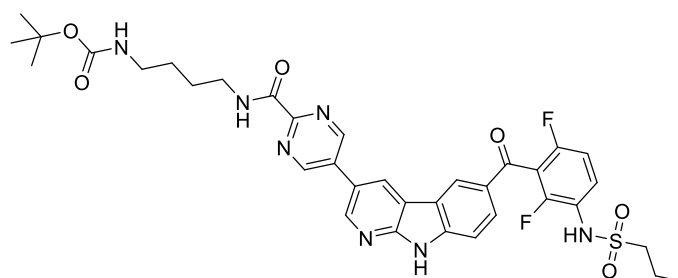


Chemical Formula: $\text{C}_{36}\text{H}_{38}\text{F}_2\text{N}_6\text{O}_6\text{S}$
Molecular Weight: 720,79

***Tert*-butyl (4-(5-(6-(2,6-difluoro-3-(propylsulfonamido)benzoyl)-9H-pyrido[2,3-b]indol-3-yl)pyrimidine-2-carboxamido)butyl)carbamate (41)**

Following standard procedure C for Suzuki coupling *N*-(2,4-difluoro-3-(3-(4,4,5,5-tetramethyl-1,3,2-dioxaborolan-2-yl)-9H-pyrido[2,3-*b*]indole-6-carbonyl)phenyl)propane-1-sulfonamide (180 mg, 324 μmol , 1 eq), *tert*-butyl (4-(5-bromopyrimidine-2-carboxamido)butyl)carbamate (133 mg, 356.7 μmol , 1.1 eq), K_2CO_3 (90 mg, 648 μmol , 2 eq) and $\text{Pd}(\text{PPh}_3)_4$ (19 mg, 16 μmol , 5 mol%) were suspended in 1,4-dioxane/water (1:1, v/v, 3.5 mL) and yielded the product as a colorless solid (20 mg, 62 μmol , 19%).

^1H NMR (200 MHz, DMSO) δ 12.72 (s, 1H), 9.83 (s, 1H), 9.40 (s, 2H), 9.28 (s, 1H), 9.02 (s, 2H), 8.81 (s, 1H), 8.04 (d, $J = 7.6$ Hz, 1H), 7.71 (d, $J = 8.9$ Hz, 2H), 7.35 (s, 1H), 6.80 (s, 1H), 4.22 – 4.06 (m, 8H), 3.04 – 2.98 (m, 2H), 1.74 (s, 2H), 1.36 (s, 12H), 0.93



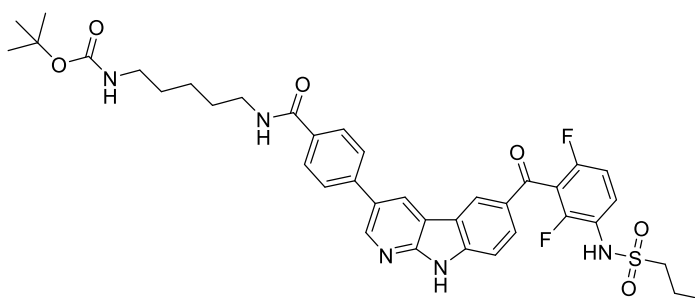
Chemical Formula: $\text{C}_{35}\text{H}_{37}\text{F}_2\text{N}_7\text{O}_6\text{S}$
Molecular Weight: 721,78

(d, $J = 7.1$ Hz, 3H) ppm. ^{13}C NMR (50 MHz, DMSO) δ 187.1, 155.0, 152.5, 132.4, 128.7, 122.5, 115.9, 79.2, 48.7, 43.9, 39.5, 28.3, 12.6 ppm.

***Tert*-butyl (5-(4-(6-(2,6-difluoro-3-(propylsulfonamido)benzoyl)-9*H*-pyrido[2,3-*b*]indol-3-yl)benzamido)pentyl)carbamate (42)**

Following standard procedure C for Suzuki coupling *N*-(2,4-difluoro-3-(3-(4,4,5,5-tetramethyl-1,3,2-dioxaborolan-2-yl)-9*H*-pyrido[2,3-*b*]indole-6-carbonyl)phenyl)propane-1-sulfonamide (104 mg, 187 μmol , 1 eq), *tert*-butyl (5-(4-bromobenzamido)pentyl)carbamate (60 mg, 156 μmol , 1 eq), K_2CO_3 (65 mg, 467 μmol , 3 eq) and $\text{Pd}(\text{PPh}_3)_4$ (14 mg, 12 μmol , 8 mol%) were suspended in 1,4-dioxane/water (1:1, v/v, 3.5 mL) and yielded the product as a colorless solid (40 mg, 55 μmol , 35%).

^1H NMR (400 MHz, MeOD) δ 8.76 (d, $J = 2.0$ Hz, 1H), 8.71 (d, $J = 1.3$ Hz, 1H), 8.67 (s, 1H), 8.05 (dd, $J = 8.7, 1.3$ Hz, 1H), 7.92 (d, $J = 8.3$ Hz, 2H), 7.78 (d, $J = 8.4$ Hz, 2H), 7.72 (td, $J = 9.0, 5.8$ Hz, 1H), 7.61 (d, $J = 8.6$ Hz, 1H), 7.21 – 7.16 (m, 1H),



Chemical Formula: $\text{C}_{38}\text{H}_{41}\text{F}_2\text{N}_5\text{O}_6\text{S}$
Molecular Weight: 733,83

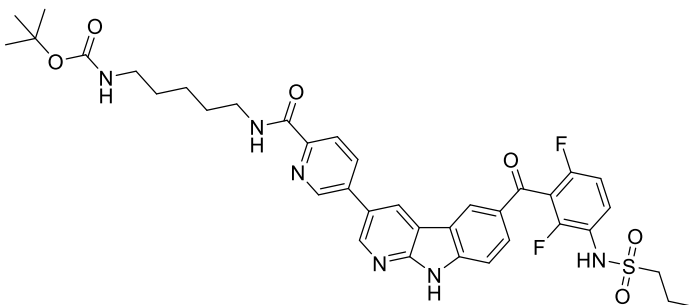
3.41 (t, $J = 7.1$ Hz, 2H), 3.18 – 3.11 (m, 2H), 3.07 (dd, $J = 11.7, 6.6$ Hz, 2H), 1.92 – 1.80 (m, 2H), 1.71 – 1.61 (m, 2H), 1.54 (dt, $J = 14.2, 7.1$ Hz, 2H), 1.43 (bs, 12H), 1.00 (t, $J = 7.5$ Hz, 3H) ppm. ^{13}C NMR (101 MHz, MeOD) δ 188.9, 169.8, 158.6, 158.20 (dd, $J = 248.5, 7.0$ Hz), 153.88 (dd, $J = 249.2, 8.2$ Hz), 153.5, 146.6, 145.2, 142.8, 134.6, 130.5, 130.1, 129.75 (dd, $J = 9.3, 1.6$ Hz), 129.5, 129.1, 129.0, 128.1, 126.0, 123.54 (dd, $J = 13.2, 3.8$ Hz), 122.3, 119.14 (dd, $J = 23.8, 22.1$ Hz), 117.9, 113.36 (d, $J = 25.9$ Hz), 113.0, 79.9, 55.2, 49.0, 41.2, 41.0, 30.7, 30.2, 28.8, 25.3, 18.3, 13.2 ppm. ESI-MS (m/z) 756.0 $[\text{M}+\text{Na}]^+$.

***Tert*-butyl (5-(5-(6-(2,6-difluoro-3-(propylsulfonamido)benzoyl)-9*H*-pyrido[2,3-*b*]indol-3-yl)picolinamido)pentyl)carbamate (43)**

Following standard procedure C for Suzuki coupling *N*-(2,4-difluoro-3-(3-(4,4,5,5-tetramethyl-1,3,2-dioxaborolan-2-yl)-9*H*-pyrido[2,3-*b*]indole-6-carbonyl)phenyl)propane-

1-sulfonamide (200 mg, 360 μmol , 1 eq), *tert*-butyl (6-((5-bromopyridin-2-yl)amino)-6-oxohexyl)carbamate (167 mg, 432 μmol , 1.1 eq), K_2CO_3 (100 mg, 720 μmol , 2 eq) and $\text{Pd}(\text{PPh}_3)_4$ (21 mg, 18 μmol , 5 mol%) were suspended in 1,4-dioxane/water (1:1, v/v, 3.5 mL) and yielded the product as a colorless solid (84 mg, 114 μmol , 32%).

^1H NMR (200 MHz, MeOD) δ 8.89 (d, $J = 1.1$ Hz, 1H), 8.75 (d, $J = 1.7$ Hz, 1H), 8.70 (d, $J = 1.5$ Hz, 1H), 8.63 (s, 1H), 8.19 (dd, $J = 8.1, 1.8$ Hz, 1H), 8.09 (d, $J = 8.3$ Hz, 1H), 8.01 (d, $J = 8.4$ Hz, 1H), 7.69 (td, $J = 8.9, 6.0$ Hz, 1H), 7.58 (d, $J = 8.6$



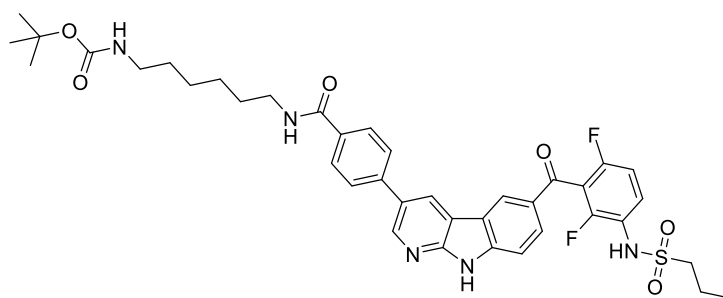
Chemical Formula: $\text{C}_{37}\text{H}_{40}\text{F}_2\text{N}_6\text{O}_6\text{S}$
Molecular Weight: 734,82

Hz, 1H), 7.16 (t, $J = 8.4$ Hz, 1H), 3.45 (t, $J = 6.7$ Hz, 2H), 3.13 (dd, $J = 8.6, 6.9$ Hz, 2H), 2.94 (t, $J = 7.4$ Hz, 2H), 1.99 (s, 2H), 1.87 – 1.60 (m, 6H), 1.49 (d, $J = 6.8$ Hz, 2H), 1.36 (s, 9H), 0.98 (t, $J = 7.4$ Hz, 3H) ppm. ^{13}C NMR (50 MHz, MeOD) δ 179.4, 140.1, 138.4, 137.1, 135.7, 128.6, 127.2, 121.1, 120.1, 119.6, 117.3, 113.8, 112.7, 108.5, 103.6, 45.8, 39.5, 31.1, 30.6, 20.6, 18.7, 13.9 ppm. ESI-MS (m/z) 756.8 $[\text{M}+\text{Na}]^+$.

***Tert*-butyl (6-(4-(6-(2,6-difluoro-3-(propylsulfonamido)benzoyl)-9*H*-pyrido[2,3-*b*]indol-3-yl)benzamido)hexyl)carbamate (44)**

Following standard procedure C for Suzuki coupling *N*-(2,4-difluoro-3-(3-(4,4,5,5-tetramethyl-1,3,2-dioxaborolan-2-yl)-9*H*-pyrido[2,3-*b*]indole-6-carbonyl)phenyl)propane-1-sulfonamide (100 mg, 180 μmol , 1.1 eq), *tert*-butyl (6-(4-bromobenzamido)hexyl)carbamate (60 mg, 150 μmol , 1 eq), K_2CO_3 (62 mg, 451 μmol , 3 eq) and $\text{Pd}(\text{PPh}_3)_4$ (14 mg, 12 μmol , 8 mol%) were suspended in 1,4-dioxane/water (1:1, v/v, 3.5 mL) and yielded the product as a colorless solid (199 mg, 271 μmol , 75%).

^1H NMR (400 MHz, MeOD) δ 8.74 (d, $J = 2.1$ Hz, 1H), 8.70 (d, $J = 2.1$ Hz, 1H), 8.66 (s, 1H), 8.05 (dd, $J = 8.7, 1.5$ Hz, 1H), 7.91 (t, $J = 7.0$ Hz, 2H), 7.77 (d, $J = 8.4$ Hz, 2H), 7.72 (td, $J = 9.0, 5.8$ Hz, 1H), 7.60 (d, $J = 8.6$ Hz, 1H), 7.21 –



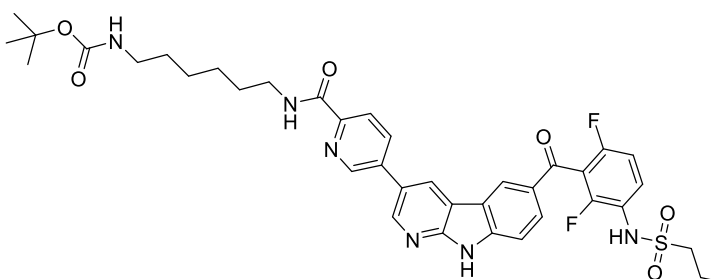
Chemical Formula: $\text{C}_{39}\text{H}_{43}\text{F}_2\text{N}_5\text{O}_6\text{S}$
Molecular Weight: 747,86

7.15 (m, 1H), 3.40 (t, $J = 7.1$ Hz, 2H), 3.19 – 3.12 (m, 2H), 3.04 (t, $J = 6.9$ Hz, 2H), 1.91 – 1.80 (m, 2H), 1.70 – 1.61 (m, 2H), 1.54 – 1.46 (m, 2H), 1.43 (s, 9H), 1.40 (m, 4H), 1.00 (t, $J = 7.5$ Hz, 3H) ppm. ^{13}C NMR (101 MHz, MeOD) δ 188.9, 169.7, 158.6, 158.19 (dd, $J = 248.3, 7.2$ Hz), 153.87 (dd, $J = 249.4, 8.1$ Hz), 153.5, 146.6, 145.2, 142.8, 134.6, 130.5, 130.1, 129.74 (d, $J = 9.8$ Hz), 129.5, 129.1, 129.0, 128.1, 126.0, 123.52 (dd, $J = 13.3, 3.9$ Hz), 122.3, 119.12 (dd, $J = 23.8, 22.0$ Hz), 117.9, 113.35 (dd, $J = 22.8, 3.9$ Hz), 112.9, 79.8, 55.2, 49.0, 41.2, 41.0, 30.9, 30.5, 28.8, 27.7, 27.5, 18.3, 13.2 ppm. ESI-MS (m/z) 770.0 $[\text{M}+\text{Na}]^+$.

***Tert*-butyl (6-(5-(6-(2,6-difluoro-3-(propylsulfonamido)benzoyl)-9H-pyrido[2,3-*b*]indol-3-yl)picolinamido)hexyl)carbamate (45)**

Following standard procedure C for Suzuki coupling *N*-(2,4-difluoro-3-(3-(4,4,5,5-tetramethyl-1,3,2-dioxaborolan-2-yl)-9H-pyrido[2,3-*b*]indole-6-carbonyl)phenyl)propane-1-sulfonamide (200 mg, 360 μmol , 1 eq), *tert*-butyl (6-(5-bromopicolinamido)hexyl)carbamate (159 mg, 396 μmol , 1.1 eq), K_2CO_3 (100 mg, 720 μmol , 2 eq) and $\text{Pd}(\text{PPh}_3)_4$ (21 mg, 18 μmol , 5 mol%) were suspended in 1,4-dioxane/water (1:1, v/v, 3.5 mL) and yielded the product as a colorless solid (80 mg, 107 μmol , 30%).

^1H NMR (200 MHz, DMSO) δ 12.65 (s, 1H), 9.83 (s, 1H), 9.21 (d, $J = 1.7$ Hz, 1H), 9.09 (s, 1H), 8.96 (d, $J = 1.8$ Hz, 1H), 8.84 (s, 1H), 8.81 – 8.77 (m, 1H), 8.41 (dd, $J = 8.1, 1.8$ Hz, 1H), 8.14 (d, $J = 8.5$ Hz, 1H), 8.04 (d, $J = 8.4$ Hz,



Chemical Formula: $\text{C}_{38}\text{H}_{42}\text{F}_2\text{N}_6\text{O}_6\text{S}$
Molecular Weight: 748,85

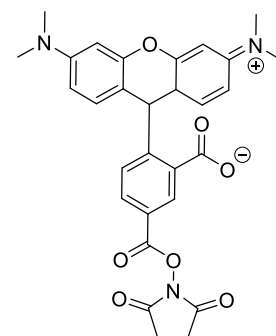
1H), 7.75 – 7.59 (m, 2H), 7.35 (t, $J = 8.9$ Hz, 1H), 6.76 (t, $J = 5.2$ Hz, 1H), 3.32 – 3.26 (m, 1H), 3.21 – 3.09 (m, 2H), 2.89 (dd, $J = 11.8, 6.2$ Hz, 2H), 1.73 (dd, $J = 15.2, 7.4$ Hz, 2H), 1.55 (s, 1H), 1.36 (s, 9H), 1.29 (s, 4H), 0.91 (t, $J = 7.4$ Hz, 3H) ppm. ^{13}C NMR (50 MHz, DMSO) δ 163.6, 152.8, 148.8, 146.5, 146.4, 143.6, 136.1, 135.5, 128.5, 128.4, 125.1, 125.0, 122.1, 120.8, 115.8, 77.3, 53.5, 39.5, 30.0, 29.5, 29.3, 29.2, 28.3, 26.2, 26.0, 16.8, 12.6 ppm. ESI-MS (m/z) 773.0 $[\text{M}+\text{Na}]^+$.

6.3.5. 5-TAMRA implementation

2-(6-(Dimethylamino)-3-(dimethyliminio)-9,9a-dihydro-3H-xanthen-9-yl)-5-(((2,5-dioxopyrrolidin-1-yl)oxy)carbonyl)benzoate (46)

5-Carboxytetramethylrhodamin (40 mg, 93 μmol , 1 eq) was dissolved in DMF (1 mL) and subsequently N,N' -disuccinimidyl carbonate (38 mg, 149 μmol , 1.6 eq) and DMAP (20 mg, 167 μmol , 1.8 eq) was added and stirred over night at room temperature. The reaction mixture was diluted with chloroform and the organic phase was washed with water and saturated sodium chloride solution. After removing the solvent under vacuum conditions, the crude product was obtained as purple solid (47 mg, 88.9 μmol , 95%).

^1H NMR (200 MHz, DMSO) δ 8.54 (s, 1H), 8.41 (dd, $J = 8.0, 1.5$ Hz, 1H), 7.50 (d, $J = 8.4$ Hz, 1H), 6.65 (d, $J = 8.7$ Hz, 2H), 6.52 (s, 4H), 2.96 (s, 12H), 2.93 (s, 4H) ppm. ESI-MS (m/z) 549.9 $[\text{M}+\text{Na}]^+$.



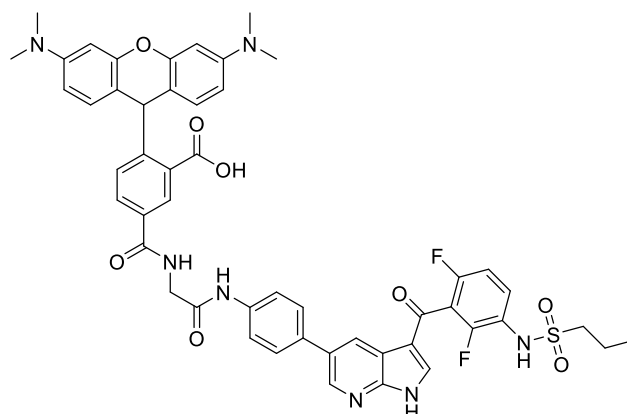
Chemical Formula: $\text{C}_{29}\text{H}_{27}\text{N}_3\text{O}_7$
Molecular Weight: 529,55

2-(3,6-Bis(dimethylamino)-9H-xanthen-9-yl)-5-(((2-((4-(3-(2,6-difluoro-3-(propylsulfonamido)benzoyl)-1H-pyrrolo[2,3-b]pyridin-5-yl)phenyl)amino)-2-oxoethyl)carbamoyl)benzoic acid (47)

Tert-butyl 2-(((4-(3-(2,6-difluoro-3-(propylsulfonamido)benzoyl)-1H-pyrrolo[2,3-b]pyridin-5-yl)phenyl)amino)-2-oxoethyl)carbamate (12 mg, 19.12 μmol , 1 eq) was dissolved in toluene/TFA (10:1, v/v) and stirred for 3 hours. Then the solvent was evaporated under reduced pressure and the residue was dissolved again in DMF (0.5 mL). The mixture was added to a solution of 5-TAMRA-SE (50 mg, 95 μmol , 5 eq) and DIPEA (66 μL , 379 μmol , 20 eq) in DMF. After 3 hours at room temperature the solvent was removed under reduced

pressure. The crude product was purified using column chromatography (RP, water/ACN/FA, v/v/v, 90:9:1–30:69:1) to provide the desired product as purple solid (13 mg, 14 μmol , 73%).

^1H NMR (400 MHz, DMSO) δ 12.85 – 12.80 (bs, 1H), 10.26 (s, 1H), 9.29 (s, 1H), 8.70 (s, 1H), 8.54 (s, 1H), 8.30 (d, J = 7.6 Hz, 1H), 8.24 – 8.23 (m, 1H), 8.21 (s, 1H), 7.83 – 7.68 (m, 4H), 7.57 (dd, J = 14.9, 9.1 Hz, 1H), 7.36 (d, J = 8.3 Hz, 1H), 7.25 (t, J = 8.6 Hz, 1H), 6.57 – 6.48 (m, 6H), 4.17 (d, J = 3.9 Hz, 2H), 3.12 – 3.06 (m, 1H), 2.95 (s, 12H), 1.73 (dd, J =



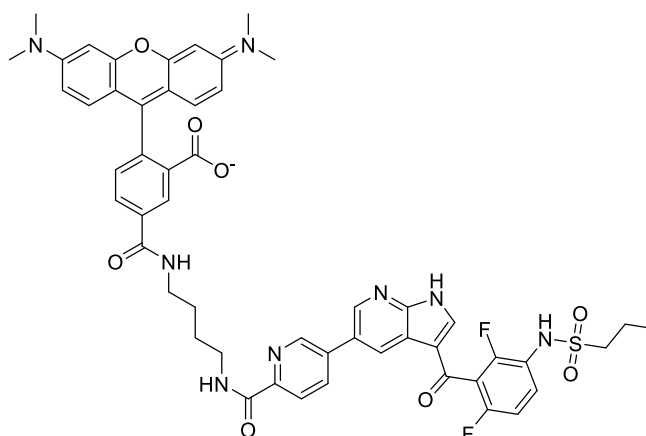
Chemical Formula: $\text{C}_{50}\text{H}_{45}\text{F}_2\text{N}_7\text{O}_8\text{S}$
Molecular Weight: 942,01

14.0, 6.9 Hz, 2H), 0.95 (t, J = 7.1 Hz, 3H) ppm. ^{13}C NMR (101 MHz, DMSO) δ 168.5, 166.8, 165.3, 155.7, 152.1, 151.8, 148.7, 138.9, 138.6, 136.1, 134.7, 134.6, 133.3, 128.5, 128.5, 127.5, 127.5, 126.6, 125.0, 124.3, 123.5, 123.1, 119.9, 117.6, 115.7, 112.3, 108.9, 105.3, 98.3, 98.0, 84.8, 53.5, 43.6, 40.0 (under DMSO-signal), 16.8, 12.7 ppm. IR 3238, 1590, 1482, 1407, 1316, 1187, 1137, 825, 496 cm^{-1} . ESI-HRMS (m/z) $[\text{M}+\text{H}]^+$ theor. 940.29347, measured 940.29283.

5-((4-(5-(3-(2,6-Difluoro-3-(propylsulfonamido)benzoyl)-1*H*-pyrrolo[2,3-*b*]pyridin-5-yl)picolinamido)butyl)carbonyl)-2-(3-(dimethyl-14-azaneylidene)-6-(dimethylamino)-3*H*-xanthen-9-yl)benzoate (48)

Following general procedure D for amide coupling of 5-TAMRA derivatives, **40** (85 mg, 126 μmol , 1 eq), 5-TAMRA (25 mg, 58 μmol , 1 eq), HATU (22 mg, 58 μmol , 1 eq) and DIPEA (61 μL , 248 μmol , 6 eq) in DMF (1 mL) yielded after column chromatography (RP, water/ACN/FA, v/v/v, 90:9:1–30:69:1) the pure product as a purple solid (17 mg, 17 μmol , 30%).

^1H NMR (600 MHz, DMSO) δ 13.35 (bs, 1H), 13.12 (s, 1H), 9.76 (s, 1H), 9.03 (s, 1H), 8.91 (t, $J = 5.1$ Hz, 1H), 8.83 (d, $J = 1.0$ Hz, 1H), 8.76 (s, 1H), 8.69 (s, 1H), 8.39 (d, $J = 7.0$ Hz, 1H), 8.30 (d, $J = 7.0$ Hz, 1H), 8.16 (d, $J = 8.1$ Hz, 1H), 7.63 – 7.53 (m, $J = 16.8, 8.7$ Hz, 1H), 7.29 (t, $J = 8.6$ Hz), 7.03 (bs, 4H), 6.94 (bs, 2H), 3.40 (dd, $J = 11.3, 5.3$ Hz, 4H),



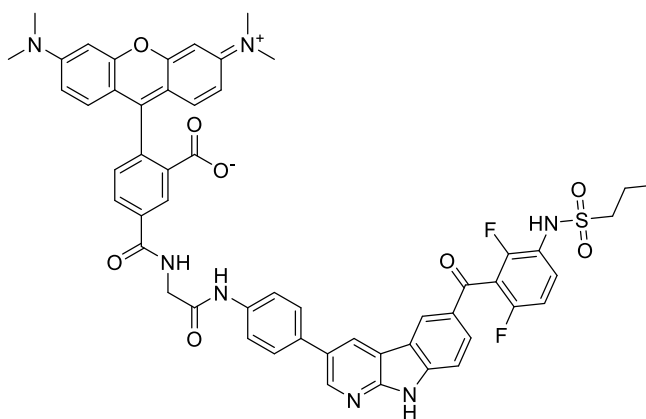
Chemical Formula: $\text{C}_{52}\text{H}_{48}\text{F}_2\text{N}_8\text{O}_8\text{S}^-$
Molecular Weight: 983,06

3.25 (s, 12H), 3.15 - 3.11 (m, 2H), 1.74 (dq, $J = 14.6, 7.3$ Hz, 2H), 1.70 – 1.61 (m, 4H), 0.96 (t, $J = 7.3$ Hz, 3H) ppm. ^{13}C NMR (151 MHz, DMSO) δ 180.7, 164.5, 163.6, 156.0 (dd, $J = 246.8, 6.8$ Hz), 152.4 (dd, $J = 249.6, 8.4$ Hz), 149.4, 149.0, 146.7, 144.3, 139.3, 136.1, 128.9 (d, $J = 7.4$ Hz), 127.7, 122.1, 121.9 (dd, $J = 14.1, 2.9$ Hz), 118.25 – 117.71 (m), 117.5, 115.8, 112.4 (d, $J = 23.0$ Hz), 96.3, 53.5, 40.5, 39.5, 38.6, 26.9, 26.6, 16.8, 12.6 ppm. IR 2933, 1650, 1584, 1347, 1184, 1123 cm^{-1} . ESI-HRMS (m/z) $[\text{M}+\text{H}]^+$ theor. 983.33566, measured 983.33491.

5-((2-((4-(6-(2,6-Difluoro-3-(propylsulfonamido)benzoyl)-9H-pyrido[2,3-b]indol-3-yl)phenyl)amino)-2-oxoethyl)carbamoyl)-2-(6-(dimethylamino)-3-(dimethyliminio)-3H-xanthen-9-yl)benzoate (49)

Following general procedure D for amide coupling of 5-TAMRA derivatives, **34** (64 mg, 94 μmol , 2 eq), 5-TAMRA (20 mg, 46 μmol , 1 eq), HATU (18 mg, 46 μmol , 1 eq) and DIPEA (32 μL , 186 μmol , 4 eq) in DMF (1 mL) yielded after column chromatography (DCM/MeOH/TFA, v/v/v, 90:9.5:0.5) the pure product as a purple solid (24 mg, 24 μmol , 52%).

^1H NMR (400 MHz, DMSO) δ 12.49 (s, 1H), 10.24 (s, 1H), 9.82 (s, 1H), 9.27 (s, 1H), 9.03 (s, 1H), 8.81 (s, 2H), 8.57 (s, 1H), 8.31 (d, $J = 7.0$ Hz, 1H), 8.03 (d, $J = 7.9$ Hz, 1H), 7.78 (s, 4H), 7.67 (d, $J = 7.8$ Hz, 2H), 7.44 – 7.31 (m, 1H), 6.56 (bs, 6H), 4.18 (s, 1H), 3.20 – 3.14 (m, 2H), 2.99 (s, 12H), 1.80 – 1.68 (m, 2H), 0.93 (t, $J = 7.1$ Hz, 3H) ppm. ^{13}C NMR



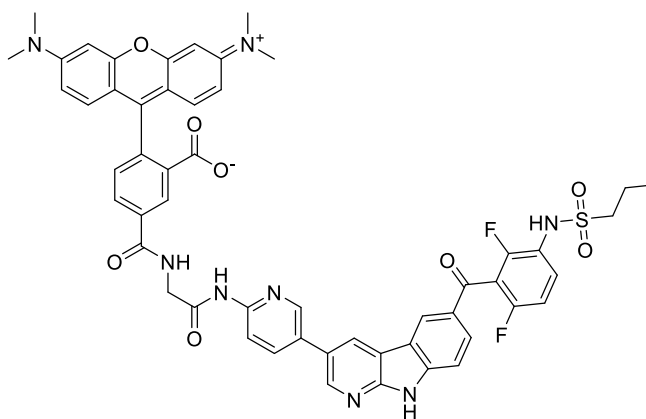
Chemical Formula: $\text{C}_{54}\text{H}_{45}\text{F}_2\text{N}_7\text{O}_8\text{S}$
Molecular Weight: 990,05

(101 MHz, DMSO) δ 193.8, 186.9, 167.6, 165.2, 151.9, 147.0, 143.4, 141.1, 138.2, 135.6, 129.6, 129.1, 128.4, 128.2, 127.3, 127.2, 127.1, 125.5, 125.0, 120.7, 119.7, 113.0, 112.4, 109.7, 98., 53.4, 43.4, 40.2 (under DMSO signal), 16.8, 12.5 ppm. IR 2966, 1589, 1482, 1339, 1184, 1131, 701 cm^{-1} . ESI-HRMS (m/z) $[\text{M}+\text{H}]^+$ 990.30912, measured 990.30875.

5-((2-((5-(6-(2,6-Difluoro-3-(propylsulfonamido)benzoyl)-9*H*-pyrido[2,3-*b*]indol-3-yl)pyridin-2-yl)amino)-2-oxoethyl)carbonyl)-2-(6-(dimethylamino)-3-(dimethyliminio)-3*H*-xanthen-9-yl)benzoate (50)

Following general procedure D for amide coupling of 5-TAMRA derivatives, **35** (59 mg, 87 μmol , 1.5 eq), 5-TAMRA (25 mg, 58 μmol , 1 eq), HATU (22 mg, 58 μmol , 1 eq) and DIPEA (52 μL , 290 μmol , 5 eq) in DMF (1 mL) yielded after column chromatography (DCM/MeOH/TFA, v/v/v, 90:9.5:0.5) the pure product as a purple solid (17 mg, 17 μmol , 30%).

^1H NMR (600 MHz, DMSO) δ 12.55 (s, 1H), 10.81 (s, 1H), 9.65 – 9.59 (m, 1H), 9.24 (t, $J = 5.6$ Hz, 1H), 9.12 (d, $J = 1.8$ Hz, 1H), 8.88 (d, $J = 1.9$ Hz, 1H), 8.82 (d, $J = 3.7$ Hz, 2H), 8.54 (s, 1H), 8.27 (dd, $J = 16.7, 5.5$ Hz, 1H), 8.21 (d, $J = 8.1$ Hz, 1H), 8.04 (d, $J = 8.6$ Hz, 1H), 7.70 – 7.64 (m, 2H), 7.35 (dd, $J = 14.3, 8.3$ Hz, 2H), 6.56 (d, $J = 8.7$ Hz, 2H),



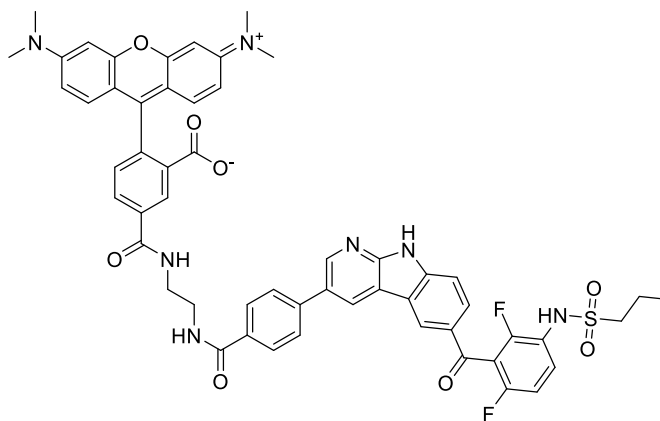
Chemical Formula: $\text{C}_{53}\text{H}_{44}\text{F}_2\text{N}_8\text{O}_8\text{S}$
Molecular Weight: 991,04

6.53 – 6.48 (m, 4H), 4.24 (d, $J = 5.2$ Hz, 2H), 3.15 (dd, $J = 8.4, 6.9$ Hz, 2H), 2.95 (s, 12H), 1.73 (dq, $J = 14.9, 7.4$ Hz, 2H), 0.92 (t, $J = 7.4$ Hz, 3H) ppm. ^{13}C NMR (151 MHz, DMSO) δ 187.0, 168.5, 168.4, 165.3, 155.1, 152.3, 152.2, 152.0, 151.0, 145.9, 145.6, 143.5, 136.3, 135.6, 134.6, 129.3, 128.5, 128.4, 127.5, 127.0, 125.5, 125.1, 124.3, 123.4, 122.3, 122.2, 122.2, 122.2, 120.7, 115.7, 113.3, 112.6, 112.4, 112.1, 109.0, 105.5, 98.0, 84.8, 53.5, 43.5, 39.5, 16.8, 12.6 ppm. IR 2962, 1589, 1486, 1343, 1180, 1139, 820, 698, 497 cm^{-1} . ESI-HRMS (m/z) $[\text{M}+\text{H}]^+$ 991.30436, measured 991.30267.

5-((2-(4-(6-(2,6-Difluoro-3-(propylsulfonamido)benzoyl)-9H-pyrido[2,3-b]indol-3-yl)benzamido)ethyl)carbonyl)-2-(6-(dimethylamino)-3-(dimethyliminio)-3H-xanthen-9-yl)benzoate (51)

Following general procedure D for amide coupling of 5-TAMRA derivatives, **36** (30 mg, 43 μmol , 2 eq), 5-TAMRA (28 mg, 65 μmol , 1 eq), HATU (25 mg, 65 μmol , 1 eq) and DIPEA (43 μL , 260 μmol , 4 eq) in DMF (1 mL) yielded after column chromatography (DCM/MeOH/TFA, v/v/v, 90:9.5:0.5) the pure product as a purple solid (35 mg, 54 μmol , 54%).

¹H NMR (400 MHz, DMSO) δ 12.58 (s, 1H), 9.83 (s, 1H), 9.14 (s, 1H), 9.04 (s, 1H), 8.91 (s, 1H), 8.85 (s, 1H), 8.74 (s, 1H), 8.62 (s, 1H), 8.02 (d, J = 7.9 Hz, 4H), 7.94 (d, J = 7.8 Hz, 1H), 7.86 (s, 1H), 7.68 (d, J = 8.4 Hz, 2H), 7.49 (s, 1H), 7.35 (t, J = 8.4 Hz, 1H), 6.79 (bs, 4H), 6.51 – 6.37 (m, 3H), 3.55 (s, 4H), 3.15 (dd, J = 12.5, 5.8 Hz, 2H),



Chemical Formula: C₅₅H₄₇F₂N₇O₈S

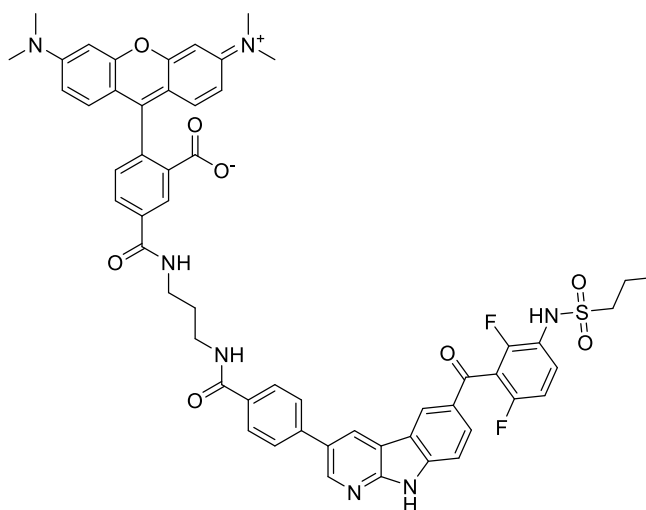
Molecular Weight: 1004.08

3.11 (s, 9H), 2.89 (s, 2H), 1.80 – 1.67 (m, 2H), 0.92 (t, J = 7.1 Hz, 3H) ppm. ¹³C NMR (101 MHz, DMSO) δ 187.0, 166.3, 152.5, 146.3, 143.5, 136.3, 133.1, 129.4, 128.4, 128.0, 126.5, 125.4, 122.07 (d, J = 14.3 Hz), 120.8, 115.7, 53.5, 16.81, 12.6 ppm. IR 1589, 1482, 1351, 1176, 1223, 922, 702 cm⁻¹. ESI-HRMS (m/z) [M+H]⁺ 1004.32477, measured 1004.32334.

5-((3-(4-(6-(2,6-Difluoro-3-(propylsulfonamido)benzoyl)-9H-pyrido[2,3-b]indol-3-yl)benzamido)propyl)carbamoyl)-2-(6-(dimethylamino)-3-(dimethyliminio)-3H-xanthen-9-yl)benzoate (52)

Following general procedure D for amide coupling of 5-TAMRA derivatives, **37** (26 mg, 37 μ mol, 1 eq), 5-TAMRA (16 mg, 37 μ mol, 1 eq), HATU (14 mg, 37 μ mol, 1 eq) and DIPEA (52 μ L, 297 μ mol, 8 eq) in DMF (1 mL) yielded after column chromatography (DCM/MeOH/TFA, v/v/v, 90:9.5:0.5) the pure product as a purple solid (26 mg, 24 μ mol, 65%).

^1H NMR (400 MHz, DMSO) δ 13.41 (bs, 1H), 12.56 (s, 1H), 9.83 (s, 1H), 9.09 (s, 1H), 8.91 (t, $J = 4.7$ Hz, 1H), 8.87 (s, 1H), 8.82 (s, 1H), 8.61 (t, $J = 4.9$ Hz, 2H), 8.26 (d, $J = 7.8$ Hz, 1H), 8.02 (s, 1H), 8.00 (d, $J = 8.4$ Hz, 1H), 7.91 (d, $J = 8.1$ Hz, 2H), 7.68 (d, $J = 8.5$ Hz, 2H), 7.67 – 7.64 (m, 1H), 7.47 (bs, 1H), 7.35 (t, $J = 8.6$ Hz, 1H), 6.80 (bs, 4H), 6.72 (bs, 2H), 3.46 – 3.40 (m, 6H), 3.19 – 3.14 (m, 2H), 3.11 (s, 12H), 1.88 (m,



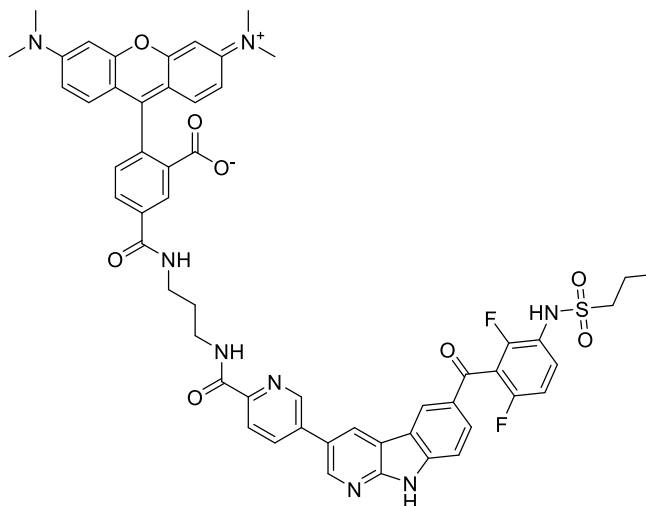
Chemical Formula: $\text{C}_{56}\text{H}_{49}\text{F}_2\text{N}_7\text{O}_8\text{S}$
Molecular Weight: 1018,11

2H), 1.74 (m, 2H), 0.93 (t, $J = 7.4$ Hz, 3H) ppm. ^{13}C NMR (101 MHz, DMSO) δ 187.0, 165.8, 164.6, 152.4, 151.1, 146.0, 143.5, 141.3, 140.6, 136.0, 133.1, 130.7, 128.4, 127.9, 127.8, 126.5, 120.8, 115.7, 112.0, 53.5, 39.5, 29.0, 16.8, 12.6 ppm. IR 1597, 1487, 1346, 1189, 1130 cm^{-1} . ESI-HRMS (m/z) $[\text{M}+\text{H}]^+$ 1018.34042, measured 1018.33986.

5-((3-(5-(6-(2,6-Difluoro-3-(propylsulfonamido)benzoyl)-9H-pyrido[2,3-b]indol-3-yl)picolinamido)propyl)carbonyl)-2-(6-(dimethylamino)-3-(dimethyliminio)-3H-xanthen-9-yl)benzoate (53)

Following general procedure D for amide coupling of 5-TAMRA derivatives, **38** (82 mg, 116 μmol , 2 eq), 5-TAMRA (25 mg, 58 μmol , 1 eq), HATU (22 mg, 58 μmol , 1 eq) and DIPEA (101 μL , 581 μmol , 10 eq) in DMF (1 mL) yielded after column chromatography (DCM/MeOH/TFA, v/v/v, 90:9.5:0.5) the pure product as a purple solid (35 mg, 34 μmol , 59%).

^1H NMR (400 MHz, DMSO) δ 13.39 (s, 1H), 12.64 (s, 1H), 9.83 (s, 1H), 9.16 (s, 1H), 9.08 (s, 1H), 9.00 (t, $J = 6.0$ Hz, 1H), 8.93 (s, 1H), 8.93 – 8.90 (m, 1H), 8.81 (s, 1H), 8.55 (s, 1H), 8.41 (dd, $J = 8.0, 1.7$ Hz, 1H), 8.26 (d, $J = 7.8$ Hz, 1H), 8.15 (d, $J = 8.1$ Hz, 1H), 8.02 (d, $J = 8.4$ Hz, 1H), 7.69 (d, $J = 8.6$ Hz, 1H), 7.66 (dd, $J = 9.1, 6.5$ Hz, 1H), 7.44 (s, 1H), 7.35 (t, $J = 8.6$ Hz, 1H), 6.62 (s, 2H), 3.45 (dd, $J = 13.1, 6.2$ Hz, 4H),



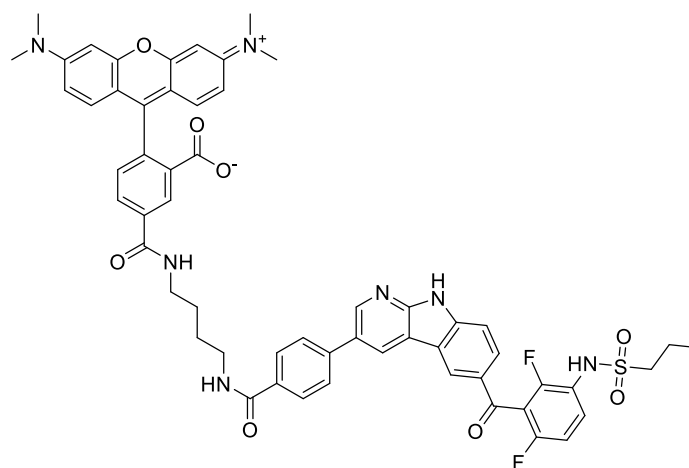
Chemical Formula: $\text{C}_{55}\text{H}_{48}\text{F}_2\text{N}_8\text{O}_8\text{S}$
Molecular Weight: 1019,09

3.18 – 3.12 (m, 2H), 3.03 (s, 12H), 1.94 – 1.83 (m, 2H), 1.73 (dq, $J = 15.1, 7.4$ Hz, 2H), 0.92 (t, $J = 7.4$ Hz, 3H) ppm. ^{13}C NMR (101 MHz, DMSO) δ 164.6, 163.7, 152.7, 148.6, 146.4, 143.5, 136.0, 135.5, 128.5, 124.8, 122.2, 122.0, 120.8, 118.8, 115.8, 112.1, 76.2, 66.4, 53.5, 40.4, 39.5, 16.8, 13.9, 12.6 ppm. IR 1589, 1490, 1343, 1180, 1131 cm^{-1} . ESI-HRMS (m/z) $[\text{M}+\text{H}]^+$ 1019.33566, measured 1019.33486.

5-((4-(4-(6-(2,6-Difluoro-3-(propylsulfonamido)benzoyl)-9H-pyrido[2,3-b]indol-3-yl)benzamido)butyl)carbonyl)-2-(6-(dimethylamino)-3-(dimethyliminio)-3H-xanthen-9-yl)benzoate (54)

Following general procedure D for amide coupling of 5-TAMRA derivatives, **39** (105 mg, 146 μmol , 2 eq), 5-TAMRA (30 mg, 70 μmol , 1 eq), HATU (27 mg, 70 μmol , 1 eq) and DIPEA (49 μL , 279 μmol , 4 eq) in DMF (1 mL) yielded after column chromatography (DCM/MeOH/TFA, v/v/v, 90:9.5:0.5) the pure product as a purple solid (28 mg, 27 μmol , 39%).

^1H NMR (400 MHz, DMSO) δ 12.57 (s, 1H), 9.83 (s, 1H), 9.13 (s, 1H), 8.90 (s, 1H), 8.84 (s, 2H), 8.58 (s, 1H), 8.48 (s, 1H), 8.24 (d, $J = 6.8$ Hz, 1H), 8.03 (s, 1H), 8.00 (d, $J = 8.5$ Hz, 2H), 7.92 (d, $J = 7.5$ Hz, 1H), 7.68 (d, $J = 8.2$ Hz, 2H), 7.35 (t, $J = 6.6$ Hz, 2H), 6.54 (s, 6H), 3.30 (m, 2H, under water peak), 3.18 – 3.13 (m, 2H), 2.96 (s, 12H), 1.78 – 1.68



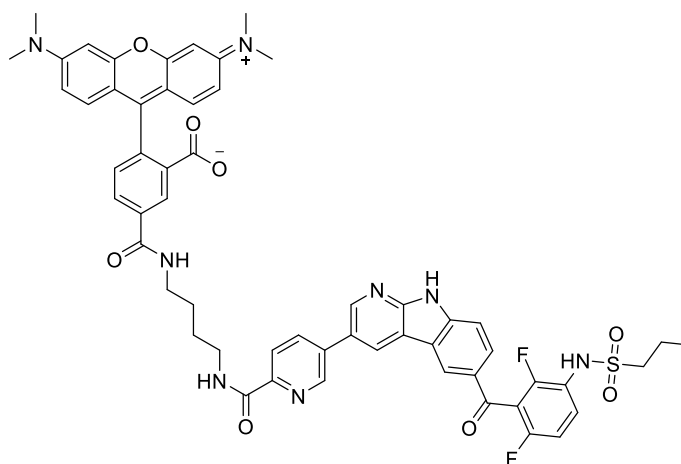
Chemical Formula: $\text{C}_{57}\text{H}_{51}\text{F}_2\text{N}_7\text{O}_8\text{S}$
Molecular Weight: 1032,13

(m, 2H), 1.64 (s, 4H), 0.92 (t, $J = 7.0$ Hz, 3H) ppm. ^{13}C NMR (101 MHz, DMSO) δ 186.9, 165.6, 164.6, 152.4, 146.0, 134.2, 129.3, 128.7, 128.1, 128.0, 126.5, 125.2, 124.3, 123.4, 123.4, 112.1, 109.4, 97.8, 53.5, 39.8, 39.1, 26.7, 26.5, 16.7, 12.5 ppm. IR 2962, 1593, 1482, 1347, 1184, 1135, 1037, 697 cm^{-1} . ESI-HRMS (m/z) $[\text{M}+\text{H}]^+$ 1032.35607, measured 1032.35455.

5-((6-(5-(6-(2,6-Difluoro-3-(propylsulfonamido)benzoyl)-9H-pyrido[2,3-b]indol-3-yl)picolinamido)hexyl)carbamoyl)-2-(6-(dimethylamino)-3-(dimethyliminio)-3H-xanthen-9-yl)benzoate (55)

Following general procedure D for amide coupling of 5-TAMRA derivatives, **40** (45 mg, 39 μmol , 1.3 eq), 5-TAMRA (20 mg, 46 μmol , 1 eq), HATU (18 mg, 46 μmol , 1 eq) and DIPEA (146 μL , 836 μmol , 18 eq) in DMF (1 mL) yielded after column chromatography (DCM/MeOH/TFA, v/v/v, 90:9.5:0.5) the pure product as a purple solid (12 mg, 11 μmol , 24%).

$^1\text{H-NMR}$ (400 MHz, DMSO) δ 12.60 (s, 1H), 9.21 (d, $J = 2.2$ Hz, 1H), 9.10 (d, $J = 2.2$ Hz, 1H), 8.97 (t, $J = 2.4$ Hz, 1H), 8.87 (dd, $J = 11.2, 5.0$ Hz, 1H), 8.84 (s, 1H), 8.45 (s, 1H), 8.41 (dd, $J = 8.2, 2.2$ Hz, 1H), 8.23 (dd, $J = 8.1, 1.5$ Hz, 1H), 8.16 (d, $J = 8.2$ Hz, 1H), 8.03 (dd, $J = 8.6, 1.6$ Hz, 1H), 7.69 (d, $J = 8.8$ Hz, 1H), 7.64 (dt, $J = 9.1, 4.6$ Hz, 1H), 7.32 (t, $J =$



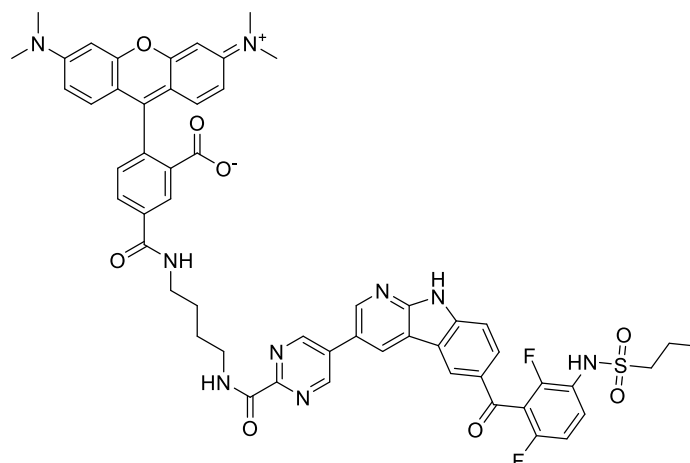
Chemical Formula: $\text{C}_{56}\text{H}_{50}\text{F}_2\text{N}_8\text{O}_8\text{S}$
Molecular Weight: 1033,12

7.9 Hz, 1H), 6.54 – 6.45 (m, 6H), 3.42 – 3.35 (m, 4H), 3.17 – 3.08 (m, 2H), 2.93 (s, 12H), 1.72 (td, $J = 15.0, 7.5$ Hz, 2H), 1.63 (s, 4H), 0.91 (t, $J = 7.4$ Hz, 3H) ppm. $^{13}\text{C NMR}$ (101 MHz, DMSO) δ 187.0, 168.4, 164.6, 163.6, 154.8, 152.8, 152.1, 152.0, 148.7, 146.4, 146.2, 143.5, 136.2, 136.1, 135.5, 128.5, 128.4, 128.4, 126.8, 124.9, 124.1, 123.1, 122.0, 120.7, 118.6, 115.8, 114.9, 112.2, 109.0, 105.6, 98.0, 84.7, 53.5, 40.2, 39.9, 39.7, 39.5, 39.5, 39.3, 39.1, 38.9, 26.9, 26.5, 26.2, 21.7, 16.9, 12.6 ppm. IR 1597, 1490, 1347, 1184, 1139 cm^{-1} . ESI-HRMS m/z $[\text{M}+\text{H}]^+$ 1033.35131, measured 1033. 35050. mp 195 – 197 $^\circ\text{C}$.

5-((4-(5-(6-(2,6-Difluoro-3-(propylsulfonamido)benzoyl)-9H-pyrido[2,3-b]indol-3-yl)pyrimidine-2-carboxamido)butyl)carbonyl)-2-(6-(dimethylamino)-3-(dimethyliminio)-3H-xanthen-9-yl)benzoate (56)

Following general procedure D for amide coupling of 5-TAMRA derivatives, **41** (40 mg, 34 μmol , 1.3 eq), 5-TAMRA (18 mg, 42 μmol , 1 eq), HATU (18 mg, 42 μmol , 1 eq) and DIPEA (73 μL , 418 μmol , 10 eq) in DMF (1 mL) yielded after column chromatography (RP, water/ACN/TFA, v/v/v, 50:49.5:0.5) the pure product as a purple solid (18 mg, 17 μmol , 42%).

^1H NMR (400 MHz, DMSO) δ 13.47 – 13.26 (bs, 1H), 12.73 (s, 1H), 9.84 (s, 1H), 9.42 (s, 2H), 9.29 (s, 1H), 9.04 (d, $J = 1.3$ Hz, 1H), 9.03 – 9.01 (m, 1H), 8.92 (t, $J = 4.9$ Hz, 1H), 8.82 (s, 1H), 8.68 (s, 1H), 8.30 (d, $J = 8.1$ Hz, 1H), 8.03 (d, $J = 8.3$ Hz, 1H), 7.71 (d, $J = 8.5$ Hz, 1H), 7.69 – 7.63 (m, 1H), 7.56 (d, $J = 6.5$ Hz, 1H), 7.36 (t, $J = 8.5$ Hz, 1H),



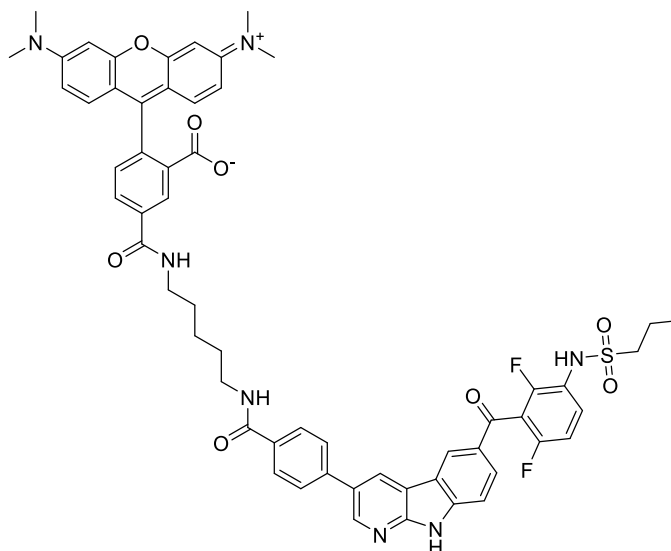
Chemical Formula: $\text{C}_{55}\text{H}_{49}\text{F}_2\text{N}_9\text{O}_8\text{S}$
Molecular Weight: 1034,11

7.02 (s, 4H), 6.92 (s, 2H), 3.42 – 3.36 (m, 4H), 3.24 (s, 12H), 3.17 – 3.12 (m, 3H), 1.73 (dd, $J = 15.0, 7.5$ Hz, 3H), 1.66 (s, 4H), 0.92 (t, $J = 7.4$ Hz, 3H) ppm. ^{13}C NMR (101 MHz, DMSO) δ 187.0, 181.2, 169.3, 167.1, 164.5, 162.3, 154.9, 153.0, 143.6, 136.1, 132.3, 128.6, 128.3, 124.8, 124.7, 121.8, 121.4, 120.7, 115.8, 112.3, 108.6, 96.3, 53.5, 40.4, 39.5, 26.8, 26.6, 16.8, 12.5 ppm. IR 1584, 1482, 1343, 1184, 1139 cm^{-1} . ESI-HRMS (m/z) $[\text{M}+\text{H}]^+$ 1034,34656, measured 1034.34456.

5-((5-(4-(6-(2,6-Difluoro-3-(propylsulfonamido)benzoyl)-9H-pyrido[2,3-b]indol-3-yl)benzamido)pentyl)carbonyl)-2-(6-(dimethylamino)-3-(dimethyliminio)-3H-xanthen-9-yl)benzoate (57)

Following general procedure D for amide coupling of 5-TAMRA derivatives, **42** (51 mg, 70 μmol , 1.5 eq), 5-TAMRA (20 mg, 46 μmol , 1 eq), HATU (18 mg, 46 μmol , 1 eq) and DIPEA (146 μL , 836 μmol , 18 eq) in DMF (1 mL) yielded after column chromatography (DCM/MeOH/TFA, v/v/v, 90:9.5:0.5) the pure product as a purple solid (15 mg, 14 μmol , 30%).

^1H NMR (600 MHz, DMSO) δ 13.37 (bs, 1H), 12.55 (s, 1H), 9.83 (s, 1H), 9.04 (s, 1H), 8.82 (dd, $J = 15.7, 6.2$ Hz, 1H), 8.60 (bs, 1H), 8.52 (t, $J = 5.4$ Hz, 1H), 8.21 (dd, $J = 7.9, 1.5$ Hz, 1H), 8.01 (d, $J = 8.5$ Hz, 1H), 7.97 (d, $J = 8.3$ Hz, 2H), 7.87 (d, $J = 8.2$ Hz, 2H), 7.69 (d, $J = 8.6$ Hz, 1H), 7.69 – 7.64 (m, 1H), 7.42 (bs, 1H), 7.35 (t, $J = 8.6$ Hz, 1H), 6.85 (s, 4H), 6.69 (s, 2H), 3.39 – 3.36 (m, 2H), 3.20 – 3.14 (m, 3H), 3.12 (s, 12H), 1.74 (m, 2H), 1.63



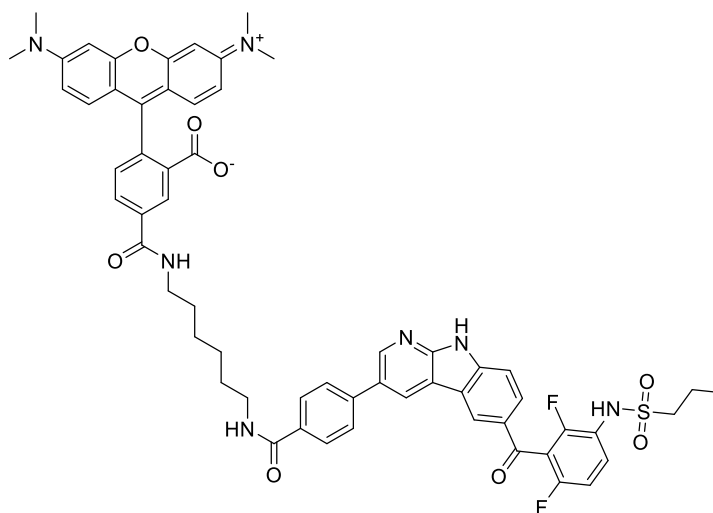
Chemical Formula: $\text{C}_{58}\text{H}_{53}\text{F}_2\text{N}_7\text{O}_8\text{S}$
Molecular Weight: 1046,16

(dq, $J = 14.6, 7.1$ Hz, 4H), 1.42 (m, 2H), 0.93 (t, $J = 7.4$ Hz, 3H) ppm. ^{13}C NMR (151 MHz, DMSO) δ 186.9, 165.7, 164.6, 156.09 (dd, $J = 248.1, 6.8$ Hz), 152.4, 152.30 (dd, $J = 251.0, 8.3$ Hz), 145.9, 143.5, 140.4, 136.2, 133.2, 129.21 (d, $J = 9.4$ Hz), 128.4, 128.2, 127.9, 127.8, 127.7, 126.4, 124.8, 122.08 (d, $J = 13.3$ Hz), 120.9, 117.56 (t, $J = 23.1$ Hz), 115.6, 112.53 (d, $J = 23.6$ Hz), 112.0, 66.3, 53.5, 40.2, 39.5, 28.8, 28.6, 23.7, 16.8, 12.6 ppm. IR 1588, 1486, 1347, 1188, 1131 cm^{-1} . ESI-HRMS (m/z) $[\text{M}+\text{H}]^+$ 1046.37172, measured 1046.37040.

5-(((6-(4-(6-(2,6-Difluoro-3-(propylsulfonamido)benzoyl)-9H-pyrido[2,3-b]indol-3-yl)benzamido)hexyl)carbonyl)-2-(6-(dimethylamino)-3-(dimethyliminio)-3H-xanthen-9-yl)benzoate (58)

Following general procedure D for amide coupling of 5-TAMRA derivatives, **44** (46 mg, 62 μmol , 1.3 eq), 5-TAMRA (20 mg, 46 μmol , 1 eq), HATU (18 mg, 46 μmol , 1 eq) and DIPEA (146 μL , 836 μmol , 18 eq) in DMF (1 mL) yielded after column chromatography (DCM/MeOH/TFA, v/v/v, 90:9.5:0.5) the pure product as a purple solid (12 mg, 11 μmol , 24%).

^1H NMR (600 MHz, DMSO) δ 13.36 (bs, 1H), 12.56 (d, $J = 10.7$ Hz, 1H), 9.83 (s, 1H), 9.12 (d, $J = 1.9$ Hz, 1H), 8.88 (d, $J = 2.2$ Hz, 2H), 8.84 (s, 1H), 8.68 (s, 1H), 8.55 (t, $J = 5.5$ Hz, 1H), 8.29 (d, $J = 7.9$ Hz, 1H), 8.02 (d, $J = 8.9$ Hz, 1H), 7.99 (d, $J = 8.3$ Hz, 2H), 7.91 (d, $J = 8.3$ Hz, 2H), 7.70 – 7.64 (m, 2H), 7.54 (d, $J = 7.2$ Hz, 1H), 7.35 (t, $J = 8.6$ Hz, 1H), 7.02 (bs, 4H), 6.91



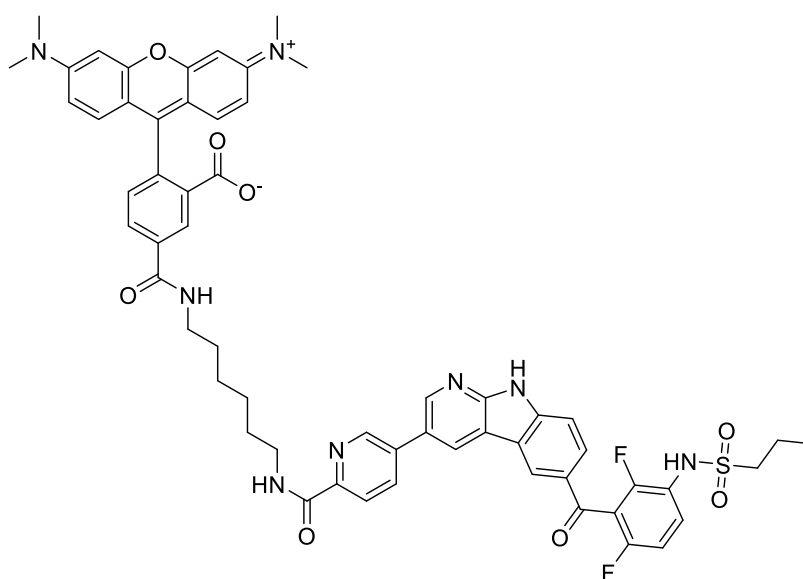
Chemical Formula: $\text{C}_{59}\text{H}_{55}\text{F}_2\text{N}_7\text{O}_8\text{S}$
Molecular Weight: 1060,19

(s, 2H), 3.36 (dd, $J = 12.8, 6.6$ Hz, 4H), 3.32 (dd, $J = 12.8, 6.6$ Hz, 2H), 3.24 (bs, 12H), 3.18 – 3.14 (m, 2H), 1.73 (m, 2H), 1.65 – 1.56 (m, 4H), 1.41 (s, 4H), 0.92 (t, $J = 7.4$ Hz, 3H) ppm. ^{13}C NMR (151 MHz, DMSO) δ 187.0, 165.7, 164.5, 156.10 (dd, $J = 248.8, 7.1$ Hz), 152.4, 152.28 (dd, $J = 250.8, 8.4$ Hz), 146.0, 143.5, 140.5, 136.2, 133.3, 129.20 (d, $J = 9.9$ Hz), 128.4, 128.0, 127.7, 126.5, 125.1, 122.1 (d, $J = 13.6$ Hz), 120.8, 117.54 (t, $J = 23.2$ Hz), 115.7, 112.53 (d, $J = 22.3$ Hz), 112.1, 96.4, 66.3, 53.5, 40.5, 39.5, 29.2, 29.0, 26.3, 16.8, 12.6 ppm. IR 2937, 1589, 1486, 1347, 1184, 1127 cm^{-1} . ESI-HRMS (m/z) $[\text{M}+\text{H}]^+$ 1060.38737, measured 1060.38695.

5-((4-(5-(6-(2,6-Difluoro-3-(propylsulfonamido)benzoyl)-9*H*-pyrido[2,3-*b*]indol-3-yl)picolinamido)butyl)carbamoyl)-2-(6-(dimethylamino)-3-(dimethyliminio)-3*H*-xanthen-9-yl)benzoate (59)

Following general procedure D for amide coupling of 5-TAMRA derivatives, **45** (109 mg, 134 μm , 2.5 eq), 5-TAMRA (23 mg, 53 μm , 1 eq), HATU (20 mg, 53 μmol , 1 eq) and DIPEA (75 μL , 427 μmol , 8 eq) in DMF (1 mL) yielded after column chromatography (DCM/MeOH/TFA, v/v/v, 90:9.5:0.5) the pure product as a purple solid (27 mg, 25 μmol , 47%).

^1H NMR (600 MHz, DMSO) δ 13.36 (bs, 1H), 12.56 (d, $J = 10.7$ Hz, 1H), 9.83 (s, 1H), 9.12 (d, $J = 1.9$ Hz, 1H), 8.88 (d, $J = 2.2$ Hz, 2H), 8.84 (s, 1H), 8.68 (s, 1H), 8.55 (t, $J = 5.5$ Hz, 1H), 8.29 (d, $J = 7.9$ Hz, 1H), 8.02 (d, $J = 8.9$ Hz, 1H), 7.99 (d, $J = 8.3$ Hz, 2H), 7.91 (d, $J = 8.3$ Hz, 1H), 7.70 – 7.64 (m, 2H),



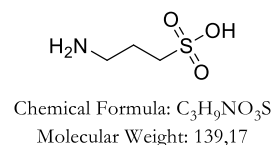
Chemical Formula: $\text{C}_{58}\text{H}_{54}\text{F}_2\text{N}_8\text{O}_8\text{S}$
Molecular Weight: 1061,17

7.54 (d, $J = 7.2$ Hz, 1H), 7.35 (t, $J = 8.6$ Hz, 1H), 7.02 (s, 4H), 6.91 (s, 2H), 3.36 (dd, $J = 12.8, 6.6$ Hz, 2H), 3.32 (dd, $J = 12.8, 6.6$ Hz, 2H), 3.24 (s, 12H), 3.18 – 3.14 (m, 2H), 1.73 (m, 2H), 1.65 – 1.56 (m, 4H), 1.41 (s, 4H), 0.92 (t, $J = 7.4$ Hz, 3H) ppm. ^{13}C NMR (151 MHz, DMSO) δ 187.0, 165.7, 164.5, 156.10 (dd, $J = 248.8, 7.1$ Hz), 152.4, 152.28 (dd, $J = 250.8, 8.4$ Hz), 146.0, 143.5, 140.5, 136.2, 133.3, 129.20 (d, $J = 9.9$ Hz), 128.4, 128.0, 127.7, 126.5, 125.1, 122.07 (d, $J = 13.6$ Hz), 120.8, 117.54 (t, $J = 23.2$ Hz), 115.7, 112.53 (d, $J = 22.3$ Hz), 112.1, 96.4, 66.3, 53.5, 40.5, 39.5, 29.2, 29.0, 26.3, 16.8, 12.6 ppm. IR 2937, 1589, 1486, 1347, 1184, 1127 cm^{-1} . ESI-HRMS (m/z) $[\text{M}+\text{H}]^+$ 1060.38737, measured 1060.38695.

6.3.6. Sulfonamide linker**3-Aminopropane-1-sulfonic acid (60)**

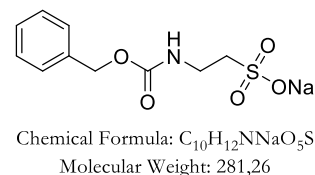
1,2-Oxathiolane 2,2-dioxide (1 g, 8.19 mmol, 1 eq) was dissolved in MeOH and ammonia (7M in MeOH) was added dropwise at room temperature and stirred for 4 hours. After full consumption of the starting material, the solvent was removed under reduced pressure and recrystallized in acetone (560 mg, 4.02 mmol, 49%).

^1H NMR (200 MHz, D_2O) δ 3.28 – 3.11 (m, 1H), 3.01 (t, $J = 7.4$ Hz, 1H), 2.13 (td, $J = 14.8, 8.5$ Hz, 1H) ppm. ^{13}C NMR (50 MHz, D_2O) δ 47.7, 46.2, 21.2 ppm

**Sodium 2-(((benzyloxy)carbonyl)amino)ethane-1-sulfonate (61)**

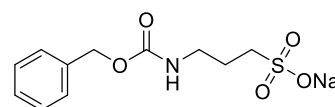
2-Aminoethane-1-sulfonic acid (1 g, 7.99 mmol, 1 eq) was in NaOH (20 mL, 2 M) and benzyl carbonochloridate (1.25 mL, 8.79 mmol, 1.1 eq) was added dropwise and stirred for 17 hours at room temperature. Subsequently the aqueous phase was extracted with EtOAc and evaporated under reduced pressure. The crude product (2.25 g, 7.99 mmol, quant.) was washed with EtOH and dried under reduced pressure

^1H NMR (200 MHz, D_2O) δ 7.39 (s, 5H), 5.07 (s, 2H), 3.52 (dd, $J = 14.3, 7.2$ Hz, 2H), 3.18 – 3.05 (m, 2H). ^{13}C NMR (50 MHz, D_2O) δ 157.8, 136.2, 128.7, 128.3, 127.6, 66.9, 50.3, 36.3 ppm.

**Sodium 3-(((benzyloxy)carbonyl)amino)propane-1-sulfonate (62)**

3-Aminopropane-1-sulfonic acid (560 mg, 4.02 mmol, 1 eq) was in NaOH (20 mL, 2M) and benzyl carbonochloridate (632 μL , 4.43 mmol, 1.1 eq) was added dropwise and stirred for 17 hours at room temperature. Subsequently the aqueous phase was extracted with EtOAc and evaporated under reduced pressure. The crude product (1.19 g, 4.02 mmol, quant.) was washed with EtOH and dried under reduced pressure.

^1H NMR (200 MHz, D_2O) δ 7.37 (s, 5H), 5.06 (d, $J = 7.2$ Hz, 2H), 3.42 - 3.26 (s, 2H), 3.19 (d, $J = 6.2$ Hz, 2H), 2.06 - 1.86 (m, 2H) ppm. ^{13}C NMR (50 MHz, D_2O) δ 158.3, 136.3, 128.8, 128.3, 127.8, 66.8, 48.4, 39.2, 24.5 ppm.

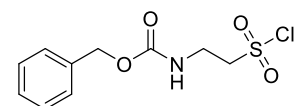


Chemical Formula: $\text{C}_{11}\text{H}_{14}\text{NNaO}_5\text{S}$
Molecular Weight: 295,28

Benzyl (2-(chlorosulfonyl)ethyl)carbamate (63)

Triphenylphosphine (2.98 g, 11.4 mmol, 1.6 eq) was suspended in DCM (15 mL), cooled to 0°C and sulfuryl chloride (1.01 mL, 12.4 mmol, 1.8 eq) was added. After 1 hour the sodium salt of 2-(((benzyloxy)carbonyl)amino)ethane-1-sulfonic acid (2.01 g, 7.1 mmol, 1 eq) was added and stirred for an additional hour. The solvent was removed under reduced pressure and the crude product was purified by column chromatography (PE/EtOAc, v/v, 30 - 50%) to obtain a colorless oil (1.46 g, 5.3 mmol, 74%).

^1H NMR (200 MHz, CDCl_3) δ 7.35 (s, 5H), 5.38 (s, 1H), 5.13 (s, 2H), 3.95 - 3.77 (m, 4H) ppm.

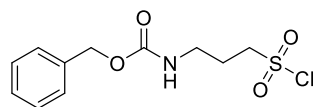


Chemical Formula: $\text{C}_{10}\text{H}_{12}\text{ClNO}_4\text{S}$
Molecular Weight: 277,72

Benzyl (3-(chlorosulfonyl)propyl)carbamate (64)

Triphenylphosphine (640 mg, 2.4 mmol, 1.6 eq) was suspended in DCM (5 mL), cooled to 0°C and sulfuryl chloride (0.22 mL, 2.7 mmol, 1.75 eq) was added. After 1 hour the sodium salt of 2-(((benzyloxy)carbonyl)amino)ethane-1-sulfonic acid (450 mg, 1.5 mmol, 1 eq) was added and stirred for an additional hour. The solvent was removed under reduced pressure and the crude product was purified by column chromatography (PE/EtOAc, v/v, 30 - 50%) to obtain a colorless oil (260 mg, 0.89 mmol, 58%).

^1H NMR (200 MHz, CDCl_3) δ 7.35 (s, 5H), 5.38 (s, 1H), 5.13 (s, 2H), 4.01 - 3.72 (m, 6H) ppm.



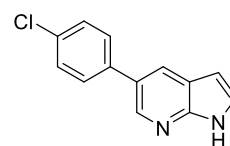
Chemical Formula: $\text{C}_{11}\text{H}_{14}\text{ClNO}_4\text{S}$
Molecular Weight: 291,75

5-(4-Chlorophenyl)-1H-pyrrolo[2,3-*b*]pyridine (65)

5-Bromo-1H-pyrrolo[2,3-*b*]pyridin (8 g, 40.6 mmol, 1 eq), potassium carbonate (11.2 g, 81.2 mmol, 2 eq) and (4-chlorophenyl)boronic acid was suspended in ACN/ H_2O (4:1 v/v, 40 mL, 1M) and degassed with argon. After adding $\text{Pd}(\text{PPh}_3)$ (470 mg, 406 mM, 1 mol%) the suspension was stirred under reflux conditions over night. The mixture was cooled to room

temperature and the precipitate was collected, washed with excess water and MeCN and dried under vacuum conditions to obtain a yellow solid (6.4 g, 28 mmol, 69%).

^1H NMR (400 MHz, DMSO) δ 11.76 (s, 1H), 8.51 (d, $J = 2.1$ Hz, 1H), 8.20 (d, $J = 1.9$ Hz, 1H), 7.72 (d, $J = 8.5$ Hz, 2H), 7.57 – 7.43 (m, 3H), 6.50 (dd, $J = 3.2, 1.7$ Hz, 1H) ppm. ^{13}C NMR (101 MHz, DMSO) δ 148.2, 141.4, 138.0, 131.7, 128.9, 128.6, 127.1, 126.9, 126.1, 119.7, 100.2 ppm.

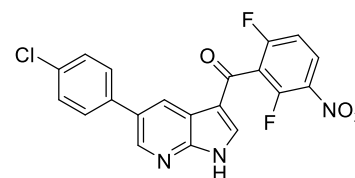


Chemical Formula: $\text{C}_{13}\text{H}_9\text{ClN}_2$
Molecular Weight: 228,68

(5-(4-Chlorophenyl)-1*H*-pyrrolo[2,3-*b*]pyridin-3-yl)(2,6-difluoro-3-nitrophenyl)methanone (66)

5-(4-Chlorophenyl)-1*H*-pyrrolo[2,3-*b*]pyridine (6 g, 26.2 mmol, 1 eq) and AlCl_3 (21 g, 157 mmol, 6 eq) was dissolved in DCM (50 mL) and stirred for 1 hour. Meanwhile 2,6-difluoro-3-nitrobenzoic acid (5.7 g, 28.9 mmol, 1.1 eq) was suspended in DCM (30 mL) and oxalyl chloride (3.7 mL, 28.9 mmol, 1.1 eq) and DMF (0.5 mL) was added dropwise. After the gas evolution stopped, both mixtures were combined and stirred for 6 hours at 40 °C. The reaction was stopped by adding MeOH and water and the forming precipitate (7.6 g, 18.4 mmol, 70%) was collected and dried under vacuum conditions.

^1H NMR (400 MHz, DMSO) δ 13.13 (s, 1H), 8.75 – 8.68 (m, 2H), 8.50 – 8.38 (m, 2H), 7.80 (d, $J = 8.5$ Hz, 2H), 7.59 – 7.49 (m, 3H) ppm. ^{13}C NMR (101 MHz, DMSO) δ 178.8, 161.5 (dd, $J = 257.1$ Hz, 7.5 Hz) 152.7 (dd, $J = 264.2, 9.4$ Hz), 149.1, 144.1, 139.8, 136.9, 134.3 (dd, $J = 7.6$ Hz, 3.6 Hz), 132.5, 130.4,



Chemical Formula: $\text{C}_{20}\text{H}_{10}\text{ClF}_2\text{N}_3\text{O}_3$
Molecular Weight: 413,76

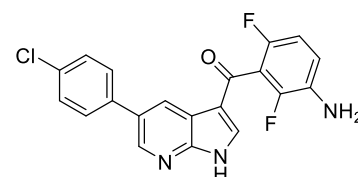
129.0, 128.9, 127.2, 119.5 (dd, $J = 25$ Hz, 23.4 Hz), 117.4, 115.4, 113.2 (dd, $J = 24.1$ Hz, 3.7 Hz) ppm.

(3-Amino-2,6-difluorophenyl)(5-(4-chlorophenyl)-1*H*-pyrrolo[2,3-*b*]pyridin-3-yl)methanone (67)

(5-(4-Chlorophenyl)-1*H*-pyrrolo[2,3-*b*]pyridin-3-yl)(2,6-difluoro-3-nitrophenyl)methanone (6 g, 14.5 mmol, 1 eq) was dissolved in THF/EtOAc (1:1, 0.06M, 500 mL) and heated to 60 °C. Stannous chloride dihydrate (11.45 g, 50.75 mmol, 3.5 eq) was added and stirred

overnight. The reaction was stopped by adding sodium bicarbonate solution, filtered through a pad of celite and washed with saturated sodium chloride solution. After drying over sodium sulfate and removing the solvent, the crude product precipitated in MTBE and was dried under vacuum conditions (2.68 g, 6.98 mmol, 48%).

^1H NMR (400 MHz, DMSO) δ 12.95 (s, 1H), 8.70 (d, J = 1.9 Hz, 1H), 8.64 (2, 1H), 7.78 (d, J = 8.4 Hz, 2H), 7.55 (d, J = 8.4 Hz, 2H), 7.00 – 6.87 (m, 2H), 5.24 (s, 2H) ppm. ^{13}C NMR (101 MHz, DMSO) δ 182.2, 149.2 (dd, 235.1 Hz, 6.7 Hz), 148.9, 146.0 (dd, J = 241.2 Hz, 8.0 Hz), 143.7, 138.0, 137.1, 133.4 (dd, J = 13.1 Hz, 2.3 Hz), 132.4, 130.1, 129.0, 128.8, 127.0, 117.5, 116.6 (dd, J = 7.9 Hz, 6.2 Hz), 115.9, 111.3 (dd, J = 22.1 Hz, 3.3 Hz) ppm.

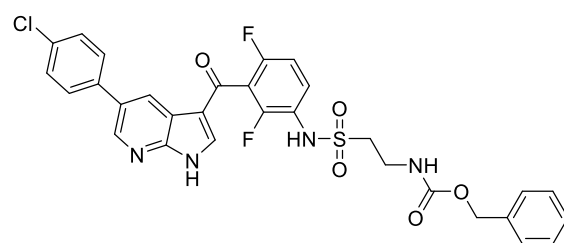


Chemical Formula: $\text{C}_{20}\text{H}_{12}\text{ClF}_2\text{N}_3\text{O}$
Molecular Weight: 383,78

Benzyl (2-(*N*-(3-(5-(4-chlorophenyl)-1*H*-pyrrolo[2,3-*b*]pyridine-3-carbonyl)-2,4-difluorophenyl)sulfamoyl)ethyl)carbamate (68)

(3-Amino-2,6-difluorophenyl)(5-(4-chlorophenyl)-1*H*-pyrrolo[2,3-*b*]pyridin-3-yl)methanone (900 mg, 2.35 mmol, 1 eq) was dissolved in pyridine (1 mL, 1M) and stirred for 1 hour under argon-atmosphere. Subsequently benzyl (2-(chlorosulfonyl)ethyl)carbamate (977 mg, 3.52 mmol, 1.5 eq) in THF (3 mL) was added dropwise and stirred for 6 hours at room temperature. The reaction was stopped by adding ethyl acetate, and water. The organic phases were washed with saturated sodium chloride solution and dried over sodium sulfate. The yellow solid (433 mg, 692 μmol , 30%) was obtained after column chromatography (DCM/MeOH, v/v, 0-5%).

^1H NMR (200 MHz, DMSO) δ 13.04 (s, 1H), 9.90 (s, 1H), 8.72 (d, J = 2.2 Hz, 1H), 8.66 (s, 1H), 8.24 (s, 1H), 7.80 (d, J = 8.5 Hz, 2H), 7.57 (d, J = 8.4 Hz, 4H), 7.36 (d, J = 21.0 Hz, 8H), 5.76 (s, 1H), 5.00 (s, 2H), 3.47 (d, J = 15.4 Hz, 2H), 3.33 – 3.27 (m, 2H, under H_2O -Peak)



Chemical Formula: $\text{C}_{30}\text{H}_{23}\text{ClF}_2\text{N}_4\text{O}_5\text{S}$
Molecular Weight: 625,04

ppm. ^{13}C NMR (50 MHz, DMSO) δ 181.5, 156.8, 149.9, 144.8, 139.9, 137.9, 137.7, 133.4,

131.1, 130.0, 129.8, 129.2, 128.7, 128.6, 128.0, 122.6, 122.6, 122.4, 122.3, 118.4, 116.5, 113.5, 113.4, 113.1, 113.0, 66.4, 52.1, 36.2 ppm. ESI-MS (m/z) 646.7 $[M + Na]^+$.

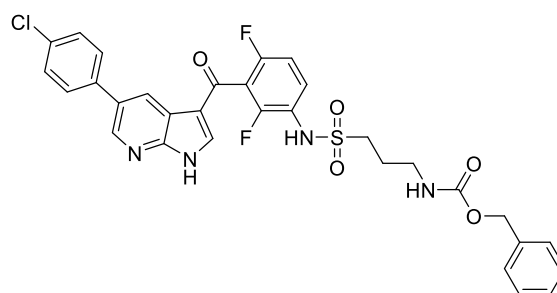
Benzyl (3-(*N*-(3-(5-(4-chlorophenyl)-1*H*-pyrrolo[2,3-*b*]pyridine-3-carbonyl)-2,4-difluorophenyl)sulfamoyl)propyl)carbamate (69)

(3-Amino-2,6-difluorophenyl)(5-(4-chlorophenyl)-1*H*-pyrrolo[2,3-*b*]pyridin-3-yl)methanone (900 mg, 2.35 mmol, 1 eq) was dissolved in pyridine (1 mL, 1M) and stirred for 1 hour under argon-atmosphere. Subsequently benzyl (2-(chlorosulfonyl)ethyl)carbamate (977 mg, 3.52 mmol, 1.5 eq) in THF (3 mL) was added dropwise and stirred for 6 hours at room temperature. The reaction was stopped by adding ethyl acetate, and water. The organic phases were washed with saturated sodium chloride solution and dried over sodium sulfate. The yellow solid (433 mg, 692 μ mol, 30%) was obtained after column chromatography (DCM/MeOH, v/v, 0-5%).

1H NMR (200 MHz, DMSO) δ 13.03 (s, 1H), 9.82 (s, 1H), 8.71 (t, $J = 2.6$ Hz, 1H), 8.65 (s, 1H), 8.24 (s, 1H), 7.79 (d, $J = 8.3$ Hz, 2H), 7.57 (m, 4H), 7.30 - 7.20 (m, 5H), 6.94 (d, $J = 8.2$ Hz, 1H), 4.97 (s, 2H), 3.12 (s, 4H), 1.87 (s, 2H)

ppm. ^{13}C NMR (50 MHz, DMSO) δ 181.5, 156.8, 149.9, 144.8, 139.9, 137.9, 137.7, 133.4,

131.1, 130.0, 129.1, 129.2, 128.7, 128.6, 128.0, 122.6, 122.6, 122.4, 122.3, 118.4, 116.5, 113.5, 113.4, 113.1, 113.0, 66.4, 57.1, 52.1, 36.2 ppm. ESI-MS (m/z) 661.1 $[M + Na]^+$.



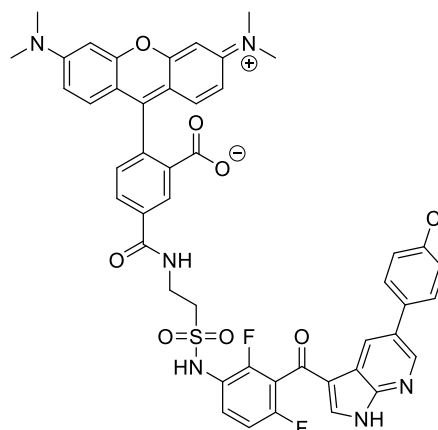
Chemical Formula: $C_{31}H_{25}ClF_2N_4O_5S$
Molecular Weight: 639,07

5-((2-(*N*-(3-(5-(4-chlorophenyl)-1*H*-pyrrolo[2,3-*b*]pyridine-3-carbonyl)-2,4-difluorophenyl)sulfamoyl)ethyl)carbamoyl)-2-(6-(dimethylamino)-3-(dimethyliminio)-3*H*-xanthen-9-yl)benzoate (70)

Benzyl(2-(*N*-(3-(5-(4-chlorophenyl)-1*H*-pyrrolo[2,3-*b*]pyridine-3-carbonyl)-2,4-difluorophenyl)sulfamoyl)ethyl)carbamate (300 mg, 480 μ mol, 5 eq) was suspended in EtOH (3 mL) and HCl (1 mL, 6N). The solution was stirred in the microwave (100W, 100 °C, 60 minutes) until complete conversion of the starting material. After removing the solvent under vacuum conditions, the crude product was solved in DMF (2 mL). DIPEA

(290 μL , 1.7 mmol, 20 eq) and 5-Tamra-SE (45 mg, 85 μmol , 1 eq) was added and the mixture was stirred overnight at room temperature. The purple product was purified using column chromatography (acetone + 1% triethylamine) and precipitated from *n*-pentane/isopropanol (9:1, v/v) (62 mg, 60 μmol , 72%).

^1H NMR (400 MHz, DMSO) δ 13.02 (s, 1H), 9.94 (s, 1H), 9.02 (t, $J = 4.5$ Hz, 1H), 8.70 (d, $J = 1.3$ Hz, 1H), 8.63 (s, 1H), 8.41 (s, 1H), 8.24 (s, 1H), 8.18 (d, $J = 8.1$ Hz, 1H), 7.77 (d, $J = 8.2$ Hz, 1H), 7.66 (dd, $J = 14.8, 8.9$ Hz, 1H), 7.55 (d, $J = 8.4$ Hz, 1H), 7.31 (t, $J = 7.9$ Hz, 1H), 6.48 (q, $J = 8.6$ Hz, 1H), 3.76 (dd, $J = 12.2, 6.5$ Hz, 2H), 3.50 (t, $J = 6.8$ Hz, 2H), 2.93 (s, 12H) ppm. ^{13}C NMR (101 MHz, DMSO) δ 180.4, 168.3, 164.9, 152.1, 152.0, 148.9, 143.8, 138.8, 137.0, 135.6, 134.3, 132.4, 130.2, 129.0, 128.8, 128.3, 127.0, 124.2, 117.4, 115.6, 109.0, 105.5, 98.4, 51.7, 34.6 ppm. ESI-MS (m/z) 902.7 $[\text{M} + \text{H}]^+$.

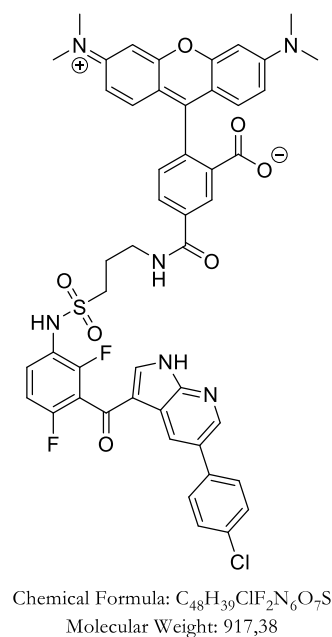


Chemical Formula: $\text{C}_{46}\text{H}_{34}\text{ClF}_2\text{N}_6\text{O}_7\text{S}^+$
Molecular Weight: 888,32

5-((3-(*N*-(3-(5-(4-chlorophenyl)-1*H*-pyrrolo[2,3-*b*]pyridine-3-carbonyl)-2,4-difluorophenyl)sulfamoyl)propyl)carbamoyl)-2-(6-(dimethylamino)-3-(dimethyliminio)-3*H*-xanthen-9-yl)benzoate (71)

Benzyl(3-(*N*-(3-(5-(4-chlorophenyl)-1*H*-pyrrolo[2,3-*b*]pyridine-3-carbonyl)-2,4-difluorophenyl)sulfamoyl)propyl)carbamate (60 mg, 94 μ mol, 5 eq) was suspended in EtOH (1 mL) and HCl (0.35 mL, 6N). The solution was stirred in the microwave (100W, 100 °C, 60 minutes) until complete conversion of the starting material. After removing the solvent under vacuum conditions, the crude product was solved in DMF (1 mL). DIPEA (33 μ L, 190 μ mol, 10 eq) and 5-Tamra-SE (10 mg, 19 μ M, 1 eq) was added and the mixture was stirred overnight at room temperature. The purple product was purified using column chromatography (acetone + 1% triethylamine) and precipitated from *n*pentane/isopropanol (9:1, v/v) (13 mg, 14 μ mol, 73%).

^1H NMR (400 MHz, DMSO) δ 8.94 (t, $J = 5.2$ Hz, 1H), 8.68 (s, 1H), 8.60 (s, 1H), 8.43 (s, 1H), 8.37 (s, 1H), 8.21 (d, $J = 8.0$ Hz, 1H), 8.10 (s, 1H), 7.95 – 7.95 (m, 1H), 7.77 (d, $J = 8.2$ Hz, 2H), 7.55 (d, $J = 7.9$ Hz, 2H), 7.52 – 7.46 (m, 1H), 7.28 (d, $J = 8.0$ Hz, 1H), 7.05 (t, $J = 7.0$ Hz, 1H), 6.47 (q, $J = 8.8$ Hz, 6H), 3.41 (d, $J = 5.2$ Hz, 4H), 3.11 – 3.05 (m, 2H), 2.92 (s, 12H), 1.99 (s, 2H) ppm. ^{13}C NMR (101 MHz, DMSO) δ 180.4, 168.29 – 167.99 (m), 164.9, 152.1, 152.0, 148.9, 143.8, 138.80 – 138.50 (m), 137.0, 135.6, 134.3, 132.4, 130.2, 129.0, 128.8, 128.3, 127.0, 124.2, 117.4, 115.6, 109.0, 105.5, 98.4, 57.1, 51.7, 34.6 ppm. ESI-MS (m/z) 917.9 [M - H] $^-$.

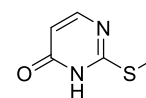


6.3.7. Aminopyrimidine series

2-(Methylthio)pyrimidin-4-ol (74)

2-Thiouracil (10 g, 78 mmol, 1 eq) and grinded sodium hydroxide pellets (3.28 g, 82 mmol, 1.05 mmol) were dissolved in a mixture of water (60 mL) and EtOH (120 mL) and heated to 45 °C until the solution was clear. After cooling the mixture to 0 °C iodomethane (5.1 mL, 82 mmol, 1.05 mmol) was added slowly and heated to 60 °C for 20 hours. The resulting solids were filtered, washed with water, and the filtrate was cooled to -20 °C. Overnight a colorless precipitate formed which was collected and dried under reduced pressure. The pure product (7.5 g, 49 mmol, 63%) was used without further purification.

¹H NMR (200 MHz, DMSO) δ 12.68 (s, 1H), 7.85 (d, *J* = 6.5 Hz, 1H), 6.08 (d, *J* = 6.5 Hz, 1H), 2.46 (s, 3H) ppm. ¹³C NMR (50 MHz, DMSO) δ 163.4, 162.9, 153.9, 109.8, 39.5, 12.9 ppm.

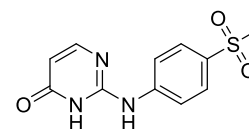


Chemical Formula: C₅H₆N₂OS
Molecular Weight: 142,18

2-((4-(Methylsulfonyl)phenyl)amino)pyrimidin-4(3H)-on (75)

4-(Methylsulfonyl)aniline (9 g, 52.8 mmol, 1.5 eq) was melted at 140 °C and 2-(methylthio)pyrimidin-4-ol (5 g, 35.2 mmol, 1 eq) was added. The mixture was heated to 180 °C until the TLC showed full consumption. The resulting solid was crushed in acetonitrile and filtered to yield the pure product (6.8 g, 25.9 mmol, 73%).

¹H NMR (400 MHz, DMSO) δ 11.15 (s, 1H), 9.50 (s, 1H), 7.91 (d, *J* = 8.7 Hz, 2H), 7.82 (d, *J* = 8.9 Hz, 2H), 6.00 (d, *J* = 4.8 Hz, 1H), 3.15 (s, 3H) ppm. ¹³C NMR (101 MHz, DMSO) δ 164.8, 156.4, 144.2, 133.3, 128.2, 118.8, 44.0, 39.5 ppm. ESI-MS (*m/z*) 267.8 [M + H]⁺.



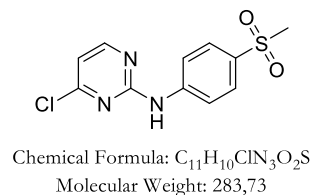
Chemical Formula: C₁₁H₁₁N₃O₃S
Molecular Weight: 265,29

4-Chloro-*N*-(4-(methylsulfonyl)phenyl)pyrimidin-2-amine (76)

2-((4-(Methylsulfonyl)phenyl)amino)pyrimidin-4(3H)-on (1.24 g, 4.67 mmol) was dissolved in POCl₃ (10 mL) and heated to reflux for 1 hour. The resulting solution was poured on ice water. After 1 hour a yellow precipitate was formed which was collected via filtration and subsequently resolved in acetonitrile. After 1 hour stirring in acetonitrile, the light-yellow

solid (900 mg, 3.17 mmol, 68%) was isolated with a suction funnel and used without further purification.

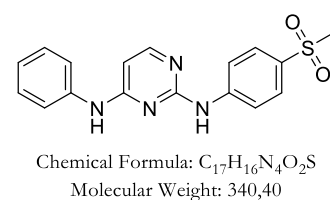
^1H NMR (400 MHz, DMSO) δ 10.54 (s, 1H), 8.52 (d, J = 5.2 Hz, 1H), 7.96 (d, J = 8.9 Hz, 2H), 7.84 (d, J = 8.8 Hz, 2H), 7.09 (d, J = 5.2 Hz, 1H), 3.15 (s, 3H) ppm. ^{13}C NMR (101 MHz, DMSO) δ 160.2, 160.2, 159.3, 144.4, 133.3, 128.1, 118.6, 113.1, 44.0, 39.5 ppm.



N2-(4-(methylsulfonyl)phenyl)-N4-phenylpyrimidine-2,4-diamine (77)

Following the general procedure for nucleophilic aromatic substitutions, the treatment of chloro-pyrimidine (40 mg, 141 μmol , 1 eq), K_2CO_3 (39 mg, 423 μmol , 3 eq) and aniline (49 mg, 353 μmol , 2.5 eq) in DMF afforded the product after purification as a white solid (14 mg, 41 μmol , 29%).

^1H NMR (400 MHz, DMSO) δ 9.73 (s, 1H), 9.48 (s, 1H), 8.09 (d, J = 5.8 Hz, 1H), 8.04 – 7.95 (m, 2H), 7.78 – 7.73 (m, 2H), 7.69 (dd, J = 8.5, 0.9 Hz, 2H), 7.40 – 7.30 (m, 2H), 7.06 (tt, J = 7.6, 1.1 Hz, 1H), 6.33 (d, J = 5.8 Hz, 1H), 3.14 (s, 3H) ppm. ^{13}C

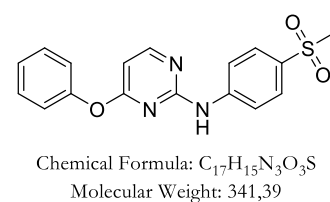


NMR (101 MHz, DMSO) δ 160.6, 159.0, 155.9, 145.7, 139.7, 131.7, 128.7, 127.8, 122.5, 120.4, 118.0, 100.0, 44.1 ppm. IR 3065, 3011, 1572, 1519, 1488, 1458, 1413, 1288, 1216, 1190, 1140, 1092, 1049, 986, 960, 834, 762, 717, 687, 656 cm^{-1} . ESI-MS (m/z) 339.2 [$\text{M} - \text{H}$].

N-(4-(methylsulfonyl)phenyl)-4-phenoxy pyrimidin-2-amine (78)

Following the general procedure for nucleophilic aromatic substitutions, treatment of the chloro-pyrimidine (60 mg, 211 μmol , 1 eq), K_2CO_3 (88 mg, 634 μmol , 3 eq) and phenol (50 mg, 529 μmol , 2.5 eq) in DMF afforded the product after purification as a light yellow solid (430 mg, 126 μmol , 60%).

^1H NMR (400 MHz, DMSO) δ 10.13 (s, 1H), 8.45 (d, J = 5.6 Hz, 1H), 7.71 (d, J = 8.9 Hz, 2H), 7.61 – 7.57 (m, 2H), 7.56 – 7.50 (m, 2H), 7.40 – 7.35 (m, 1H), 7.30 – 7.25 (m, 2H), 6.59 (d, J = 5.6 Hz, 1H), 3.11 (s, 3H) ppm. ^{13}C NMR (101 MHz, DMSO) δ 169.5,

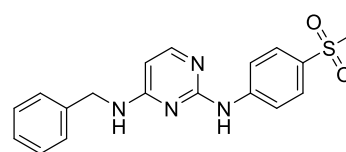


160.1, 159.0, 152.4, 144.9, 132.3, 129.9, 127.7, 125.7, 122.1, 117.9, 99.7, 44.0, 39.5 ppm. IR 3356, 1598, 1576, 1532, 1511, 1483, 1438, 1410, 1329, 1281, 1257, 1215, 1135, 1089, 798, 766, 750, 694, 662 cm^{-1} .

N4-benzyl-N2-(4-(methylsulfonyl)phenyl)pyrimidine-2,4-diamine (79)

Following the general procedure for nucleophilic aromatic substitutions, treatment of the chloro-pyrimidine (90 mg, 317 μmol , 1 eq), K_2CO_3 (132 mg, 952 μmol , 3 eq) and amine (85 mg, 793 μmol , 2.5 eq) in DMF afforded the product after purification as a colorless solid (93 mg, 262 μmol , 83%).

^1H NMR (400 MHz, DMSO) δ 9.56 (s, 1H), 7.97 – 7.83 (m, 4H), 7.68 (d, J = 8.8 Hz, 2H), 7.39 – 7.31 (m, 4H), 7.28 – 7.21 (m, 1H), 6.11 (s, 1H), 4.57 (s, 2H), 3.11 (s, 3H) ppm. ^{13}C NMR (101 MHz, DMSO) δ 162.5, 159.3, 154.9, 146.0, 139.6, 131.2,



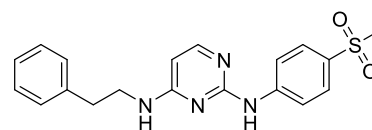
Chemical Formula: $\text{C}_{18}\text{H}_{18}\text{N}_4\text{O}_2\text{S}$
Molecular Weight: 354.43

128.3, 127.8, 127.1, 126.8, 117.5, 99.0, 44.1, 43.5, 39.5 ppm. IR 3423, 3085, 3055, 3020, 2928, 2882, 1620, 1575, 1535, 1507, 1466, 1413, 1337, 1294, 1253, 1224, 1139, 1088, 959, 793, 774, 759, 732, 695, 661 cm^{-1} .

N2-(4-(methylsulfonyl)phenyl)-N4-phenethylpyrimidine-2,4-diamine (80)

Following the general procedure for nucleophilic aromatic substitutions, treatment of the chloro-pyrimidine (90 mg, 317 μmol , 1 eq), K_2CO_3 (132 mg, 952 μmol , 3 eq) and amine (96 mg, 793 μmol , 2.5 eq) in DMF afforded the product after purification and recrystallization in a mixture of EtOAc and *n*-hexane as a colorless solid (64 mg, 174 μmol , 55%).

^1H NMR (400 MHz, DMSO) δ 9.56 (s, 1H), 8.05 – 7.98 (m, 2H), 7.86 (s, 1H), 7.75 – 7.67 (m, 2H), 7.47 (s, 1H), 7.30 (m, 4H), 7.22 (ddd, J = 6.0, 3.6, 1.7 Hz, 1H), 6.05 (d, J = 5.8 Hz, 1H), 3.57 (s, 2H), 3.12 (s, 3H), 2.87 (t, J = 7.5 Hz, 2H) ppm.



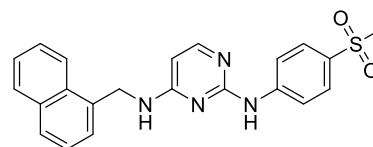
Chemical Formula: $\text{C}_{19}\text{H}_{20}\text{N}_4\text{O}_2\text{S}$
Molecular Weight: 368.46

^{13}C NMR (101 MHz, DMSO) δ 162.5, 159.3, 154.5, 146.1, 139.5, 131.2, 128.7, 128.3, 127.8, 126.1, 117.6, 99.0, 44.1, 41.7, 39.5, 35.0 ppm.

N2-(4-(methylsulfonyl)phenyl)-N4-(naphthalen-1-ylmethyl)pyrimidine-2,4-diamine (81)

Following the general procedure for nucleophilic aromatic substitutions, treatment of the chloro-pyrimidine (90 mg, 317 μmol , 1 eq), K_2CO_3 (132 mg, 952 μmol , 3 eq) and amine (125 mg, 793 μmol , 2.5 eq) in DMF afforded the product after purification and recrystallization in a mixture of EtOAc and *n*-hexane as a colorless solid (33 mg, 205 μmol , 65%).

^1H NMR (400 MHz, DMSO) δ 9.56 (s, 1H), 8.15 (d, $J = 7.8$ Hz, 1H), 8.00 – 7.96 (m, 1H), 7.91 (d, $J = 5.8$ Hz, 2H), 7.88 – 7.84 (m, 1H), 7.82 (s, 2H), 7.59 (tt, $J = 10.8, 3.5$ Hz, 2H), 7.47 (m, 4H), 6.18 (s, 1H), 5.04 (s, 2H), 3.04 (s, 3H) ppm. ^{13}C



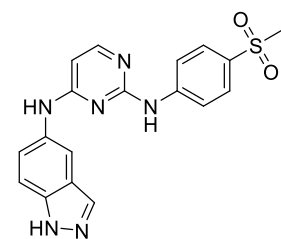
Chemical Formula: $\text{C}_{22}\text{H}_{20}\text{N}_4\text{O}_2\text{S}$
Molecular Weight: 404,49

NMR (101 MHz, DMSO) δ 162.4, 159.3, 154.8, 145.9, 133.4, 131.1, 130.94 128.6, 127.6, 127.4, 126.3, 125.9, 125.5, 124.6, 123.4, 117.5, 44.0, 41.5, 39.5 ppm. IR 3398, 1627, 1579, 1538, 1505, 1470, 1417, 1341, 1315, 1295, 1225, 1138, 1091, 989, 952, 852, 813, 793, 769, 736, 707, 663 cm^{-1} .

N4-(1H-indazol-5-yl)-N2-(4-(methylsulfonyl)phenyl)pyrimidine-2,4-diamine (82)

Following the general procedure for nucleophilic aromatic substitutions, treatment of the chloro-pyrimidine (90 mg, 317 μmol , 1 eq), K_2CO_3 (132 mg, 952 μmol , 3 eq) and amine (106 mg, 793 μmol , 2.5 eq) in DMF afforded the product after purification and recrystallization in a mixture of EtOAc and *n*-hexane as a colorless solid (24 mg, 63 μmol , 20%).

^1H NMR (400 MHz, DMSO) δ 13.02 (s, 1H), 9.70 (s, 1H), 9.44 (s, 1H), 8.14 (s, 1H), 8.05 (t, $J = 6.1$ Hz, 1H), 8.00 (d, $J = 8.8$ Hz, 1H), 7.70 (d, $J = 8.9$ Hz, 2H), 7.54 (d, $J = 8.8$ Hz, 1H), 7.45 (dd, $J = 8.9, 1.9$ Hz, 1H), 6.29 (d, $J = 5.8$ Hz, 1H), 3.13 (s, 3H) ppm. ^{13}C NMR (101 MHz, DMSO) δ 161.0, 155.8, 145.8, 136.9, 133.2, 132.4, 131.6, 127.8, 123.0, 122.29, 118.0, 111.6, 110.2, 99.4, 44.1, 39.5, 25.5 ppm.



Chemical Formula: $\text{C}_{18}\text{H}_{16}\text{N}_6\text{O}_2\text{S}$
Molecular Weight: 380,43

IR 1578, 1501, 1415, 1294, 1218, 1140, 790, 772, 721, 698, 668 cm^{-1} .

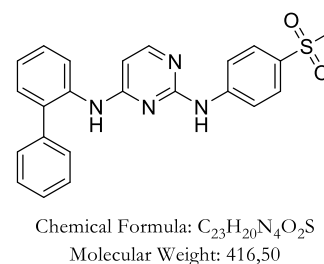
N4-cyclohexyl-N2-(4-(methylsulfonyl)phenyl)pyrimidine-2,4-diamine (83)

Following the general procedure for nucleophilic aromatic substitutions, treatment of the chloro-pyrimidine (90 mg, 317 μmol , 1 eq), K_2CO_3 (132 mg, 952 μmol , 3 eq) and amine (106 mg, 793 μmol , 2.5 eq) in DMF afforded the product after purification and recrystallization in a mixture of EtOAc and *n*-hexane as a colorless solid (24 mg, 63 μmol , 20%).

***N*4-([1,1'-biphenyl]-2-yl)-*N*2-(4-(methylsulfonyl)phenyl)pyrimidine-2,4-diamine (84)**

Following the general procedure for nucleophilic aromatic substitutions, treatment of the chloro-pyrimidine (90 mg, 317 μmol , 1 eq), K_2CO_3 (132 mg, 952 μmol , 3 eq) and amine (134 mg, 793 μmol , 2.5 eq) in DMF afforded the product after purification and recrystallization in a mixture of EtOAc and *n*-hexane as a colorless solid (34 mg, 82 μmol , 26%)

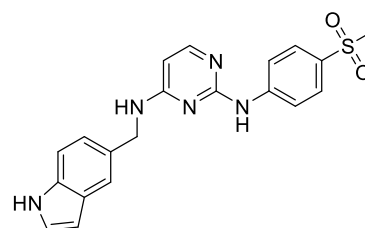
^1H NMR (400 MHz, DMSO) δ 9.58 (s, 1H), 8.87 (s, 1H), 7.93 (d, $J = 5.8$ Hz, 1H), 7.88 (d, $J = 8.9$ Hz, 2H), 7.61 (d, $J = 8.9$ Hz, 2H), 7.53 (d, $J = 7.5$ Hz, 1H), 7.49 – 7.26 (m, 8H), 6.06 (d, $J = 5.8$ Hz, 1H), 3.11 (s, 3H) ppm. ^{13}C NMR (101 MHz, DMSO) δ 162.1, 159.0, 156.0, 145.9, 139.2, 137.8, 135.7, 131.2, 130.6, 128.70, 128.3, 128.3, 128.0, 127.6, 127.1, 126.3, 117.6, 98.3, 44.1, 39.5 ppm. IR 1570, 1507, 1405, 1322, 1293, 1139, 1090, 952, 767, 743, 700, 661 cm^{-1} .



***N*4-((1*H*-indol-5-yl)methyl)-*N*2-(4-(methylsulfonyl)phenyl)pyrimidine-2,4-diamine (85)**

Following the general procedure for nucleophilic aromatic substitutions, treatment of the chloro-pyrimidine (90 mg, 317 μmol , 1 eq), K_2CO_3 (132 mg, 952 μmol , 3 eq) and amine (116 mg, 793 μmol , 2.5 eq) in DMF afforded the product after purification and recrystallization in a mixture of EtOAc and *n*-hexane as a colorless solid (28 mg, 71 μmol , 22%).

^1H NMR (400 MHz, DMSO) δ 11.02 (s, 1H), 9.55 (s, 1H), 7.97 (d, $J = 8.2$ Hz, 2H), 7.86 (dd, $J = 12.6, 5.0$ Hz, 1H), 7.81 (s, 1H), 7.70 (d, $J = 8.9$ Hz, 2H), 7.52 (s, 1H), 7.36 (d, $J = 8.3$ Hz, 1H), 7.32 – 7.29 (m, 1H), 7.11 (dd, $J = 8.4, 1.4$ Hz, 1H), 6.40 – 6.36 (m, 1H), 6.11 (d, $J = 5.4$ Hz, 1H), 4.63 (s, 2H), 3.11 (s, 3H) ppm. ^{13}C NMR (101 MHz, DMSO) δ 162.5,



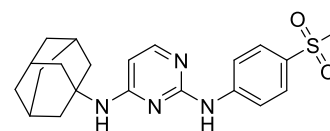
Chemical Formula: $\text{C}_{20}\text{H}_{19}\text{N}_5\text{O}_2\text{S}$
Molecular Weight: 393,47

159.3, 154.6, 146.1, 135.1, 131.1, 129.6, 127.8, 127.6, 125.60, 120.9, 118.6, 117.5, 111.3, 100.9, 99.1, 59.8, 44.1, 39.5, 20.8, 14.1 ppm. IR 1724, 1601, 1575, 1511, 1480, 1401, 1348, 1327, 1282, 1243, 1220, 1138, 1085, 1042, 964, 927, 894, 835, 794, 765, 725, 659 cm^{-1} .

N4-(adamantan-1-yl)-N2-(4-(methanesulfonyl)phenyl)pyrimidine-2,4-diamine (86)

Following the general procedure for nucleophilic aromatic substitutions, treatment of the chloro-pyrimidine (90 mg, 317 μmol , 1 eq), K_2CO_3 (132 mg, 952 μmol , 3 eq) and amine (119 mg, 793 μmol , 2.5 eq) in DMF afforded the product after purification and recrystallization in a mixture of EtOAc and *n*-hexane as a colorless solid (25 mg, 63 μmol , 20%).

^1H NMR (400 MHz, DMSO) δ 9.40 (s, 1H), 8.01 (d, $J = 1.8$ Hz, 2H), 7.79 (d, $J = 5.9$ Hz, 1H), 7.72 (d, $J = 8.9$ Hz, 2H), 6.87 (s, 1H), 6.07 (d, $J = 5.9$ Hz, 1H), 3.13 (s, 3H), 2.11 (s, 9H), 1.77 – 1.65 (m, 6H) ppm. ^{13}C NMR (101 MHz, DMSO) δ 162.2, 158.6,



Chemical Formula: $\text{C}_{21}\text{H}_{26}\text{N}_4\text{O}_2\text{S}$
Molecular Weight: 398,53

154.0, 146.1, 131.1, 127.8, 117.5, 100.1, 51.2, 44.1, 40.9, 39.5, 36.0, 28.9 ppm. IR 3339, 2929, 1601, 1577, 1534, 1497, 1403, 1347, 1305, 1256, 1220, 1141, 1087, 975, 948, 851, 804, 755, 722, 690, 654 cm^{-1} .

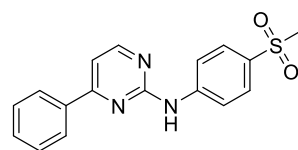
N-(4-(methanesulfonyl)phenyl)-4-phenylpyrimidin-2-amine (87)

A solution of 4-chloro-*N*-(4-(methanesulfonyl)phenyl)pyrimidin-2-amine (122 mg, 430 μmol , 1 eq), K_2CO_3 (150 mg, 1.07 mmol, 2.5 eq) and phenylboronic acid (105 mg, 860 μmol , 2 eq) in EtOH/water (3:1, v/v, 2 mL) was purged with argon for 15 minutes. To the mixture $\text{Pd}(\text{dppf})_2\text{Cl}_2$ (20 mg, 22 μmol , 5 mol%) was added and heated to 55 $^\circ\text{C}$ for 2 hours. After TLC indicated full consumption of the starting material, the mixture was diluted with EtOAc and washed with water and brine. The organic phase was dried over sodium sulphate,

concentrated, and purified by column chromatography (PE/EtOAc, 10 – 50%) to provide the product as white solid (93 mg, 286 μmol , 60%).

^1H NMR (400 MHz, DMSO) δ 10.26 (s, 1H), 8.65 (d, $J = 5.2$ Hz, 1H), 8.24 – 8.18 (m, 2H), 8.14 – 8.08 (m, 2H), 7.89 – 7.83 (m, 2H), 7.58 (ddd, $J = 4.7, 4.1, 2.6$ Hz, 3H), 7.55 (s, 1H), 3.16 (s, 3H) ppm.

^{13}C NMR (101 MHz, DMSO) δ 163.9, 159.7, 159.2, 145.3, 136.3, 132.3, 131.1, 129.0, 128.1, 127.0, 118.0, 109.3, 44.0, 39.5 ppm. IR 3342, 1420, 1305, 1144, 1090, 828, 763, 738, 688 cm^{-1} . ESI-MS (m/z) 348.1 $[\text{M} + \text{H}]^+$.



Chemical Formula: $\text{C}_{17}\text{H}_{15}\text{N}_3\text{O}_2\text{S}$
Molecular Weight: 325,39

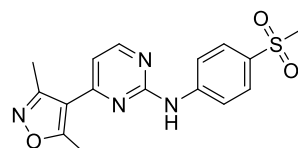
4-(3,5-Dimethylisoxazol-4-yl)-*N*-(4-(methylsulfonyl)phenyl)pyrimidin-2-amine (88)

A solution of 4-chloro-*N*-(4-(methylsulfonyl)phenyl)pyrimidin-2-amine (60 mg, 211 μmol , 1 eq), K_2CO_3 (74 mg, 529 μmol , 3 eq) and (3,5-dimethylisoxazol-4-yl)boronic acid (60 mg, 423 μmol , 2 eq) in EtOH/water (3:1, v/v, 2 mL) was purged with argon for 15 minutes. To the mixture $\text{Pd}(\text{dppf})_2\text{Cl}_2$ (30 mg, 35 μmol , 5 mol%) was added and heated to 50 $^\circ\text{C}$ for 1 hours. After TLC indicated full consumption the mixture was diluted with EtOAc and washed with water and brine. The organic phase was dried over sodium sulphate, concentrated, and purified by column chromatography to provide the product as white solid (55 mg, 116 μmol , 55%).

^1H NMR (400 MHz, DMSO) δ 10.17 (s, 1H), 8.62 (d, $J = 5.2$ Hz, 1H), 8.07 – 7.96 (m, 2H), 7.91 – 7.80 (m, 2H), 7.13 (d, $J = 5.2$ Hz, 1H), 3.15 (s, 2H), 2.67 (s, 3H), 2.45 (s, 3H) ppm. ^{13}C NMR (101

MHz, DMSO) δ 169.8, 159.5, 158.8, 158.4, 158.1, 145.1, 132.5,

128.0, 118.2, 113.8, 111.8, 44.0, 12.8, 11.5 ppm. IR 2922, 2853, 1570, 1532, 1413, 1292, 1252, 1220, 1141, 1089, 1052, 1000, 968, 885, 834, 811, 772, 755, 694, 661 cm^{-1} . ESI-MS (m/z) 343.3 $[\text{M} - \text{H}]^-$.

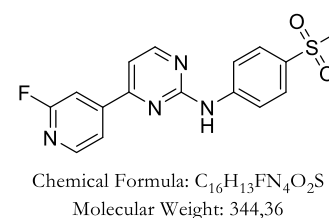


Chemical Formula: $\text{C}_{16}\text{H}_{16}\text{N}_4\text{O}_3\text{S}$
Molecular Weight: 344,39

4-(2-Fluoropyridin-4-yl)-N-(4-(methylsulfonyl)phenyl)pyrimidin-2-amine (89)

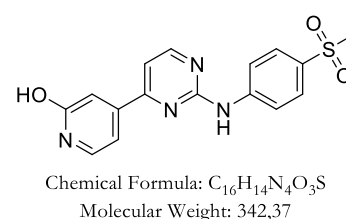
A solution of 4-chloro-*N*-(4-(methylsulfonyl)phenyl)pyrimidin-2-amine (200 mg, 705 μmol , 1 eq), K_2CO_3 (294 mg, 2.11 mmol, 3 eq) and (2-fluoropyridin-4-yl)boronic acid (199 mg, 1.4 mmol, 2 eq) in 1,4-dioxane/water (3:1, v/v, 2 mL) was purged with argon for 15 minutes. To the mixture XPhos Pd G3 (30 mg, 35 μmol , 5 mol%) was added and heated to 100 °C for 1 hours. After TLC indicated full consumption the mixture was diluted with EtOAc and washed with water and brine. The organic phase was dried over sodium sulphate, concentrated, and purified by column chromatography to provide the product as white solid (102 mg, 296 μmol , 42%).

^1H NMR (400 MHz, DMSO) δ 10.41 (s, 1H), 8.79 (d, $J = 5.0$ Hz, 1H), 8.47 (d, $J = 5.1$ Hz, 1H), 8.12 – 8.08 (m, 1H), 8.07 (d, $J = 8.3$ Hz, 2H), 7.88 (d, $J = 7.6$ Hz, 3H), 7.71 (d, $J = 5.0$ Hz, 1H), 3.17 (s, 3H) ppm. ^{13}C NMR (101 MHz, DMSO) δ 164.04 (d, $J = 235.1$ Hz), 160.3, 160.3, 159.7, 149.75 (d, $J = 8.2$ Hz), 148.78 (d, $J = 15.3$ Hz), 144.9, 132.7, 128.1, 119.45 (d, $J = 4.1$ Hz) 118.3, 110.2, 107.3, 106.9, 44.0 ppm. IR 3302, 1601, 1571, 1529, 1444, 1399, 1314, 1286, 1196, 1140, 1089, 992, 966, 885, 868, 839, 813, 767, 733, 707, 664 cm^{-1} . ESI-MS (m/z) 343.2 [$\text{M} - \text{H}$] $^-$.

**4-(2-((4-(Methylsulfonyl)phenyl)amino)pyrimidin-4-yl)pyridin-2-ol (90)**

4-(2-Fluoropyridin-4-yl)-*N*-(4-(methylsulfonyl)phenyl)pyrimidin-2-amine (30 mg, 87 μmol) was dissolved in acetic acid (100 %, 2 mL) and heated up to 100 °C for 17 hours. After cooling to room temperature colorless crystals precipitated over 72 hours. The crystals were collected via suction filtration and washed with water to yield the pure product (18 mg, 53 μmol , 60%).

^1H NMR (400 MHz, DMSO) δ 10.42 (s, 1H), 8.80 (d, $J = 5.1$ Hz, 1H), 8.47 (d, $J = 5.2$ Hz, 1H), 8.11 (d, $J = 5.1$ Hz, 1H), 8.07 (d, $J = 8.8$ Hz, 2H), 7.90 – 7.85 (m, 2H), 7.74 – 7.71 (m, 1H), 3.16 (s, 3H) ppm. ^{13}C NMR (101 MHz, DMSO) δ 165.3, 160.4,



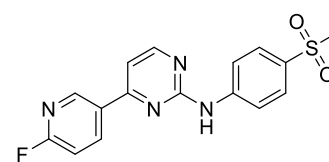
159.8, 149.9, 149.8, 149.0 148.8, 145.0, 132.8, 128.2, 119.6 119.5, 118.4, 110.3, 107.4, 107.0,

44.0 ppm. IR 3305, 1602, 1571, 1529, 1444, 1398, 1314, 1286, 1196, 1140, 1089, 993, 967, 869, 839, 813, 767, 733, 707, 663 cm^{-1} .

4-(6-Fluoropyridin-3-yl)-*N*-(4-(methylsulfonyl)phenyl)pyrimidin-2-amine (91)

A solution of 4-chloro-*N*-(4-(methylsulfonyl)phenyl)pyrimidin-2-amine (200 mg, 705 μmol , 1 eq), K_2CO_3 (294 mg, 2.11 mmol, 3 eq) and (6-fluoropyridin-3-yl)boronic acid (199 mg, 1.4 mmol, 2 eq) in 1,4-dioxane/water (3:1, v/v, 2 mL) was purged with argon for 15 minutes. To the mixture XPhos Pd G3 (30 mg, 35 μmol , 5 mol%) was added and heated to 100 $^\circ\text{C}$ for 1 hours. After TLC indicated full consumption the mixture was diluted with EtOAc and washed with water and brine. The organic phase was dried over sodium sulphate, concentrated, and purified by column chromatography to provide the product as white solid (150 mg, 436 μmol , 62%).

^1H NMR (400 MHz, DMSO) δ 10.32 (s, 1H), 9.04 (d, $J = 2.5$ Hz, 1H), 8.75 – 8.69 (m, 1H), 8.70 – 8.67 (m, 1H), 8.09 – 8.03 (m, 1H), 7.89 – 7.84 (m, 1H), 7.62 (d, $J = 5.2$ Hz, 1H), 7.39 (dd, $J = 8.6, 2.6$ Hz, 1H), 3.17 (s, 3H) ppm. ^{13}C NMR (101 MHz, DMSO) δ 160.7, 164.35 (d, $J = 239.6$ Hz), 159.61 (d, $J = 3.4$ Hz),



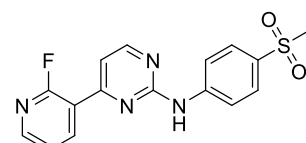
Chemical Formula: $\text{C}_{16}\text{H}_{13}\text{FN}_4\text{O}_2\text{S}$
Molecular Weight: 344,36

146.95 (d, $J = 16.0$ Hz), 145.1, 140.80 (d, $J = 8.9$ Hz), 130.71 (d, $J = 4.4$ Hz), 132.5, 128.1, 118.2, 110.02 (d, $J = 37.7$ Hz), 109.4, 44.0 ppm. IR 1598, 1578, 1538, 1485, 1445, 1418, 1368, 1320, 1297, 1241, 1202, 1145, 1115, 1091, 1024, 973, 820, 789, 766 cm^{-1} .

4-(2-Fluoropyridin-3-yl)-*N*-(4-(methylsulfonyl)phenyl)pyrimidin-2-amine (92)

A solution of 4-chloro-*N*-(4-(methylsulfonyl)phenyl)pyrimidin-2-amine (200 mg, 705 μmol , 1 eq), K_2CO_3 (294 mg, 2.11 mmol, 3 eq) and (2-fluoropyridin-3-yl)boronic acid (199 mg, 1.4 mmol, 2 eq) in 1,4-dioxane/water (3:1, v/v, 2 mL) was purged with argon for 15 minutes. To the mixture XPhos Pd G3 (30 mg, 35 μmol , 5 mol%) was added and heated to 100 $^\circ\text{C}$ for 1 hours. After TLC indicated full consumption the mixture was diluted with EtOAc and washed with water and brine. The organic phase was dried over sodium sulphate, concentrated, and purified by column chromatography to provide the product as white solid (170 mg, 494 μmol , 70%).

¹H NMR (400 MHz, DMSO) δ 10.37 (s, 1H), 8.62 (ddd, $J = 9.8$, 7.6, 2.0 Hz, 1H), 8.42 (ddd, $J = 4.7, 1.8, 1.1$ Hz, 1H), 8.08 – 8.04 (m, 2H), 7.88 – 7.83 (m, 2H), 7.60 (ddd, $J = 7.3, 4.8, 1.9$ Hz, 1H), 7.42 (dd, $J = 5.1, 2.2$ Hz, 1H), 3.16 (s, 3H). ¹³C NMR (101 MHz,



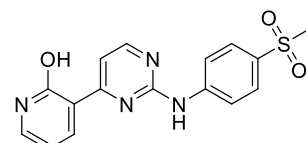
Chemical Formula: C₁₆H₁₃FN₄O₂S
Molecular Weight: 344,36

DMSO) δ 160.36 (d, $J = 240.5$ Hz), 159.61 (d, $J = 1.8$ Hz), 158.92 (d, $J = 6.8$ Hz), 149.42 (d, $J = 15.5$ Hz), 145.0, 141.59 (d, $J = 2.5$ Hz), 132.6, 128.1, 122.90 (d, $J = 3.9$ Hz), 119.71 (d, $J = 25.9$ Hz), 118.2, 112.76 (d, $J = 9.4$ Hz), 44.0 ppm. IR 3273, 3184, 3101, 1599, 1575, 1522, 1408, 1296, 1251, 1206, 1142, 1090, 991, 950, 830, 813, 786, 762, 727, 690, 663 cm⁻¹. ESI-MS (m/z) 343.2 [M - H]⁻.

3-(2-((4-(Methylsulfonyl)phenyl)amino)pyrimidin-4-yl)pyridin-2-ol (93)

4-(2-Fluoropyridin-3-yl)-*N*-(4-(methylsulfonyl)phenyl)pyrimidin-2-amine (30 mg, 87 μ mol) was dissolved in acetic acid (100%, 2 mL) and heated up to 100 °C for 17 hours. After cooling to room temperature colorless crystals precipitated over 72 hours. The crystals were collected via suction filtration and washed with water to yield the pure product (15 mg, 44 μ mol, 50%).

¹H NMR (400 MHz, DMSO) δ 12.18 (s, 1H), 10.13 (s, 1H), 8.62 (d, $J = 7.0$ Hz, 1H), 8.58 (d, $J = 5.0$ Hz, 1H), 8.16 (t, $J = 15.3$ Hz, 1H), 8.05 (d, $J = 8.5$ Hz, 2H), 7.85 (d, $J = 8.5$ Hz, 2H), 7.67 (d, $J = 5.4$ Hz, 1H), 6.49 (t, $J = 6.6$ Hz, 1H), 3.15 (s, 3H) ppm. ¹³C NMR



Chemical Formula: C₁₆H₁₄N₄O₃S
Molecular Weight: 342,37

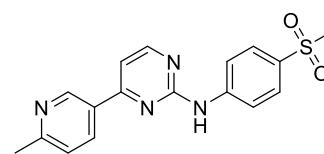
(101 MHz, DMSO) δ 161.2, 160.6, 159.1, 158.8, 145.4, 141.6, 138.8, 132.0, 128.1, 124.4, 117.8, 112.0, 105.5, 44.1 ppm. IR 1576, 1526, 1491, 1446, 1406, 1297, 1245, 1137, 1088, 1058, 961, 910, 841, 768, 720, 701, 663 cm⁻¹.

4-(2-(6-Methylpyridin-3-yl)-*N*-(4-(methylsulfonyl)phenyl)pyrimidin-2-amine (94)

A solution of 4-chloro-*N*-(4-(methylsulfonyl)phenyl)pyrimidin-2-amine (200 mg, 705 μ mol, 1 eq), K₂CO₃ (294 mg, 2.11 mmol, 3 eq) and (6-methylpyridin-3-yl)boronic acid (193 mg, 1.4 mmol, 2 eq) in 1,4-dioxane/water (3:1, v/v, 2 mL) was purged with argon for 15 minutes. To the mixture XPhos Pd G3 (30 mg, 35 μ mol, 5 mol%) was added and heated to 100 °C for 1 hours. After TLC indicated full consumption the mixture was diluted with EtOAc and washed with water and brine. The organic phase was dried over sodium sulphate,

concentrated, and purified by column chromatography to provide the product as white solid (166 mg, 488 μmol , 69%).

^1H NMR (400 MHz, DMSO) δ 10.33 (s, 1H), 8.68 (d, $J = 4.9$ Hz, 1H), 8.58 (d, $J = 3.2$ Hz, 1H), 8.04 (d, $J = 8.7$ Hz, 2H), 7.92 (d, $J = 7.5$ Hz, 1H), 7.83 (d, $J = 8.6$ Hz, 1H), 7.40 (dd, $J = 7.3, 5.1$ Hz, 1H), 7.22 (d, $J = 5.0$ Hz, 1H), 3.15 (s, 3H), 2.62 (s, 3H) ppm. ^{13}C



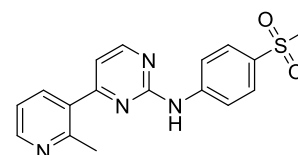
Chemical Formula: $\text{C}_{17}\text{H}_{16}\text{N}_4\text{O}_2\text{S}$
Molecular Weight: 340,40

NMR (101 MHz, DMSO) δ 165.7, 159.35, 158.7, 155.5, 149., 145.1, 137.0, 136.55, 133.0, 132.9, 132.4, 128.0, 121.4, 118.1, 113.4, 44.0, 23.4 ppm. IR 3317, 1599, 1571, 1524, 1493, 1325, 1291, 1245, 1201, 1138, 1090, 1028, 989, 966, 829, 803, 776, 713, 699, 663 cm^{-1} .

4-(6-Methylpyridin-3-yl)-N-(4-(methylsulfonyl)phenyl)pyrimidin-2-amine (95)

A solution of 4-chloro-*N*-(4-(methylsulfonyl)phenyl)pyrimidin-2-amine (200 mg, 705 μmol , 1 eq), K_2CO_3 (294 mg, 2.11 mmol, 3 eq) and (2-methylpyridin-3-yl)boronic acid (193 mg, 1.4 mmol, 2 eq) in 1,4-dioxane/water (3:1, v/v, 2 mL) was purged with argon for 15 minutes. To the mixture XPhos Pd G3 (30 mg, 35 μmol , 5 mol%) was added and heated to 100 $^\circ\text{C}$ for 1 hours. After TLC indicated full consumption the mixture was diluted with EtOAc and washed with water and brine. The organic phase was dried over sodium sulphate, concentrated, and purified by column chromatography to provide the product as white solid (166 mg, 488 μmol , 69%).

^1H NMR (400 MHz, DMSO) δ 10.29 (s, 1H), 9.24 (s, 1H), 8.67 (d, $J = 5.1$ Hz, 1H), 8.42 (d, $J = 8.2$ Hz, 1H), 8.08 (d, $J = 8.7$ Hz, 2H), 7.86 (d, $J = 8.5$ Hz, 2H), 7.60 (d, $J = 5.1$ Hz, 1H), 7.46 (d, $J = 8.1$ Hz, 1H), 3.16 (s, 3H), 2.57 (s, 3H) ppm. ^{13}C NMR (101 MHz, DMSO) δ 162.0, 160.7, 159.7, 159.3, 147.7, 145.2, 134.7, 132.4,



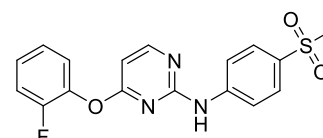
Chemical Formula: $\text{C}_{17}\text{H}_{16}\text{N}_4\text{O}_2\text{S}$
Molecular Weight: 340,40

129.2, 128.1, 123.3, 118.1, 109.2, 44.0, 24.1 ppm. IR 3340, 1595, 1574, 1552, 1521, 1461, 1419, 1288, 1250, 1200, 1140, 1090, 991, 961, 837, 813, 772, 740, 722, 691, 662 cm^{-1} .

4-(2-Fluorophenoxy)-*N*-(4-(methylsulfonyl)phenyl)pyrimidin-2-amine (96)

Following the general procedure for nucleophilic aromatic substitutions, treatment of the chloro-pyrimidine (50 mg, 176 μmol , 1 eq), K_2CO_3 (146 mg, 1.06 mmol, 1.5 eq) and phenol (40 mg, 352 μmol , 2 eq) in DMF afforded the product after purification and recrystallization in a mixture of EtOAc and *n*hexane as a colorless solid (23 mg, 75 μmol , 36%).

^1H NMR (400 MHz, DMSO) δ 10.19 (s, 1H), 8.49 (d, $J = 5.3$ Hz, 1H), 7.64 (d, $J = 8.4$ Hz, 2H), 7.58 (d, $J = 8.4$ Hz, 2H), 7.54 – 7.31 (m, 1H), 6.72 (d, $J = 5.3$ Hz, 1H), 3.11 (s, 3H) ppm. ^{13}C



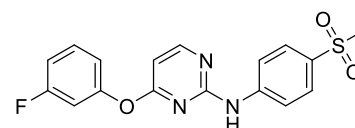
Chemical Formula: $\text{C}_{17}\text{H}_{14}\text{FN}_3\text{O}_3\text{S}$
Molecular Weight: 359,38

NMR (101 MHz, DMSO) δ 168.6, 160.5, 159.0, 154.03 (d, $J = 247.0$ Hz), 144.7, 139.33 (d, $J = 12.6$ Hz), 132.5, 127.6, 127.47 (d, $J = 7.3$ Hz), 125.5, 124.5, 117.9, 116.91 (d, $J = 18.4$ Hz), 99.1, 43.9 ppm. IR 3262, 3182, 3092, 3049, 3022, 1599, 1574, 1521, 1495, 1455, 1415, 1296, 1251, 1218, 1179, 1142, 1092, 1053, 952, 836, 771, 696, 660 cm^{-1} .

4-(3-Fluorophenoxy)-*N*-(4-(methylsulfonyl)phenyl)pyrimidin-2-amine (97)

Following the general procedure for nucleophilic aromatic substitutions, treatment of the chloro-pyrimidine (50 mg, 176 μmol , 1 eq), K_2CO_3 (146 mg, 1.06 mmol, 1.5 eq) and phenol (40 mg, 352 μmol , 2 eq) in DMF afforded the product after purification and recrystallization in a mixture of EtOAc and *n*hexane as a colorless solid (27 mg, 75 μmol , 43%).

^1H NMR (400 MHz, DMSO) δ 10.16 (s, 1H), 8.47 (d, $J = 5.6$ Hz, 1H), 7.73 (d, $J = 8.8$ Hz, 2H), 7.62 (d, $J = 8.9$ Hz, 2H), 7.56 (dd, $J = 15.1, 8.2$ Hz, 1H), 7.29 (dt, $J = 10.0, 2.3$ Hz, 1H), 7.23 (td, $J = 8.6, 2.3$ Hz, 1H), 7.16 (dd, $J = 8.1, 1.8$ Hz, 1H), 6.63 (d, $J = 5.6$ Hz, 1H), 3.11 (s, 3H). ^{13}C NMR (101 MHz, DMSO) δ 169.1, 162.62 (d, $J = 245.2$ Hz), 160.3, 159.1, 153.38 (d, $J = 11.2$ Hz), 144.9, 132.5, 131.15 (d, $J = 9.7$ Hz), 118.40 (d, $J = 2.8$ Hz), 118.1, 112.69 (d, $J = 21.0$ Hz), 110.14 (d, $J = 24.1$ Hz), 99.8, 44.0 ppm. IR 1600, 1574, 1524, 1484, 1456, 1416, 1301, 1252, 1218, 1139, 1092, 1055, 948, 858, 834, 806, 770, 688, 659 cm^{-1} .



Chemical Formula: $\text{C}_{17}\text{H}_{14}\text{FN}_3\text{O}_3\text{S}$
Molecular Weight: 359,38

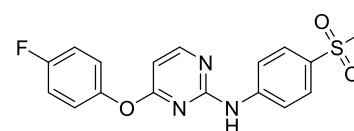
4-(4-Fluorophenoxy)-*N*-(4-(methylsulfonyl)phenyl)pyrimidin-2-amine (98)

Following the general procedure for nucleophilic aromatic substitutions, treatment of the chloro-pyrimidine (80 mg, 211 μmol , 1 eq), K_2CO_3 (88 mg, 634 μmol , 3 eq) and phenol (47 mg, 423 μmol , 2 eq) in DMF afforded the product after purification and recrystallization in a mixture of EtOAc and *n*hexane as a colorless solid (41 mg, 114 μmol , 54%).

^1H NMR (600 MHz, DMSO) δ 10.13 (s, 1H), 8.45 (d, $J = 5.6$ Hz, 1H), 7.72 (d, $J = 8.7$ Hz, 2H), 7.63 (d, $J = 8.9$ Hz, 2H), 7.39 – 7.31 (m, 4H), 6.60 (d, $J = 5.6$ Hz, 1H), 3.11 (s, 3H) ppm.

^{13}C NMR (151 MHz, DMSO) δ 160.2, 159.66 (d, $J = 242.4$

Hz), 159.1, 148.40 (d, $J = 2.9$ Hz), 144.8, 132.4, 127.7, 123.96 (d, $J = 9.5$ Hz), 118.0, 116.44 (d, $J = 23.8$ Hz), 99.7, 44.0 ppm. IR 1600, 1571, 1522, 1499, 1457, 1419, 1333, 1302, 1221, 1182, 1137, 1088, 1053, 987, 956, 836, 800, 770, 703 cm^{-1} .



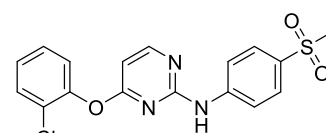
Chemical Formula: $\text{C}_{17}\text{H}_{14}\text{FN}_3\text{O}_3\text{S}$
Molecular Weight: 359,38

4-(2-Chlorophenoxy)-*N*-(4-(methylsulfonyl)phenyl)pyrimidin-2-amine (99)

Following the general procedure for nucleophilic aromatic substitutions, treatment of the chloro-pyrimidine (50 mg, 176 μmol , 1 eq), K_2CO_3 (73 mg, 529 μmol , 3 eq) and phenol (45 mg, 352 μmol , 2 eq) in DMF afforded the product after purification and recrystallization in a mixture of EtOAc and *n*hexane as a colorless solid (43 mg, 114 μmol , 65%).

^1H NMR (400 MHz, DMSO) δ 10.18 (s, 1H), 8.49 (d, $J = 5.5$ Hz, 1H), 7.70 (d, $J = 7.9$ Hz, 1H), 7.61 (d, $J = 8.6$ Hz, 2H), 7.56 (d, $J = 8.6$ Hz, 2H), 7.51 (d, $J = 7.5$ Hz, 1H), 7.45 (m, 2H), 6.71 (d, $J = 5.5$ Hz, 1H), 3.11 (s, 3H) ppm. ^{13}C NMR (101 MHz, DMSO)

δ 168.6, 160.5, 159.0, 148.3, 144.7, 132.4, 130.5, 128.8, 127.6, 127.5, 126.4, 124.6, 117.8, 99.2, 43.9 ppm. IR 3318, 3100, 2920, 1569, 1517, 1487, 1457, 1409, 1286, 1251, 1220, 1135, 1091, 1046, 986, 946, 840, 820, 797, 765, 738, 687, 658 cm^{-1} . ESI-MS (m/z) 374.3 [$\text{M} - \text{H}$].



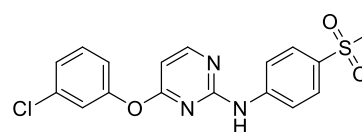
Chemical Formula: $\text{C}_{17}\text{H}_{14}\text{ClN}_3\text{O}_3\text{S}$
Molecular Weight: 375,83

4-(3-Chlorophenoxy)-*N*-(4-(methylsulfonyl)phenyl)pyrimidin-2-amine (100)

Following the general procedure for nucleophilic aromatic substitutions, treatment of the chloro-pyrimidine (60 mg, 211 μmol , 1 eq), K_2CO_3 (88 mg, 634 μmol , 3 eq) and phenol (54

mg, 423 μmol , 2 eq) in DMF afforded the product after purification and recrystallization in a mixture of EtOAc and *n*hexane as a colorless solid (38 mg, 101 μmol , 49%).

^1H NMR (400 MHz, DMSO) δ 10.16 (s, 1H), 8.47 (d, $J = 5.6$ Hz, 1H), 7.73 (d, $J = 8.9$ Hz, 2H), 7.64 (d, $J = 8.9$ Hz, 2H), 7.55 (t, $J = 8.1$ Hz, 1H), 7.49 (t, $J = 2.1$ Hz, 1H), 7.47 – 7.43



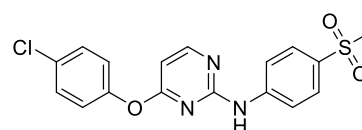
Chemical Formula: $\text{C}_{17}\text{H}_{14}\text{ClN}_3\text{O}_3\text{S}$
Molecular Weight: 375,83

(m, 1H), 7.28 (ddd, $J = 8.1, 2.2, 0.9$ Hz, 1H), 6.64 (d, $J = 5.6$ Hz, 1H), 3.11 (s, 3H) ppm. ^{13}C NMR (101 MHz, DMSO) δ 169.1, 160.3, 159.0, 153.1, 144.8, 133.7, 132.5, 131.2, 127.7, 125.8, 122.6, 121.0, 118.0, 99.8, 44.0 ppm. IR 1593, 1571, 1522, 1453, 1414, 1302, 1267, 1218, 1198, 1139, 1092, 1054, 963, 897, 833, 810, 776, 710, 679 cm^{-1} . ESI-MS (m/z) 374.2 [$\text{M} - \text{H}$] $^-$.

4-(4-Chlorophenoxy)-N-(4-(methylsulfonyl)phenyl)pyrimidin-2-amine (101)

Following the general procedure for nucleophilic aromatic substitutions, treatment of the chloro-pyrimidine (60 mg, 211 μmol , 1 eq), K_2CO_3 (88 mg, 634 μmol , 3 eq) and phenol (54 mg, 423 μmol , 2 eq) in DMF afforded the product after purification and recrystallization in a mixture of EtOAc and *n*hexane as a colorless solid (15 mg, 40 μmol , 19%).

^1H NMR (400 MHz, DMSO) δ 10.11 (d, $J = 15.6$ Hz, 1H), 8.46 (d, $J = 5.6$ Hz, 1H), 7.72 (d, $J = 8.5$ Hz, 2H), 7.63 (d, $J = 8.4$ Hz, 2H), 7.58 (d, $J = 8.2$ Hz, 2H), 7.33 (d, $J = 8.2$ Hz, 2H), 6.63 (d, $J = 5.6$ Hz, 1H), 3.11 (s, 3H) ppm. ^{13}C NMR (101



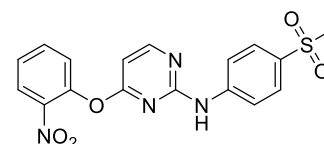
Chemical Formula: $\text{C}_{17}\text{H}_{14}\text{ClN}_3\text{O}_3\text{S}$
Molecular Weight: 375,83

MHz, DMSO) δ 169.3, 160.2, 159.0, 151.2, 144.8, 132.5, 129.9, 129.8, 127.6, 124.1, 118.1, 99.8, 44.0 ppm.

N-(4-(methylsulfonyl)phenyl)-4-(2-nitrophenoxy)pyrimidin-2-amine (102)

Following the general procedure for nucleophilic aromatic substitutions, treatment of the chloro-pyrimidine (100 mg, 352 μmol , 1 eq), K_2CO_3 (146 mg, 1.06 mmol, 3 eq) and phenol (98 mg, 705 μmol , 2 eq) in DMF afforded the product after purification and recrystallization in a mixture of EtOAc and *n*hexane as a colorless solid (57 mg, 148 μmol , 42%).

^1H NMR (400 MHz, DMSO) δ 10.18 (s, 1H), 8.51 (s, 1H), 8.26 (d, $J = 8.0$ Hz, 1H), 7.94 (t, $J = 7.8$ Hz, 1H), 7.65 (q, $J = 9.1$ Hz, 2H), 7.59 (s, 4H), 6.77 (d, $J = 5.6$ Hz, 1H), 3.11 (s, 3H) ppm. ^{13}C



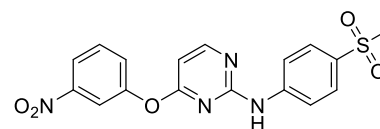
Chemical Formula: $\text{C}_{17}\text{H}_{14}\text{N}_4\text{O}_5\text{S}$
Molecular Weight: 386,38

NMR (101 MHz, DMSO) δ 168.5, 160.6, 158.8, 144.9, 144.5, 142.1, 135.7, 132.6, 127.6, 127.2, 125.8, 125.8, 117.9, 99.6, 43.9 ppm. IR 3276, 3262, 3186, 3102, 3015, 1601, 1574, 1520, 1417, 1347, 1294, 1263, 1209, 1136, 1084, 1050, 829, 794, 767, 703, 664 cm^{-1} . ESI-MS (m/z) 385.3 $[\text{M} - \text{H}]^-$.

***N*-(4-(methylsulfonyl)phenyl)-4-(3-nitrophenoxy)pyrimidin-2-amine (103)**

Following the general procedure for nucleophilic aromatic substitutions, treatment of the chloro-pyrimidine (50 mg, 176 μmol , 1 eq), K_2CO_3 (73 mg, 529 μmol , 3 eq) and phenol (49 mg, 352 μmol , 2 eq) in DMF afforded the product after purification and recrystallization in a mixture of EtOAc and *n*hexane as a colorless solid (42 mg, 109 μmol , 61%).

^1H NMR (400 MHz, DMSO) δ 10.18 (s, 1H), 8.51 (s, 1H), 8.26 (d, $J = 8.0$ Hz, 1H), 7.94 (t, $J = 7.8$ Hz, 1H), 7.65 (q, $J = 9.1$ Hz, 2H), 7.59 (s, 4H), 6.77 (d, $J = 5.6$ Hz, 1H), 3.11 (s, 3H) ppm. ^{13}C NMR (101 MHz, DMSO) δ 168.5, 160.6,



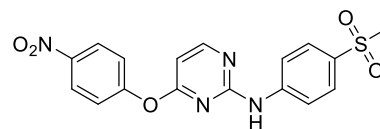
Chemical Formula: $\text{C}_{17}\text{H}_{14}\text{N}_4\text{O}_5\text{S}$
Molecular Weight: 386,38

158.8, 144.9, 144.5, 142.1, 135.7, 132.6, 127.6, 127.2, 125.8, 125.8, 117.9, 99.6, 43.9 ppm. IR 3276, 3262, 3186, 3102, 3015, 1601, 1574, 1520, 1417, 1347, 1294, 1263, 1209, 1136, 1084, 1050, 829, 794, 767, 703, 664 cm^{-1} . ESI-MS (m/z) 385.3 $[\text{M} - \text{H}]^-$.

***N*-(4-(methylsulfonyl)phenyl)-4-(4-nitrophenoxy)pyrimidin-2-amine (104)**

Following the general procedure for nucleophilic aromatic substitutions, treatment of the chloro-pyrimidine (200 mg, 705 μmol , 1 eq), K_2CO_3 (146 mg, 1.06 mmol, 1.5 eq) and phenol (147 mg, 1.06 mmol, 1.5 eq) in DMF afforded the product after purification and recrystallization in a mixture of EtOAc and *n*hexane as a colorless solid (100 mg, 259 μmol , 37%).

¹H NMR (400 MHz, DMSO) δ 10.17 (s, 1H), 8.53 (t, *J* = 5.1 Hz, 1H), 8.43 – 8.34 (m, 3H), 7.74 (d, *J* = 8.9 Hz, 2H), 7.65 (d, *J* = 8.9 Hz, 2H), 7.63 – 7.55 (m, 2H), 6.73 (d, *J* = 5.6 Hz, 1H), 3.10 (s, 3H) ppm. ¹³C NMR (101 MHz, DMSO) δ 168.6, 160.7, 159.0, 157.5, 144.8, 144.6, 132.7, 127.7, 125.6, 123.1, 118.2, 100.3, 43.9 ppm. IR 3261, 3105, 3011, 1612, 1573, 1521, 1450, 1417, 1346, 1301, 1252, 1201, 1137, 1091, 1051, 988, 964, 855, 832, 809, 762, 704, 664 cm⁻¹. ESI-MS (*m/z*) 385.2 [M - H]⁻.

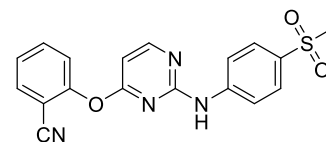


Chemical Formula: C₁₇H₁₄N₄O₅S
Molecular Weight: 386,38

2-((2-((4-(Methylsulfonyl)phenyl)amino)pyrimidin-4-yl)oxy)benzonitrile (105)

Following the general procedure for nucleophilic aromatic substitutions, treatment of the chloro-pyrimidine (80 mg, 282 μmol, 1 eq), K₂CO₃ (117 mg, 846 μmol, 3 eq) and phenol (67 mg, 564 μmol, 2 eq) in DMF afforded the product after purification and recrystallization in a mixture of EtOAc and *n*hexane as a colorless solid (78 mg, 213 μmol, 76%).

¹H NMR (400 MHz, DMSO) δ 10.24 (s, 1H), 8.55 (d, *J* = 5.6 Hz, 1H), 8.05 (dd, *J* = 7.8, 1.3 Hz, 1H), 7.91 (ddd, *J* = 8.3, 7.6, 1.7 Hz, 1H), 7.68 – 7.53 (m, 6H), 6.81 (d, *J* = 5.6 Hz, 1H), 3.11 (s, 3H) ppm. ¹³C NMR (101 MHz, DMSO) δ 168.7, 161.1, 160.8, 158.9, 153.9, 144.6, 135.4, 134.0, 133.9, 132.7, 127.7, 126.8, 123.9, 117.9, 115.4, 106.6, 99.8, 99.4, 43.8 ppm. IR 1578, 1522, 1419, 1290, 1248, 1217, 1139, 1091, 1047, 962, 832, 790, 763, 661 cm⁻¹. ESI-MS (*m/z*) 365.1 [M - H]⁻.

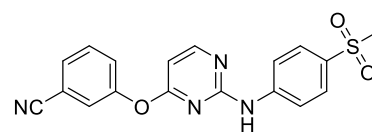


Chemical Formula: C₁₈H₁₄N₄O₃S
Molecular Weight: 366,40

3-((2-((4-(Methylsulfonyl)phenyl)amino)pyrimidin-4-yl)oxy)benzonitrile (106)

Following the general procedure for nucleophilic aromatic substitutions, treatment of the chloro-pyrimidine (50 mg, 176 μmol, 1 eq), K₂CO₃ (146 mg, 1.06 mmol, 1.5 eq) and phenol (42 mg, 352 μmol, 2 eq) in DMF afforded the product after purification and recrystallization in a mixture of EtOAc and *n*hexane as a colorless solid (41 mg, 112 μmol, 64%).

¹H NMR (400 MHz, DMSO) δ 10.16 (s, 1H), 8.49 (d, *J* = 5.4 Hz, 1H), 7.93 (s, 1H), 7.86 (d, *J* = 7.4 Hz, 1H), 7.76 – 7.60 (m, 6H), 6.69 (d, *J* = 5.4 Hz, 1H), 3.11 (s, 3H) ppm. ¹³C NMR



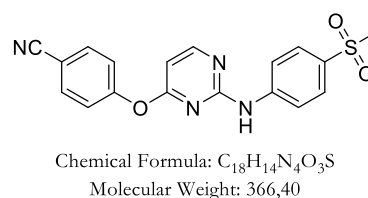
Chemical Formula: C₁₈H₁₄N₄O₃S
Molecular Weight: 366,40

(101 MHz, DMSO) δ 160.4, 152.5, 144.7, 132.6, 131.3, 129.7, 127.7, 126.1, 121.3, 118.1, 112.5, 99.9, 43.9 ppm. IR 3254, 3185, 3097, 3069, 3035, 3004, 2231, 1569, 1521, 1454, 1415, 1293, 1234, 1217, 1141, 1092, 1051, 989, 972, 934, 834, 811, 762, 708, 687, 653, 663 cm^{-1} . ESI-MS (m/z) 365.2 $[\text{M} - \text{H}]^-$.

4-((2-((4-(Methylsulfonyl)phenyl)amino)pyrimidin-4-yl)oxy)benzonitrile (107)

Following the general procedure for nucleophilic aromatic substitutions, treatment of the chloro-pyrimidine (200 mg, 705 μmol , 1 eq), K_2CO_3 (146 mg, 1.06 mmol, 1.5 eq) and phenol (147 mg, 1.06 mmol, 1.5 eq) in DMF afforded the product after purification and recrystallization in a mixture of EtOAc and *n*hexane as a colorless solid (100 mg, 259 μmol , 37%).

^1H NMR (400 MHz, DMSO) δ 10.16 (s, 1H), 8.51 (d, $J = 5.6$ Hz, 1H), 8.05 – 7.99 (m, 2H), 7.72 (d, $J = 8.9$ Hz, 2H), 7.68 – 7.63 (m, 2H), 7.56 – 7.51 (m, 2H), 6.70 (d, $J = 5.6$ Hz, 1H), 3.12 (s, 3H) ppm. ^{13}C NMR (101 MHz, DMSO) δ 168.7,

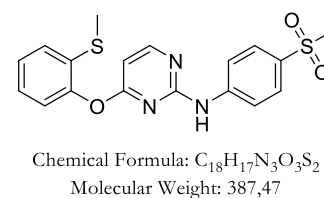


160.6, 159.0, 156.0, 144.7, 134.4, 132.6, 127.7, 123.4, 118.4, 118.1, 108.4, 100.1, 43.9 ppm. IR 3278, 3187, 3102, 3056, 3014, 1570, 1526, 1491, 1452, 1413, 1292, 1206, 1139, 1089, 1048, 1016, 987, 950, 879, 836, 813, 762, 695, 659 cm^{-1} . ESI-MS (m/z) 365.3 $[\text{M} - \text{H}]^-$.

N-(4-(methylsulfonyl)phenyl)-4-(2-(methylthio)phenoxy)pyrimidin-2-amine (108)

Following the general procedure for nucleophilic aromatic substitutions, treatment of the chloro-pyrimidine (50 mg, 176 μmol , 1 eq), K_2CO_3 (73 mg, 529 μmol , 3 eq) and phenol (34 mg, 352 μmol , 2 eq) in DMF afforded the product after purification and recrystallization in a mixture of EtOAc and *n*hexane as a colorless solid (48 mg, 124 μmol , 70%).

^1H NMR (400 MHz, DMSO) δ 10.14 (s, 1H), 8.45 (d, $J = 5.6$ Hz, 1H), 7.66 (d, $J = 8.4$ Hz, 2H), 7.58 (d, $J = 8.4$ Hz, 2H), 7.46 (d, $J = 7.8$ Hz, 1H), 7.41 (t, $J = 7.5$ Hz, 1H), 7.33 (t, $J = 7.5$ Hz, 1H), 7.27 (d, $J = 7.9$ Hz, 1H), 6.61 (d, $J = 5.6$ Hz, 1H), 3.11 (s, 3H), 2.40 (s, 3H) ppm. ^{13}C NMR (101 MHz, DMSO) δ 168.9, 160.2, 159.1, 148.9, 144.8, 132.3,



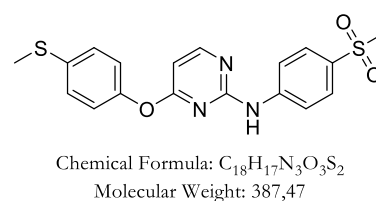
131.9, 127.6, 126.7, 126.7, 126.0, 122.8, 117.9, 99.2, 44.0, 14.0 ppm. IR 3342, 1601, 1574,

1517, 1443, 1410, 1285, 1220, 1198, 1128, 1087, 1069, 1050, 958, 840, 805, 765, 721, 704, 677, 656 cm⁻¹.

***N*-(4-(methylsulfonyl)phenyl)-4-(4-(methylthio)phenoxy)pyrimidin-2-amine (109)**

Following the general procedure for nucleophilic aromatic substitutions, treatment of the chloro-pyrimidine (80 mg, 282 μmol, 1 eq), K₂CO₃ (117 mg, 846 μmol, 3 eq) and phenol (79 mg, 564 μmol, 2 eq) in DMF afforded the product after purification and recrystallization in a mixture of EtOAc and *n*hexane as a colorless solid (55 mg, 142 μmol, 50%).

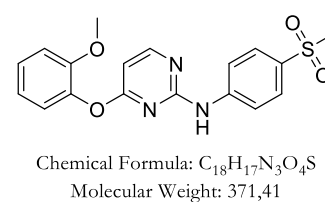
¹H NMR (400 MHz, DMSO) δ 10.12 (s, 1H), 8.44 (d, *J* = 5.6 Hz, 1H), 7.72 (d, *J* = 8.9 Hz, 2H), 7.62 (d, *J* = 8.9 Hz, 1H), 7.43 – 7.38 (m, 2H), 7.26 – 7.19 (m, 2H), 6.59 (d, *J* = 5.6 Hz, 1H), 3.11 (s, 1H), 2.54 (s, 3H) ppm. ¹³C NMR (101 MHz, DMSO) δ 169.6, 160.1, 159.1, 149.9, 144.9, 135.2, 132.4, 127.6, 122.8, 118.1, 99.6, 44.0, 15.3 ppm.



4-(2-Methoxyphenoxy)-*N*-(4-(methylsulfonyl)phenyl)pyrimidin-2-amine (110)

Following the general procedure for nucleophilic aromatic substitutions, treatment of the chloro-pyrimidine (50 mg, 176 μmol, 1 eq), K₂CO₃ (73 mg, 529 μmol, 3 eq) and phenol (44 mg, 352 μmol, 2 eq) in DMF afforded the product after purification and recrystallization in a mixture of EtOAc and *n*hexane as a colorless solid (41 mg, 110 μmol, 63%).

¹H NMR (400 MHz, DMSO) δ 10.11 (s, 1H), 8.42 (d, *J* = 5.6 Hz, 1H), 7.65 (d, *J* = 8.4 Hz, 2H), 7.57 (d, *J* = 8.5 Hz, 2H), 7.36 (t, *J* = 7.8 Hz, 1H), 7.28 – 7.22 (m, 1H), 7.06 (t, *J* = 7.6 Hz, 1H), 6.58 (d, *J* = 5.6 Hz, 1H), 3.71 (s, 3H), 3.10 (s, 3H) ppm. ¹³C NMR



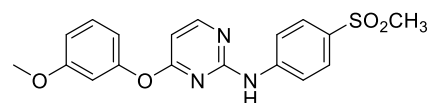
(101 MHz, DMSO) δ 169.2, 159.9, 159.1, 151.3, 144.9, 140.9, 132.2, 127.6, 126.9, 123.1, 121.0, 117.7, 113.2, 99.1, 55.7, 44.0 ppm. IR 1573, 1522, 1497, 1414, 1303, 1251, 1220, 1143, 1112, 1093, 1056, 1041, 953, 840, 788, 766, 694, 660 cm⁻¹.

4-(3-Methoxyphenoxy)-*N*-(4-(methylsulfonyl)phenyl)pyrimidin-2-amine (111)

Following the general procedure for nucleophilic aromatic substitutions, treatment of the chloro-pyrimidine (50 mg, 176 μmol, 1 eq), K₂CO₃ (73 mg, 529 μmol, 3 eq) and phenol (44

mg, 352 μmol , 2 eq) in DMF afforded the product after purification and recrystallization in a mixture of EtOAc and *n*hexane as a colorless solid (38 mg, 102 μmol , 58%).

^1H NMR (400 MHz, DMSO) δ 10.14 (s, 1H), 8.44 (d, $J = 5.6$ Hz, 1H), 7.76 (d, $J = 8.3$ Hz, 1H), 7.62 (d, $J = 8.3$ Hz, 2H), 7.42 (t, $J = 8.1$ Hz, 2H), 6.94 (d, $J = 8.4$ Hz, 1H), 6.88 (s, 1H), 6.84 (d, $J = 8.0$ Hz, 1H), 6.57 (d, $J = 5.6$ Hz, 1H), 3.77 (s, 3H), 3.11 (s, 3H). ^{13}C NMR (101 MHz, DMSO) δ 169.4, 160.6, 160.1, 159.1, 153.3, 144.9, 132.4, 130.33, 127.64, 118.01, 114.00, 111.51, 107.98, 99.63, 55.43, 43.97.

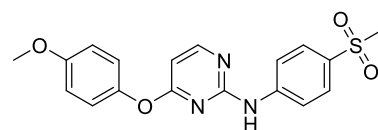


Chemical Formula: $\text{C}_{18}\text{H}_{17}\text{N}_3\text{O}_4\text{S}$
Molecular Weight: 371,41

4-(4-Methoxyphenoxy)-*N*-(4-(methylsulfonyl)phenyl)pyrimidin-2-amine (112)

Following the general procedure for nucleophilic aromatic substitutions, treatment of the chloro-pyrimidine (50 mg, 176 μmol , 1 eq), K_2CO_3 (73 mg, 529 μmol , 3 eq) and phenol (44 mg, 352 μmol , 2 eq) in DMF afforded the product after purification and recrystallization in a mixture of EtOAc and *n*hexane as a colorless solid (39 mg, 105 μmol , 60%).

^1H NMR (400 MHz, DMSO) δ 10.10 (s, 1H), 8.42 (d, $J = 5.6$ Hz, 1H), 7.74 (d, $J = 8.9$ Hz, 2H), 7.62 (d, $J = 8.9$ Hz, 2H), 7.26 – 7.13 (m, 2H), 7.11 – 7.01 (m, 2H), 6.54 (d, $J = 5.6$ Hz, 1H), 3.81 (s, 1H), 3.11 (s, 3H). ^{13}C NMR (101 MHz, DMSO)



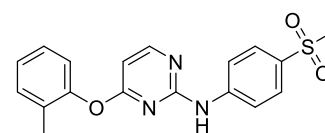
Chemical Formula: $\text{C}_{18}\text{H}_{17}\text{N}_3\text{O}_4\text{S}$
Molecular Weight: 371,41

δ 169.9, 160.0, 159.1, 157.0, 145.7, 145.5, 144.9, 132.3, 127.7, 123.0, 118.0, 114.9, 99.5, 55.5, 44.0 ppm. IR 3074, 3005, 2926, 1599, 1574, 1526, 1497, 1456, 1417, 1295, 1239, 1220, 1182, 1141, 1089, 1052, 1028, 990, 951, 831, 787, 765, 690, 658 cm^{-1} .

***N*-4-(methylsulfonyl)phenyl)-4-(*o*-tolylloxy)pyrimidin-2-amine (113)**

Following the general procedure for nucleophilic aromatic substitutions, treatment of the chloro-pyrimidine (60 mg, 211 μmol , 1 eq), K_2CO_3 (88 mg, 634 μmol , 3 eq) and phenol (46 mg, 423 μmol , 2 eq) in DMF afforded the product after purification and recrystallization in a mixture of EtOAc and *n*hexane as a colorless solid (40 mg, 113 μmol , 53%).

^1H NMR (400 MHz, DMSO) δ 10.13 (s, 1H), 8.44 (d, $J = 5.6$ Hz, 1H), 7.64 (d, $J = 8.9$ Hz, 2H), 7.56 (d, $J = 8.9$ Hz, 2H), 7.41 (dd, $J = 6.7, 0.8$ Hz, 1H), 7.38 – 7.26 (m, 2H), 7.19 (dd, $J = 7.8, 1.3$ Hz, 1H), 6.59 (d, $J = 5.6$ Hz, 1H), 3.10 (s, 1H), 2.11 (s, 3H) ppm.



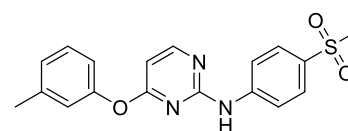
Chemical Formula: $\text{C}_{18}\text{H}_{17}\text{N}_3\text{O}_3\text{S}$
Molecular Weight: 355,41

^{13}C NMR (101 MHz, DMSO) δ 169.2, 160.2, 159.2, 151.3, 150.9, 144.9, 132.3, 131.3, 130.3, 127.7, 127.5, 126.0, 122.4, 117.8, 99.2, 44.0, 15.9 ppm. IR 3337, 1600, 1570, 1519, 1491, 1455, 1411, 1295, 1215, 1173, 1135, 1088, 1053, 987, 960, 838, 817, 797, 764, 714, 663 cm^{-1} . ESI-MS (m/z) 354.3 $[\text{M} - \text{H}]^-$.

***N*-4-(methylsulfonyl)phenyl)-4-(*m*-tolylloxy)pyrimidin-2-amine (114)**

Following the general procedure for nucleophilic aromatic substitutions, treatment of the chloro-pyrimidine (60 mg, 211 μmol , 1 eq), K_2CO_3 (88 mg, 34 μmol , 3 eq) and phenol (46 mg, 423 μmol , 2 eq) in DMF afforded the product after purification and recrystallization in a mixture of EtOAc and *n*hexane as a colorless solid (45 mg, 127 μmol , 60%).

^1H NMR (400 MHz, DMSO) δ 10.13 (s, 1H), 8.44 (d, $J = 5.6$ Hz, 1H), 7.74 (d, $J = 8.9$ Hz, 2H), 7.61 (d, $J = 8.9$ Hz, 1H), 7.40 (t, $J = 7.8$ Hz, 1H), 7.17 (t, $J = 7.7$ Hz, 1H), 7.08 – 7.04 (m, 1H), 6.56 (d, $J = 5.6$ Hz, 1H), 3.11 (s, 3H), 2.36 (s, 3H) ppm.



Chemical Formula: $\text{C}_{18}\text{H}_{17}\text{N}_3\text{O}_3\text{S}$
Molecular Weight: 355,41

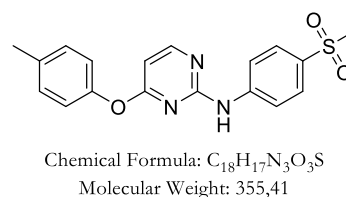
^{13}C NMR (101 MHz, DMSO) δ 169.5, 160.1, 159.2, 152.3, 144.9, 139.7, 132.3, 129.6, 127.7, 126.3, 122.4, 119.0, 118.0, 99.7, 44.0, 20.9 ppm. IR 1570, 1517, 1412, 1300, 1216, 1137, 1095, 1054, 962, 925, 790, 768, 692, 657 cm^{-1} . ESI-MS (m/z) 354.2 $[\text{M} - \text{H}]^-$.

***N*-4-(methylsulfonyl)phenyl)-4-(*p*-tolylloxy)pyrimidin-2-amine (115)**

Following the general procedure for nucleophilic aromatic substitutions, treatment of the chloro-pyrimidine (60 mg, 211 μmol , 1 eq), K_2CO_3 (88 mg, 34 μmol , 3 eq) and phenol (46

mg, 423 μmol , 2 eq) in DMF afforded the product after purification and recrystallization in a mixture of EtOAc and *n*hexane as a colorless solid (35 mg, 98 μmol , 47%).

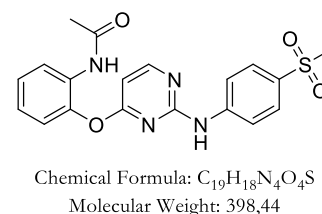
^1H NMR (400 MHz, DMSO) δ 10.09 (s, 1H), 8.42 (d, $J = 5.6$ Hz, 1H), 7.73 (d, $J = 8.9$ Hz, 2H), 7.61 (d, $J = 8.9$ Hz, 2H), 7.31 (d, $J = 8.1$ Hz, 2H), 7.14 (d, $J = 8.4$ Hz, 2H), 6.55 (d, $J = 5.6$ Hz, 1H), 3.11 (s, 1H), 2.38 (s, 3H) ppm. ^{13}C NMR (101 MHz, DMSO) 169.7, 160.0, 159.1, 150.2, 144.9, 134.9, 132.3, 130.3, 127.7, 121.8, 118.1, 99.6, 44.0, 20.4 ppm. IR 3266, 1611, 1570, 1518, 1413, 1300, 1210, 1141, 1091, 1057, 955, 836, 790, 771, 724, 681, 660 cm^{-1} . ESI-MS (m/z) 354.3 [M - H].



***N*-(2-((2-((4-(Methylsulfonyl)phenyl)amino)pyrimidin-4-yl)oxy)phenyl)acetamide (116)**

Following the general procedure for nucleophilic aromatic substitutions, treatment of the chloro-pyrimidine (50 mg, 176 μmol , 1 eq), K_2CO_3 (73 mg, 529 μmol , 3 eq) and phenol (45 mg, 352 μmol , 2 eq) in DMF afforded the product after purification and recrystallization in a mixture of EtOAc and *n*hexane as a colorless solid (45 mg, 113 μmol , 64%).

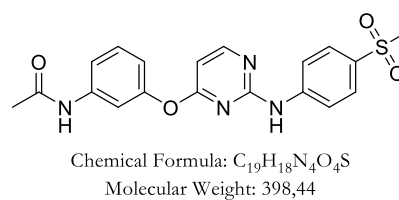
^1H NMR (400 MHz, DMSO) δ 10.15 (s, 1H), 8.45 (d, $J = 5.6$ Hz, 1H), 7.74 (d, $J = 8.9$ Hz, 2H), 7.64 – 7.58 (m, 3H), 7.47 – 7.40 (m, 2H), 6.94 (dt, $J = 6.9, 2.1$ Hz, 1H), 6.59 (d, $J = 5.6$ Hz, 1H), 3.11 (s, 3H), 2.04 (s, 3H) ppm. ^{13}C NMR (101 MHz, DMSO) δ 169.4, 168.6, 160.2, 159.1, 152.5, 144.9, 140.8, 132.4, 129.9, 127.7, 118.0, 116.4, 116.0, 112.4, 99.7, 44.0, 24.0 ppm. IR 1569, 1511, 1447, 1409, 1292, 1220, 1139, 1091, 953, 768 cm^{-1} .



***N*-(3-((2-((4-(methylsulfonyl)phenyl)amino)pyrimidin-4-yl)oxy)phenyl)acetamide (117)**

Following the general procedure for nucleophilic aromatic substitutions, treatment of the chloro-pyrimidine (60 mg, 211 μmol , 1 eq), K_2CO_3 (88 mg, 34 μmol , 3 eq) and phenol (64 mg, 423 μmol , 2 eq) in DMF afforded the product after purification and recrystallization in a mixture of EtOAc and *n*hexane as a colorless solid (55 mg, 138 μmol , 65%).

^1H NMR (400 MHz, DMSO) δ 10.15 (s, 1H), 8.45 (d, J = 5.6 Hz, 1H), 7.74 (d, J = 8.9 Hz, 2H), 7.64 – 7.58 (m, 3H), 7.47 – 7.40 (m, 2H), 6.94 (dt, J = 6.9, 2.1 Hz, 1H), 6.59 (d, J = 5.6 Hz, 1H), 3.11 (s, 3H), 2.04 (s, 3H) ppm. ^{13}C NMR

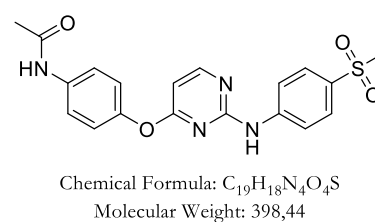


(101 MHz, DMSO) δ 169.4, 168.6, 160.2, 159.1, 152.5, 144.9, 140.8, 132.4, 129.9, 127.7, 118.0, 116.4, 116.0, 112.4, 99.7, 44.0, 24.0 ppm. IR 1573, 1539, 1490, 1444, 1410, 1271, 1251, 1223, 1135, 1087, 1031, 964, 766, 712, 689, 667 cm^{-1} .

***N*-(4-((2-((4-(methylsulfonyl)phenyl)amino)pyrimidin-4-yl)oxy)phenyl)acetamide (118)**

Following the general procedure for nucleophilic aromatic substitutions, treatment of the chloro-pyrimidine (60 mg, 211 μmol , 1 eq), K_2CO_3 (88 mg, 634 μmol , 3 eq) and phenol (64 mg, 423 μmol , 2 eq) in DMF afforded the product after purification and recrystallization in a mixture of EtOAc and *n*hexane as a colorless solid (80 mg, 201 μmol , 95%).

^1H NMR (600 MHz, DMSO) δ 10.10 (d, J = 4.9 Hz, 2H), 8.42 (d, J = 5.6 Hz, 1H), 7.72 – 7.65 (m, 4H), 7.61 (d, J = 8.9 Hz, 2H), 7.23 – 7.14 (m, 2H), 6.56 (d, J = 5.6 Hz, 1H), 3.10 (s, 3H), 2.08 (s, 3H) ppm. ^{13}C NMR (151 MHz, DMSO) δ

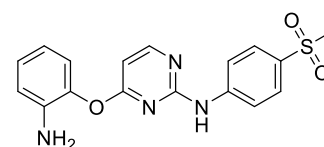


169.8, 168.3, 160.0, 159.1, 147.5, 144.9, 137.0, 132.3, 127.6, 122.3, 120.4, 118.0, 99.5, 43.9, 23.9 ppm. IR 3347, 3266, 3096, 3023, 1613, 1598, 1573, 1522, 1503, 1448, 1420, 1301, 1252, 1219, 1188, 1141, 1093, 1052, 987, 964, 833, 806, 773, 693, 656 cm^{-1} .

3-((2-((4-(Methylsulfonyl)phenyl)amino)pyrimidin-4-yl)oxy)benzoic acid (119)

3-((2-((4-(Methylsulfonyl)phenyl)amino)pyrimidin-4-yl)oxy)benzonitrile (81 mg, 221 μmol , 1 eq) was dissolved in HCl (12 N, 2 mL) and heated to 100 $^\circ\text{C}$ for 2 hours. After TLC indicated complete consumption, the mixture was cooled to 0 $^\circ\text{C}$. Overnight a crystallized solid precipitated and was collected via suction filtration and washed with EtOH. After drying under reduced pressure, the pure product (42 mg, 109 μmol , 49%) was obtained.

¹H NMR (400 MHz, DMSO) δ 10.10 (s, 1H), 8.40 (d, *J* = 5.6 Hz, 1H), 7.75 (d, *J* = 8.8 Hz, 2H), 7.63 – 7.56 (m, 2H), 7.08 – 7.03 (m, 1H), 6.98 (dd, *J* = 7.9, 1.3 Hz, 1H), 6.86 (dd, *J* = 8.0, 1.5 Hz, 1H), 6.63 (ddd, *J* = 7.9, 6.2, 1.5 Hz, 1H), 6.52 (d, *J* = 5.6 Hz, 1H),



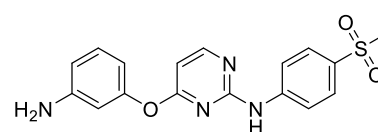
Chemical Formula: C₁₇H₁₆N₄O₃S
Molecular Weight: 356,40

4.98 (s, 1H), 3.10 (s, *J* = 6.7 Hz, 3H) ppm. ¹³C NMR (101 MHz, DMSO) δ 169.4, 159.7, 159.2, 145.1, 141.3, 141.0, 138.6, 132.1, 127.7, 126.4, 122.6, 119.1, 118.0, 117.0, 116.2, 116.1, 99.7, 44.0 ppm. IR 1600, 1570, 1521, 1444, 1412, 1294, 1220, 1138, 1091, 1051, 958, 805, 767, 690, 659 cm⁻¹. ESI-MS (*m/z*) 355.2 [M - H]⁻.

4-(3-aminophenoxy)-*N*-(4-(methylsulfonyl)phenyl)pyrimidin-2-amine (122)

N-(4-(methylsulfonyl)phenyl)-4-(3-nitrophenoxy)pyrimidin-2-amine (30 mg, 78 μmol, 1 eq) was dissolved in MeOH (3 mL) and a small portion of Raney nickel (slurry in water) was added. The mixture was stirred under hydrogen atmosphere for 48 hours. After removing the solvent under reduced pressure, the residue was recrystallized in a mixture of EtOAc and *n*hexane and the product could be obtained as a colorless solid (21 mg, 59 μmol, 76%).

¹H NMR (400 MHz, DMSO) δ 10.13 (s, 1H), 8.41 (d, *J* = 5.6 Hz, 1H), 7.82 (d, *J* = 8.8 Hz, 2H), 7.66 (d, *J* = 8.9 Hz, 2H), 7.12 (t, *J* = 8.0 Hz, 1H), 6.53 (dt, *J* = 6.9, 3.4 Hz, 1H), 6.49 (d, *J* = 5.6 Hz, 1H), 6.39 (t, *J* = 2.0 Hz, 1H), 6.34 (dd, *J* =



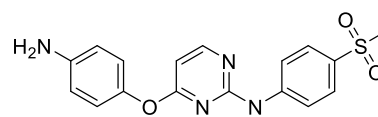
Chemical Formula: C₁₇H₁₆N₄O₃S
Molecular Weight: 356,40

7.9, 1.7 Hz, 1H), 5.38 (s, 2H), 3.11 (s, 3H). ¹³C NMR (101 MHz, DMSO) δ 169.7, 160.0, 159.2, 153.3, 150.5, 145.0, 132.3, 130.0, 127.8, 118.0, 111.3, 108.5, 106.8, 99.5, 44.0 ppm. ESI-MS (*m/z*) 355.3 [M - H]⁻.

4-(4-Aminophenoxy)-*N*-(4-(methylsulfonyl)phenyl)pyrimidin-2-amine (123)

4-(4-Ethylphenoxy)-*N*-(4-(methylsulfonyl)phenyl)pyrimidin-2-amine (80 mg, 207 μmol, 1 eq) was dissolved in MeOH (7 mL) and a small portion of Raney nickel (slurry in water) was added. The mixture was stirred under hydrogen atmosphere for 17 hours. After removing the solvent under reduced pressure, the residue was recrystallized in a mixture of EtOAc and *n*hexane and the product could be obtained as a colorless solid (55 mg, 154 μmol, 75%).

^1H NMR (400 MHz, DMSO) δ 10.09 (s, 1H), 8.37 (d, J = 5.7 Hz, 1H), 7.81 (d, J = 8.9 Hz, 2H), 7.66 (d, J = 8.9 Hz, 2H), 6.89 (d, J = 8.7 Hz, 1H), 6.65 (d, J = 8.7 Hz, 2H), 6.44 (d, J = 5.7 Hz, 1H), 5.14 (s, 2H), 3.12 (s, 3H) ppm. ^{13}C NMR



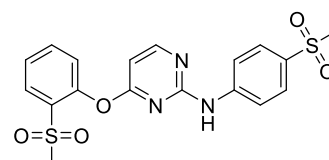
Chemical Formula: $\text{C}_{17}\text{H}_{16}\text{N}_4\text{O}_3\text{S}$
Molecular Weight: 356,40

(101 MHz, DMSO) δ 170.3, 159.7, 159.2, 146.7, 145.0, 142.2, 132.2, 127.7, 122.1, 118.0, 114.4, 99.3, 44.0 ppm. IR 1573, 1523, 1502, 1457, 1417, 1285, 1222, 1190, 1140, 1091, 1054, 958, 830, 808, 773, 660 cm^{-1} . ESI-MS (m/z) 355.0 $[\text{M} - \text{H}]^-$.

4-(2-(methylsulfonyl)phenoxy)-*N*-(4-(methylsulfonyl)phenyl)pyrimidin-2-amine (124)

3-Chloroperoxybenzoic acid (46 mg, 197 μmol , 75% in water, 2.2 eq) was dissolved in DCM (5 mL) and washed with saturated sodium chloride solution and dried over sodium sulphate. Then the organic was separated and cooled to 0 $^\circ\text{C}$. A solution of *N*-(4-(methylsulfonyl)phenyl)-4-(4-(methylthio)phenoxy)pyrimidin-2-amine (33 mg, 85 μmol , 1 eq) was added in DCM (2 mL) and stirred for 17 hours. TLC analysis indicated full consumption of the starting material and subsequently the solvent was removed under reduced pressure. The residue was recrystallized in a mixture of EtOAc and *n*-hexane and afforded the product as a colorless solid (29 mg, 69 μmol , 81%).

^1H NMR (400 MHz, DMSO) δ 10.15 (s, 1H), 8.45 (d, J = 5.6 Hz, 1H), 7.65 (d, J = 8.9 Hz, 2H), 7.57 (d, J = 8.9 Hz, 2H), 7.46 (dd, J = 7.9, 1.6 Hz, 1H), 7.40 (td, J = 7.5, 1.5 Hz, 1H), 7.33 (td, J = 7.6, 1.7 Hz, 1H), 7.27 (dd, J = 7.9, 1.4 Hz, 1H), 6.61 (d, J = 5.6 Hz, 1H), 3.11 (s, 3H), 2.40 (s, 3H) ppm. ^{13}C NMR (101 MHz,



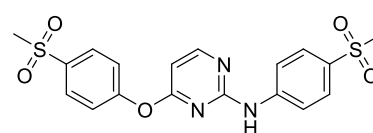
Chemical Formula: $\text{C}_{18}\text{H}_{17}\text{N}_3\text{O}_5\text{S}_2$
Molecular Weight: 419,47

DMSO) δ 168.9, 160.2, 159.1, 148.9, 144.9, 132.3, 131.9, 127.6, 126.7, 126.0, 122.8, 117.9, 99.3, 44.0, 14.0 ppm. IR 3342, 1601, 1574, 1518, 1443, 1411, 1287, 1220, 1199, 1129, 1087, 1069, 1051, 958, 840, 805, 766, 744, 722, 656 cm^{-1} .

4-(4-(Methylsulfonyl)phenoxy)-*N*-(4-(methylsulfonyl)phenyl)pyrimidin-2-amine (125)

3-Chloroperoxybenzoic acid (46 mg, 197 μ mol, 75% in water, 2.2 eq) was dissolved in DCM (5 mL) and washed with saturated sodium chloride solution and dried over sodium sulphate. Then the organic was separated and cooled to 0 °C. A solution of *N*-(4-(methylsulfonyl)phenyl)-4-(4-(methylthio)phenoxy)pyrimidin-2-amine (33 mg, 85 μ mol, 1 eq) was added in DCM (2 mL) and stirred for 17 hours. TLC analysis indicated full consumption and subsequently the solvent was removed under reduced pressure. The residue was recrystallized in a mixture of EtOAc and *n*hexane and afforded the product as a colorless solid (30 mg, 72 μ mol, 84%).

¹H NMR (400 MHz, DMSO) δ 10.16 (s, 1H), 8.48 (d, J = 5.5 Hz, 1H), 7.85 (d, J = 7.6 Hz, 2H), 7.69 (d, J = 8.3 Hz, 2H), 7.61 (d, J = 8.2 Hz, 2H), 7.51 (d, J = 7.6 Hz, 2H), 6.67 (d, J = 5.5 Hz, 1H), 3.10 (s, 3H), 2.83 (s, 3H) ppm. ¹³C NMR (101



Chemical Formula: C₁₈H₁₇N₃O₅S₂
Molecular Weight: 419,47

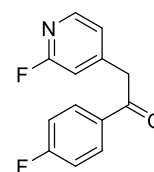
MHz, DMSO) δ 169.2, 160.4, 159.0, 154.2, 144.7, 143.3, 132.5, 127.6, 125.6, 123.1, 118.1, 99.8, 43.9, 43.2 ppm. IR 3263, 1565, 1517, 1443, 1410, 1294, 1259, 1219, 1197, 1140, 1093, 1036, 1012, 967, 829, 780, 701 cm⁻¹.

6.3.8. Thioimidazole series

1-(4-Fluorophenyl)-2-(2-fluoropyridin-4-yl)ethan-1-one (126)

Ethyl 4-fluorobenzoate (726 μ L, 4.95 mmol, 1.1 eq) and 2-fluoro-4-methylpyridine (500 mg, 4.5 mmol, 1 eq) were dissolved in THF (10 mL) and cooled to 0 °C. Then a cooled solution of LiHMDS (1M in THF, 9 mL, 9 mmol, 2 eq) in THF (5 mL) was added slowly via a dropping funnel over 45 minutes. After warming up to room temperature, HCl solution was added (1 M, 5 mL) and the reaction mixture was extracted with EtOAc. The organic phase was separated, dried over sodium sulphate and the solvent removed by rotary evaporation. The crude yellow solid (982 mg, 4.21 mmol, 93%) was used without further purification.

^1H NMR (400 MHz, CDCl_3) δ 8.18 (d, $J = 5.1$ Hz, 1H), 8.05 – 7.99 (m, 2H), 7.21 – 7.14 (m, 2H), 7.12 – 7.06 (m, 1H), 6.85 (s, 1H), 4.30 (s, 2H) ppm. ^{13}C NMR (101 MHz, CDCl_3) δ 193.7, 166.29 (d, $J = 256.4$ Hz), 165.84 (d, $J = 253.5$ Hz), 149.01 (d, $J = 8.1$ Hz), 147.84 (d, $J = 15.3$ Hz), 132.20 (d, $J = 9.3$ Hz), 131.27 (d, $J = 9.5$ Hz), 122.77 (d, $J = 4.1$ Hz), 116.26 (d, $J = 22.0$ Hz), 110.77 (d, $J = 37.6$ Hz), 44.30 (d, $J = 3.0$ Hz) ppm. ESI-MS (m/z) 232.2 $[\text{M} - \text{H}]^-$.

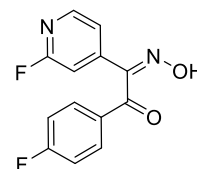


Chemical Formula: $\text{C}_{13}\text{H}_9\text{F}_2\text{NO}$
Molecular Weight: 233,22

1-(4-Fluorophenyl)-2-(2-fluoropyridin-4-yl)-2-(hydroxyimino)ethan-1-one (127)

1-(4-Fluorophenyl)-2-(2-fluoropyridin-4-yl)ethan-1-one (2 g, 8.6 mmol, 1 eq) was dissolved in glacial acetic acid (40 mL) and cooled to 10 °C. After slowly adding an aqueous solution of sodium nitrite (3.5M, 7.35 mL, 25.7 mmol, 3 eq) through a dropping funnel, the reaction mixture was stirred until TLC indicated full consumption of the starting material. Then the mixture diluted with ice water (50 mL) and stirred for an additional hour. The forming precipitate was collected via suction funnel and dried under reduced pressure. The resulting yellow solid (1.45 g, 5.21 mmol, 61%) was used without further purification.

^1H NMR (400 MHz, DMSO) δ 12.72 (bs, 1H), 8.30 (d, $J = 5.0$ Hz, 1H), 7.98 – 7.91 (m, 2H), 7.42 (dd, $J = 14.4, 6.3$ Hz, 2H), 7.38 (d, $J = 4.2$ Hz, 1H), 7.19 (s, 1H) ppm. ^{13}C NMR (101 MHz, DMSO) δ 192.1, 166.06 (d, $J = 254.9$ Hz), 163.55 (d, $J = 235.6$ Hz), 151.92 (d, $J = 6.7$ Hz), 148.88 (d, $J = 15.5$ Hz), 144.37 (d, $J = 8.4$ Hz), 132.26 (d, $J = 10.1$ Hz), 130.87 (d, $J = 2.5$ Hz), 118.29 (d, $J = 4.1$ Hz), 116.76 (d, $J = 22.4$ Hz), 105.43 (d, $J = 39.9$ Hz) ppm. ESI-MS (m/z) 261.1 $[\text{M} - \text{H}]^-$.



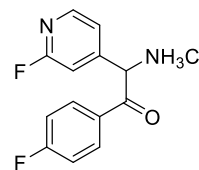
Chemical Formula: $\text{C}_{13}\text{H}_8\text{F}_2\text{N}_2\text{O}_2$
Molecular Weight: 262,22

2-Amino-1-(4-fluorophenyl)-2-(2-fluoropyridin-4-yl)ethan-1-one HCl (128)

1-(4-fluorophenyl)-2-(2-fluoropyridin-4-yl)-2-(hydroxyimino)ethan-1-one (1.4 g, 5.32 mmol, 1 eq) was dissolved in FA/MeOH-mixture (1:1, v/v) and cooled to 10 °C. Then zinc dust (522 mg, 7.98 mmol, 1.5 eq) was added in portions and the suspension was stirred at room temperature for 20 hours. The resulting solid was filtered through a glass frit and the clear filtrate was dried under reduced pressure. The crude product was resolved in EtOAc

and HCl in 1,4-dioxane (4N) was added dropwise. The precipitating colorless solid (445 mg, 1-79 mmol, 34%) was collected and used without further purification.

^1H NMR (400 MHz, DMSO) δ 9.28 (s, 3H), 8.32 (s, 1H), 8.21 (s, 2H), 7.51 (s, 2H), 7.39 (s, 2H), 6.55 (s, 1H) ppm. ^{13}C NMR (101 MHz, DMSO) δ 148.71 (d, $J = 15.0$ Hz), 132.19 (d, $J = 9.9$ Hz), 121.6, 116.20 (d, $J = 22.2$ Hz), 109.79 (d, $J = 39.4$ Hz) 56.2 ppm. ESI-MS (m/z) 246.9 [M - H].

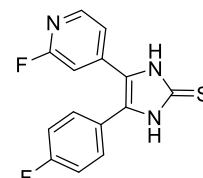


Chemical Formula: $\text{C}_{13}\text{H}_{11}\text{ClF}_2\text{N}_2\text{O}$
Molecular Weight: 284,69

4-(4-Fluorophenyl)-5-(2-fluoropyridin-4-yl)-1,3-dihydro-2H-imidazole-2-thione (129)

2-Amino-1-(4-fluorophenyl)-2-(2-fluoropyridin-4-yl)ethan-1-one HCl (440 mg, 1.55 mmol, 1 eq) and potassium thiocyanate (300 mg, 3.09 mmol, 2 eq) were suspended in dry DMF (5 mL) and heated to 100 °C for 45 minutes. After TLC analysis indicated full consumption of the starting material, the solution was diluted with ice water and stored at 7 °C for 72 hours. The precipitating yellow solid was collected and purified using column chromatography (PE/EtOAc, 10 – 80%).

^1H NMR (400 MHz, DMSO) δ 12.83 (s, 2H), 8.13 (d, $J = 5.4$ Hz, 1H), 7.52 – 7.47 (m, 2H), 7.36 – 7.27 (m, 2H), 7.15 – 7.12 (m, 1H), 7.11 (s, 1H) ppm. ^{13}C NMR (101 MHz, DMSO) δ 164.7, 163.8, 162.5, 162.4, 161.3, 148.05 (d, $J = 16.1$ Hz), 141.18 (d, $J = 9.1$ Hz), 131.22 (d, $J = 8.5$ Hz), 128.1, 124.33 (d, $J = 3.2$ Hz), 120.96 (d, $J = 3.7$ Hz), 116.16 (d, $J = 21.8$ Hz), 105.64 (d, $J = 40.2$ Hz) ppm. ESI-MS (m/z) 287.7 [M - H].

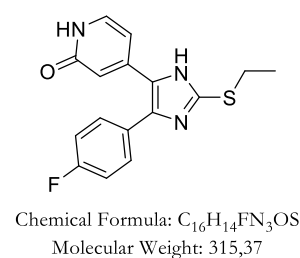


Chemical Formula: $\text{C}_{14}\text{H}_9\text{F}_2\text{N}_3\text{S}$
Molecular Weight: 289,30

4-(2-(Ethylthio)-4-(4-fluorophenyl)-1H-imidazol-5-yl)pyridin-2(1H)-one (133)

Following standard procedure F S-alkylation of mercaptoimidazole and acidic hydrolysis 4-(4-fluorophenyl)-5-(2-fluoropyridin-4-yl)-1,3-dihydro-2H-imidazole-2-thione (80 mg, 277 μmol , 1 eq), iodoethane (27 μL , 332 μmol , 1.2 eq) and K_2CO_3 (46 mg, 332 μmol , 1.2 eq) were suspended in THF (3 mL) and yielded the product as an off-white solid (65 mg, 206 μmol , 75%).

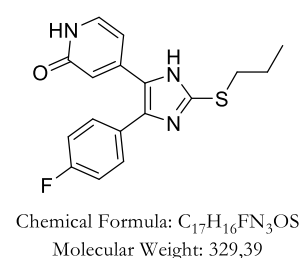
^1H NMR (400 MHz, DMSO) δ 12.74 (s, 0.6H), 12.69 (s, 0.4H), 11.36 (s, 1H), 7.56 – 7.42 (m, 2H), 7.36 (m, 3H), 6.36 (s, 2H), 6.23 (d, J = 6.7 Hz, 0.6H), 6.00 (d, J = 6.5 Hz, 0.4H), 3.19 – 3.06 (m, 2H), 1.32 (t, J = 7.3 Hz, 3H). ^{13}C NMR (101 MHz, DMSO) δ 131.10 (d, J = 8.4 Hz), 130.25 (d, J = 7.8 Hz), 126.72 (d, J = 3.0 Hz), 115.79 (d, J = 21.7 Hz), 115.25 (d, J = 21.4 Hz) ppm. ^{13}C NMR (101 MHz, DMSO) δ 162.59, 162.35, 162.06 (d, J = 246.1 Hz), 161.55 (d, J = 243.6 Hz), 146.1, 142.5, 141.8, 140.9, 139.9, 135.4, 134.7, 134.0, 130.7, 125.2, 115.3, 114.5, 103.9, 103.7, 26.9, 26.7, 15.2. IR 3078, 2946, 1629, 1606, 1559, 1413, 1366, 1221, 1158, 1068, 968, 918, 895, 839, 800, 735, 719, 699, 681 cm^{-1} . ESI-MS (m/z) 314.3 [M - H] $^-$.



4-(4-(4-Fluorophenyl)-2-(propylthio)-1H-imidazol-5-yl)pyridin-2(1H)-one (134)

Following standard procedure F S-alkylation of mercaptoimidazole and acidic hydrolysis 4-(4-fluorophenyl)-5-(2-fluoropyridin-4-yl)-1,3-dihydro-2H-imidazole-2-thione (73 mg, 252 μmol , 1 eq), 1-iodopropane (38 μL , 303 μmol , 1.2 eq) and K_2CO_3 (42 mg, 303 μmol , 1.2 eq) were suspended in THF (3 mL) and yielded the product as an off-white solid (52 mg, 158 μmol , 57%).

^1H NMR (400 MHz, DMSO) δ 12.70 (d, J = 17.2 Hz, 1H), 11.35 (s, 1H), 7.55 – 7.44 (m, 2H), 7.38 – 7.26 (m, 2H), 7.26 – 7.15 (m, 1H), 6.36 (d, J = 5.7 Hz, 1H), 6.21 (d, J = 6.3 Hz, 0.6H), 6.00 (d, J = 6.4 Hz, 0.4H), 3.10 (dd, J = 13.9, 6.9 Hz, 2H), 1.76 – 1.61 (m, 2H), 1.01 – 0.94 (m, 3H) ppm. ^{13}C NMR (101 MHz, DMSO) δ 162.55, 162.31, 141.05, 133.89, 131.14, 131.06, 126.73, 121.33, 115.89, 115.67, 103.83, 34.48, 22.73, 13.04 ppm. IR 1636, 1497, 1430, 1223, 1156, 1094, 1069, 973, 837, 794 cm^{-1} . ESI-MS (m/z) 328.3 [M - H] $^-$.

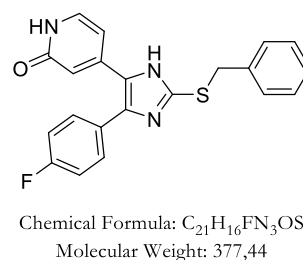


4-(2-(Benzylthio)-4-(4-fluorophenyl)-1H-imidazol-5-yl)pyridin-2(1H)-one (135)

Following standard procedure F S-alkylation of mercaptoimidazole and acidic hydrolysis 4-(4-fluorophenyl)-5-(2-fluoropyridin-4-yl)-1,3-dihydro-2H-imidazole-2-thione (50 mg, 173 μmol , 1 eq), benzylbromide (25 μL , 207 μmol , 1.2 eq) and K_2CO_3 (29 mg, 207 μmol , 1.2

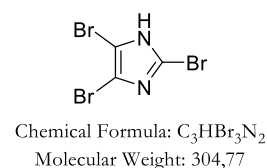
eq) were suspended in THF (3 mL) and yielded the product as an off-white solid (21 mg, 56 μmol , 32%).

^1H NMR (400 MHz, DMSO) δ 12.76 (s, 1H), 11.38 (s, 1H), 7.55 – 7.16 (m, 10H), 6.37 (s, 1H), 6.24 (s, 0.6H), 5.99 (s, 0.4H), 4.40 (s, 2H) ppm. ^{13}C NMR (101 MHz, DMSO) δ 162.55, 137.86, 133.95, 131.05 (d, $J = 6.9$ Hz), 128.90, 128.42, 127.26, 115.80 (d, $J = 21.8$ Hz), 114.53, 103.84, 36.62 ppm. IR 1637, 1607, 1495, 1221, 1156, 1092, 1068, 974, 839, 697 cm^{-1} .



2,4,5-Tribromo-1*H*-imidazole (133)

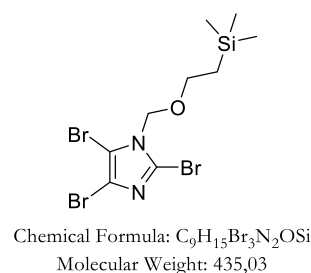
Imidazole (34 g, 500 mmol, 1 eq) and KHCO_3 (150.2 g, 1.5 mol, 3 eq) were dissolved in DMF (250 mL, 2 M) and stirred with a KPG stirrer. After cooling the reaction mixture to 0 $^\circ\text{C}$ bromide (78.1 mL, 1.3 mol, 3.05 eq) was added slowly over 4 hours and then stirred at 70 $^\circ\text{C}$ until TLC indicated full consumption of the starting material. The reaction was stopped by adding ice water (1.5 L) and an off-white solid (92.4 g, 303 mmol, 61%) precipitated, which was collected via suction funnel, washed with ice water and dried in vacuum.



^1H NMR (400 MHz, DMSO) δ 14.05 (s, 1H) ppm. ^{13}C NMR (101 MHz, DMSO) δ 116.1 ppm. ESI-MS (m/z) 303.0 $[\text{M} - \text{H}]^-$.

2,4,5-Tribromo-1-((2-(trimethylsilyl)ethoxy)methyl)-1*H*-imidazole (134)

2,4,5-tribromo-1*H*-imidazole (40 g, 131 mmol, 1 eq) was dissolved in THF (525 mL, 0.25 M) and NaH (6.04 g, 151 mmol, 1.15 eq, 60 % in mineral oil) was added under room temperature and stirred for 30 minutes. Then SEM-Cl (24.4 mL, 138 mmol, 1.05 eq) was added and stirred until HPLC indicated full consumption of the starting material. The reaction was stopped with saturated ammonium chloride solution and extracted with EtOAc. The pure product could be obtained after column chromatography (PE/EtOAc, v/v, 10:1) as a yellow oil (24.2 g, 56 mmol, 42%).

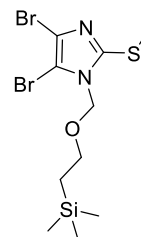


^1H NMR (400 MHz, CDCl_3) δ 5.32 (s, 2H), 3.66 – 3.56 (m, 2H), 0.99 – 0.87 (m, 2H), -0.01 (d, $J = 3.3$ Hz, 9H) ppm. ^{13}C NMR (101 MHz, CDCl_3) δ 119.2, 117.7, 105.8, 76.0, 67.4, 17.9, -1.3 ppm. ESI-MS (m/z) 435.5 [$\text{M} - \text{H}$].

4,5-Dibromo-2-(methylthio)-1-((2-(trimethylsilyl)ethoxy)methyl)-1*H*-imidazole (135)

2,4,5-Tribromo-1-((2-(trimethylsilyl)ethoxy)methyl)-1*H*-imidazole (11.19 g, 25.7 mmol, 1 eq) was dissolved in THF (86 mL, 0.3 M) under argon atmosphere and cooled to -78 °C. Subsequently *n*BuLi (10.3 mL, 25.7 mmol, 1 eq, 2.5 M) was added and stirred for 90 minutes. Then dimethyldisulfide (2.29 mL, 25.7 mmol, 1 eq) was added and stirred under slowly warming up to room temperature. After 20 hours the reaction was stopped by adding HCl solution (1M) and extracted with diethyl ether. The product could be obtained after removing of the solvent as a yellow oil (9.8 g, 24.4 mmol, 95%).

^1H NMR (400 MHz, CDCl_3) δ 5.28 (s, $J = 15.3$ Hz, 2H), 3.58 (ddd, $J = 8.3, 5.7, 2.1$ Hz, 2H), 2.64 – 2.60 (m, 3H), 0.95 – 0.89 (m, 2H), -0.01 (d, $J = 3.3$ Hz, 9H) ppm.

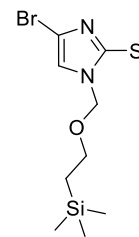


Chemical Formula: $\text{C}_{10}\text{H}_{18}\text{Br}_2\text{N}_2\text{OSSi}$
Molecular Weight: 402,22

5-Bromo-2-(methylthio)-1-((2-(trimethylsilyl)ethoxy)methyl)-1*H*-imidazole (136)

4,5-Dibromo-2-(methylthio)-1-((2-(trimethylsilyl)ethoxy)methyl)-1*H*-imidazole (19.26 g, 48 mol, 1 eq) was dissolved in THF (96 mL, 0.5M) and cooled to -78 °C under argon atmosphere. *n*BuLi (19.15 mL, 48 mmol, 1 eq, 2.5M) was added and the reaction was stopped after 15 minutes by adding ammonium chloride solution. The aqueous phase was extracted with EtOAc and after removing of the organic solvent, the crude product (14.60 g, 45.2 mmol, 94%) was used without further purification.

^1H NMR (400 MHz, DMSO) δ 7.52 (d, $J = 4.1$ Hz, 1H), 5.22 (s, 2H), 3.53 – 3.47 (m, 2H), 2.52 (d, $J = 1.5$ Hz, 3H), 0.87 – 0.82 (m, 2H), -0.03 (s, 9H). ^{13}C NMR (101 MHz, DMSO) δ 143.1, 121.5, 113.6, 74.6, 73.4, 65.7, 17.1, 15.7, -1.4 ppm.

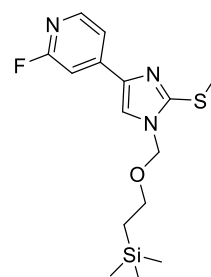


Chemical Formula: $\text{C}_{10}\text{H}_{19}\text{BrN}_2\text{OSSi}$
Molecular Weight: 323,32

2-Fluoro-4-(2-(methylthio)-1-((2-(trimethylsilyl)ethoxy)methyl)-1*H*-imidazol-5-yl)pyridine (140)

5-Bromo-2-(methylthio)-1-((2-(trimethylsilyl)ethoxy)methyl)-1*H*-imidazole (729 mg, 2.25 mmol, 1 eq) was suspended in degassed 1,4-dioxane (30 mL). A previously degassed aqueous solution of K_3PO_4 (10 mL, 1.5 M, 3.5 eq) was added under vigorous stirring. The reaction mixture was frozen with nitrogen and carefully degassed under vacuum and backfilled with argon. XPhos Pd G4 (95 mg, 0.11 mmol, 5 mol%) was added under an argon flow, and the mixture was heated to 65 °C. (2-Fluoropyridin-4-yl)boronic acid (953 mg, 6.76 mmol, 3 eq) was added to the reaction mixture in small portions (95 mg) over 4 hours. After full consumption of the starting material the suspension was cooled to room temperature, quenched by the addition of a saturated ammonium chloride solution, and extracted with EtOAc. The combined organic layers were dried over sodium sulphate, filtered, and the solvents removed by rotary evaporation. The pure product (610 mg, 1.80 mmol, 80%) could be obtained after column chromatography (PE/EtOAc, v/v, 10–50%).

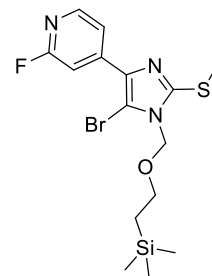
1H NMR (400 MHz, $CDCl_3$) δ 8.17 (d, $J = 5.3$ Hz, 1H), 7.50 (m, 2H), 7.32 (s, 1H), 5.29 (d, $J = 6.3$ Hz, 2H), 2.71 (s, 3H), 1.64 (s, 2H), 0.97 – 0.91 (m, 2H), 0.02 – -0.03 (m, 9H) ppm. ^{13}C NMR (101 MHz, $CDCl_3$) δ 148.0, 147.9, 119.4, 117.2, 104.3, 75.5, 67.0, 17.9, 16.4, -1.3 ppm.



Chemical Formula: $C_{15}H_{22}FN_3OSSi$
Molecular Weight: 339,50

4-(4-Bromo-2-(methylthio)-1-((2-(trimethylsilyl)ethoxy)methyl)-1*H*-imidazol-5-yl)-2-fluoropyridine (141)

2-Fluoro-4-(2-(methylthio)-1-((2-(trimethylsilyl)ethoxy)methyl)-1*H*-imidazol-5-yl)pyridine (710 mg, 2.09 mmol, 1 eq) was dissolved in acetonitrile (25 mL) and cooled to -30 °C. NBS (372 mg, 2.09 mmol, 1 eq) dissolved in acetonitrile (10 mL) was added via a syringe and stirred at -30 °C for 1 hour. After warming up to room temperature, the reaction was stopped by adding a sodium thiosulphate solution and extracted with EtOAc. The combined organic layers were dried over sodium sulphate, filtered, and the solvent removed by rotary



Chemical Formula: $C_{15}H_{21}BrFN_3OSSi$
Molecular Weight: 418,40

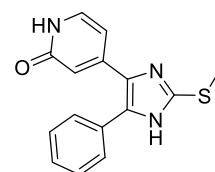
evaporation. The pure product (600 mg, 1.43 mmol, 69%) could be obtained after column chromatography (PE/EtOAc, v/v, 10–50%).

^1H NMR (400 MHz, CDCl_3) δ 8.22 (d, $J = 5.3$ Hz, 1H), 7.89 – 7.84 (m, 1H), 7.60 (s, 1H), 5.35 (s, 2H), 3.70 – 3.55 (m, 2H), 2.70 (s, 3H), 0.99 – 0.91 (m, 9H), 0.02 – -0.02 (m, 9H) ppm. ^{13}C NMR (101 MHz, CDCl_3) δ 164.5 (d, $J = 236.6$ Hz), 147.8 (d, $J = 15.5$ Hz), 146.9, 145.7 (d, $J = 9.1$ Hz), 135.8 (d, $J = 4.1$ Hz), 118.3 (d, $J = 3.9$ Hz) 105.97 (d, $J = 39.6$ Hz), 103.45, 74.04, 67.13, 1, 15.8, -1.3 ppm.

4-(2-(Methylthio)-5-phenyl-1*H*-imidazol-4-yl)pyridin-2(1*H*)-one (142)

Following standard procedure E for Suzuki coupling imidazole and acidic hydrolysis 4-(4-bromo-2-(methylthio)-1-((2-(trimethylsilyl)ethoxy)methyl)-1*H*-imidazol-5-yl)-2-fluoropyridine (250 mg, 598 μmol , 1 eq), phenylboronic acid (182 mg, 1.49 mmol, 2.5 eq), K_3PO_4 (380 mg, 1.79 mmol, 3 eq) and *t*BuXPhos Pd G3 (14 mg, 12 μmol , 2 mol%) were suspended in 1,4-dioxane/water (4:1, v/v, 3 mL) and yielded the product as an off-white solid (20 mg, 71 μmol , 30%).

^1H NMR (400 MHz, DMSO) δ 12.66 (bs, 1H), 11.31 (bs, 1H), 8.19 (d, $J = 5.1$ Hz, 0.4H), 8.17 – 8.11 (m, 0.6H), 7.42 (dd, $J = 18.1, 9.1$ Hz, 6H), 7.25 (dd, $J = 7.6, 3.9$ Hz, 1.6H), 7.10 (s, 0.4H), 6.38 (d, $J = 1.2$ Hz, 1H), 6.25 (s, 1H), 6.02 (s, 0.6H), 2.61 (s, 3H). ^{13}C NMR (101 MHz, DMSO) δ 162.6, 162.5, 147.1, 147.0, 146.2, 134.7, 131.3, 128.8, 128.4, 123.9, 116.0, 115.8, 114.5, 111.0, 110.6, 103.9, 14.9 ppm. IR 1634, 1610, 1551, 1488, 1413, 1364, 1313, 1226, 1172, 1137, 1114, 1072, 1032, 998, 968, 912, 886, 841, 800, 763, 730, 693 cm^{-1} .



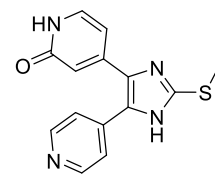
Chemical Formula: $\text{C}_{15}\text{H}_{13}\text{N}_3\text{OS}$
Molecular Weight: 283.35

4-(2-(Methylthio)-5-(pyridin-4-yl)-1*H*-imidazol-4-yl)pyridin-2(1*H*)-one (143)

Following standard procedure E for Suzuki coupling imidazole and acidic hydrolysis 4-(4-bromo-2-(methylthio)-1-((2-(trimethylsilyl)ethoxy)methyl)-1*H*-imidazol-5-yl)-2-fluoropyridine (150 mg, 369 μmol , 1 eq), pyridin-4-ylboronic acid (66 mg, 538 μmol , 2.5 eq), K_3PO_4 (228 mg, 1.08 mmol, 3 eq) and *t*BuXPhos Pd G3 (6 mg, 7 μmol , 2 mol%) were

suspended in 1,4-dioxane/water (4:1, v/v, 3 mL) and yielded the product as a yellow solid (26 mg, 127 μmol , 35%).

^1H NMR (400 MHz, DMSO) δ 13.06 (bs, 1H), 11.77 (bs, 1H), 8.71 (d, $J = 3.7$ Hz, 2H), 7.88 (s, 2H), 7.45 (d, $J = 6.1$ Hz, 1H), 6.48 (s, 1H), 6.20 (d, $J = 5.8$ Hz, 1H), 2.65 (s, 3H) ppm. ^{13}C NMR (101 MHz, DMSO) δ 162.2, 158.42, 154.7, 145.7, 144.2, 144.1, 136.3, 122.6, 118.0, 115.1, 104.6, 14.6 ppm. IR ESI-MS (m/z) 287.7 [M - H] $^-$.

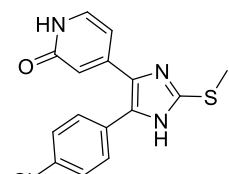


Chemical Formula: $\text{C}_{14}\text{H}_{12}\text{N}_4\text{OS}$
Molecular Weight: 284,34

4-(4-(4-Chlorophenyl)-2-(methylthio)-1H-imidazol-5-yl)pyridin-2(1H)-one (144)

Following standard procedure E for Suzuki coupling imidazole and acidic hydrolysis 4-(4-bromo-2-(methylthio)-1-((2-(trimethylsilyl)ethoxy)methyl)-1H-imidazol-5-yl)-2-fluoropyridine (150 mg, 369 μmol , 1 eq), (4-chlorophenyl)boronic acid (140 mg, 896 μmol , 2.5 eq), K_3PO_4 (228 mg, 1.08 mmol, 3 eq) and *t*BuXPhos Pd G3 (6 mg, 7 μmol , 2 mol%) were suspended in 1,4-dioxane/water (4:1, v/v, 3 mL) and yielded the product as an off-white solid (24 mg, 21 μmol , 21%).

^1H NMR (400 MHz, DMSO) δ 12.70 (s, 1H), 11.37 (s, 1H), 7.60 – 7.41 (m, 4H), 7.34 – 7.20 (m, 1H), 6.36 (s, 1H), 6.24 – 6.16 (m, 0.6H), 6.01 – 5.99 (m, 0.4 H), 2.61 (s, 3H) ppm. ^{13}C NMR (101 MHz, DMSO) δ 162.27, 130.41, 129.90, 128.79, 128.36, 114.83, 103.88, 14.88. IR 1620, 1500, 1485, 1434, 1402, 1368, 1316, 1231, 1173, 117, 1088, 1069, 1016, 967, 913, 884, 827, 795, 731, 697, 682 cm^{-1} . ESI-MS (m/z) 287.7 [M - H] $^-$.

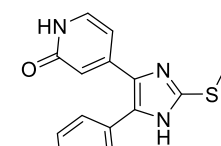


Chemical Formula: $\text{C}_{15}\text{H}_{12}\text{ClN}_3\text{OS}$
Molecular Weight: 317,79

4-(5-(4-Hydroxyphenyl)-2-(methylthio)-1H-imidazol-4-yl)pyridin-2(1H)-one (145)

Following standard procedure E for Suzuki coupling imidazole and acidic hydrolysis 4-(4-bromo-2-(methylthio)-1-((2-(trimethylsilyl)ethoxy)methyl)-1H-imidazol-5-yl)-2-fluoropyridine (150 mg, 369 μmol , 1 eq), (4-hydroxyphenyl)boronic acid (74 mg, 538 μmol , 1.5 eq), K_3PO_4 (228 mg, 1.08 mmol, 3 eq) and *t*BuXPhos Pd G3 (6 mg, 7 μmol , 2 mol%) were suspended in 1,4-dioxane/water (4:1, v/v, 3 mL) and yielded the product as an off-white solid (42 mg, 140 μmol , 39%).

^1H NMR (600 MHz, DMSO) δ 12.71 (bs, 1H), 9.82 (s, 1H), 8.07 (dd, $J = 12.8, 5.5$ Hz, 1H), 7.31 (d, $J = 5.2$ Hz, 1H), 7.29 – 7.25 (m, 2H), 7.08 (s, 1H), 6.86 (d, $J = 8.5$ Hz, 2H), 2.62 (s, 3H) ppm. ^{13}C NMR (151 MHz, DMSO) δ 164.5, 163.0, 162.9, 158.0, 147.6, 147.4, 130.2, 118.2, 115.8, 104.6, 104.4, 15.0 ppm. IR 1663, 1609, 1539, 1499, 1468, 1437, 1405, 1363, 1277, 1201, 1171, 1137, 1005, 879, 840, 798, 730, 687, 654 cm^{-1} . ESI-MS (m/z) 287.7 [$\text{M} - \text{H}$].

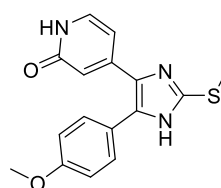


Chemical Formula: $\text{C}_{15}\text{H}_{13}\text{N}_3\text{O}_2\text{S}$
Molecular Weight: 299,35

4-(5-(4-Methoxyphenyl)-2-(methylthio)-1H-imidazol-4-yl)pyridin-2(1H)-one (146)

Following standard procedure E for Suzuki coupling imidazole and acidic hydrolysis 4-(4-bromo-2-(methylthio)-1-((2-(trimethylsilyl)ethoxy)methyl)-1H-imidazol-5-yl)-2-fluoropyridine (150 mg, 369 μmol , 1 eq), (4-methoxyphenyl)boronic acid (109 mg, 717 μmol , 2 eq), K_3PO_4 (228 mg, 1.08 mmol, 3 eq) and *t*BuXPhos Pd G3 (6 mg, 7 μmol , 2 mol %) were suspended in 1,4-dioxane/water (4:1, v/v, 3 mL) and yielded the product as a yellow solid (20 mg, 63 μmol , 53%).

^1H NMR (400 MHz, DMSO) δ 12.62 (s, 1H), 11.31 (s, 1H), 7.37 (d, $J = 8.5$ Hz, 2H), 7.23 (d, $J = 6.8$ Hz, 1H), 7.01 (d, $J = 8.3$ Hz, 2H), 6.39 (s, 1H), 6.20 (s, 1H), 3.80 (s, 3H), 2.60 (s, 3H) ppm. ^{13}C NMR (101 MHz, DMSO) δ 162.6, 159.2, 134.7, 130.1, 114.3, 114.1, 103.8, 55.2, 15.0 ppm. IR 1609, 1491, 1434, 1412, 1367, 1294, 1247, 1225, 1169, 1110, 1066, 1033, 1000, 965, 882, 828, 795, 734, 699, 679 cm^{-1} . ESI-MS (m/z) 287.7 [$\text{M} - \text{H}$].

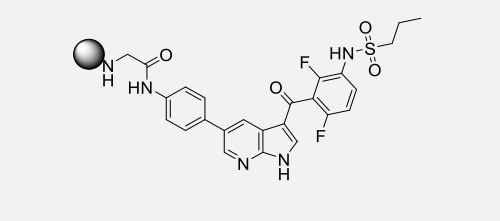
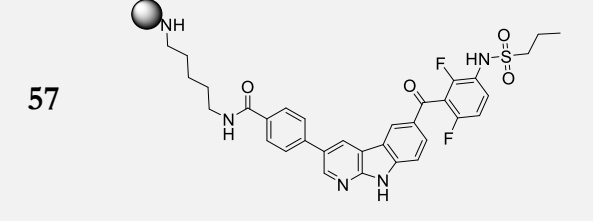
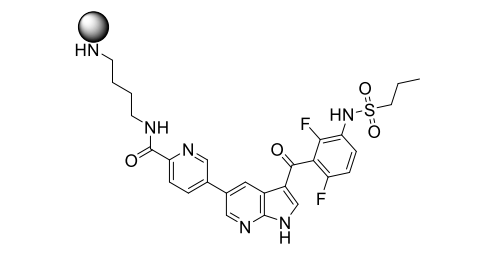
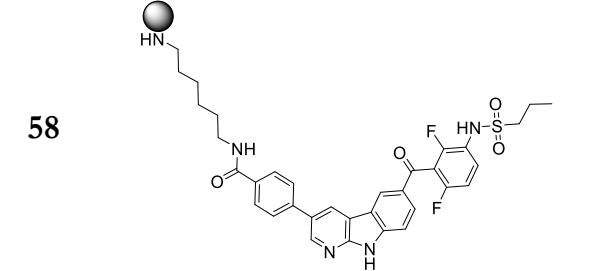
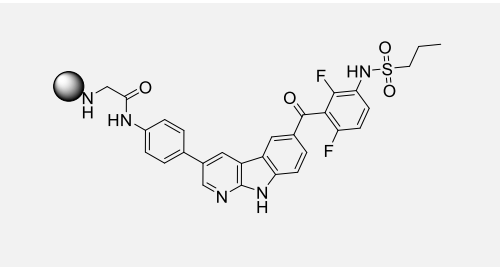
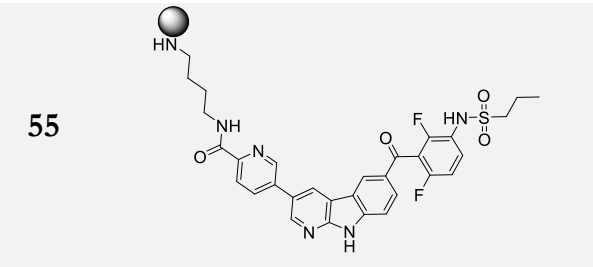
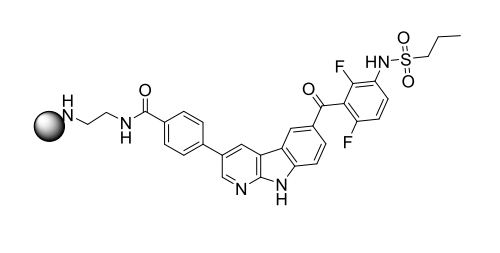
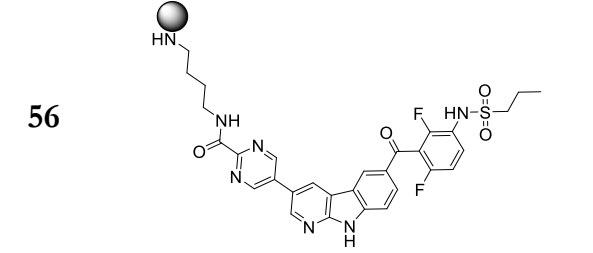
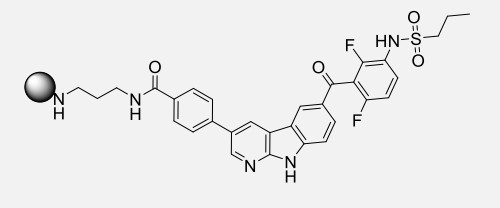
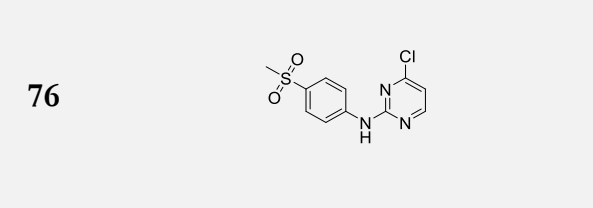
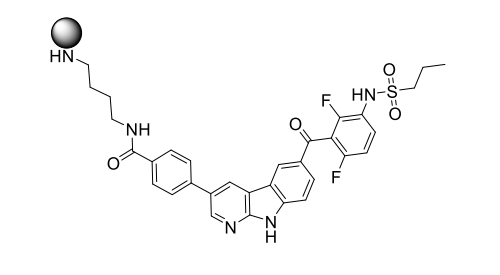
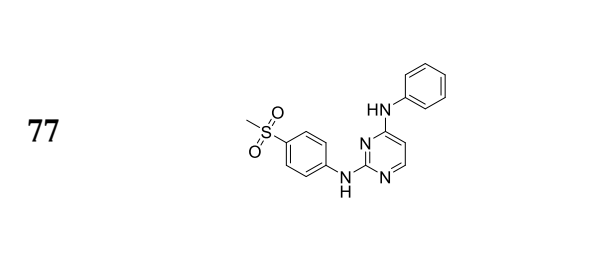


Chemical Formula: $\text{C}_{16}\text{H}_{15}\text{N}_3\text{O}_2\text{S}$
Molecular Weight: 313,38

7. Appendix

No.	Structure	No.	Structure
27		34	
29		36	
30		39	
31		44	
32		40	
		41	

APPENDIX

No.	Structure	No.	Structure
47		57	
48		58	
49		55	
51		56	
52		76	
54		77	

APPENDIX

No.	Structure	No.	Structure
78		88	
79		89	
80		90	
81		91	
82		92	
83		93	
84		94	
85		95	
86		96	
87		97	

APPENDIX

No.	Structure	No.	Structure
98		108	
99		109	
100		110	
101		111	
102		112	
103		113	
104		114	
105		115	
106		116	
107		117	

APPENDIX

No.	Structure	No.	Structure
118		135	
119		142	
120		143	
121		144	
122		145	
123		146	
124			
125			
133			
134			

APPENDIX

<i>No.</i>	<i>POC^{MKK4}</i>	<i>Conc.</i> [μ M]	<i>No.</i>	<i>POC^{MKK4}</i>	<i>Conc.</i> [μ M]	<i>No.</i>	<i>POC^{MKK4}</i>	<i>Conc.</i> [μ M]
27	15	0.1	72	0.25	1	105	100	0.1
29	1.9	0.1	73	0.4	1	106	106	0.1
30	2	0.1	76	90	1	107	78	0.1
31	7.2	0.1	77	73	1	108	100	0.1
32	5.3	0.1	78	15	1	109	96	0.1
34	9.2	0.1	79	62	1	110	100	0.1
36	3.5	0.1	80	62	1	111	100	0.1
39	5.2	0.1	81	100	1	112	98	0.1
44	21	0.1	82	28	1	113	100	0.1
47	11	0.1	83	46	1	114	100	0.1
48	57	0.1	84	60	1	115	91	0.1
49	13	0.1	85	70	1	116	89	0.1
51	19	0.1	86	62	1	117	98	0.1
52	13	0.1	87	31	0.1	118	99	0.1
54	4.3	0.1	88	96	0.1	119	81	0.1
55	1.3	0.1	89	100	0.1	120	100	0.1
56	9.3	0.1	90	94	0.1	121	96	0.1
57	32	0.1	91	100	0.1	122	100	0.1
58	6.6	0.1	92	63	0.1	123	99	0.1
70	98	0.1	93	99	0.1	124	100	0.1
71	95	0.1	94	83	0.1	125	100	0.1
			95	100	0.1	133	68	0.1
			96	100	0.1	134	98	0.1
			97	100	0.1	135	87	0.1
			98	100	0.1	142	26	0.1
			99	100	0.1	143	96	0.1
			100	98	0.1	144	100	0.1
			101	100	0.1	145	100	0.1
			102	100	0.1	146	68	0.1
			103	100	0.1	147	100	1
			104	92	0.1	148	92	0.1

8. Bibliography

- [1] a) C. H. Arrowsmith, J. E. Audia, C. Austin, J. Baell, J. Bennett, J. Blagg, C. Bountra, P. E. Brennan, P. J. Brown, M. E. Bunnage et al., *Nat. Chem. Biol.* **2015**, *11*, 536; b) J. Quancard, B. Cox, D. Finsinger, S. M. Guéret, I. V. Hartung, H. F. Koolman, J. Messinger, G. Sbardella, S. Laufer, *ChemMedChem* **2020**.
- [2] J. Xiao, F. Wang, N.-K. Wong, J. He, R. Zhang, R. Sun, Y. Xu, Y. Liu, W. Li, K. Koike et al., *J. Hepatol.* **2019**, *71*, 212.
- [3] K. M. Field, C. Dow, M. Michael, *Lancet Oncol.* **2008**, *9*, 1092.
- [4] S. A. Mao, J. M. Glorioso, S. L. Nyberg, *Transl. Res.* **2014**, *163*, 352.
- [5] A. Abu Rmilah, W. Zhou, E. Nelson, L. Lin, B. Amiot, S. L. Nyberg, *WIREs Dev. Biol.* **2019**, *8*, 340.
- [6] T. Matsumoto, T. Kinoshita, Y. Kirii, K. Yokota, K. Hamada, T. Tada, *Biochem. Biophys. Res. Commun.* **2010**, 369.
- [7] a) B. Nolen, S. Taylor, G. Ghosh, *Mol. Cell* **2004**, *15*, 661; b) D. K. Treiber, N. P. Shah, *Chem. Biol.* **2013**, *20*, 745.
- [8] T. Matsumoto, T. Kinoshita, Y. Kirii, K. Yokota, K. Hamada, T. Tada, *Biochem. Biophys. Res. Commun.* **2010**, 369.
- [9] T. Matsumoto, T. Kinoshita, Y. Kirii, T. Tada, A. Yamano, *Biochem. Biophys. Res. Commun.* **2012**, 195.
- [10] F. Ardito, M. Giuliani, D. Perrone, G. Troiano, L. Lo Muzio, *Int. J. Mol. Med.* **2017**, *40*, 271.
- [11] A. Cuenda, *Int. J. Biochem. Cell Biol.* **2000**, *32*, 581.
- [12] D. Fabbro, S. W. Cowan-Jacob, H. Moebitz, *Br. J. Pharmacol.* **2015**, *172*, 2675.
- [13] F. Zuccotto, E. Ardini, E. Casale, M. Angiolini, *J. Med. Chem.* **2010**, *53*, 2681.
- [14] M. Gehring, *Covalent Kinase Inhibitors: An Overview*, Springer, Berlin, Heidelberg, **2020**.
- [15] G. J. Hannon, J. J. Rossi, *Nature* **2004**, *431*, 371.
- [16] T. Wuestefeld, M. Pesic, R. Rudalska, D. Dauch, T. Longerich, T.-W. Kang, T. Yevsa, F. Heinzmann, L. Hoenicke, A. Hohmeyer et al., *Cell* **2013**, *153*, 389.
- [17] W. Haeusgen, T. Herdegen, V. Waetzig, *Eur. J. Cell Biol.* **2011**, *90*, 536.

- [18] D. E. Lee, K. W. Lee, S. Byun, S. K. Jung, N. Song, S. H. Lim, Y.-S. Heo, J. E. Kim, N. J. Kang, B. Y. Kim et al., *J. Biol. Chem.* **2011**, *286*, 14246.
- [19] a) L. Xu, Y. Ding, W. J. Catalona, X. J. Yang, W. F. Anderson, B. Jovanovic, K. Wellman, J. Killmer, X. Huang, K. A. Scheidt et al., *J. Natl. Cancer Inst.* **2009**, *101*, 1141; b) R. Cohen, B. Schwartz, I. Peri, E. Shimoni, *J. Agr. Food Chem.* **2011**, *59*, 7932.
- [20] N. Kim, J. Park, C. G. Gadhe, S. J. Cho, Y. Oh, D. Kim, K. Song, *PloS one* **2014**, *9*, 91037.
- [21] G. Bollag, J. Tsai, J. Zhang, C. Zhang, P. Ibrahim, K. Nolop, P. Hirth, *Nat. Rev. Drug Discov.* **2012**, *11*, 873.
- [22] H. Vin, S. S. Ojeda, G. Ching, M. L. Leung, V. Chitsazzadeh, D. W. Dwyer, C. H. Adelman, M. Restrepo, K. N. Richards, L. R. Stewart et al., *eLife* **2013**, *2*, 969.
- [23] P. Klövekorn, B. Pfaffenrot, M. Juchum, R. Selig, W. Albrecht, L. Zender, S. A. Laufer, *Eur. J. Med. Chem.* **2020**, 112963.
- [24] M. Juchum, R. Selig, S. Laufer, W. Albrecht, WO2019243315A1.
- [25] T. Lowinger, M. Shimazaki, Sat, Hiroki, Tanaka, Kazuho, N. Tsuno, K. Marx, M. Yamamoto, Urbahns, Klaus, Gantner, Florian, H. Okigami, Nakashima, Kosuke, Takeshita, Leisuke, K. B. Bacon et al., WO2003037898A1.
- [26] K. K. Deibler, R. K. Mishra, M. R. Clutter, A. Antanasijevic, R. Bergan, M. Caffrey, K. A. Scheidt, *ACS Chem. Biol.* **2017**, *12*, 1245.
- [27] A. J. Kwong, K. A. Scheidt, *Bioorg. Med. Chem. Lett.* **2020**, *30*, 127203.
- [28] L. Q. M. Chow, S. G. Eckhardt, *J. Clin. Oncol.* **2007**, *25*, 884.
- [29] Y. Li, W. Xie, G. Fang, *Anal. Bioanal. Chem.* **2008**, *390*, 2049.
- [30] D. A. Bachovchin, S. J. Brown, H. Rosen, B. F. Cravatt, *Nat. Biotechnol.* **2009**, *27*, 387.
- [31] P. W. Atkins, J. de Paula, C. Hartmann, *Kurzlehrbuch Physikalische Chemie*, 5. Aufl., Wiley-VCH, Weinheim, **2019**, 511.
- [32] D. Frackowiak, *J. Photochem. Photobiol.* **1988**, *2*, 399.
- [33] M. Born, R. Oppenheimer, *Annalen der Physik* **1927**, *389*, 457.
- [34] E. U. Condon, *Am. J. Phys.* **1947**, *15*, 365.
- [35] G. Gauglitz (Hrsg.) *Handbook of Spectroscopy*, Wiley-VCH, Weinheim, **2003**, 37.
- [36] J. B. Lambert, S. Gronert, H. F. Shurvell, D. A. Lightner, *Spektroskopie. Strukturaufklärung in der organischen Chemie*, 2. Aufl., Pearson, München, **2012**.

- [37] K. S. Sarkisyan, I. V. Yampolsky, K. M. Solntsev, S. A. Lukyanov, K. A. Lukyanov, A. S. Mishin, *Sci. Rep.* **2012**, *2*, 608.
- [38] J. R. Lakowicz, *Principles of Fluorescence Spectroscopy*, Springer US, Boston, **2006**, 81.
- [39] X. Shu, S. J. Remington, *Protein Sci.* **2008**, 2703.
- [40] D. C. Prasher, V. K. Eckenrode, W. W. Ward, F. G. Prendergast, M. J. Cormier, *Gene* **1992**, *111*, 229.
- [41] H. Zheng, X.-Q. Zhan, Q.-N. Bian, X.-J. Zhang, *Chem. Biol.* **2013**, *49*, 429.
- [42] R. Sjöback, J. Nygren, M. Kubista, *Spectrochim. Acta A Mol. Biomol. Spectrosc.* **1995**, *51*, 7-21.
- [43] D. M. Jameson, J. A. Ross, *Chem. Rev.* **2010**, *110*, 2685.
- [44] L. D. Lavis, *Annu. Rev. Biochem.* **2017**, *86*, 825.
- [45] M. Savarese, A. Aliberti, I. de Santo, E. Battista, F. Causa, P. A. Netti, N. Rega, *J. Phys. Chem.* **2012**, *116*, 7491.
- [46] D. Sheehan, *Physical biochemistry. Principles and applications*, 2. Aufl., Wiley-Blackwell, Chichester, **2009**, 55.
- [47] M. Sauer, J. Hofkens, J. Enderlein, *Handbook of Fluorescence Spectroscopy and Imaging*, Wiley-VCH, Weinheim, Germany, **2011**, 18.
- [48] M. D. Hall, A. Yasgar, T. Peryea, J. C. Braisted, A. Jadhav, A. Simeonov, N. P. Coussens, *Methods Appl. Fluoresc.* **2016**, *4*, 22001.
- [49] N. J. Moerke, *Curr. Protoc. Chem. Biol.* **2009**, *1*, 1.
- [50] W. A. Lea, A. Simeonov, *Expert Opin. Drug Discov.* **2011**, *6*, 17.
- [51] A. Simeonov, A. Jadhav, C. J. Thomas, Y. Wang, R. Huang, N. T. Southall, P. Shinn, J. Smith, C. P. Austin, D. S. Auld et al., *J. Med. Chem.* **2008**, *51*, 2363.
- [52] C. Hauser, R. Wodtke, R. Löser, M. Pietsch, *J. Amino Acids* **2017**, *49*, 567.
- [53] G. M. Thurber, K. S. Yang, T. Reiner, R. H. Kohler, P. Sorger, T. Mitchison, R. Weissleder, *Nat. Commun.* **2013**, *4*, 1504.
- [54] E. Kim, K. S. Yang, R. H. Kohler, J. M. Dubach, H. Mikula, R. Weissleder, *Bioconjug. Chem.* **2015**, *26*, 1513.
- [55] E. Shevchenko, A. Poso, T. Pantsar, *Comput. Struct. Biotechnol. J.* **2020**, *18*, 2687.
- [56] T. Kircher, T. Pantsar, A. Oder, J. Peter von Kries, M. Juchum, B. Pfaffenrot, P. Kloevekorn, W. Albrecht, R. Selig, S. Laufer, *Eur. J. Med. Chem.* **2020**, 112901.

- [57] W. Albrecht, S. Laufer, R. Selig, P. Klövekorn, B. Präfke, WO2018134254A1.
- [58] Z. Zhang, Z. Yang, H. Wong, J. Zhu, N. A. Meanwell, J. F. Kadow, T. Wang, *J. Org. Chem.* **2002**, *67*, 6226.
- [59] A. J. J. Lennox, G. C. Lloyd-Jones, *Chem. Soc. Rev.* **2014**, *43*, 412.
- [60] K. Belasri, F. Fülöp, I. Szatmári, *Molecules* **2019**, *24*, 3578.
- [61] A. V. Afonin, I. A. Ushakov, S. Y. Kuznetsova, O. V. Petrova, E. Y. Schmidt, A. I. Mikhaleva, *Magn. Reson. Chem.* **2002**, *40*, 114.
- [62] S. T. Handy, Y. Zhang, *Chem. Commun.* **2006**, 299.
- [63] R. J. Abraham, M. Reid, *J. Chem. Soc.* **2002**, 1081.
- [64] Y. Garcia, F. Schoenebeck, C. Y. Legault, C. A. Merlic, K. N. Houk, *J. Am. Chem. Soc.* **2009**, *131*, 6632.
- [65] P. Ruiz-Castillo, S. L. Buchwald, *Chem. Rev.* **2016**, *116*, 12580.
- [66] J. K. Laha, P. Petrou, G. D. Cuny, *J. Org. Chem.* **2009**, *74*, 3152.
- [67] J. R. Dunetz, J. Magano, G. A. Weisenburger, *Org. Process Res. Dev.* **2016**, *20*, 140.
- [68] C. Nájera, *Synlett* **2002**, 1388.
- [69] I. W. Ashworth, B. G. Cox, B. Meyrick, *J. Org. Chem.* **2010**, *75*, 8117.
- [70] a) F. Ciruela, *Curr. Opin. Biotechnol.* **2008**, *19*, 338; b) M. Tomura, N. Yoshida, J. Tanaka, S. Karasawa, Y. Miwa, A. Miyawaki, O. Kanagawa, *Proc. Natl. Acad. Sci. USA* **2008**, *105*, 10871.
- [71] P. Pal, H. Zeng, G. Durocher, D. Girard, R. Giasson, L. Blanchard, L. Gaboury, L. Villeneuve, *J. Photochem. Photobiol.* **1996**, *98*, 65.
- [72] S. M. Menchen, S. Fung, EP0272007A2.
- [73] K. F. Byth, A. Thomas, G. Hughes, C. Forder, A. McGregor, C. Geh, S. Oakes, C. Green, M. Walker, N. Newcombe et al., *Mol. Cancer Ther.* **2009**, *8*, 1856.
- [74] D. J. Wood, S. Korolchuk, N. J. Tatum, L. Z. Wang, J. A. Endicott, M. Noble, M. P. Martin, *Cell Chem. Biol.* **2018**, 121.
- [75] M. Anderson, D. M. Andrews, A. J. Barker, C. A. Brassington, J. Breed, K. F. Byth, J. D. Culshaw, M. R. V. Finlay, E. Fisher, H. H. J. McMiken et al., *Bioorg. Med. Chem. Lett.* **2008**, *18*, 5487.
- [76] P. M. Cromm, K. T. G. Samarasinghe, J. Hines, C. M. Crews, *J. Am. Chem. Soc.* **2018**, *140*, 17019.

- [77] S. C. Ceide, A. G. Montalban, *Tetrahedron Lett.* **2006**, *47*, 4415.
- [78] S. M. Smith, S. L. Buchwald, *Org. Lett.* **2016**, *18*, 2180.
- [79] M. Maddess, R. Carter, *Synthesis* **2012**, *44*, 1109.
- [80] P. A. Cox, A. G. Leach, A. D. Campbell, G. C. Lloyd-Jones, *J. Am. Chem. Soc.* **2016**, *138*, 9145.
- [81] S. A. Laufer, G. K. Wagner, D. A. Kotschenreuther, W. Albrecht, *J. Med. Chem.* **2003**, *46*, 3230.
- [82] C. Gruetter, J. R. Simard, D. Rauh, *J. Am. Chem. Soc.* **2009**, 13286.
- [83] D. A. Shabalin, J. E. Camp, *Org. Biomol. Chem.* **2020**, *18*, 3950.
- [84] F. Bellina, S. Cauteruccio, R. Rossi, *Tetrahedron* **2007**, *63*, 4571.
- [85] M. Günther, J. Lategahn, M. Juchum, E. Döring, M. Keul, J. Engel, H. L. Tumbrink, D. Rauh, S. Laufer, *J. Med. Chem.* **2017**, *60*, 5613.
- [86] John A. Joule, Keith Mills, *Heterocyclic Chemistry*, Wiley-Blackwell, **2010**, 146.
- [87] Z. Wang, *Radziszewski Reaction*, Wiley-VCH, New York, **2001**.
- [88] S. Laufer, D. Hauser, A. Liedtke, *Synthesis* **2008**, *2008*, 253.
- [89] K. Hofmann, *Imidazole and its Derivatives*, Interscience Publishers, New York, **1953**, 79.
- [90] R. Gompper, *Angew. Chem.* **1964**, *76*, 412.
- [91] H. L. Bradlow, C. A. Vanderwerf, *J. Org. Chem.* **1949**, *14*, 509.
- [92] W. R. Dolbier, *Guide to Fluorine NMR for Organic Chemists*, Wiley, Hoboken, New Jersey, **2016**, 109.
- [93] F. Milletti, A. Vulpetti, *J. Chem. Inf. Model.* **2010**, *50*, 1062.
- [94] F. Muth, M. Günther, S. M. Bauer, E. Döring, S. Fischer, J. Maier, P. Drückes, J. Köppler, J. Trappe, U. Rothbauer et al., *J. Med. Chem.* **2015**, *58*, 443.
- [95] B. Iddon, B. L. Lim, *J. Am. Chem. Soc.* **1983**, 735.
- [96] V. Snieckus, *Pure Appl. Chem.* **1990**, *62*, 2047.
- [97] B. H. Lipshutz, W. Vaccaro, B. Huff, *Tetrahedron Lett.* **1986**, *27*, 4095.
- [98] G. L. Schmir, L. A. Cohen, *Biochemistry* **1965**, *4*, 533.
- [99] B. Iddon, A. K. Petersen, J. Becher, N. J. Christensen, *J. Am. Chem. Soc.* **1995**, 1475.
- [100] B. Iddon, N. Khan, *J. Am. Chem. Soc.* **1987**, 1445.
- [101] P. A. Cox, M. Reid, A. G. Leach, A. D. Campbell, E. J. King, G. C. Lloyd-Jones, *J. Am. Chem. Soc.* **2017**, *139*, 13156.

- [102] a) A. F. Littke, C. Dai, G. C. Fu, *J. Am. Chem. Soc.* **2000**, *122*, 4020; b) J. P. Wolfe, R. A. Singer, B. H. Yang, S. L. Buchwald, *J. Am. Chem. Soc.* **1999**, *121*, 9550.
- [103] E. Lyngvi, F. Schoenebeck, *Tetrahedron* **2013**, *69*, 5715.
- [104] M. A. Fabian, W. H. Biggs, D. K. Treiber, C. E. Atteridge, M. D. Azimioara, M. G. Benedetti, T. A. Carter, P. Ciceri, P. T. Edeen, M. Floyd et al., *Nat. Biotechnol.* **2005**, *23*, 329.
- [105] Z. Karoulia, Y. Wu, T. A. Ahmed, Q. Xin, J. Bollard, C. Krepler, X. Wu, C. Zhang, G. Bollag, M. Herlyn et al., *Cancer Cell* **2016**, *30*, 485.
- [106] J. D. Rodgers, D. J. Robinson, A. G. Arvanitis, T. P. Maduskuie, S. Shepard, L. Storace, H. Wang, M. Rafalski, R. Kumar, J. Andrew *et al.*, US 20090215766A1.
- [107] J. Frank, A. R. Katritzky, *J. Am. Chem. Soc.* **1976**, 1428.